# SYNTHESIS, CHARACTERIZATION, AND APPLICATION OF ZIRCONIA AND SULFATED ZIRCONIA DERIVED FROM SINGLE SOURCE PRECURSORS

By

**MOHAMMED H. AL-HAZMI**

Bachelor of Science
King Saud University
Riyadh, Saudi Arabia
1995

Master of Science
King Saud University
Riyadh, Saudi Arabia
1999

Submitted to the Faculty of the
Graduate College of the
Oklahoma State University
In partial fulfilment of
The requirements for
The Degree of
DOCTOR OF PHILOSOPHY
May, 2005

**SYNTHESIS, CHARACTERIZATION, AND APPLICATION OF ZIRCONIA AND SULFATED ZIRCONIA DERIVED FROM SINGLE SOURCE PRECURSORS**

**Thesis Approved:**

**_____Dr. Allen Apblett_____**

**Thesis Adviser**

**_____**

**_____Dr. K. Darrell Berlin_____**

**_____Dr. LeGrand Slaughter_____**

**_____Dr. Gary Foutch_____**

**_____Dr. A. Gordon Emslie_____**

**Dean of the Graduate College**

## ACKNOWLEDGMENTS

The words are inadequate to express my truthful and profound thanks to my phenomenal advisor Dr. Allen W. Apblett for his advice and guidance, continued support, tremendous help, encouragements, and insight and sharp criticism. Since the time that he offered and accepted me to work in this intriguing project, and during the last four and half years, I have learned lots of things from his way of thinking and his research methodology. When encountering some problems and difficulties in different research issues, he simply gives the guidance and the strength to embellish an acceptable idea into a great one. I can honestly say that this Ph.D. dissertation work would not be accomplished without his outstanding supervision, scientific knowledge and experience, and his magnanimous and warm personality of research.

My committee members, Dr. Berlin, Dr. Slaughter, and Dr. Foutch are deeply appreciated for their assistance, reading, editing, and invaluable discussion and comments. I would like to express my sincere acknowledge to my colleagues, all Dr. Apblett's group members, faculty and staff at the Department of Chemistry of Oklahoma State University for their support, kindness and indispensable help during my research period. Furthermore, I extend my warm thanks to Dr. Resasco and his group members at the Department of the Chemical Engineering, University of Oklahoma for performing the X-ray photoelectron spectroscopy analysis.

I would also like to express many thanks to Dr. Margaret Eastman for her effort in performing solid state NMR experiments and Mrs. Phoebe Doss from the electron microscopy laboratory for doing some SEM morphological images.

My utmost sincerest gratitude need to be directed also to Dr. Khalid Karim, Dr. Esam Jami, and Mr. Irhsad Zahir at SABIC R&T, Saudi Arabia, for performing some elemental analysis and pore volume measurements. I am also grateful to SABIC management for their financial support during my study.

Deep appreciations and enormous grateful tribute to my wife (Wafaa AL-Hazmi), my children and my parents for their love, patience, care, sacrifice and trust during my study. Without that, I would never be succeeding in my life. Thank you so much for continuous assistance no matter what the need was.

Finally and humbly, I would like to express my sincere thanks and appreciation to God for giving me the strength and dedication to achieve and complete this degree.

THANK YOU ALL

## TABLE OF CONTENTS

## LIST OF TABLES

**Table** **page**

## LIST OF FIGURES

**Figure** **page**

# CHAPTER 1

## GENERAL INTRODUCTION

### BACKGROUND AND AIM OF RESEARCH:

Zirconia is a widely used ceramic in many technological applications. This is clearly attributed to its unique mechanical and chemical properties such as surface acidity and basicity, oxidation and reduction properties, porosity, stable surface area at high temperatures, high melting point, good mechanical strength, low thermal conductivity, and corrosion resistance [1]. Zirconia is used as an effective catalyst in many important reactions such as dehydration, elimination, hydrogenation, and oxidation reactions. Moreover, zirconia can be acidified to give a strong acid catalyst which can be effective in many reactions, such as alkene isomerization, hydrocracking, and alkylation [2]. Additionally, the high thermal stability and high ionic conductivity of zirconia make it a useful material for refractory purposes and in oxygen sensors. Zirconia has four polymorphs; namely, cubic, tetragonal, monoclinic, and orthorhombic. The latter formed only at elevated pressures. Zirconia can be modified by doping with other metal oxides such as magnesia and yttria. The tetragonal to monoclinic phase transformation significantly enhances the strength and toughness of partially stabilized zirconia [3]. Customarily, zirconia is prepared through base precipitation of zirconium hydroxide,

followed by thermal calcination. Similarly, the traditional method for the synthesis of sulfated zirconia involves treating zirconium hydroxide or oxide with an aqueous solution of sulfuric acid prior to the thermal treatment. The aim of this work is to synthesize a single source precursors composed of zirconium carboxylates and zirconium sulfonates that are suitable for formation of zirconia and sulfated zirconia upon thermal calcination. The variation of the ligands coordinated to zirconium metal will eventually influence properties of the final oxide catalysts such as specific surface area, surface morphology, phase composition, number of active sites, and surface acidity. Furthermore, another purpose of this work is to study the catalytic behavior of the synthesized sulfated zirconia for several reactions, such as alkylation of aromatics and ketone condensation reactions, and relate the catalytic activity with the physical and chemical properties.

## AQUEOUS CHEMISTRY AND STRUCTURE OF ZIRCONIUM (IV):

Zirconium has nearly equal energy of the 4d and 5s levels, and this allows most of the zirconium chemistry to involve the four electrons in these two levels. The $Zr^{4+}$ is a highly charged ion with a relatively large radius (0.86 Å). The Zr(IV) compounds exhibit high coordination numbers because Zr(IV) does not have a partially filled shell. Therefore, Zr(IV) does not display a stable lower valence species. Solutions of zirconium salts can exhibit many chemical reactions such as hydrolysis, polymerization and hydration, depending on conditions. Zirconium salts dissociate in water at low pH value. For example, $Zr^{4+}$ ions hydrate with bonding to eight water molecules to form a square antiprism [4]. In solution, these species hydrolyze by proton transfer from a zirconium-water linkage to liberate hydronium ions as shown in Equation 1-1.

$$[Zr(H_2O)_8]^{4+} + H_2O \longrightarrow [Zr(H_2O)_7(OH)]^{3+} + H_3O^+$$

$$[Zr(H_2O)_7(OH)]^{3+} \xrightarrow{H_2O} [Zr(H_2O)_6(OH)_2]^{2+} + H_3O^+$$

**Eq. 1-1**

The structure of $ZrOCl_2 \cdot 8H_2O$ was determined by Clearfield and coworkers [4]. Single crystal X-ray analysis showed the isolated polymeric tetramer cations of composition $[Zr_4(OH)_8(H_2O)_{16}]^{8+}$ with chlorine counterions to balance the charges. The four $Zr^{4+}$ ions form a slightly distorted square and are connected together with bridging hydroxide groups. The neutral water molecules are bonded directly to zirconium to complete an 8-fold coordination shell of the zirconium atoms. The authors concluded that there are no bonds between zirconium and chlorine formed in either the solid state or in solution. Figure 1-1 shows the structure of the polymeric tetramer cation.

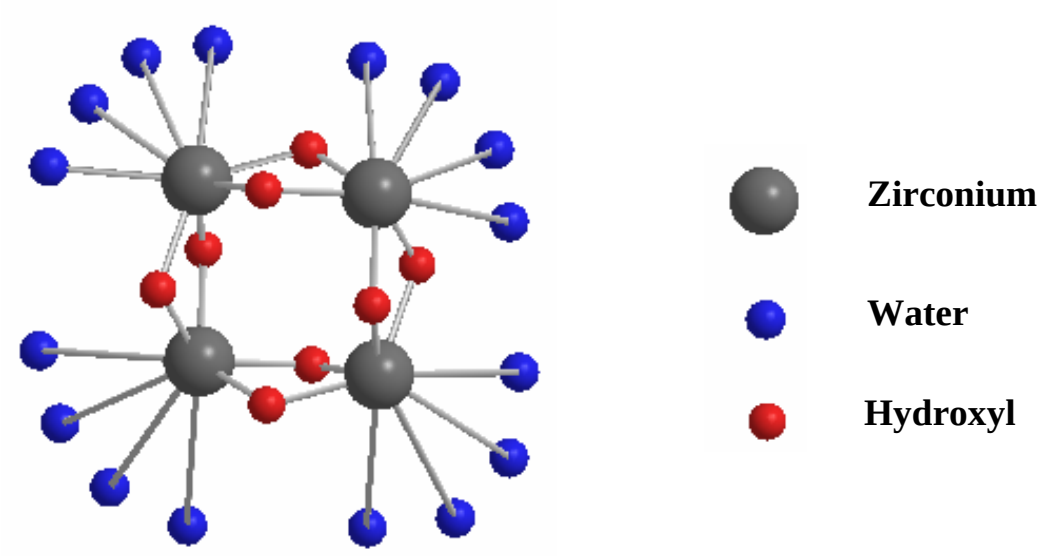


**Figure 1-1: The structure of $[Zr_4(OH)_8(H_2O)_{16}]^{8+}$ polymeric tetramer zirconium complex cation [4].**

**HYDROUS ZIRCONIUM OXIDE:**

The chemical and physical nature of the gels that form upon addition of the hydroxide base ions to an aqueous solution of zirconium salts have been the subject of enormous research interest [5-9]. The pH, aging time, precipitation agent, and zirconium salt are important parameters that play a critical rule on the characteristic properties of the final oxide produced [5,6]. Several authors believe that the structure of the materials obtained by precipitation of a zirconium salt using base is not completely a pure zirconium hydroxide. In fact, the product is believed to be hydrated oxide $ZrO_x(OH)_y$. Clearfield [7] suggested that a polymeric tetrameric zirconium species was formed from a Zr(IV) solution via addition of a base which displaced the bonded water in hydroxyl groups. The tetramers are bonded together, via bridging hydroxyl groups, to form sheets which bind together via a condensation of hydroxyl groups to form a three dimensional zirconia units and water molecules as shown in Figure 1-2. However, electron diffraction studies of this hydrated oxide demonstrated that the particle size is very small and not large enough to give X-ray diffraction patterns, and therefore an amorphous pattern was obtained.

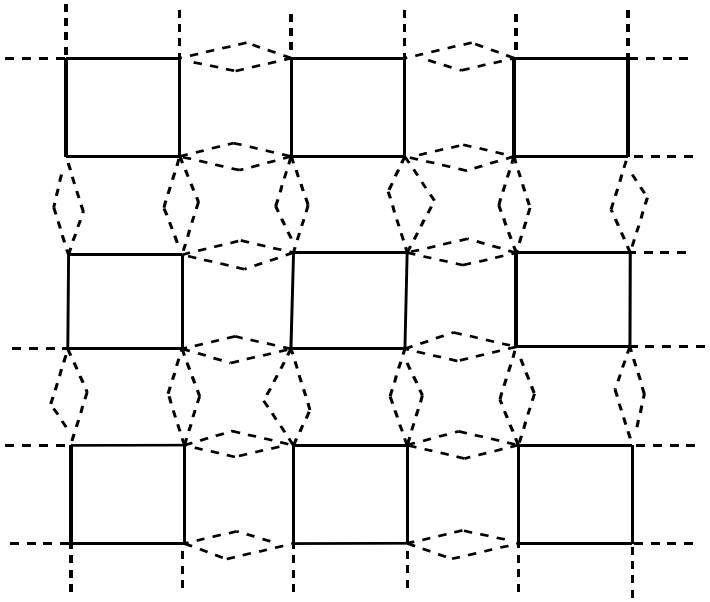

**Figure 1-2: The structure the ordered sheet polymeric species in solution formed by the tetrameric Zr(IV) complex. $Zr_4(OH)_8$ tetrameric units are represented by the solid square lines, the dashed line represent the hydroxyl groups, and the bridging hydroxyl groups are represented by the bent dash lines [7].**

Ultrafine pure zirconia can also be prepared by a hydrolytic polycondensation of zirconium alkoxides [8,9]. This procedure provides a better way to control the rapid hydrolysis. The organic groups of the zirconium alkoxide react with hydroxyl groups of water molecules to form an alcohol and corresponding oxide as shown below (Equation 1-2). The degree of hydrolysis and polymerization depend on many factors such as reaction temperature, pH, nature of the R groups, and the $OH^-$ concentration.

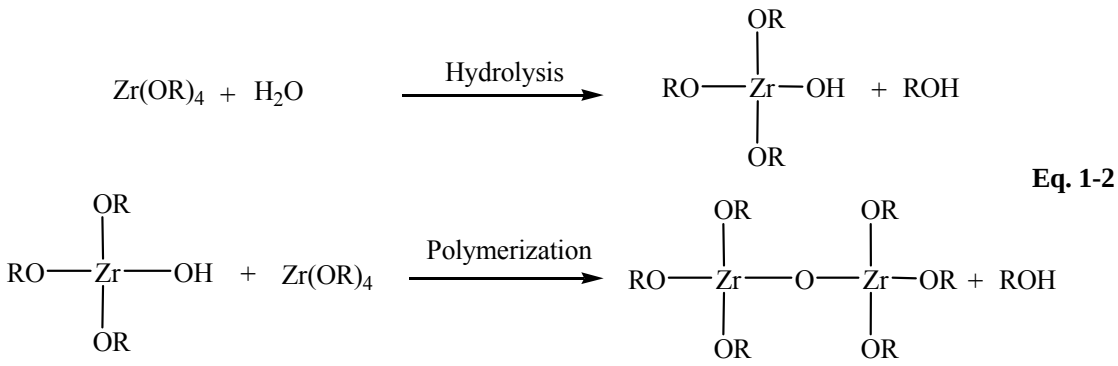


**Eq. 1-2**

**ZIRCONIUM OXIDE:**

Zirconium (IV) oxide is an extremely important oxide, and it has an extensive number of applications. It is used as a solid state electrolyte, in industrial ceramics, and in the catalysis area. Furthermore, the extraordinarily high melting point and low thermal coefficient of expansion make it a major component of refractories. Another important reported application is that heated zirconia can be utilized as a source of infrared radiation and white light [10]. The high electrical resistance of the zirconia makes it an excellent oxide material for use as a ceramic insulator [11]. Table 1-1 summarizes the physical properties of the zirconium (IV) oxide.

**Table 1-1: Physical properties of zirconium oxide ($ZrO_2$)**

| Property | Value |
|---|---|
| Boiling point (°C) | 4300 |
| Coefficient of thermal expansion at -80 °C (cm/cm/°C) | $8 \times 10^{-6}$ |
| Color | White |
| Density (gm/ml) | |
| Monoclinic | 5.68 |
| Tetragonal | 6.10 |
| Cubic | 6.27 |
| Entropy of formation at 298 K (Cal.) | - 46.5 |
| Heat of Formation at 298 K (Kg Cal./mol) | -261.5 |
| Heat of fusion (Kg Cal./mol) | 20.8 |
| Formula weight (gm/ mol) | 123.22 |
| Melting point (°C) | 2900 |
| Solubility | |
| Soluble in | HF, Conc. $H_2SO_4$, molten glass |
| Insoluble in | Water, alkalies, organic solvents |
| Thermal conductivity at 100 °C (Cal. Sec/cm/cm$^2$/°C) | 0.004 |

**CRYSTAL STRUCTURE OF ZIRCONIUM OXIDE:**

**Cubic phase:** Smith has identified the crystal structure of cubic zirconia [12]. The cubic phase is stable above 2370 ºC to melting point. The cubic phase has a fluorite-type structure with a unit cell dimension of 5.27 Å. Each $Zr^{4+}$ ion is coordinated to eight oxygen atoms, while each oxygen atom is bonded to four zirconium atoms in a tetrahedral manner. Figures 1-3 [13] and 1-4(c) show the structure of cubic zirconia.

**Monoclinic phase:** The crystal structure of the monoclinic phase revealed the unit cell parameters to a = 5.169 Å, b = 5.232 Å, and c = 5.341 Å with β = 99º. The crystal structure of this phase demonstrates that the zirconium cations are seven-fold

coordinated with oxygen. Oxygen coordinates nearly tetrahedral to zirconium cations with one angle slightly larger than the tetrahedral angle (109.5º). Another property of this structure is the existence of two alternative layers forming the seven-fold coordination. The seven coordination site of $Zr^{4+}$ arises from the fact that there are two parallel oxygen layers present in the structure of the monoclinic zirconium oxide in which the zirconium atom layer is located between these oxygen layers parallel to the 100 planes. The first layer is the $Zr^{4+}$ coordinated to four oxygen atoms which form a square plane similar to half of an eight-fold cubic structure. In the second layer, the $Zr^{4+}$ ion is coordinated to the three other oxygen atoms which form a trigonal shape with the plane parallel to the phase of the first layer as shown in Figure 1-4 (a and d). The monoclinic phase is stable at room temperature to about 1170 °C [14].

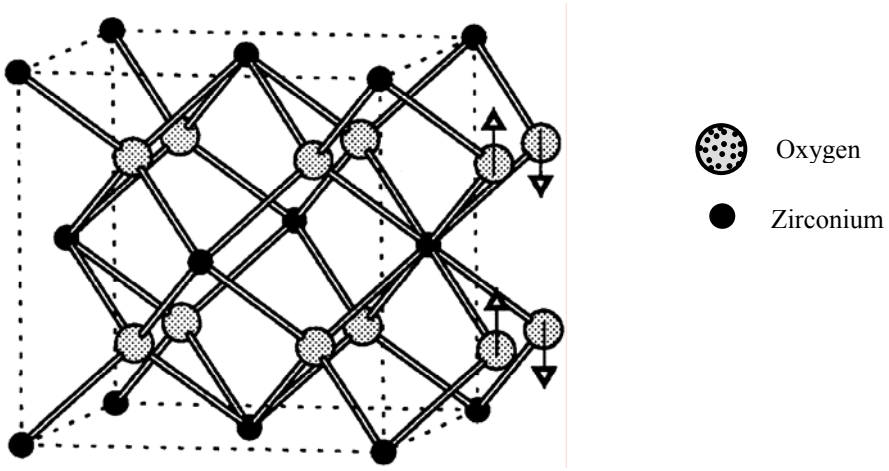


**Figure 1-3: The atomic positions of zirconium and oxygen atoms in the cubic zirconia crystal structure [14].**

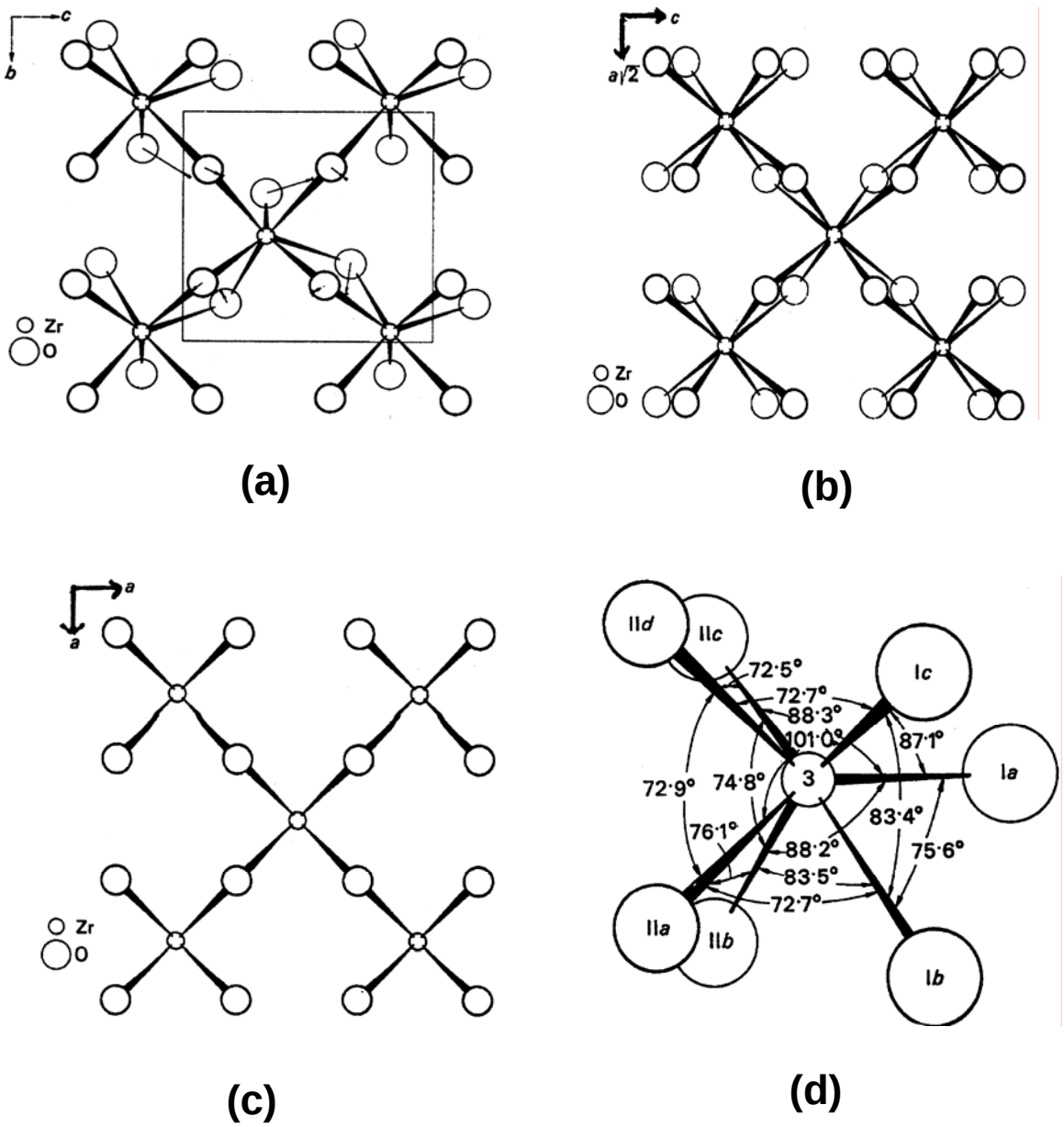


**Figure 1-4: The crystal structure of zirconia: (a) projection for the $ZrO_7$ layer of monoclinic phase, (b) projection for the layer of the $ZrO_8$ of the tetragonal phase, (c) projection of the $ZrO_8$ layer of cubic phase, and (d) angle and interatomic distances in the monoclinic $ZrO_7$ layer [12].**

**Tetragonal phase:** The tetragonal phase is stable above 1170 ºC and below the cubic range temperature of about 2370 ºC. The tetragonal zirconia structure is very similar to the cubic structure with a slight difference. The former still maintains the eight-fold coordination of the zirconium cation. However, the bond distances between the zirconium ions and the four oxygens is 2.45 Å, while the distances to the other four oxygen atoms is slightly shorter, 2.065 Å [Figure 1-4(b)] [12,15].

**PHASE TRANSFORMATION:**

Zirconia can exhibit phase transformation from one structure to another as a function of temperature and pressure as follows [1]:

$$\text{Monoclinic} \underset{950\ ^\circ\text{C}}{\overset{1170\ ^\circ\text{C}}{\rightleftharpoons}} \text{Tetragonal} \overset{2370\ ^\circ\text{C}}{\rightleftharpoons} \text{Cubic} \overset{2680\ ^\circ\text{C}}{\rightleftharpoons} \text{Liquid}$$

The monoclinic–tetragonal phase transformation has been extensively studied due to its theoretical and practical importance [16-21]. Upon phase transformation, the lattice parameters change, and zirconia undergoes contraction on heating and expansion on cooling through the transformation. X-ray diffraction analysis [16] showed that the transformation does not occur at a fixed temperature, but the extent of transformation is changed with changing the temperature. Earlier, Wolten [17] illustrated that the monoclinic-tetragonal transition was thermodynamically reversible and exhibited a large thermal hysteresis between cooling and heating cycles. Furthermore, the transformation rate was dependent upon the particle size of the zirconia powder. The larger the particle size of the prepared zirconia, the faster the phase transformation occurs.

One of the major advantageous of the monoclinic to tetragonal transformation is the volume contraction which can dramatically improve the fracture toughness and strength of zirconia ceramics [3]. However, the volume expansion of the tetragonal to monoclinic phase transformation, which occurs upon cooling through the transformation temperature, can indeed induce cracking of the materials. Therefore, stabilization of zirconia ceramics with other oxide materials, such as yttria and magnesia, is required in order to improve the mechanical properties of zirconia [18].

A metastable tetragonal phase can be achieved at low temperatures using a variety of synthetic approaches. Garvie et al. [19,20] attributed the low temperature stability of the tetragonal phase to the low surface energy of the tetragonal phase compared to that of the monoclinic phase. They claimed that the critical size for stabilization of the tetragonal phase was 30 nm. When the crystallite size exceeded 30 nm, the material exhibited a transformation from tetragonal phase to more stable monoclinic phase. Additionally, the presence of water, upon calcination, was found to increase the rate of aggregation to form large particles and enhance the transformation [21]. This is also probably attributed to the lowering of the monoclinic surface energy as a result of water adsorption. Morgan [22], however, prepared a monoclinic zirconia with a crystallite size smaller than 30 nm. This contradiction arises a question whether the tetragonal phase is the more stable phase or it is a metastable phase. Addition of sulfate anions can also play an important rule in phase transformation. Bridging sulfate ions stabilize the structure of zirconia since it can retard the formation of oxo bonds between zirconium atoms and oxygen atoms. This will prevent sintering at high temperature, and hence, prevent rapid phase transformation and will stabilize the surface area [23,24]. Furthermore, bridging

sulfate groups are believed to contribute to thermal stabilization by increasing of the Zr-O-Zr separation from 3.4 Å to about 4.3 Å [23-25]. There are, in fact, other factors which also influence the phase transformation such as the precursor, pH, and aging time [26,27]. Srinivasan, et al. [26] precipitated zirconia at different pH values within the range 3-13. The samples were calcined at 500 °C for different periods of time. They found that the sample precipitated at low pH exhibited fast phase transition from tetragonal to monoclinic. Furthermore, the phase transformation occurred more rapidly in an oxygen environment than in an inert gas atmosphere. The role of oxygen adsorption is believed to be as follows; the oxygen creates defect sites which generate more strains and dislocations sites which, in turn, initiate the phase transformation [1].

Several authors have studied extensively the thermal behaviour of the precipitated zirconium hydroxide using thermal gravimetric analysis (TGA) and differential thermal analysis (DTA) [27-29]. All authors observed similar results, indicating that the phase transformation of the amorphous phase into tetragonal phase, which is called glow crystallization, occurred at about 400 °C. Blesa et al. [30] suggested a scheme for the transformation of the precipitated zirconium hydroxide. (Equation 1-3).

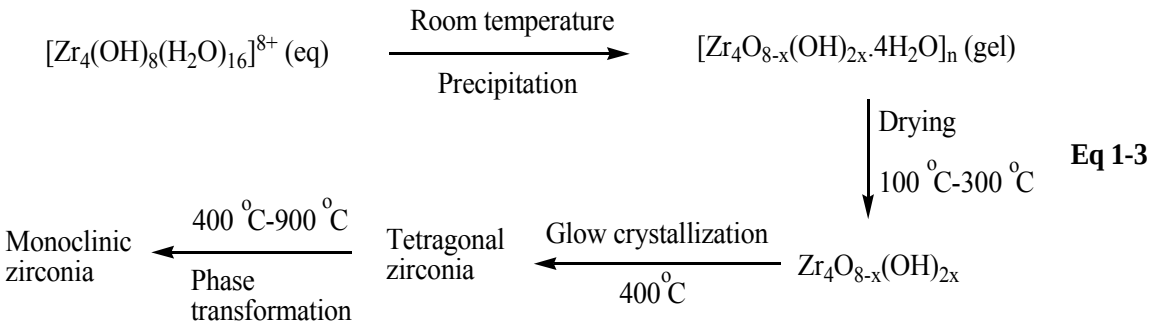


**Eq 1-3**

To conclude, the phase transformation phenomenon of amorphous zirconia is influenced by the crystallization time, the calcination temperature, the environment in which the sample is calcined, the precursor, and the precipitation process. Under most conditions, the initial zirconia formed was in the tetragonal phase when calcined to 400 °C. Upon further heating, the transformation of the tetragonal phase to monoclinic phase occurs and the transformation rate depends on the mentioned factors.

## SULFATED ZIRCONIA, A STRONG ACID MATERIAL:

The utilization of liquid acid catalysts is very important in commercial and industrial applications. However, the uses of these liquid catalysts have some safety and environmental drawbacks such as toxicity, corrosivity, pollution, separation of products, and problems associated with storage, disposal, transportation and handling. Therefore, replacing those acids with more environmentally friendly, solid acids is extremely favored. Among these strong acids, sulfated zirconia has attracted much attention since it exhibited a promising catalytic activity in many reactions such as isomerzation, hydrocracking, alkylations, condensations, and oligomerizations [31]. Arata et al. [32] was the first to report that sulfated zirconia is active for *n*-butane isomerization at moderate temperatures. A 100% sulfuric acid, the threshold of the super acidity according to the definition by Cillespic [33], was not able to catalyze the skeletal isomerization of *n*-butane. That indicated that the reaction mechanism involved the formation of carbenium ions via protonation of the alkane, and this accentuated the superacidity of sulfated zirconia. However, the acid strength is not the only important factor which affects the catalytic activity of sulfated zirconia, but also the type of the acid sites,

Brønsted and Lewis acid sites, plays an important role in determining the catalytic properties.

It is generally accepted that the essential properties of sulfated zirconia, such as the acid strength, the nature of the Lewis and Brønsted acid sites, and catalytic properties, are strongly influenced by the method of preparation, nature of the starting materials, types of sulfation agent, and thermal treatment [34,35]. Conventional sulfated zirconia is generally synthesized by two step methods [36-38]. In the first step, zirconium hydroxide is prepared by hydrolysis of an aqueous solution of a zirconium salt. The second step involves treatment of the zirconium hydroxide with a suitable sulfating agent to form strong acid zirconia upon pyrolysis. An alternative one step preparation procedure has also been developed for the synthesis of sulphated zirconia. In the one step method, alcogel is formed by mixing the zirconium alkoxide, usually zirconium propoxide, in alcohol with nitric acid in the presence of sulfuric acid. The alcohol is then dried to form aerogel which in turn forms sulfated zirconia when calcined at high temperature [39]. These methods are affected by the type of hydrolyzing and precipitation agents, pH of the solution, type of the zirconium precursor, sulfating agents, and finally the drying and calcination procedure. Typical sulfating agents reported in the literature are $H_2SO_4$, $(NH_4)_2SO_4$, $SO_2$, $H_2S$, $CS_2$, and $SO_2Cl_2$, and typical zirconium precursors are zirconium chloride, zirconium nitrate, zirconium isopropoxide, and zirconium oxychloride [40,41].

**NATURE OF THE ACTIVE SITES ON SULFATED ZIRCONIA:**

Several studies have been conducted in order to understand the nature and the structure of the acid active sites of sulfated zirconia. Norman et al. [23,24] reported that the transformation of zirconium hydroxide to oxide proceeds via loss of weakly bonded water molecules and hydroxyl groups during the thermal decomposition to form hydroxyl bridges as a preliminary step to form oxide. Upon sulfation, they suggested that sulfate groups form a bridging structure which improves the thermal stability. Furthermore, the sulfate ions delay the formation of oxo bonds which can facilitate the quick crystallization and phase transformation. This will eventually retard the sintering and stabilize the surface area and lead to fine oxide particles [42,43]. The first structure of sulfated zirconia was proposed by Yamaguchi et al. [44] [Figure 1-5(I)]. They claimed that only Lewis sites existed on the surface. Ward et al. [39] proposed a modified structure which illustrates the observation of Brønsted acid sites [Figure 1-5(II)].


(I) (II)

**Figure 1-5: Proposed sulfated zirconia model; (I): model proposed by Yamaguchi [44], (II): model proposed by Ward [39].**

Morterra et al. [45] suggested that the surface sulfates are highly covalent and have a strong ability to accept electrons from incoming basic molecules. The presence of the adsorbed water molecules, which act as Lewis bases, tends to reduce the covalency of

the surface sulfates, resulting in formation of an ionic form of sulfate species, and hence reduce the Lewis acidic character. Davies et al. [25] proposed a scheme that describes the mechanism of loss of a sulfur species from the surface of the materials in the form of $SO_3$ at high temperature [Figure 1-6)].

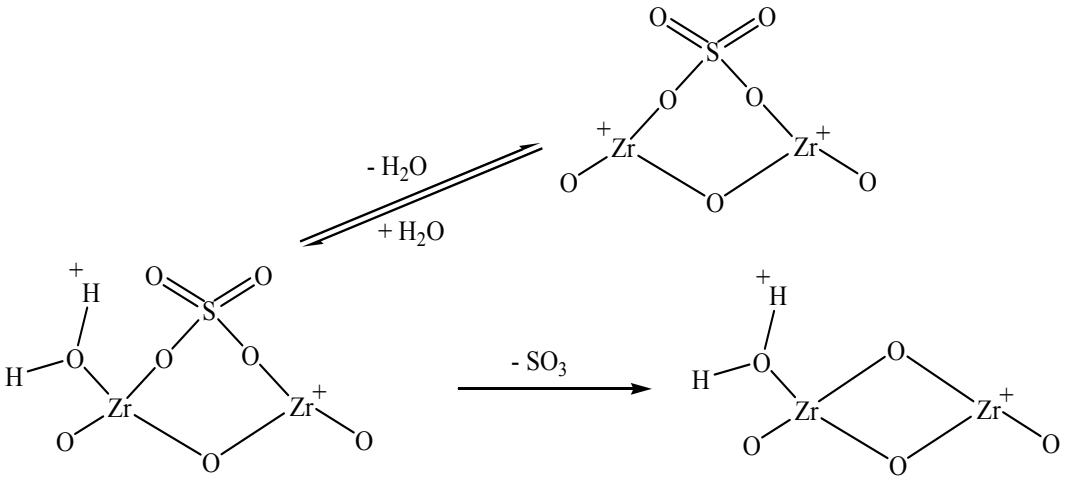


**Figure 1-6: Sulfated zirconia model proposed by Davis [25].**

Clearfield et al. [46] proposed a mechanism for the formation of both Lewis and Brønsted acid sites upon thermal treatment of the sulfonated zirconium hydroxide. Their assumption was based on the displacement of the bridge hydroxyl groups of hydrated zirconia by the chemisorption of bisulfate ions. Lewis acid sites are formed as a result of the reaction of the bisulfate ions with an adjacent hydroxyl group, as indicated by asterisk in Figure 1-7. The Brønsted acid sites are formed as a result of the reaction of two adjacent hydroxyl groups. This results in formation of Lewis acid sites as well as bisulfate groups which act as strong Brønsted acid sites. The strong acidity of these Brønsted sites is attributed to the adjacent Lewis sites which tend to withdraw the electrons from bisulfate. As a result, the oxygen-hydrogen bond in the bisulfate is

weakened [Figure 1-7]. The presence of both acid sites was confirmed by adsorption of pyridine via the use of IR spectroscopy analysis [47]. The bisulfate anions are probably responsible for the high Lewis activity of sulfated zirconia. This is due to the inductive effect of these bisulfate groups which withdraw electron density from the three-coordinate zirconium cation through the bridging oxygen.

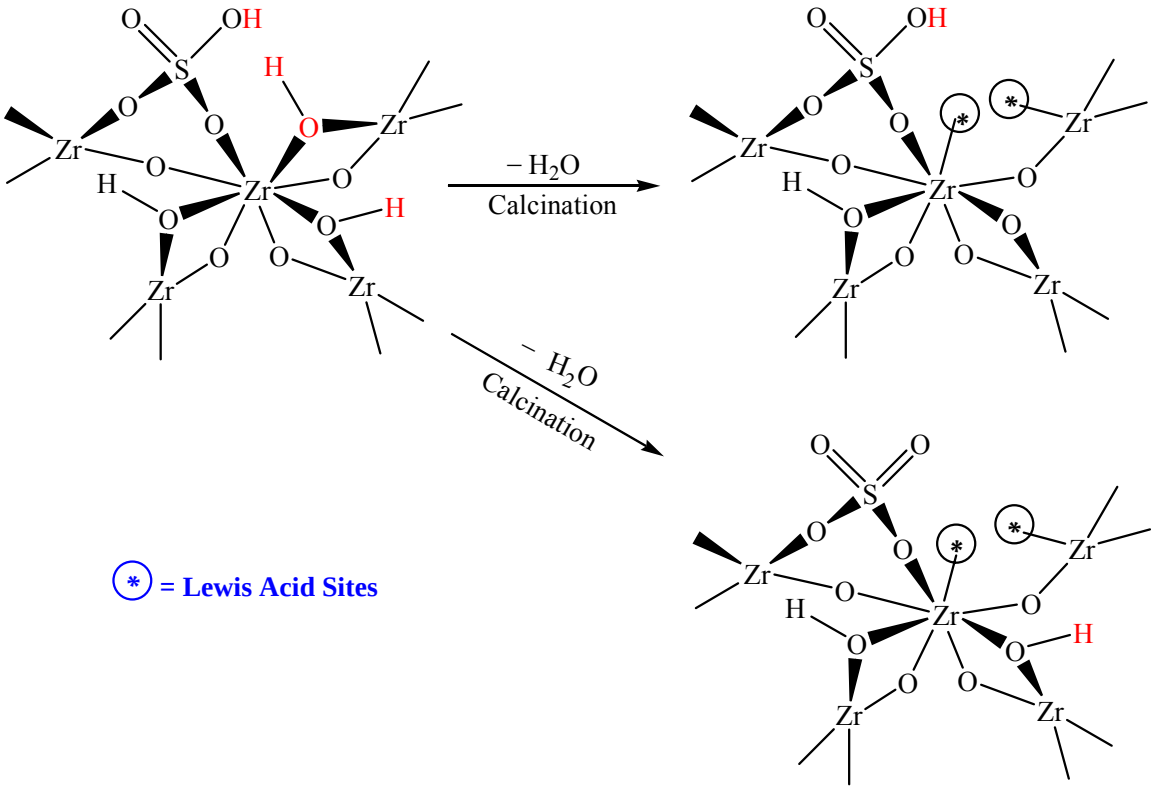


**Figure 1-7: Sulfated zirconia model proposed by Clearfield [46].**

A slightly different evaluation was proposed by Babou et al. [48]. They suggested that the protons of the sulfuric acid are trapped on the surface of the zirconium hydroxide to form an ionic surface. The sulfate ions ($SO_4^{2-}$) are then adsorbed on the positively charged surfaces. Drying at temperatures below 200 °C led to a loss of the first water

molecule. Further heating above 200 °C led to the elimination of the second water molecule with formation of a chemisorbed $SO_3$ group [Figure 1-8].

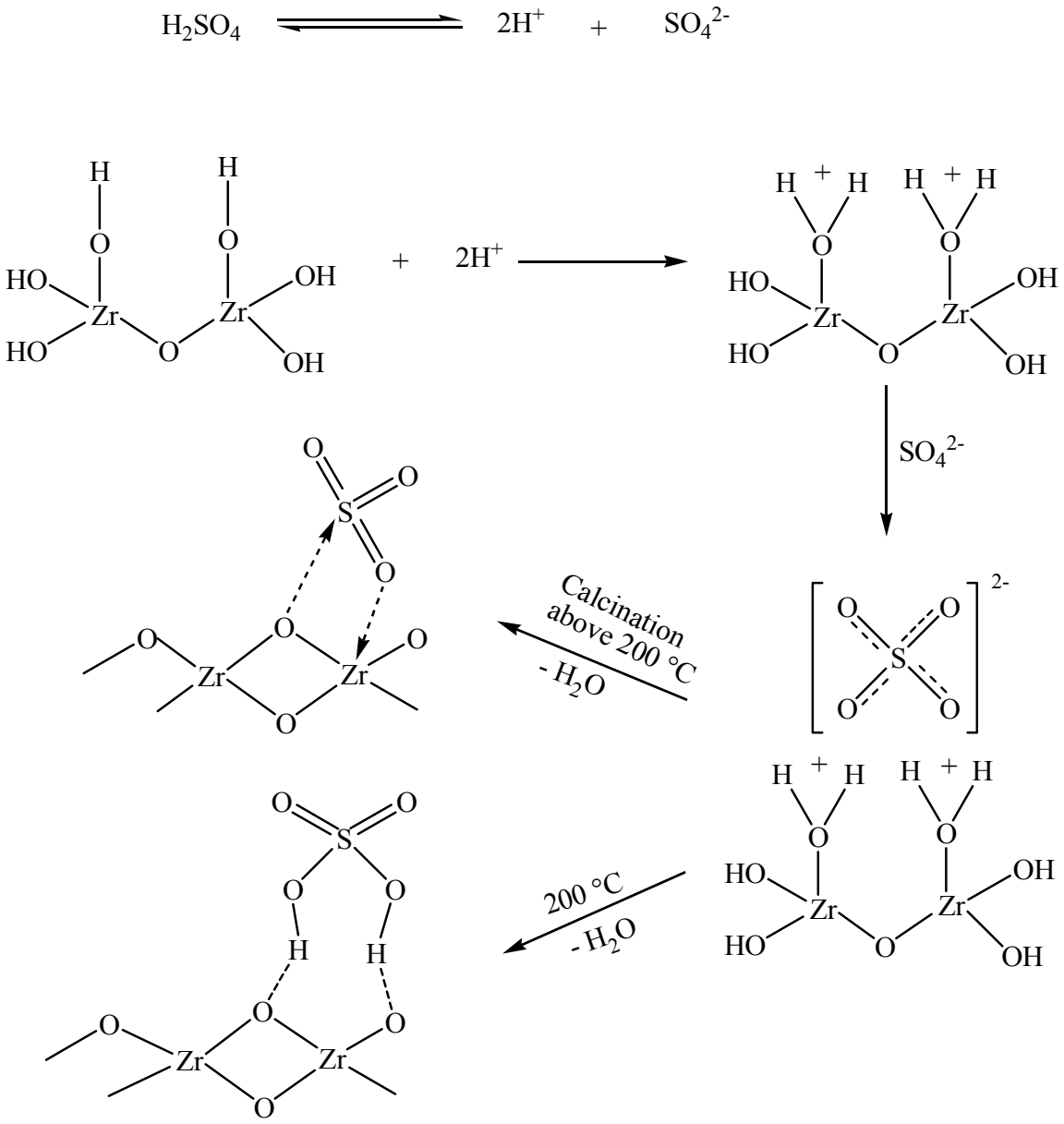


**Figure 1-8: Sulfated zirconia model proposed by Babou [48].**

A different structure of sulfated zirconia with 5-coordination surface atoms was proposed by White et al. [49]. Each sulfur atom in this structure is surrounded by five oxygen atoms. [Figure 1-9].

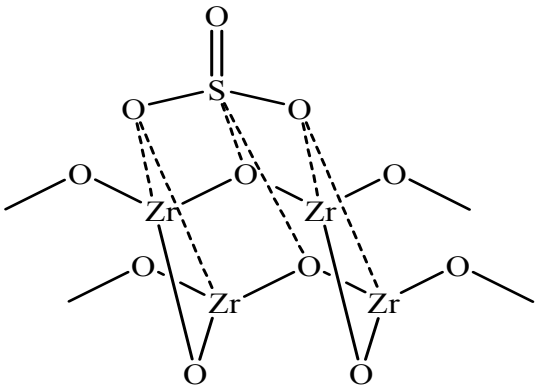


**Figure 1-9: Sulfated zirconia model proposed by White [49].**

**ACIDIC PROPERTIES OF SULFATED ZIRCONIA:**

The acidity is one of the most important properties of sulfated zirconia. The reactivity of the solid acid depends mainly on the nature of the active sites, Brønsted or Lewis acid sites. The properties of the solid acids are strongly influenced by the preparative conditions and other parameters such as nature of the starting materials and procedures adopted for thermal treatment and/or electric insulation [2,31]. A slight variation of the preparative procedure can strongly influence the surface acidic properties of the resulting oxide [50]. Different characterization techniques were discussed in the literature for the determination of surface acidity strength and for provision a rough impression of the number of acid sites on the solid acidic surface. Examples of these methods are the titration with base molecules using bases with diverse pKa values [51], and studying the adsorption of suitable base molecules such as ammonia, *n*-butylamine,

quinoline, and pyridine using infrared and temperature program desorption (TPD) techniques [52-56]. However, despite all the acidity studies and measurements, the superacidity of sulfated zirconia is still a subject of debate. Kustiv et al. studied the strength of the Brønsted acid sites using benzene as a weak base type probe obtained by monitoring the infrared shift of the hydroxyl groups after adsorption of benzene [57]. They concluded that the strength of the acidic sites of the sulfated zirconia is stronger than that of the silica gel, but still weaker than the zeolites, which don't exhibit super acidity. Therefore, they classify sulfated zirconia as a strong acid rather than supper acid. Pyridine and ammonia, on the other hand, are unique probes since they can be utilized to measure both Brønsted and Lewis acid sites on the catalyst surface by exploiting the infrared spectroscopic technique [58]. Pyridine and ammonia can distinguish between Brønsted and Lewis acid sites based on the fact that proton donor sites and electron pair acceptor sites can interact with the electron pair on the nitrogen atom. Therefore, there are specific characteristic IR bands associated with adsorption of ammonia and pyridine over Lewis sites while different characteristic peaks assigned for adsorption of ammonium and pyridinium ions over Brønsted acid sites [58-60]. However, it was reported for the analogous amines, such as *n*-butylamine, that ammonia and other primary and secondary amines are considered to be misleading probes for surface acidity measurements of solid acids, since these amines can dissociate to yield $NR_xH_y^-$ anions and $H^+$ cations. These anions and cations latter can be adsorbed on the acid and base sites, respectively, depend on the solid type and adsorption conditions, Eq. 3-1[61].

$$NR_xH_y \rightleftharpoons NR_xH_y^- + H^+ \qquad \textbf{Eq. 3-1}$$

Infrared spectroscopy was also utilized to estimate the Lewis and Brønsted acidity using several bases such as pyridine, ammonia, and benzene by monitoring the chemical shift of the asymmetric stretching of S=O bonds, which were observed in the range of 1370-1410 $cm^{-1}$ and OH groups around 3600 $cm^{-1}$ [62-65]. These kinds of base probes are able to identify and measure quantitively the Brønsted as well as Lewis acid sites on the surface. This approach can give valuable information about the structure of sulfated zirconia. Additionally, IR studies using base probes showed that there are several sulfate forms present on the surface [66]. It was suggested that sulfated zirconia does not exhibit a superacidity modality since its acidity is not stronger or similar to that of pure sulfuric acid or even some acidic zeolites [57,67-69].

The acid strength is defined as the ability of the solid surface to convert a neutral base into its conjugate acid. One of the most important analytical methods utilized for the evaluation of the acid strength of sulfated zirconia is Hammett indicators, which depend on a color change. These techniques are often used for characterization of liquid acids. The Hammett acidity function, known as Ho value, provides an indication about the acid strength, since the more acidic the surface, the lower the Ho and pKa values and vice versa. If the color formed is that of the acid form of the indicator, the implication is that the proton transfers from the surface to the adsorbate, indicating that the value of the Ho is the same or lower than the pKa of the conjugate acid of the indicator according to the following equation (Eq. 3-2) [53,54,58,70]:

$$HA + B \text{ (Indicator base)} \rightleftharpoons BH^{+} \text{(conjugate acid)} + A^{-} \qquad \textbf{Eq. 3-2}$$

Therefore, the acid strength expressed by Ho as shown in Eq. 3-3:

$$Ho = pKa + \log [B]/[BH^+] \qquad \textbf{Eq. 3-3}$$

Where Ka is the equilibrium constant of dissociation of the acid, [B] and $[BH^+]$ are the concentrations of the neutral base and conjugate acids, respectively. For example, a solid gives a yellow color with chalcone (pKa = -5.6) whereas it is colorless with anthraquinone (pKa = -8.2). Therefore, it can be concluded that the acid strength (Ho) of the solid is between -5.6 and -8.2. Furthermore, the solid which gives a color change with *p*-nitrotoluene (pKa = -11.4) is considered to be more acidic than 100% sulfuric acid and hence it is a superacid [71,72].

Hino et al. [71] reported that the Ho value for sulfated zirconia is about -16, which is much larger than that of the 100% $H_2SO_4$ (Ho = -11), if this method is applicable to solid acids. However, there are many limitations for this method, specially when applied to solid acids such as: difficulty in formation of the conjugate acid $BH^+$ [68]; presence of heterogeneous distribution of the indicator over the anisotropic solid surface [73]; strong interaction between solvent and catalyst surface; high sensitivity toward moisture; strong chemical bonding of the indicator (B) with the protonic acid sites on the surface; and finally difficulty to observe color change in some cases [74-76]. Furthermore, several assumptions are needed to obtain reliable acidity measurements using the Hammett indicator method. For instance, equilibrium between adsorbed indicator on the surface acid sites and the homogenous, uniformly-distributed acid surface is assumed to be maintained. Another assumption is the formation of the mobile

physisorbed $BH^+$ on the acid surface. Moreover, theoretical methods were also used to assess the acidity of sulfated zirconia using *ab intio* methods along with utilizing water and carbon monoxide as appropriate probes [69,77,78]. These measurements provide invaluable information about sulfated zirconia structure at the microscopic level. It has been confirmed that sulfated zirconia has acidity similar to that of pure sulfuric acid and yet is not considered a superacid. That was also confirmed by Adevaa and his associates using thermal methods and UV measurements [68]. They reported that the acidity of sulfated zirconia is similar to that of zeolites. They concluded that its catalytic activity towards initiating isomerization of alkanes is not only directed by the surface acidity, but also can catalyze such a reaction while zeolites can not.

Furthermore, Shibata et al. [79] reported that zirconia itself, without the incorporation of sulfate ions, is a weakly acidic oxide. They claimed the highest acidity strength of zirconia prepared with 64 $m^2/g$ specific surface area was derived calcination of zirconium hydroxide at 773 K for 3 hours. The acidity strength reported was Ho = +1.5 with an acidity amount of 60 μmol/ g. The acid sites on the zirconia surface are mainly Lewis sites. In conclusion, one can say that the catalyst properties, such as pore shape and diameter, can strongly influence the availability of the acid sites and hence the catalyst activity and selectivity. Additionally, more research work is required to develop suitable methods for characterization of acidic properties of sulfated zirconia and other solid acids.

Despite all the debate in the literature about the superacidity status and the acid strength of the sulfated zirconia, there are many researchers who reported and confirm that the sulfated zirconia is indubitably a superacid. Their conclusions were based on

acidity measurements using Hammett indicators [71,80-82], and using adsorption probes such as ammonia, pyridine, and benzene [2,62,63,65,82]. In our current research work, we corroborate the previous researchers work. Although our experimental protocol was different, we arrived at a similar conclusion that the synthesized sulfated zirconia does in fact exhibit superacidity.

**MODIFIED SULFATED ZIRCONIA:**

It was discovered that platinum-promoted, sulfated zirconia showed a higher activity towards alkane isomerization reactions in the presence of hydrogen molecules than conventional sulfated zirconia [83,84]. Several researchers studied the state of the Pt-supported over sulfated zirconia. Hattori [85] suggested that Pt-supported over sulphated zirconia is different than the usual supported Pt catalysts. Characterization techniques, such as temperature programmed desorption (TPD), X-ray photoelectron spectroscopy (XPS), and extended X-ray absorption fine structure (EXAFS) indicated most of the Pt on the sulphated zirconia support surface is in a cationic state. These results were confirmed by Ebitani [86]. Due to the redox metal-support interaction of the Pt with the acidic-sulphated zirconia support, the reducibility of the cationic Pt particles on the surface was suppressed, and no carbon monoxide chemisorption was observed, confirming the dominant presence of cationic Pt particles [87]. Furthermore, the presence of Pt and $H_2$ in a gas phase reaction is believed to help purge the active sites by hydrogenation of the coke formed during the reaction. The latter is considered the main reason for the catalyst deactivation [88]. Hattori and his associates [85] proposed a mechanistic role of Pt in the presence of $H_2$. They suggested that the hydrogen adsorbed

dissociatively on the surface of Pt particles. Subsequently, these hydrogen atoms undergo distribution onto the sulfated zirconia support. Hydrogen atoms, then, migrate to the zirconium sites which are the Lewis acid sites. As a result, an electron will be released from the hydrogen atom and converted to a proton which bonds to the adjacent surface oxygen atoms forming a new Brønsted acid site. The latter can play an important role as active sites for the acid catalyzed reactions. On the other hand, removing of an electron will result in weakened Lewis acid sites, and hence a decrease in coke formation and an increase in the catalytic activity. Figure 1-10 describes a possible mechanism of the $H_2$ distribution on the activation of sulfated zirconia.

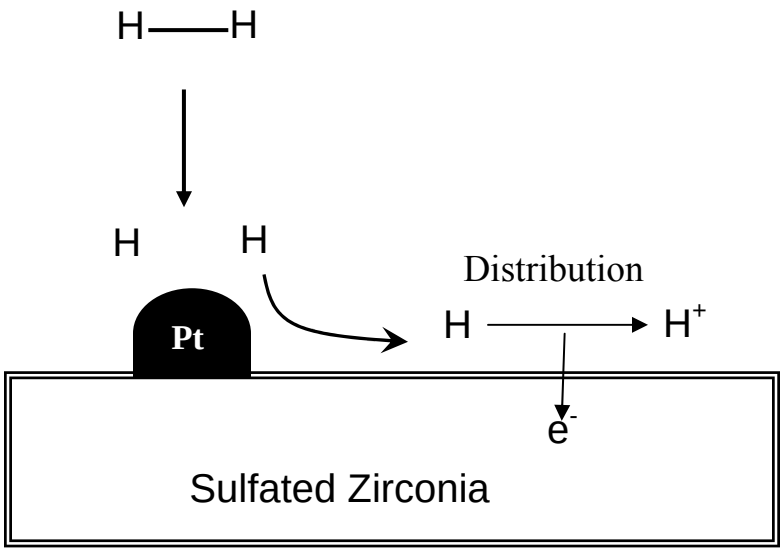


**Figure 1-10: Role of platinum and possible mechanism of $H_2$ distribution over the Pt surface to activate the sulfated zirconia (proposed by Hattori [85])**

Sulfated zirconia has recently been modified to be a more shape-selective catalyst by coating of the oxide with polymers such as polyvinyl alcohol [89,90]. Carbonylation at different calcination temperatures in inert atmosphere helps to create a barrier of carbon molecular sieves (CMS) which coat the zirconium oxide to generate a well defined pore size and distribution.

**CONCLUSIONS AND REMARKS:**

Most of the previous synthetic methods, for zirconia and sulfated zirconia utilize zirconium hydroxide as a starting material and result in formation of a monoclinic crystalline zirconia which is the less active phase compared to tetragonal zirconia. The interaction of a sulfate ion with the tetragonal phase provides highly active sites with higher catalytic activity. Additionally, moderate calcination temperatures are required for the formation of active sites and for the formation of a covalent structure between sulfate ions and tetragonal zirconia phase. High calcination temperatures will lead to the loss of sulfate ions and enhance transformation of the tetragonal phase to monoclinic phase which leads to an acute decrease in the activity. Moreover, the existence of sulfated anions on the surface of zirconia strongly enhances the Lewis acidity via increases on the electron accepting susceptibly of the zirconium cations through the bridging oxygen atoms which join the sulfur and zirconium atoms.

In this work, zirconia and sulfated zirconia will be prepared by synthesizing zirconium carboxylates and sulfonates as single source precursor complexes which undergo transformations to a stable zirconia and/or sulfated zirconia upon thermal calcination with the incorporation of the sulfate ions into the zirconia lattice. The next

two chapters discuss the synthesis and characterization of several zirconium carboxylate and sulfonate precursors. The fourth chapter of the dissertation is reserved for the synthesis and characterization of supported sulfated zirconia over Mobil Crystalline Materials MCM-41. The acidic properties of the prepared sulfated zirconia and the supported sulfated zirconia samples, using several probes such as cyclohexylamine, acetonylacetone, and Hammett base indicators, will be covered during discussions in chapters three and four. The remainder of the work will be dedicated for discussion of some application reactions, such as alkylation and aldol condensation reactions, performed over sulfated zirconia.

**REFERENCES CITED:**


1. R. Srinivasan and B. Davis, *Proceed. Am. Chem. Soc. Symp., Mat. Synth. Charact.* **1997**, 147.
2. X. Song and A. Sayari. *Cat. Rev.-Sci. Eng.*, **1996**, *38(3)*, 329.
3. M. Bocanegra-Bernal and S. Dioz De La Torre, *J. Mater. Sci*. **2002**, *37*, 4947.
4. A. Clearfield and P. Vaughan, *Acta Cryst.* **1956**, *9*, 555.
5. B. Davis, *J. Am. Ceram. Soc*, **1984**, *67(8)*, 168.
6. R. Srinivasan and B. Davis, *Catal. Lett*., **1992**, *14*, 165.
7. A. Clearfield, *Reviews of Pure and Applied Chemistry*, **1964**, *14*, 91.
8. B. Yoldas, *J. Mater. Sci*. **1986**, *21*, 1080.
9. B. Yoldas, *J. Nanocrystalline solids*, **1984**, *63*, 145.
10. M. Hall and R. Nesten, *J. Optical Soc. Am.* **1952**, *42*, 257.
11. L. Navias U.S. Patent 2,515,790, 1950.
12. D. Smith and H. Newkirk, *Acta. Cryst.,* **1965**, *18*, 983.
13. M. Finnis and T. Paxton, *Phys. Rev. Lett.*, **1998**, *81(23)*, 5149.
14. J. McCullough and K. Trueblood, *Acta. Cryst*.,**1959**, *12*, 507.
15. G. Teufer, *Acta. Cryst*., **1962**, *15*, 1187.
16. H. Goldschmidt, *Adv. X-ray Anal.*, **1962**, *5*, 191.
17. G. Wolten, *J. Am. Chem. Soc.* **1963**, *46(9)*, 418.
18. J. Hong, D. De La Torre, L. Gao, K. Miyamoto and H. Miyamoto, *J. Mater. Sci. Lett.*, **1998**, *17*, 1313.
19. R. Garvie, *J. Phys. Chem*., **1965**, *69*, 1238.

20. R. Garvie, *J. Phys. Chem*., **1985**, *82*, 218.

21. Y. Muraje and E. Kato, *J. Am. Ceram. Soc*., **1983**, *66(3)*, 196.

22. P. Morgan, *J. Am. Ceram. Soc*., **1984**, *67*, 204.

23. C. Norman, P. Goulding and I. McAlpine, *Catal. Today*, **1994**, *20*, 313.

24. C. Norman, P. Goulding and P. Moles, *Stud. Surf. Sci. Catal*., **1994**, *90*, 269.

25. B. Davis, R. Keogh and R. Srinivasan, *Catal. Tody*, **1994**, *20*, 219.

26. R. Srinivasan, R. De Angelis and B. Davis, *J. Mater. Res*., **1986**, *1*, 583.

27. R. Srinivasan, M. Harris, S. Simpson, R. De Angelis and B. Davis, *J. Mater. Res*., **1988**, *3*, 787.

28. J. Livage, K. Doi and C. Mazieres, *J. Am. Ceram. Soc*., **1968**, *51(6)*, 349.

29. M. Torralvo, M. Alario and C. Mazieres, *J. Catal*. **1984**, *86*, 473.

30. M. Blesa, A. Maroto, S. Passagio, N. Figliolia and G. Rigotti, *J. Mat. Sci.*, **1985**, *20*, 4601.

31. G. Yadav and J. Nair, *Micro. Meso. Mat.***1999**, *33*, 1.

32. K. Arata and M. Hino, *Hyomen*, **1981**, *19*, 75.

33. R. Gillespie and T. Peel, *Adv. Phys. Org. Chem*., **1972**, *9*,1.

34. A. Corma, *Chem. Rev*., **1995**, *95*, 559.

35. X. Song and A. Sayari, *Chemtech*, **1995**, 27.

36. M. Hino, S. Kobayashi and K. Arata, *J. Am. Chem. Soc*., **1979**, *101*, 6439.

37. K. Tanabe, H. Hattori and T. Yamaguchi, *Crit. Rev. Surt. Chem.*, **1990**, *1*, 1.

38. T. Yamaguchi, K. Tanabe and Y. Kung, *Mater. Chem. Phys*., **1987**, *17*, 249.

39. D. Ward and E. Ko, *J. Catal*., **1994**, *18*, 150.

40. M. Bensitel, O. Saur, J. Lavalley and G. Mabilon, *Mater. Chem. Phys*., **1987**, *17*, 249.

41. S. Baba, Y. Shibata, T. Kawamura, H. Takaoka, T. Kimara, K. Kousaka, Y. Minato, N. Yokoyama, K. Lida and T. Imai, EP. 174836, 1986.

42. B. Aiken, W. Hsu and E. Matijevic, *J. Mater, Sci*, **1990**, *25*, 1886.

43. R. Srinivasan, D. Taulbee and B. Davis, *Catal. Lett*., **1991**, *9*, 1.

44. T. Yamaguchi, T. Jin and K. Tanabe, *J. Phys. Chem.* **1986**, *90*, 3148.

45. C. Morterra, G. Cerrato, F. Pinna, M. Signoretto and G. Strukul, *J. Catal*. **1994**, *149,* 181.

46. A. Clearfield, G. Serrete and A. Khazi-Syed, *Catal. Today*, **1994**, *20*, 295.

47. H. Vesteghrni, T. Jaccon and A. Lecomte, *Rev. Phys. Appl.*, **1989**, *24*, C4.

48. F. Babou, G. Goudurier and J. Vedrine, *J. Catal*. **1995**, *152*, 341.

49. R., White; S., Sikabwej; M., Coelho and D., Resasco, *J. Catal*. **1995**, *157*, 755.

50. K. Arata, *Adv. Catal*. **1990**, *37*, 165.

51. S. Wilson, B. Lok, C. Mesina, T. Cannan and E. Flanigen, *J. Am. Chem. Soc.* **1982**, *104*, 1146.

52. D. Milburn, K. Saito, R. Keogh and B. Davis, *Appl. Catal. A: General*, **2001**, *215*, 191.

53. K. Tanabe, *Solid Acid and Basis, Their Catalytic Properties*, Academic Press: New York, 1973.

54. L. Forni, *Catal. Rev.* **1973**, *8*, 65.

55. J. Vedrine, A. Bolis, P. Dejaife, C. Naccache, P. Swiezzchowski, E. Derovane, J. Nagy, J. Gilson and J. van Hoff, *J. Catal.* **1988**, *36*, 323.

56. V. Dondur and H. Karge, *Surf. Sci.* **1987**, *189*, 873.

57. L. Kustov, V. Kazansky, F. Figueras and D. Tichit, *J. Catal.* **1994**, *150*, 341.

58. K. Tanabe, M. Misono, Y. Ono and H. Hattori, *New Solid Acids and Bases, Their Catalytic Prooeries, Stud. Surf. Sci. Catal.*, (51), Elsevier: Tokyo 1989, pp 5-25.

59. H. Knozinger, H. Kriltenbrink and P. Ratnasamy, *J. Catal*. **1977**, *48*, 436.

60. F. Van Cauwelaert and W. Keith, *Trans. Faraday Soc.*, **1970**, *66*, 454.

61. H. Karge and J. Schweckendied, In Proceeding of the Fifth International Symposium on Heterogeneous Catalysis. Varna, Bulgaria, Publishing House of the Bulgaria Acad Sci: 1983, p 429.

62. A. Corma, V. Fornes, M. Juan-Rajadell and J. Lopez Nieto, *Appl. Catal. A: General*, **1994**, *116*, 151.

63. A. Corma, A. Martinez and C. Martinez*, J. Catal.*, **1994**, *149*, 52.

64. K. Ebitani, J. Kobishi, A. Horie, H. Hattori and K. Tanabe, Acid-Base Catalysis, Kodansha, Tokyo: 1989.

65. C. Lin and C. Hsu, *J. Chem. Soc. Chem. Commun.*, **1992**, 1479.

66. C. Morterra, G. Cerrato, F. Pinna and M. Signorretto, *J. Catal*. **1995**, *157*, 109.

67. C. Morterra, G. Cerrato and V. Bolis, *Catal. Today*. **1993**, *17*, 505.

68. V. Adeeva, W. de Haan, J. Janchen, G. Lei, V. Schunemann, L. van de Ven, W. Schtler and R. van Santen. *J. Catal.* **1995**, *151*, 364.

69. F. Babou, B. Bigot and P. Sautet, *J. Phys. Chem*. **1993**, *97*, 11501.

70. C. Guo, S. Yao; J. Cao and Z. Qian, *Appl. Catal. A* **1994**, *107*, 229.

71. M. Hino and K. Arata, *J. Chem. Soc., Chem. Commun.*, **1980**, 851.

72. X. Song and A. Sayari, *Catal. Rev.-Sci. Eng.* **1996**, *38(3)*, 329.

73. M. Deeba and W. Hall, *J. Catal*. **1979**, *60*, 417.

74. G. Olah, G. Prakash and J. Sommer, *Superacids*, Wiley and Sons: New York, 1985, pp 4-29.

75. H. G. Karge; *Stud. Surf. Sci, Catal.* **1991**, *65*, 133.

76. M. Hino and K. Arata, *J. Chem. Soc. Chem. Commun*. **1980**, *18*, 851.

77. F. Babou, B. Bigto, G. Coudurier, P. Sautet and J. Vedrine, *Stud. Surf. Sci. Catal.*, **1994**, *90*, 519.

78. B. Umansky, J. Engelhardt and W. Hall, *J. Catal.* **1991**, *127*, 128.

79. K. Shibata, T. Kiyoura, J. Kitagawa, T. Sumiyoshi and K. Tanabe, *Bull. Chem. Soc. Jpn.* **1973**, *46*, 2985.

80. T. Yamaguchi, K. Tanabe and Y Kung, *Mater. Chem. Phys.* **1986**, *16*, 67.

81. M. Wen, I. Wender, and J. Tierney, *Energy Fuels,* **1990**, *4*, 372.

82. T. Okuhara, T. Nishimura, H. Watanabe and M. Misono, *J. Mol. Catal.*, **1992**, *74*, 247.

83. Y. Hao and K. Arata, *J. Chem. Soc. Chem. Commun*., **1995**, 789.

84. M. Hino and K. Arata, *J. Chem. Soc. Chem. Commun*., **1995**, 789.

85. H. Hattori, *Stud. Surf. Sci. Catal*. **1993**, *77*, 69.

86. K. Ebitani, T. Tanaka and H. Hattori, *Appl. Catal. A*, **1993**, *102(2)*, 78.

87. K. Ebitani, H. Konno, T. Tanaka and H. Hattori, *J. Catal*., **1992**, *35 (1)*, 60.

88. T. Hosoi, S. Kitada, T. Shimizu, T. Imai and S. Nojima, *Shokubai,* **1990**, *32(2)*, 117.

89. G. Yadav, J. Nair and V. Narendra, US Pat. Appl. 09/211 500, 1998.

90. G. Yadav, and J. Nair, *Langmuir*, **1999**, *16(9)*, 4072.

# CHAPTER 2

## SYNTHESIS OF ZIRCONIA POWDERS DERIVED FROM SINGLE SOURCE ZIRCONIUM CARBOXYLATE PRECURSORS

### INTRODUCTION:

Zirconia has numerous applications as a refractory ceramic material. High performance tetragonal zirconia polycrystalline oxide is one useful form, but it must be prepared with a high density, homogenous structure, and small grain size [1,2]. Synthesis of such materials depends on the zirconium starting precursor. A fine powder with little tendency toward agglomeration is required since the agglomeration forms during the precipitation and calcination steps. Generally, high purity oxides can be synthesized directly from the corresponding metal hydroxide precipitates by thermal treatment. Most interest in recent years had focused on the synthesis and development of a stable, low temperature zirconia with the use of different precursors [3]. In the work reported herein, a variety of zirconium carboxylate complexes were utilized as precursors for the synthesis of zirconium oxide. Zirconium carboxylates can be prepared easily by the reaction of sodium carboxylate with an aqueous solution of a zirconium salt [4]. Zirconium cations in the aqueous solution coordinate to the carboxylate anions. In the aqueous solution of zirconium oxychloride, for instance, the carboxylate groups displace

the water molecules in the tetrameric cation $[Zr_4(OH)_8]^{8+}$ to form monocarboxylato zirconium species. As more carboxylate ligands coordinate to zirconium, more water molecules will be displaced from the zirconium complex. The bond formed between the carboxylate ligands and the zirconium atom should be stronger and more stable than the zirconium-water bond. The number of the carboxylate ligands that coordinate to the zirconium atom depends on the stability of the carboxylate ligand bonds. Furthermore, heating the zirconium aqueous solution will tend to weaken the bonds between zirconium and carboxylate and strengthen the zirconium-water and zirconium hydroxyl bonds. Reaction of zirconium halogenides, such as zirconium oxychloride in nonaqueous system, will involve a kind of competition between the halogen atoms and the carboxylate anions for bonding with zirconium atoms. Additionally, with an increase of the carboxylate chain length, the hydrophilic nature of the zirconium carboxylate complex will be reduced. Therefore, zirconium carboxylate complexes usually do not dissolve in water but are soluble in nonpolar solvents. Additionally, zirconium carboxylates can also be prepared by the reaction of zirconium alkoxide with a carboxylic acid [5,6]. Alkoxide groups can be displaced completely by carboxylic acid ligands when heated in a nonpolar solvent. This method formed a polymerized zirconium carboxylate with high molecular weight [6]. Zirconium metal possibly coordinates to the carboxylate ligands in four different modes, that are as a free ion, a monodentate ligand, bidentate bridging ligand, and a bidentate chelating ligand as shown in Figure 2-1 [7].

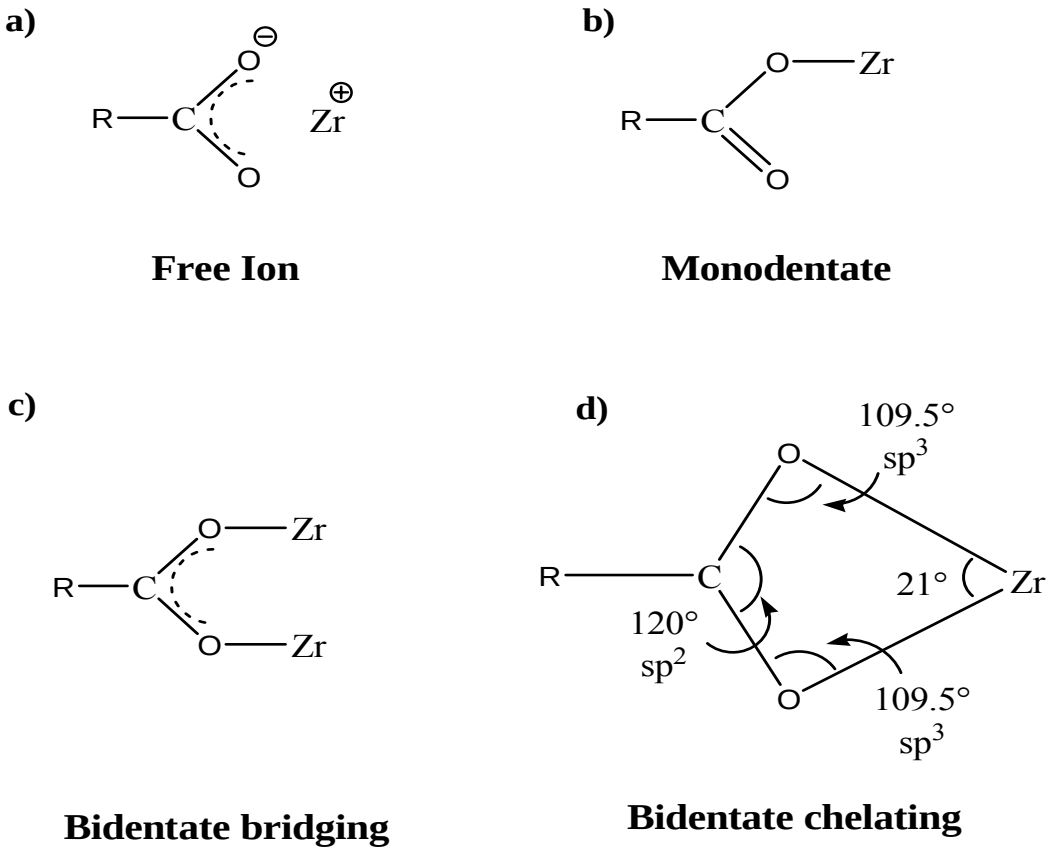


**Figure 2-1: Types of coordination of carboxylates ligands with the zirconium metal [7].**

In the monodentate coordination, the hydrogen of the carboxylic acid is replaced by a zirconium ion which eventually influences the stretching frequency of the carbonyl group in the acid. When replacing the O=C-O-H with O=C-O-Zr, the stretching frequency of the carbonyl will decrease due to an increase of the reduced mass since the vibrational frequency is inversely proportional to the mass. The carboxylate also can coordinate in a bidentate fashion in two different ways. These are bidentate bridging in which each oxygen atom of the carboxylic acid coordinates to a different zirconium atom

and bidentate chelating in which both oxygen atoms of the carboxylate ions coordinate to the same zirconium metal ion. Bidentate bridging is assumed to result in less strain than the bidentate chelating configuration. The oxygen atoms of the carboxylate ligands have $sp^3$ hybridization with an angle of 109.5° while the carbon atom has $sp^2$ hybridization with angle of 120°. Therefore, since the four bonds (two Zr-O, and two C-O) lay in the same plane to form a chelated structure and the summation of the three angles is 339°, the chelated O-Zr-O angle is left with only 21° (Figure 2-1d). This angle is too small compared to that of the eight-fold coordination Zr-atom angle which is 72° [8]. As a result, the other three bonds will be reduced leading to steric strain in the structure.

Chelating carboxylates can also influence the properties of the resulted zirconium complexes. α-Hydroxyl carboxylic acids, for example, form a chelate ring with zirconium, followed by ionization of the hydroxyl hydrogen. The structure of the chelated carboxylate is shown below as structures (I) and (II):

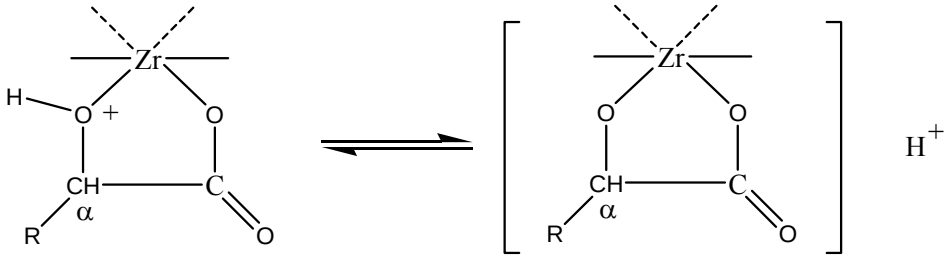


( I ) ( II )

The most available zirconium carboxylate complexes discussed extensively in the literature and utilized as a precursor for the synthesis of zirconium oxide are the zirconium acetates [9-15]. Zirconium tetraacetate was prepared by the reaction of zirconium tetrachloride with an excess of acetic acid at 80 °C [9]. Refluxing the mixture to the boiling point, resulted in formation of zirconium oxyacetate [9,10]. Zirconium oxyacetate was also prepared by refluxing of a small amount of zirconium oxychloride

with acetic acid to give a product characterized as $Zr_4O_3(CH_3COO)_{10}\cdot 3H_2O$ [11]. Recently, Gong et al. [16] reported a novel zirconium oxy-hydroxy acetate complex synthesized from zirconium oxychloride and acetic acid solution followed by precipitation with concentrated ammonium hydroxide at pH ≈ 6. The product was determined to have a formula of $Zr_4O_3(OH)_7(CH_3COO)_3\cdot 5H_2O$ and it produced a tetragonal zirconium oxide phase with a crystallite size of 30 nm when pyrolyzed at 545 °C.

Little research work has been done to investigate the preparation of zirconium oxide from the pyrolysis of zirconium carboxylate complexes and the effect on the zirconium complex precursors on the oxide properties such as the surface area, particle size, and the crystalline phase that is formed. In this chapter, zirconium carboxylate complexes were prepared and utilized as single precursors for the synthesis of zirconia powder upon thermal calcination. The temperature of the thermal composition, as well as the properties of the final oxide, showed a strong dependence on the type of carboxylate ligands used.

## EXPERIMENTAL:

### Chemicals:

All the chemicals were purchased and used without further purification. The chemicals used in this section were as follows: Aqueous ammonium hydroxide [$NH_4OH$ ACS reagent, Scientific Products]; zirconium oxychloride [$ZrOCl_2.8H_2O$, Alfa Aesar]; sodium bicarbonate [$NaHCO_3$, Alfa Aesar]; 2-ethylhexanoic acid [$C_8H_{16}O_2$, MCB], benzilic acid [$C_{14}H_{12}O_3$, Fluka]; α-hydroxyisobutyric acid [$C_4H_8O_3$, Fluka]; propanoic

acid [$C_3H_6O_2$, Aldrich]; sodium butyrate [$C_4H_7O_2Na$, Aldrich]; isobutyric acid [$C_4H_8O_2$, Aldrich]; pivalic acid [$C_5H_{10}O_2$, Aldrich]; mandelic acid [$C_8H_8O_3$, Aldrich]; and hydroxy pivalic [$C_5H_{10}O_3$, Aldrich].

**Preparation of the zirconium carboxylate precursor:**

Figure 2-2 shows the chemical structure of all carboxylic acids used for the preparation of the zirconium carboxylate complexes.

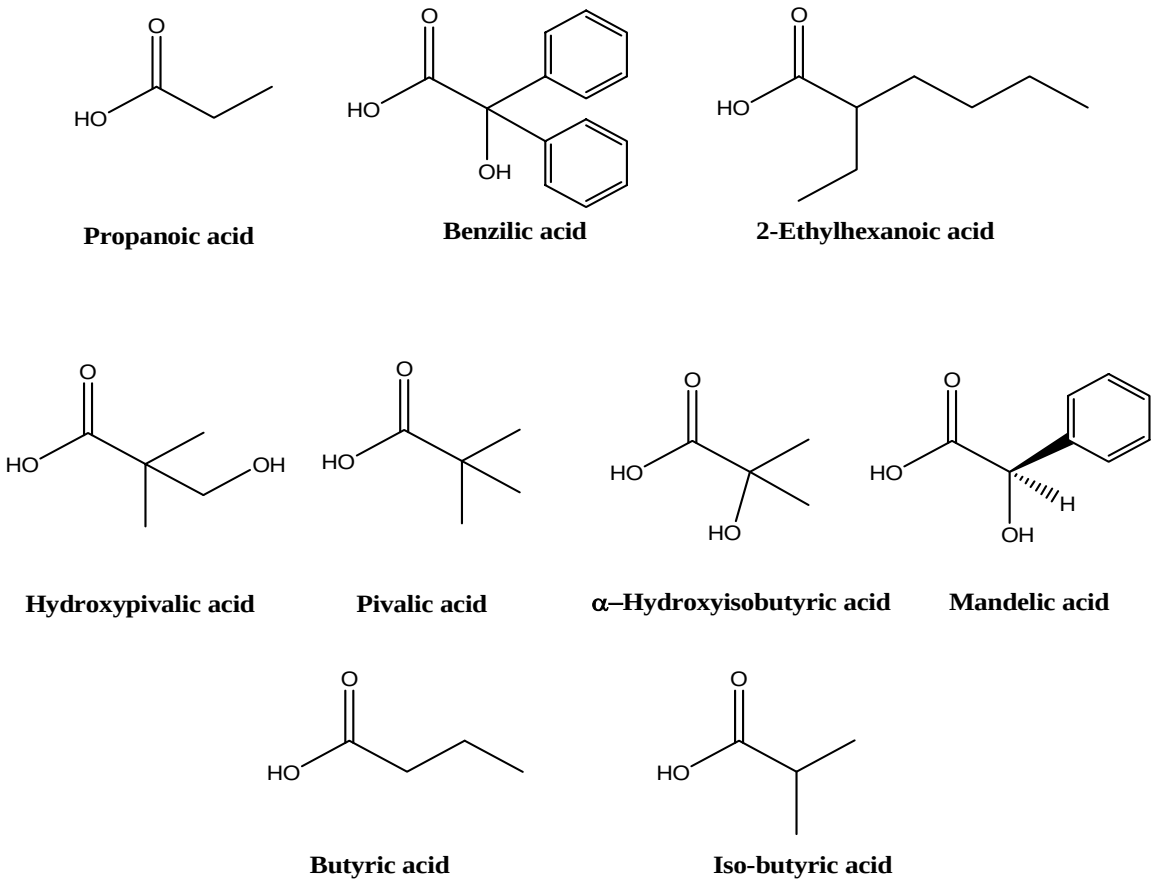


**Figure 2-2: The structure of the carboxylic acids used for the preparation of the single precursor zirconium carboxylates.**

The zirconium carboxylate precursors were synthesized simply by the reaction of the zirconium oxychloride salt with carboxylic acids or their salts.

**Reaction of $ZrOCl_2 \cdot 8H_2O$ with glacial propanoic acid:**

**$Zr_4O_2(OH)_5(OAp)_5Cl_2].8H_2O$ (Zr-1):**

A sample of 20 g (60 mmol) of zirconium oxychloride octahydrate was added to 200 ml of concentrated propanoic acid in a 500-ml, round-bottomed flask and refluxed for three days. A light golden yellow solution was created. The solution was cooled to room temperature. The resulting light yellow solid was filtered, washed with de-ionized water, and dried under vacuum for 24 hours. The reaction yielded 15.8 g of product. The solution, on the other hand, was placed in a 200-ml flask which was then left in a fume hood for crystallization and evaporation of excess acid to about 50 ml. White thin crystals formed from the solution. About 1.4 g of the crystals were collected from the latter solution. Both samples showed very similar IR absorptions. IR ($cm^{-1}$) (KBr): 3653(m, sh), 3310(s, br), 2981(s), 2944(s), 2886(m), 1562(s), 1470(s), 1440(s), 1376(m), 1303(s), 1241(w), 1084(m), 1015(w), 811(w), 665(m), 553(w), 474(m).

**Reaction of $ZrOCl_2 \cdot 8H_2O$ with the sodium propionate: $[Zr_4O_4(OH)_3(OAp)_5] \cdot 7H_2O$ (Zr-2):**

A sample of 3 g (80 mmol) of propanoic acid was diluted with 100 ml of de-ionized water in a 200-ml beaker. A sample of 3.4 g (80 mmol) of sodium bicarbonate was added gradually to the solution resulting in $CO_2$ evolution and yielding a colorless solution. An amount of 6.44 g (40 mmol) of zirconium oxychloride was dissolved in 50

ml of de-ionized water in a 250 ml beaker and added gradually to the propanoic acid solution, a white colored precipitate was observed. The precipitate was filtered and washed with enough distilled water to remove all the residual unreacted starting materials and sodium salts and was then dried under vacuum for 12 hours. The reaction yielded 4.89 g (95.6% based on $ZrOCl_2 \cdot 8H_2O$). IR($cm^{-1}$)(KBr): 3632(m, sh), 3340(s, br), 2978(s), 2941(s), 2882(m), 1560(s), 1471(s), 1439(s, sh), 1376(m), 1301(m, sh), 1239(w), 1080(m), 812(w), 651(w).

**Reaction of $ZrOCl_2 \cdot 8H_2O$ with the sodium butyrate:**

**$[Zr_4O_4(OH)_2(BUT)_6] \cdot 2H_2O$ (Zr-3):**

A sample of 11.22 g (100 mmol) of sodium butyrate (98%) was dissolved in 100 ml of de-ionized water in a 200 ml beaker. A sample of 16.1g (50 mmol) of zirconium oxychloride was dissolved in a 50 ml of de-ionized water in 250 ml beaker and added gradually to the butyrate solution. A white colored precipitate was observed. The precipitate was filtered and washed with enough distilled water to remove all the residual unreacted starting materials and sodium salts. Finally it was dried under vacuum for 12 hours. The reaction yielded 12.3 g (94% based on $ZrOCl_2.8H_2O$). IR($cm^{-1}$)(KBr): 3648(m), 3494(m), 3396(m), 3334(m), 2963(m), 2935(m), (2874(m), 1600(s), 1533(m), 1466(m), 1376(m), 1315(m), 1293(m), 1211(w), 1100(m), 668(m, br).

**Reaction of $ZrOCl_2 \cdot 8H_2O$ with the sodium isobutyrate:**

**$[Zr_4O_4(OH)_2(ISBUT)_6] \cdot 8H_2O$ (Zr-4):**

A sample of 16.7 g (190 mmol) of isobutyric acid was diluted with 100 ml of de-ionized water in a 200-ml beaker. The acid was neutralized with 16 g (190 mmol) of sodium bicarbonate to yield a colorless solution. A solution of 31 g (95 mmol) of zirconium oxychloride in 100 ml of de-ionized water was added gradually to the isobutyrate acid solution. The resulting white precipitate was filtered and washed with enough distilled water to remove all the residual unreacted starting materials and sodium salts. Finally it was dried under vacuum for 12 hours. The reaction yielded 35.6 g (100% based on $ZrOCl_2 \cdot 8H_2O$). IR($cm^{-1}$)(KBr): 3639(m, sh), 3396(s, br), 2971(s), 2930(s), 2873(m), 1716(w), 1585(s), 1487(s), 1444(s), 1361(m), 1300(m). 1170(w), 1097(w), 931(w), 666(w, br).

**Reaction of $ZrOCl_2 \cdot 8H_2O$ with ammonium pivalate: $[Zr_4O_{4.5}(PA)_7] \cdot 5H_2O$ (Zr-5):**

A sample of 6.0 g (19 mmol) of zirconium oxychloride octahydrate was dissolved in 30 ml of de-ionized water in a 250 ml beaker. Next, 4.8 g (40 mmol) of ammonium pivalate was dissolved in 100 ml of de-ionized water, and this solution was added slowly to the zirconium solution causing the formation of a white precipitate. The precipitate was filtered, washed carefully with de-ionized water to remove all the residual ammonium salts and dried under vacuum for 12 hours. The reaction yielded 6.8 g (99.2% based on $ZrOCl_2 \cdot 8H_2O$). IR($cm^{-1}$)(KBr): 3666(s, sh), 3383 (m, br), 2964(s), 2931(s), 2871(s), 1551(s), 1488(s, sh), 1431(s), 1380(s), 1364(s), 1231(s), 1030(w), 937(w), 906(m), 878(w), 814(w), 787(m, br), 606(m).

**Reaction of $ZrOCl_2 \cdot 8H_2O$ with the sodium hydroxypivalate:**

**$[Zr_4O_5(HPA)_6] \cdot 8H_2O$ (Zr-6):**

A sample of 11.8 g (100 mmol) of hydroxypivalic acid was diluted with 100 ml of de-ionized water in a 200 ml beaker. Then 8.4g (100 mmol) of sodium bicarbonate was added gradually to the solution. Carbon dioxide was released upon addition of sodium bicarbonate, and a colorless solution was formed. An amount of 16.1 g (50.0 mmol) of zirconium oxychloride was dissolved in 50 ml of de-ionized water in 250-ml beaker and added gradually to the hydroxypivalate solution. A white color precipitate formed. The precipitate was filtered and washed with a large amount of de-ionized water to remove all the residual unreacted starting materials and sodium salts. Finally, it was dried under vacuum for 12 hours. The reaction yielded 13.3 g (64.4% based on $ZrOCl_2 \cdot 8H_2O$). IR($cm^{-1}$)(KBr): 3349(s, br), 3070(m), 2968(s), 2931(s), 2874(m), 1556(s), 1480(s, sh), 1431(s, sh), 1361(m), 1272(m), 1191(w), 1046(m), 987(w), 904(w), 783(w), 659(w), 600(w), 498(w).

**Reaction of $ZrOCl_2 \cdot 8H_2O$ with the ammonium 2-ethylhexanoate:**

**$[Zr_4O_6(OH)_2(EHA)_2] \cdot 7H_2O$ (Zr-7):**

A sample of 8.1 g (50 mmol) of ammonium 2-ethylhexanoate was diluted with 50 ml of de-ionized water in a 200-ml beaker. A sample of 8.00 g (25 mmol) of zirconium oxychloride was dissolved in 30 ml of de-ionized water in 250-ml beaker. The zirconium salt solution was added gradually to the 2-ethylhexanoic acid solution, and a white colored precipitate was observed immediately. The precipitate was filtered and washed with enough amount of distilled water to remove all the residual unreacted starting

materials and ammonium hydroxide. Finally, the precipitate was dried under vacuum for 12 hours. The reaction yielded 4.8 g (74% based on $ZrOCl_2 \cdot 8H_2O$). IR($cm^{-1}$)(KBr): 3663(m), 3411(m, br), 2958(s), 2934(m), 2873(m), 1539(s), 1424(s), 1375(m), 1322(m), 1233(w), 1104(w), 950(w), 727(w, br).

**Reaction of $ZrOCl_2 \cdot 8H_2O$ with α-Hydroxy isobutyric acid**

**$[Zr_4(OH)_4(HIBUTA)_{12}] \cdot 6H_2O$ (Zr-8):**

A sample of 5.2 g (50mmol) of α-hydroxyisobutyric acid was added to 50 ml of de-ionized water in a 200-ml beaker. A sample of 8.1 g (25 mmol) of zirconium oxychloride was dissolved in 30 ml of de-ionized water in 250-ml beaker. The latter solution was added gradually to the previous solution with continuous refluxing for 4 hours. The precipitate was filtered and washed with a large amount of distilled water to remove all the residual unreacted starting materials. Finally it was dried under vacuum for 12 hours and collected. The reaction yielded 4.83 g (56% based on $ZrOCl_2 \cdot 8H_2O$). IR($cm^{-1}$)(KBr): 3325(m, br), 2983(m), 2941(m), 2884(m), 2700-2100(m, br), 1714(m, sh), 1615(s), 1555(m), 1477(m), 1431(m), 1388(s, sh), 1363(s, sh), 1267(s), 1192(m), 1167(s), 964(m, sh), 938(w), 907(m, sh), 822(w, sh), 778(w), 632(w, sh), 583(w, sh), 509(w), 436(vw).

**Reaction of $ZrOCl_2 \cdot 8H_2O$ with the sodium α-hydroxyisobutyrat**

**$[Zr_4O(OH)_4(HIBUTA)_{10}] \cdot 28H_2O$ (Zr-9):**

A sample of 5.2 g (50 mmol) of α-hydroxyisobutyric acid was added to 50 ml of de-ionized water in a 200-ml beaker. A sample of 4.2 g (50 mmol) of sodium

bicarbonate was added gradually to the solution. Carbon dioxide was released upon addition of sodium bicarbonate, and a colorless solution was formed. A sample of 8.1 g (25 mmol) of zirconium oxychloride was dissolved in 30 ml of de-ionized water in 250 ml beaker. The latter solution was added gradually to the previous solution, and a white precipitate was formed. The precipitate was filtered and washed with enough distilled water to remove all the residual unreacted starting materials. Finally it was dried under vacuum for 12 hours and collected. The reaction yielded 6.35 g (78% based on $ZrOCl_2.8H_2O$). IR($cm^{-1}$)(KBr): 3395(s, br), 2981(m), 2935(m), 2940-2200(m, br), 1551(s, br), 1475(s), 1427(m), 1377(m), 1359(m), 1332(m), 1198(w, br), 1038(w), 1003(m), 973(m), 934(w), 909(w), 835(m), 824(m), 780(w), 655(m), 634(m), 534(w), 464(w).

**Reaction of $ZrOCl_2 \cdot 8H_2O$ with mandelic acid $[Zr_4O(OH)_5(MA)_9] \cdot 4H_2O$ (Zr-10):**

A sample of 15.2 g (100 mmol) of mandelic acid was dissolved in 100 ml of de-ionized water in a 250-ml round-bottomed flask with heating at the boiling temperature. An amount of 16.1 g (50 mmol) of zirconium oxychloride was dissolved in 50 ml of de-ionized water in a 250 ml beaker. The latter solution was gradually added to the previous solution with continuous refluxing for 4 hours. The precipitate was filtered and washed with enough distilled water to remove all the residual unreacted starting materials. Finally, it was dried under vacuum for 12 hours and collected. The reaction yielded 18.9 g (72% based on $ZrOCl_2 \cdot 8H_2O$). IR($cm^{-1}$)(KBr): 3366(s, br), 3062(m), 3033(m), 2981(m,br), 2571(m, br), 1957(vw), 1894(vw), 1805(vw), 1625(s, br), 1496(m, sh), 1450(m, sh), 1374(m), 1342(m), 1280(m, sh), 1190(m, sh), 1158(vw), 1082(w), 1053(m),

1026(m), 1003(m), 962(m), 920(w), 789(w), 756(w), 695(m), 674(w), 620(m), 611(m), 534(m), 498(w).

**Reaction of $ZrOCl_2 \cdot 8H_2O$ with the sodium mandelate: $[Zr_4(OH)_8(MA)_8] \cdot 8H_2O$ (Zr-11):**

A sample of 15.2 g (100 mmol) of mandelic acid was dissolved in 100 ml of de-ionized water in a 200-ml beaker. About 8.6 g (100 mmol) of sodium bicarbonate was added gradually to the solution. Carbon dioxide was released upon addition of sodium bicarbonate, a colorless solution was formed. A sample of 16.1 g (50 mmol) of zirconium oxychloride was dissolved in 50 ml of de-ionized water in 250 ml beaker. The latter solution was added gradually to the previous solution, and a white precipitate was formed. The precipitate was filtered and washed with enough distilled water to remove all the residual unreacted starting materials. Finally, it was dried under vacuum for 12 hours and collected. The reaction yielded 18.4 g (78% based on $ZrOCl_2 \cdot 8H_2O$). IR($cm^{-1}$)(KBr): 3366(s, br), 1717(m), 1637(m), 1598(m), 1448(m), 1362(m), 1321(m), 1221(w), 1181(w), 982(w), 865(w), 677(w, br).

**Reaction of $ZrOCl_2 \cdot 8H_2O$ with benzilic acid $[Zr_4O(OH)_6(BA)_8] \cdot 4H_2O$ (Zr-12):**

A sample of 18.44 g (80 mmol) of benzilic acid was added to 100 ml of de-ionized water in a 250-ml round bottomed flask with heating at the boiling temperature. Then 12.88 g (40 mmol) of zirconium oxychloride was dissolved in 50 ml of de-ionized water in 250-ml beaker. The latter solution was gradually added to the previous solution with continuous refluxing for 4 hours. The precipitate was filtered and washed with

enough distilled water to remove all the residual unreacted starting materials. Finally, it was dried under vacuum for 12 hours and collected. The sample was washed benzilic acid reflection peaks disappeared in the X-ray powder diffraction pattern of the solid. The reaction yielded 21.8 g (88.6% based on $ZrOCl_2 \cdot 8H_2O$). IR($cm^{-1}$)(KBr): 3535(w), 3398 (w), 3052(m, sh), 2999-2000 (m, br), 1952(w), 1880(w), 1809(w), 1752(w), 1653(m), 1597(m), 1491(m), 1445(m), 1325(w), 1307(m), 1276(s, sh), 1208(m), 1188(w), 1173(m), 1089(m), 1063(m), 1031(m), 1014(m), 933(m), 783(m), 763(m), 700(s), 620(w), 601(w), 551(w), 488(w), 425(w).

**Reaction of $ZrOCl_2 \cdot 8H_2O$ with the sodium benzilate: $[Zr_4(OH)_{7.5}(BA)_{8.5}] \cdot 14H_2O$ (Zr-13):**

A sample of 18.44 g (80 mmol) of benzilic acid was added to 100 ml of de-ionized water in a 500-ml beaker. A sample of 6.72 g (80mmol) of sodium bicarbonate was added gradually to the solution. Next, a sample of 12.88 g (40 mmol) of zirconium oxychloride was dissolved in 50 ml of de-ionized water in 250 ml beaker. The latter solution was added gradually to the previous solution, and a white precipitate was observed. The precipitate was filtered and washed three times with distilled water by stirring the sample in 600 ml of water for 1 hour each time in order to remove all the residual unreacted starting materials and sodium chloride. Finally it was dried under vacuum for 12 hours. The reaction yielded 23.5 g (86% based on the $ZrOCl_2 \cdot 8H_2O$). IR($cm^{-1}$)(KBr): 3544(s, br), 3059 (m), 3034 (m), 2930(m), 1957(w), 1888(w), 1813(w), 1664(s), 1598(m), 1492(m), 1447(m), 1313(m, br), 1213(m), 1174(m), 1093(w),

1060(m), 1031(w), 1003(w), 986(w), 942(w), 914(w), 818(w), 757(m), 700(m), 677(w), 604(w), 489(w).

**Characterizations:**

The precursors and zirconium powders were characterized using several techniques. The specific surface area was obtained via a conventional Brunauer-Emmett-Teller (BET) multilayer nitrogen adsorption method using a Quantachrome Nova 1200 instrument. Thermogravimetric analyses were performed using a Seiko EXSTAR 6000 TG/DTA 6200 instrument. Scanning Electron Micrographs where obtained using a JEOL JXM 6400 SEM. Infrared spectra in the 4000-400 $cm^{-1}$ region were collected by diffuse reflectance of a ground powder diluted with potassium bromide on a Nicolet Magna-IR 750 spectrometer. The Carbon Hydrogen elemental analysis was performed by Desert Analytics. X-Ray powder diffraction patterns were obtained on a Bruker AXS D8 advance diffractomer using copper $K_\alpha$ radiation with a wavelength of 1.5418 Å. All the XRD patterns where collected at ambient temperature, and the phases were identified using the ICDD database (ICDD# 42-1164 and #37-1484). The mean crystallite sizes of the oxide samples were estimated by X-ray diffraction using a line broadening method and Scherer's equation, $C = \lambda k/\beta COS\ (2\theta)$, where $\lambda$ is the radiation wave length, k is a constant dependant on the crystallite shape, $\theta$ is the angle of the maximum intensity peak, and $\beta$ is equal to the square-root of the $\beta_t^2 - \beta_o^2$ value where $\beta_t$ and $\beta_o$ are the angular peak width measured at half of the maximum intensity line for the measured and reference compounds, respectively. The peaks were profiled with a Pearson 7 model using Topas P version 1.01 software (Bruker Analytical X-ray systems, Madison,WI,

USA, 1998). The profiles of the standard and the sample were input into the Win-Crysize version 3.05 programs (Bruker Analytical X-ray systems, Madison, WI, USA, 1997), which uses the Scherer's evaluation method to determine crystallite size and strain broadening effects [17].

The volume fraction of the tetragonal ($t$-$ZrO_2$) and monoclinic ($m$-$ZrO_2$) phases and the relative ratio of tetragonal zirconia to monoclinic zirconia were determined in a manner akin to that descried by Toraya [18]. The integrated intensity ratio (X) was calculated by using the area values of the tetragonal characteristic peak at $2\theta = 30^{\circ}$ for the (111) reflection and that of the two monoclinic characteristic peaks of the peaks at $2\theta = 28^{\circ}$ and $2\theta = 31^{\circ}$ for the $(11\bar{1})$ and (111) reflections respectively, as shown below:

$$X_{monoclinic} = \left[ \frac{\text{(A) Monoclinic (111) + (A) Monolinic } (11\bar{1})}{\text{(A) Tetragonal (111) + (A) Monoclinic (111) + (A) Monolinic } (11\bar{1})} \right]$$

$$X_{tetragonal} = \left[ \frac{\text{(A) Tetragonal (111)}}{\text{(A) Tetragonal (111) + (A) Monoclinic (111) + (A) Monolinic } (11\bar{1})} \right]$$

The volume fraction ($V$) was then calculated using the integrated intensity values taking into account the deviation from linearity between the volume fraction and the intensity ratio using the following correction equation [18]:

$$V_{monoclinic} = \frac{1.311\, X_{monoclinic}}{1+0.311\, X_{monoclinic}} \qquad V_{tetragonal} = 1 - V_{monoclinic}$$

The chloride content was determined using a conventional gravimetric analysis [19]. A sample of approximately 0.20 g of the desired sample was dissolved in 150 ml of de-ionized water in a 400-ml beaker followed by addition of 0.5 ml of concentrated nitric acid. A silver nitrate solution (0.1 M) was added dropwise to the resulting solution with continuous stirring until no more white precipitate of silver chloride was formed. The solution was then heated near its boiling point for 10 minutes. The precipitate agglomerated in the bottom of the beaker. Another 3-4 drops of silver nitrate solution was added to confirm that there was no chloride ions left in the solution. Finally, the supernatant solution was left to stand for one hour in the dark, followed by filtration and drying at 130 °C for 3 hours. The percentage of chlorine in the original sample was calculated from the amount of the silver chloride isolated.

## RESULTS AND DISCUSSION:

The zirconium carboxylate precursors were prepared from the reaction of zirconium oxychloride with different sodium or ammonium carboxylic acid salts. Zirconium carboxylate precursors prepared by this method were precipitated with a good yield. The properties of the precursors and the corresponding oxides are strongly dependent on the nature of the carboxylate ligands.

### Zirconium carboxylate precursors:

The stoichiometry and formula weight of the complexes were determined directly from the TGA curves, assuming that the calcined residue was pure zirconium oxide. The thermogravimetric analysis (TGA) of several of the zirconium carboxylate complexes are

shown in Figure 2-3 and Figure 2-4. Generally, all samples showed a loss of weight starting from room temperature to about 450-500 °C. However, slight differences were observed in the TGA in the ranges between 25 °C-100 °C, 100 °C-200 °C, 200 °C-350 °C, and 350 °C-500 °C. The first range of weight loss from room temperature to 100 °C was due to the evaporation of the water molecules. In the second thermal range from 100 °C to 200 °C, loosely bonded organic species, hydroxide ions, and carboxylate moieties may be thermally decomposed. The third range between 200 °C - 350 °C corresponds mainly to decomposition of carboxylate groups and is the major weight loss step. A slow thermal decomposition curve was observed above 350 °C and 500 °C due to the loss of the remaining portion of the carboxylate and carbonate species on the surface to give zirconium oxide, carbon dioxide, and water. The weight loss strongly depends on the nature of the carboxylate ligand coordinated to the zirconium in the precursor. Furthermore, the TGA results illustrate that the total weight loss of the zirconium α-hydroxylcarboxylate complexes (17 wt%-24 wt %) was lower than that, along with the high molecular weight, of the aliphatic zirconium carboxylates (38 wt%-47 wt %). The reason behind that is the strong tendency of the α-hydroxylcarboxylate to coordinate to zirconium metal via forming a stable, chelating, five member ring that can be seen clearly from the stoichiometric results demonstrated in Table 2-1. The proposed formulas for the resulted zirconium carboxylate complexes was estimated from the TGA results and the C,H elemental analysis results (Table 2-2). We found that the experimental C,H elemental analysis we obtained fit the theoretical values for the proposed structures within a ± 5% variation. The temperature required for complete conversion to zirconia and the ceramic yield were strongly dependant on the identity of the carboxylate ion.

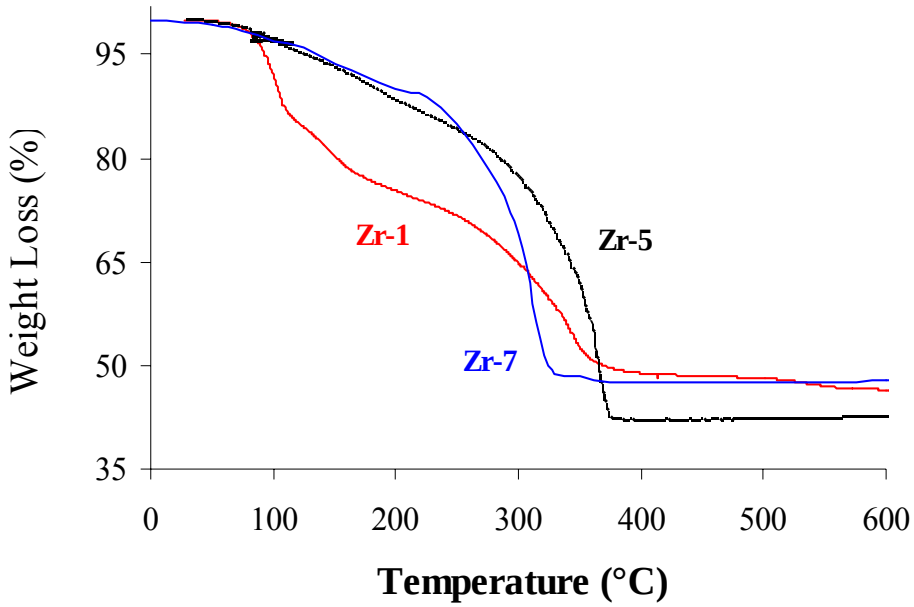


**Figure 2-3: The thermogravimetric analysis (TGA) data for the prepared zirconium carboxylates: (Zr-1: propionate; Zr-5: pivalate; and Zr-7: 2-ethyl hexanoate).**

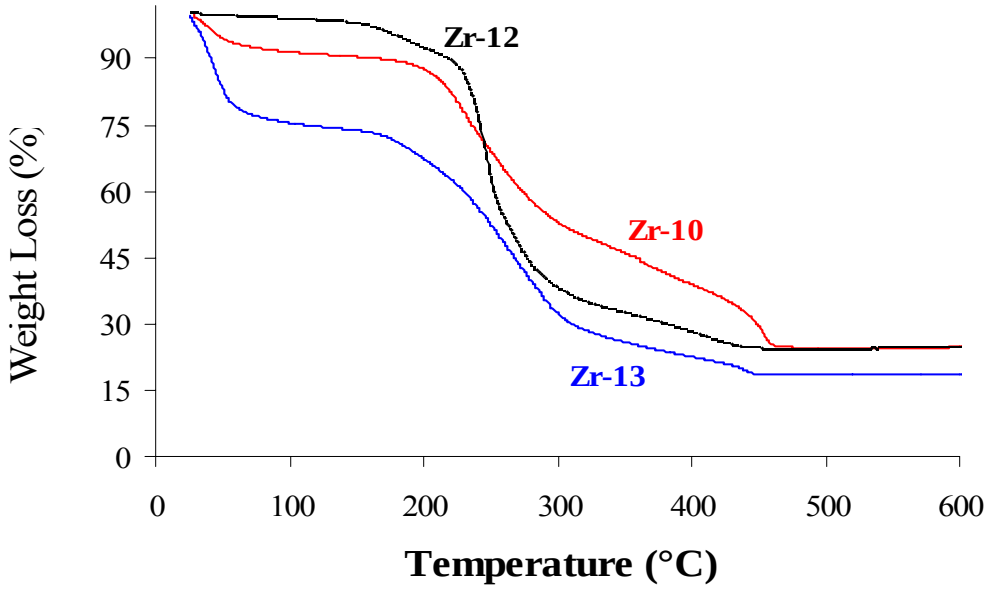


**Figure 2-4: The thermogravimetric analysis (TGA) data for the prepared zirconium carboxylates: (Zr-10: mandelate; Zr-12: benzilate; and Zr-13: benzilate (from sodium salt of benzilic acid).**

**Table 2-1: The structures and properties of the synthesized zirconium carboxylate complexes.**

| Sample code | (Initial components) $ZrOCl_2.8H_2O$ with : | Calcination to oxide | | *Oxide Temperature (°C) | ** Product proposed formula | pH | Surface Area ($m^2/g$) | Product yield (%) | Precursor crystal phase |
|---|---|---|---|---|---|---|---|---|---|
| | | $ZrO_2$ (%) | Molecular weight (g / mol) | | | | | | |
| **ZrAc** | Zirconium acetate | 58.0 | 211 | 590 | $[Zr_4O_4(OH)_3(OAc)_5]4H_2O$ | --- | 0.78 | --- | Amorphous |
| **Zr-1** | Glacial propanoic acid | 45.0 | 273 | 590 | $[Zr_4O_2(OH)_5(OAp)_5Cl_2]8H_2O$ | 0-1 | 0.56 | 97 | Crystalline |
| **Zr-2** | Sodium propionate | 48.9 | 252 | 590 | $[Zr_4O_4(OH)_3(OAp)_5]7H_2O$ | 6-7 | 1.39 | 95.6 | Amorphous |
| **Zr-3** | Sodium butyrate | 44.6 | 262 | 450 | $[Zr_4O_4(OH)_2(BUT)_6]2H_2O$ | 6 | 23.5 | 94 | Amorphous |
| **Zr-4** | Sodium isobutyrate | 42.5 | 289 | 450 | $[Zr_4O_4(OH)_2(ISBUT)_6]8H_2O$ | 6 | 36.5 | 100 | Amorphous |
| **Zr-5** | Ammonium pivalate | 40.5 | 304 | 380 | $[Zr_4O_{4.5}(PA)_7]5H_2O$ | 6 | 297 | 99.2 | Amorphous |
| **Zr-6** | Sodium hydroxypivalate | 37.7 | 326 | 590 | $[Zr_4O_5(HPA)_6]8H_2O$ | 5-6 | 14.9 | 64.4 | Crystalline |
| **Zr-7** | Ammonium 2-ethylhexanoate | 47.5 | 259 | 470 | $[Zr_4O_6(OH)_2(EHA)_2]7H_2O$ | 3-4 | 20.1 | 74 | Amorphous |
| **Zr-8** | α- Hydroxylisobutyric acid | 27.8 | 443 | 590 | $[Zr_4(OH)_4(HIBUTA)_{12}]6H_2O$ | 0-1 | 11.3 | 56 | Crystalline |
| **Zr-9** | Sodium α-hydroxyisobutyrate | 24.4 | 504 | 650 | $[Zr_4O(OH)_4(HIBUTA)_{10}]28H_2O$ | 0-1 | 6.11 | 78 | Crystalline |
| **Zr-10** | Mandelic acid | 23.1 | 532 | 500 | $[Zr_4O(OH)_5(MA)_9]4H_2O$ | 0-1 | 13.2 | 72.2 | Crystalline |
| **Zr-11** | Sodium mandelate | 26.0 | 473 | 540 | $[Zr_4(OH)_8(MA)_8]8H_2O$ | 1-2 | 1.93 | 78 | Amorphous |
| **Zr-12** | Benzilic acid | 20.5 | 600 | 470 | $[Zr_4O(OH)_6(BA)_8]4H_2O$ | 0-1 | 38.5 | 88.6 | Crystalline |
| **Zr-13** | Sodium benzilate | 18.2 | 676 | 520 | $[Zr_4(OH)_{7.5}(BA)_{8.5}]14H_2O$ | 6-7 | 31.7 | 86 | Amorphous |
| **Zr-14** | Sodium benzilate | 20.2 | 600 | 450 | $[Zr_4O(OH)_6(BA)_8]4H_2O$ | 6-7 | 241 | 86 | Crystalline |

** The minimum temperature for the complete conversion of precursor to zirconium oxide.*

*** OAp= Propionate; BA = Benzilate; PA = Pivalate; MA = BUT = Butyrate; ISBUT = Isobutyrate; Mandelate; HPA = Hydroxy pivalate; HIBA = Hydroxy isobutyrate; EHA = 2-Ethylhexanoate.*

**Table 2-2: The elemental analysis results for the synthesized zirconium carboxylate complexes.**

| Sample code | Elemental analysis (%) | | Product proposed formula | *Expt. Mwt (g/mol) | **Theoretical Mwt. (g/mol) |
|---|---|---|---|---|---|
| | C | H | | | |
| **ZrAc** | 14.1 | 2.81 | $[Zr_4O_4(OH)_3(OAc)_5]\cdot 4H_2O$ | 211 | 212 |
| **Zr-1** | 17.2 | 4.10 | $[Zr_4O_2(OH)_5(OAP)_5Cl_2]\cdot 8H_2O$ | 273 | 267 |
| **Zr-2** | 18.6 | 3.95 | $[Zr_4O_4(OH)_3(OAP)_5]\cdot 7H_2O$ | 252 | 243 |
| **Zr-3** | 28.3 | 4.68 | $[Zr_4O_4(OH)_2(BUT)_6]\cdot 2H_2O$ | 254 | 256 |
| **Zr-4** | 23.3 | 5.33 | $[Zr_4O_4(OH)_2(ISBUT)_6]\cdot 8H_2O$ | 289 | 292 |
| **Zr-5** | 35.0 | 7.08 | $[Zr_4O_{4.5}(PA)_7]\cdot 5H_2O$ | 304 | 309 |
| **Zr-6** | 27.6 | 4.93 | $[Zr_4O_5(HPA)_6]\cdot 8H_2O$ | 326 | 323 |
| **Zr-7** | 18.5 | 4.55 | $[Zr_4O_6(OH)_2(EHA)_2]\cdot 7H_2O$ | 259 | 227 |
| **Zr-8** | 36.5 | 5.27 | $[Zr_4(OH)_4(HIBA)_{12}]\cdot 6H_2O$ | 443 | 445 |
| **Zr-9** | 23.9 | 6.45 | $[Zr_4O(OH)_4(HIBA)_{10}]\cdot 28H_2O$ | 504 | 496 |
| **Zr-10** | 47.0 | 4.46 | $[Zr_4O(OH)_5(MA)_9]\cdot 4H_2O$ | 532 | 506 |
| **Zr-12** | 57.8 | 4.26 | $[Zr_4O(OH)_6(BA)_8]\cdot 4H_2O$ | 600 | 593 |
| **Zr-13** | 54.0 | 4.75 | $[Zr_4(OH)_{7.5}(BA)_{8.5}]\cdot 14H_2O$ | 676 | 669 |

** from TGA and thermal analysis*

*** from proposed formula*

The X-ray diffraction patterns (XRD) in the range of 10-70º for the zirconium benzilates are shown in Figure 2-5. XRD analysis showed that the zirconium benzilate complex (Zr-12) prepared by the reflux of benzilic acid with an aqueous solution of zirconium oxychloride was a crystalline material while the zirconium benzilate complex prepared by the reaction of a zirconium salt with the sodium salt of benzilic acid (Zr-13) was amorphous. However, when the Zr-13 sample was stirred in water for 24 hours, it showed a crystalline material with similar diffraction lines and d-spacings to that of the

Zr-12 sample. Thus, in contact with water, the amorphous phase undergoes crystallization to give the same crystalline phase that is formed under reflux conditions. However, broader XRD reflection peaks were observed for the room temperature sample indicating less extensive crystalline growth and smaller crystallite size than the high temperature sample. As the material was transformed into a more arranged structure, there was a marked increase in surface area from 31 $m^2/g$ to about 241 $m^2/g$. This demonstrates that the crystallization leads to an organization of the zirconium benzilate into a mesoporous structure. This was confirmed by the low angle XRD pattern that show the growth of a peak at $2\theta = 7^\circ$ (d = 7.02 Å). This was accompanied by a large increase in surface area as would be expected for formation of a mesoporous solid.

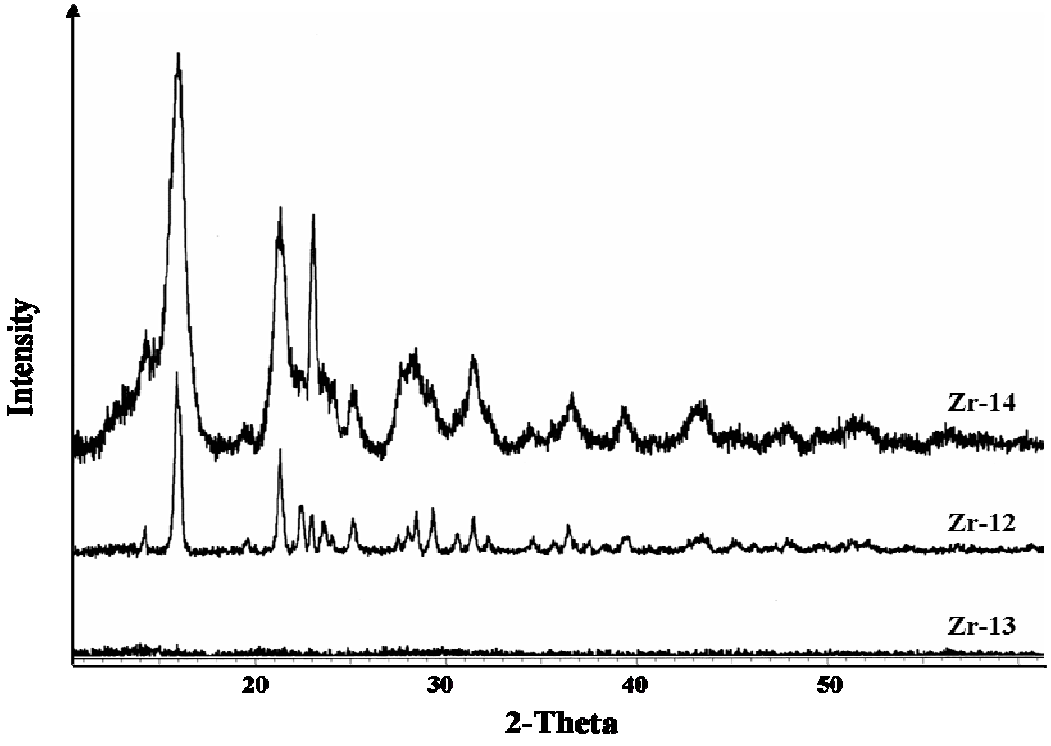


**Figure 2-5: X-Ray diffraction pattern of the zirconium benzilates from the reaction of zirconium oxychloride with: Zr-13: benzilic acid, sodium salt; Zr-12: benzilic acid; Zr-14: benzilic acid, sodium salt stirred for 24 hours in water.**

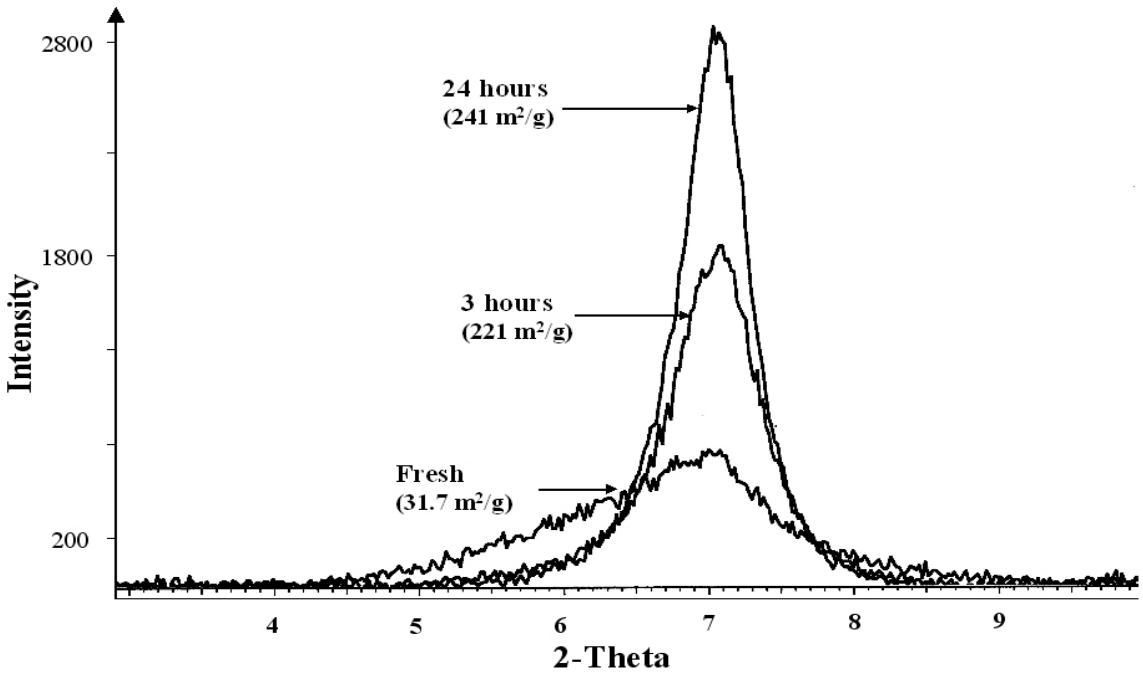


**Figure 2-6: Low angle X-ray diffraction pattern of the zirconium benzilate (Zr-13) stirred in water at different period of time.**

The low angle X-ray diffraction pattern of the calcined zirconium pivalate complex (Figure 2-7) also shows formation of a mesoporous solid. A single broad diffraction peak was observed with a d-spacing of 14.3 Å, 18.1 Å, and 20.0 Å for the fresh synthesized complex, and the complex calcined at 250 °C and 300 ºC, respectively. The breadth of the reflection peaks reflect wither distribution of pore sizes or organization of the pores in limited regions of the solid. The zirconium pivalate complex also showed a high surface area of about 297 $m^2$/g. These results, along with the low angle X-ray diffraction data, confirm the ordered porous structure of the zirconium pivalate complex. Upon thermal calcination, as shown in Figure 2-7, the d-spacing increased while the scattering intensity decreased. This provides a clear indication that the structure undergoes contraction during calcination and transformed into a less ordered

structure upon removal of the alkyl groups. This is also confirmed by the sharp decrease of the specific surface area during calcination due to the collapse of the structure. The observed increase in the d-spacing might be due to the loss of adsorbed water molecules and gradual thermal decomposition of the alkyl groups leading to longer pores and an expansion in the distance between the structure layers.

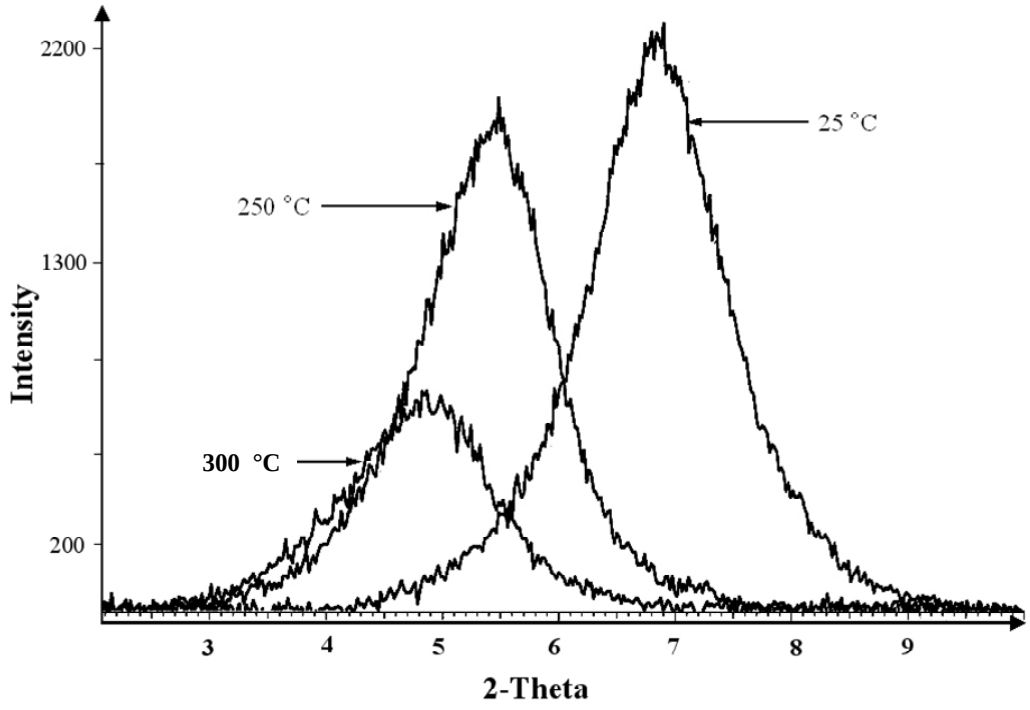


**Figure 2-7: Low angle X-ray diffraction pattern of the zirconium pivalate (Zr-5) calcined at different temperatures.**

It is expected that the polymerization of the zirconium carboxylate tetramer occurred by the presence of the -OH groups which form a bridge between two tetramers [20,21]. Apparently, a slow hydrolysis is associated with the polymerization process. The hydrogens of the incoming water molecule form a partial bond with the oxygen in

the carboxylate ligands. Thus, a displacement of some carboxylate ligands will take place to form a monodentate carboxylate. Another water molecule can attack another bridging carboxylate or attack the monodentate ligand to completely displace the carboxylate molecule. This process will form more hydroxyl groups which can link the tetramer together and form a polymeric species. With continued hydrolysis, more carboxylate ligands are displaced with more bridging tetramers formed by OH and oxo groups and hence a larger polymer will form. Additionally, it is also believed that the carboxylate ions may incorporate in the linkage of the zirconium tetramers together. Hence the properties of the ligands that coordinate to the zirconium metal are strongly influenced by the degree of the polymerization. The polymerization processes may be responsible for the formation of the high surface area porous zirconium complexes as in case of the zirconium pivalate (Zr-5) and zirconium benzilate (Zr-14). Additionally, based on the elemental analysis and the TG analysis, the Zr-13 precursor (derived from the reaction of zirconium oxychloride and benzilic acid, sodium salt) has a general chemical formula of $[Zr_4(OH)_{7.5}(BA)_{8.5}]\cdot 14H_2O$ while the Zr-14 precursor (derived from the reaction of zirconium oxychloride and benzilic acid, sodium salt stirred for a longer time) has a chemical formula of $[Zr_4O(OH)_6(BA)_8]\cdot 4H_2O$. The Zr-12 precursor showed a less amount of water, less hydroxyl, and less carboxylate ligand. This may be due to the fact that the longer aging time in solution results in oxalation in which the bridging hydroxyl groups transform into an oxo bridging group. This is often observed for hydrous metal oxides [20,21]. A schematic diagram for the polymerization process is shown in Figure 2-8 [21].

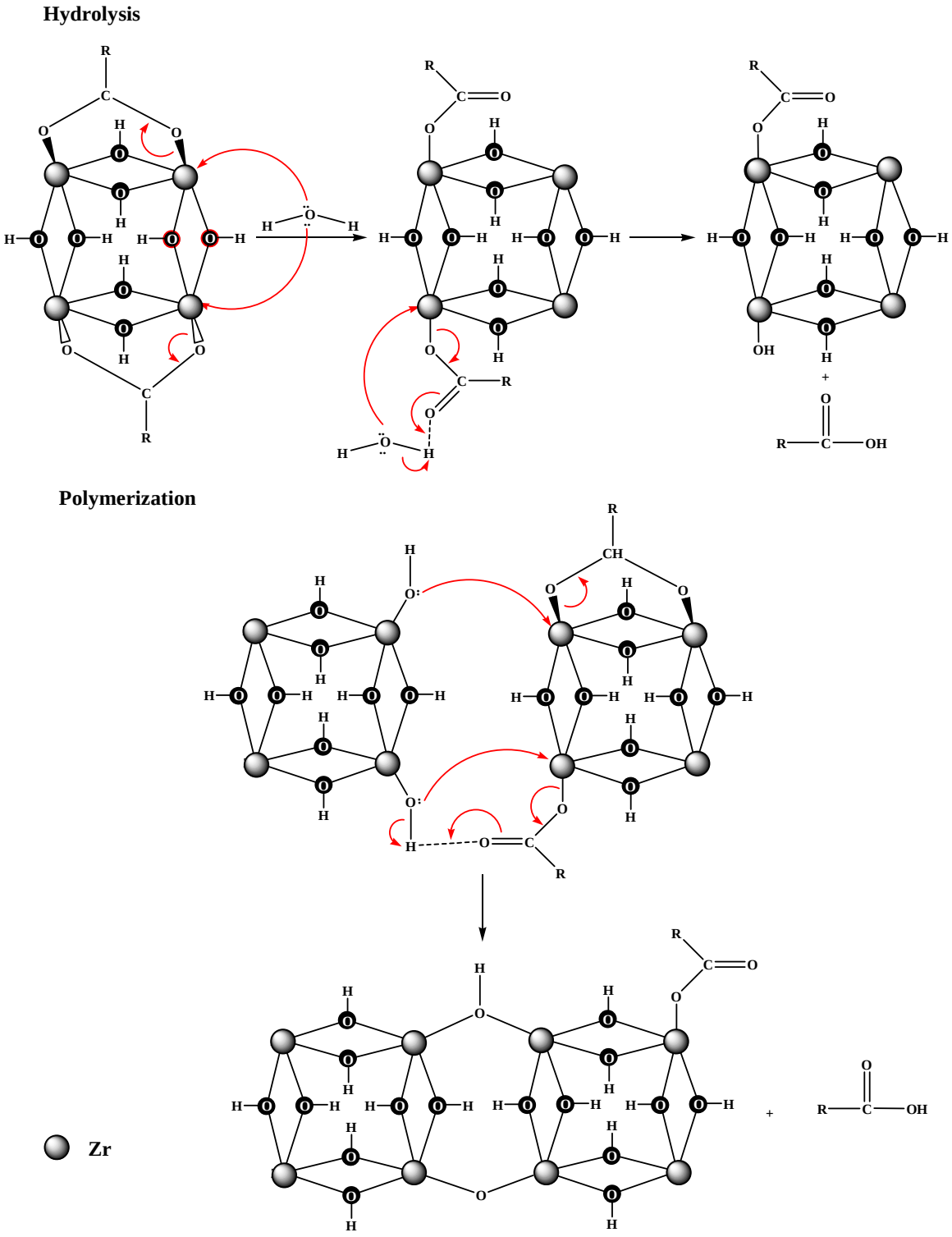


**Figure 2-8: Schematic diagram for the partial hydrolysis and polymerization of the zirconium carboxylate tetramers.**

As a matter of fact, some of the synthesized zirconium carboxylate as shown in Table 2-1 and Table 2-2 preserved a high amount of water molecules in the final complexes. This is especially true for zirconium benzilate and zirconium α-hydroxyisobutyrate. The inclusion of extra water may be attributed to the water molecules coordinated to the zirconium metal in the complexes being highly polarized and capable of strong interaction with other water molecules via hydrogen bonding. As a result of such hydrogen bonding, several stable physisorbed immobilized water layers may formed (Figure 2-9).

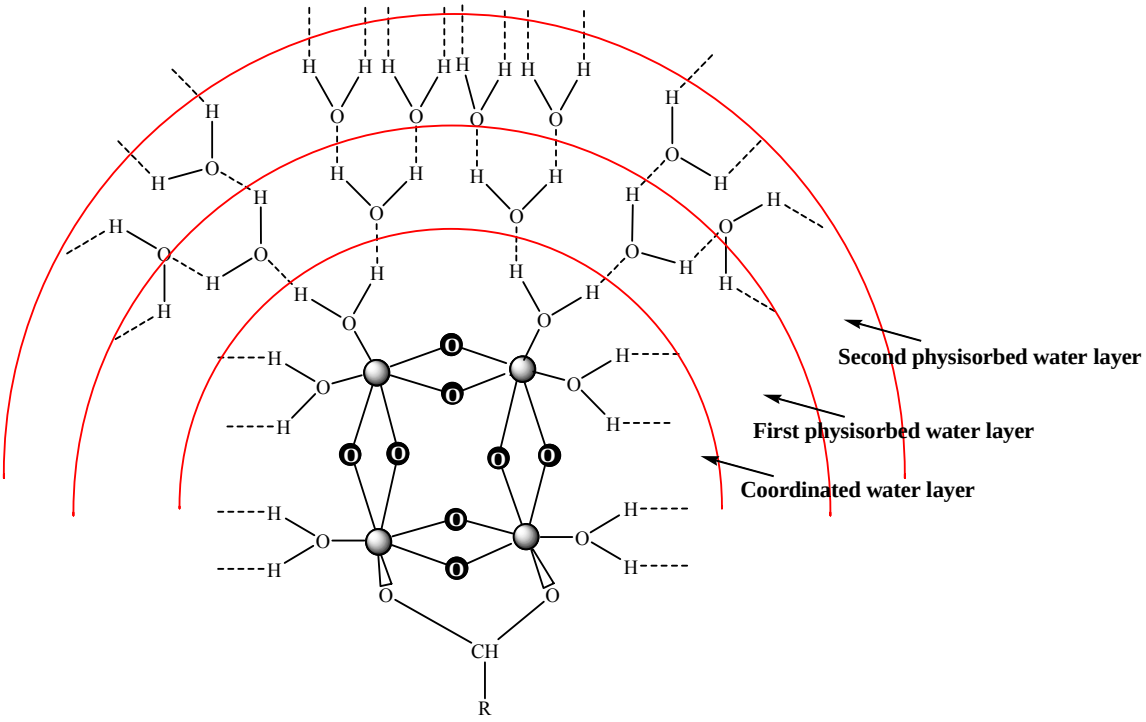


**Figure 2-9: Physisorbed water molecules on the zirconium carboxylate complexes.**

IR analysis can give significant information about the coordination mode of the carboxylate ligands. Generally, the carboxylate ligands bonded in a bridging bidentate

configuration have a $\Delta\nu$ value (splitting between the asymmetric and symmetric carbonyl stretching frequencies) of about 160 $cm^{-1}$ while chelating bidentate carboxylates give a smaller $\Delta\nu$ value (100 $cm^{-1}$ or less). Monodentate carboxylates, on the other hand, result in a greater $\Delta\nu$ value of about 200 $cm^{-1}$ [7,22]. The zirconium aliphatic carboxylates such as propionate showed a band centered at 3377 $cm^{-1}$ which corresponds to the hydrogen bonded O-H stretching band while the one at 3643 $cm^{-1}$ is related to the free O-H stretching vibration. The bands for zirconium propionate at 2980 $cm^{-1}$ and 2930 $cm^{-1}$ were assigned to the asymmetric and symmetric methyl groups of the carboxylate ligands, respectively, while that at 1340 $cm^{-1}$ was attributed to the vibration mode of the $CH_3$ groups. The bands around 1560 $cm^{-1}$ and 1439 $cm^{-1}$ correspond to the asymmetric and symmetric carboxylate stretching vibrations, respectively. The IR band at about 1470 $cm^{-1}$ belongs to the $CH_3$ and C-O-H bending frequencies.

Table 2-3 lists the stretching frequencies of the carboxylate carbonyl group $\nu_{COO(symm)}$ and $\nu_{COO(asymm)}$ and the splitting ($\Delta\nu$) between the asymmetric and symmetric carbonyl stretching frequencies of the different zirconium carboxylate complexes. In general, the results in Table 2-3 showed that the $\Delta\nu$ values are higher for the $\alpha$-hydroxy carboxylate zirconium complexes (benzilate and mandelate) than that of other zirconium carboxylate complexes. As shown in the Table 2-3, the $\Delta\nu$ values of $\alpha$-hydroxy-carboxylate zirconium complexes were in the range 230-301 $cm^{-1}$ while the other zirconium carboxylate complexes showed lower $\Delta\nu$ values in the range 120-152 $cm^{-1}$. The lower $\Delta\nu$ values for the other zirconium carboxylates are presumably attributed to the bridging bidentate bonding character of these carboxylate ligands.

**Table 2-3: Infrared carbonyl stretching frequency data for the zirconium carboxylate complexes.**

| *Sample Code | Proposed Structure | Free C=O ($cm^{-1}$) | $\nu_{COO}$ ($cm^{-1}$) | | Complex $\Delta\nu$ ($cm^{-1}$) |
|---|---|---|---|---|---|
| | | | Assym. | Symm. | |
| **Zr-1** | $[Zr_4O_2(OH)_5(OAP)_5Cl_2]\cdot 8H_2O$ | 1700 | 1564 | 1439 | 125 |
| **Zr-2** | $[Zr_4O_4(OH)_3(OAP)_5]\cdot 7H_2O$ | 1700 | 1560 | 1439 | 121 |
| **Zr-3** | $[Zr_4O_4(OH)_2(BUT)_6]\cdot 2H_2O$ | 1712 | 1600 | 1466 | 134 |
| **Zr-4** | $[Zr_4O_4(OH)_2(ISBUT)_6]\cdot 8H_2O$ | 1707 | 1585 | 1444 | 141 |
| **Zr-5** | $[Zr_4O_{4.5}(PA)_7]\cdot 5H_2O$ | 1700 | 1580 | 1428 | 152 |
| **Zr-6** | $[Zr_4O_5(HPA)_6]\cdot 8H_2O$ | 1698 | 1556 | 1431 | 125 |
| **Zr-7** | $[Zr_4O_6(OH)_2(EHA)_2]\cdot 7H_2O$ | 1720 | 1570 | 1425 | 145 |
| **Zr-8** | $[Zr_4(OH)_4(HIBA)_{12}]\cdot 6H_2O$ | 1730 | 1615 | 1388 | 227 |
| **Zr-9** | $[Zr_4O(OH)_4(HIBA)_{10}]\cdot 28H_2O$ | 1730 | 1551 | 1381 | 170 |
| **Zr-10** | $[Zr_4O(OH)_5(MA)_9]\cdot 4H_2O$ | 1716 | 1625 | 1351 | 274 |
| **Zr-11** | $[Zr_4(OH)_8(MA)_8]\cdot 8H_2O$ | 1716 | 1598 | 1383 | 215 |
| **Zr-12** | $[Zr_4O(OH)_6(BA)_8]\cdot 4H_2O$ | 1720 | 1650 | 1356 | 294 |
| **Zr-13** | $[Zr_4(OH)_{7.5}(BA)_{8.5}]\cdot 14H_2O$ | 1720 | 1593 | 1388 | 205 |
| **Zr-14** | $[Zr_4O(OH)_6(BA)_8]\cdot 4H_2O$ | 1720 | 1653 | 1352 | 301 |

** The samples specifications correspond to each samples code was described in Table 2-1.*

Bidentate bridging can occur with two different steric structures, cis and trans. In the cis structure both oxygen atoms of the carboxylate groups coordinate to the zirconium atoms on the same side of the tetramer plane, and, in the trans structure, the two oxygen atoms coordinate to the two zirconium atoms that lie on different sides of the tetramer

plane (Figure 2-9). The cis configuration is sterically less strained than the trans configuration due to the strained Zr-O angle in the trans structure.

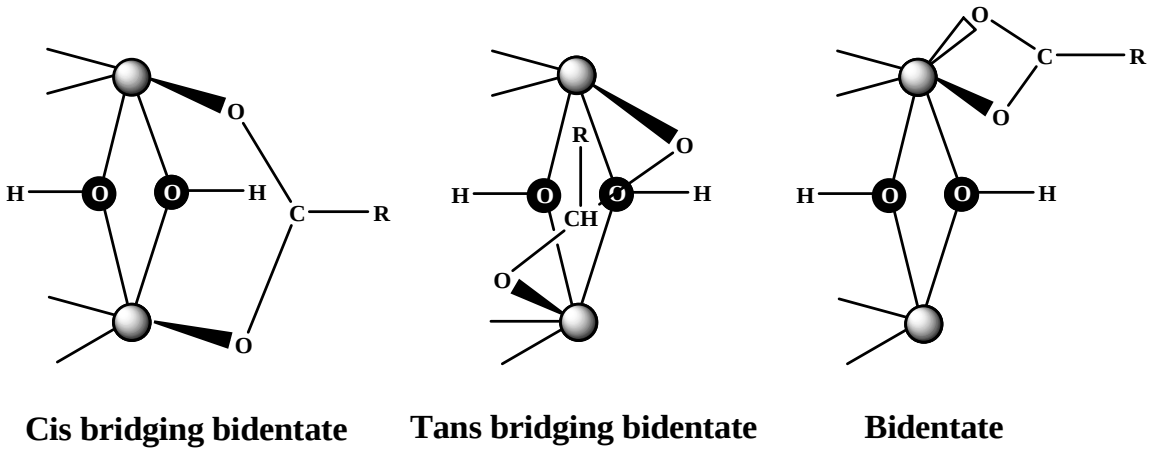


**Cis bridging bidentate** **Tans bridging bidentate** **Bidentate**

**Figure 2-10: Possible bonding types of carboxylate to the zirconium tetramer.**

The results in Table 2-3 also showed that the Δν values for the zirconium carboxylate were slightly increased with an increase in the chain length or branching of the carboxylate ligands, the propionate having the lowest Δν value of 121 $cm^{-1}$ while 2-ethylhexanoate had the highest value among the aliphatic carboxylate of 145 $cm^{-1}$. Additionally, the synthesized aliphatic zirconium carboxylate complexes, such as zirconium propionate, zirconium pivalate, zirconium hydroxypivalate, and 2-ethylhexanoiate, had lower asymmetric stretching frequencies of the carbonyl groups than the α-hydroxylcarboxylate zirconium complexes. A large shift of the carbonyl stretching frequencies between the free acid carbonyl (1700-1730 $cm^{-1}$) and the carbonyl stretching frequencies (1560-1580 $cm^{-1}$) of the complexes was observed for these complexes. This shift is due to the fact that when zirconium metal coordinates to the

oxygen of the carbonyl groups in the carboxylate ligands in a bidentate fashion, the C-O bond will be weakened due to the sharing of the carbonyl oxygen electrons in the bonding with the zirconium metal. In contrast, the α-hydroxyl zirconium carboxylate complexes showed a higher asymmetric stretching for the carbonyl groups (1620-1650 $cm^{-1}$). This is presumably due to the chelating type of bonding between the oxygen of the carbonyl group and the oxygen of the alcoholic hydroxyl group with the zirconium metal to form a five-membered ring structure. This will make the contribution of the carboxylate carbonyl group to the bonding less, leading to a higher stretching frequency.

Figure 2-11 shows the IR spectra of the zirconium benzilate complexes and benzilic acid. The stretching frequency of the carboxylate carbonyl group $\nu_{COO(symm)}$ of the benzilic acid is appeared above 1700 $cm^{-1}$ (Figure 2-11A). The strong band at about 3400 $cm^{-1}$ corresponded to the free alcoholic α-hydroxy groups ($\nu_{OH}$). When the zirconium salt reacted with sodium benzilate (Zr-13), the stretching frequency of the carboxylate carbonyl was decreased to about 1590 $cm^{-1}$ while maintaining the high intensity of the single sharp O-H peak at about 3550 $cm^{-1}$ which indicates the absence of the hydrogen bonds in this structure and emphasizes the dominance of the bidentate coordination. The results in Table 2-3 and Figure 2-11 also showed that the zirconium benzilate derived form sodium benzilate (Zr-13) has a lower $\Delta\nu$ value (205 $cm^{-1}$) which indicates bidentate coordination of the carboxylate group. Upon the stirring and polymerization of the Zr-13 complex, the carboxyl stretching frequency increased to about 1650 $cm^{-1}$, and the sharpness of the O-H band at 3550 $cm^{-1}$ decreased dramatically (Figure 2-11C). This implied that the bonding of the carboxylate to the zirconium atoms was transformed into the bridging chelating mode with incorporation of the O-H group in

the bonding to form a five-membered ring structure. Additionally, it is likely that the hydroxyl group of the carboxylate condenses with a free or bridging hydroxyl group from the zirconium tetramer to liberate a water molecule. Figure 2-12 shows the proposed two types of bonding structures for the synthesized zirconium benzilate complexes.

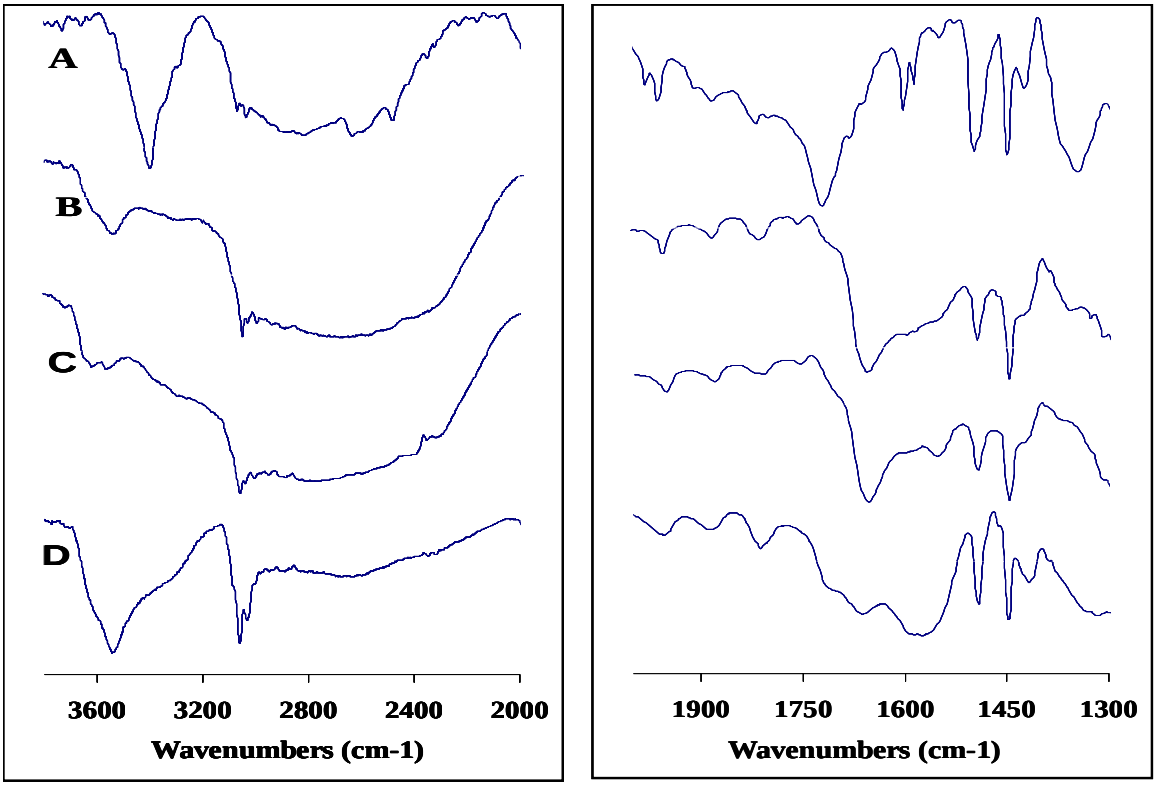


**Figure 2-11: Infrared spectra of the zirconium benzilate complexes: A: benzilic acid; B: (Zr-12) $ZrOCl_2.8H_2O$ with benzilic acid; C: (Zr-14) $ZrOCl_2.8H_2O$ with benzilic acid, sodium salt stirred for 24 hours in water; D: (Zr-13) $ZrOCl_2.8H_2O$ with benzilic acid, sodium salt.**

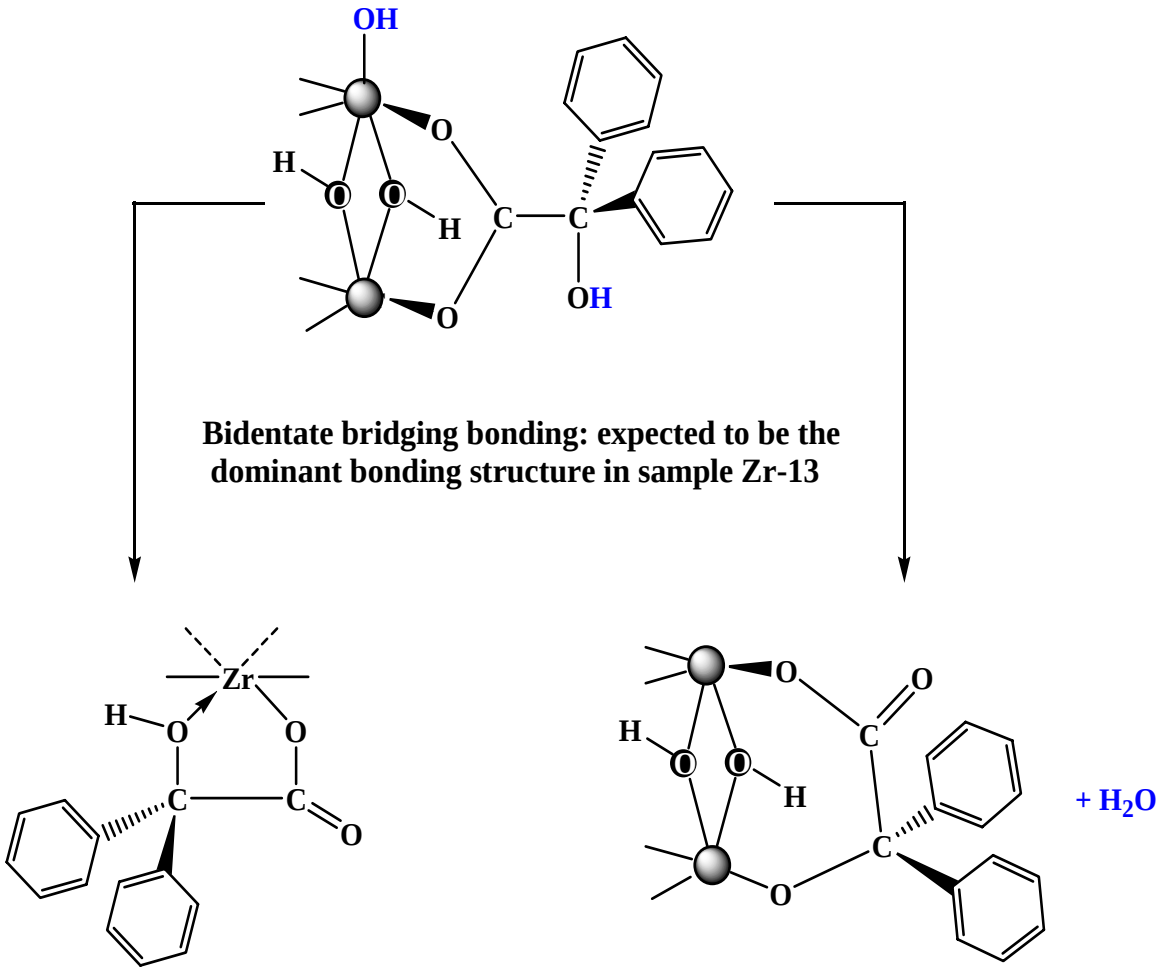


**Figure 2-12: Bonding types in the zirconium benzilate complexes.**

**Zirconium oxide from zirconium carboxylates:**

Figures 2-13 showed the IR spectra and the X-ray diffraction patterns for the products obtained from the pyrolysis of zirconium propionate at different calcination temperatures. The IR spectra (Figure 2-13) showed that the bands corresponding to the

carboxylate were still intact when the sample was heated at 230 °C. The intensity of the carboxylate band was reduced significantly in the sample calcined at 420 °C, which implied that most of the carboxylate ligands were decomposed at this temperature. The IR spectra for the calcined precursor (Figure 2- 13 B and C) showed a sharp band at about 2339 $cm^{-1}$. This band appeared due to the adsorbed $CO_2$ species on the surface. Carbon dioxide formed as a result of the thermal decomposition of the carboxylate ligand. The previous studies on the adsorption of carbon dioxide over zirconia and modified zirconia showed similar bands in the same wavenumber range [23-24]. Apparently, $CO_2$ is weakly adsorbed on the surface. This can be seen clearly from the slight frequency shift ($\Delta\nu$) with respect to the $CO_2$ free molecule which has a band at 2348 $cm^{-1}$ [23]. The peak observed at about 1424 $cm^{-1}$ for the zirconium propionate calcined at 470 °C (Figure 2-13C) probably corresponds to the presence of some carbonate species adsorbed on the surface of the tetragonal zirconium oxide. It was observed also that the calcined sample at 470 °C showed a medium broad band at 1533 $cm^{-1}$ which was attributed to bidentate carbonate species present on the oxide surface. Furthermore, the sample lost about 40% of its weight when calcined at 470 °C, which according to the TGA analysis is the appropriate temperature for zirconia formation. However, the sample color was still brown at this calcination temperature indicating that the band at 1533 $cm^{-1}$ may be due to the bidentate carbonate and carbon species deposited on the oxide surface [23,25]. The intensity of this peak decreased upon calcination to 720 °C (Figure 2-13D). The band observed at 790 $cm^{-1}$ for the sample calcined at 470 °C is probably due to the carbonate-water interaction. With the increase of the calcination temperature, the intensity of this band was decreased.

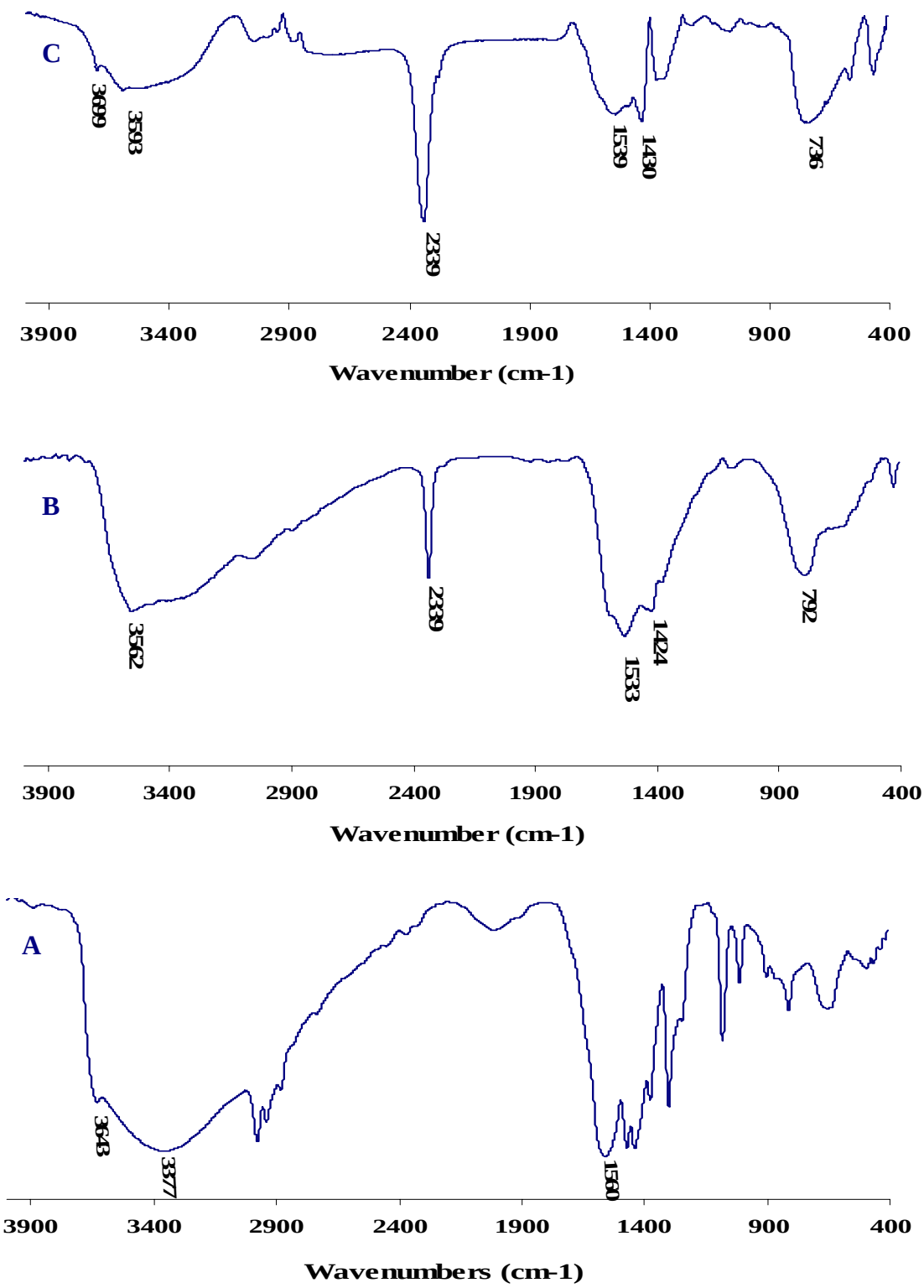


**Figure 2-13: IR spectra of the pyrolysis product of the zirconium propionate (Zr-1) at A: room temperature; B: 470 °C; and C: 720 °C.**

The pyrolysis products of the zirconium propionate at 230 °C was found to be amorphous by X-ray powder diffraction (Figure 2-14). With further heating to 420 °C, a mixture of tetragonal and cubic phases started to appear as a result of the transformation of the zirconium carboxylate to zirconium oxide. Upon heating to 590 °C, a more crystalline tetragonal zirconia phase was observed. When the oxide was heated above 600 °C, a phase transformation occurred from the tetragonal phase to monoclinic. When the oxide was further calcined to 800 °C, the monoclinic phase was the dominant phase with about 90% relative abundance.

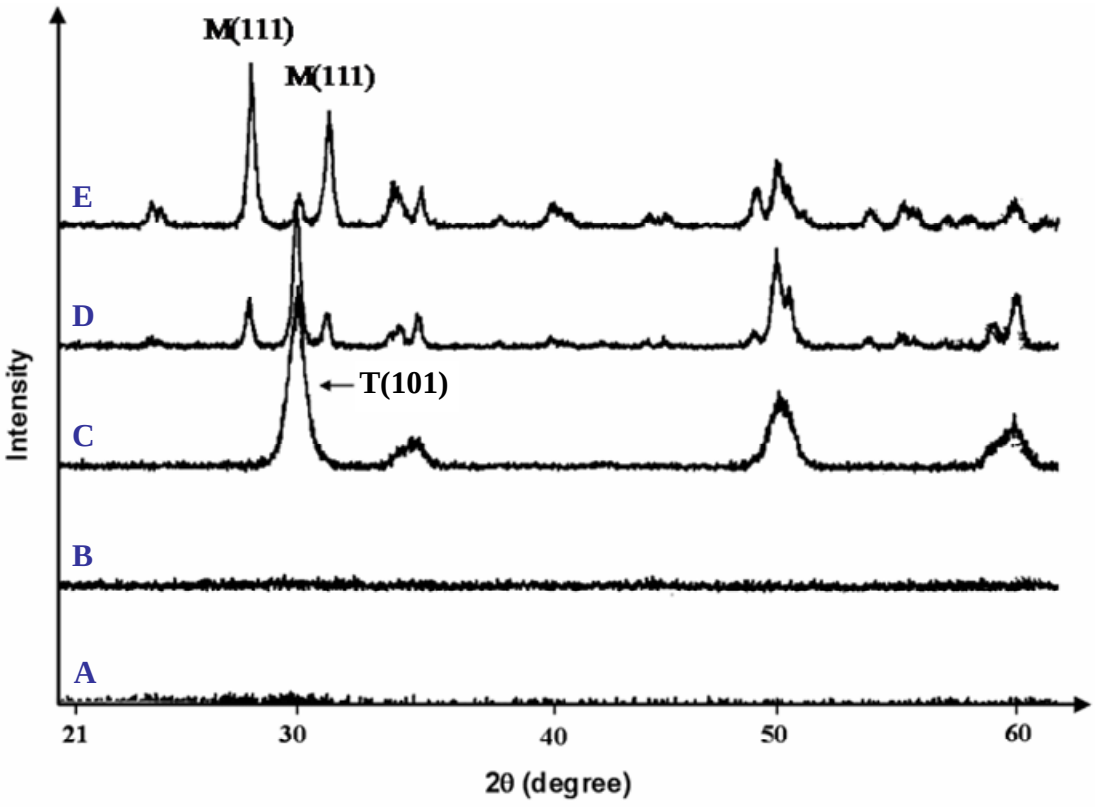


**Figure 2-14: X-Ray diffraction pattern for zirconium propionate (Zr-1) calcined at different temperature: A: room temperature; B: 230 °C; C: 590 °C; D: 720 °C; E: 800 °C. (T = Tetragonal; M = Monoclinic)**

In most cases, zirconium carboxylates showed first a transformation to a metastable tetragonal phase followed by transformation of the tetragonal to monoclinic phase. The initial crystallization of the zirconia from these complexes was observed in the temperature range of 350 °C to 450 °C. Calcination to temperatures higher than 600 °C resulted in a phase transformation of the tetragonal phase to give a mixture of tetragonal and monoclinic phases of zirconia. The general trend of the thermal calcination of zirconium carboxylates to crystalline zirconium oxide can be described as shown below:

$$\left[Zr(OH)_x(Carboxylate)_y\right].nH_2O \xrightarrow[-\ nH_2O]{130\ ^\circ C} \left[Zr(OH)_x(Carboxylate)_y\right]$$

$$\left[Zr(OH)_x(Carboxylate)_y\right] \xrightarrow{350\ ^\circ C - 500\ ^\circ C} ZrO_2\ (tetragonal) + CO_2 + H_2O$$

$$ZrO_2\ (tetragonal) \xrightarrow{600\ ^\circ C - 800\ ^\circ C} ZrO_2\ (tetragonal) + ZrO_2\ (monoclinic)$$

$$ZrO_2\ (tetragonal) + ZrO_2\ (monoclinic) \xrightarrow{> 800\ ^\circ C} ZrO_2\ (monoclinic)$$

The presence of hydroxyl ions is believed to stabilize the tetragonal phase and delay the transformation to the monoclinic phase [26]. Therefore, the transformation from tetragonal to monoclinic phase was observed in this work occurred at a higher temperature compared to that of a pure zirconium hydroxide prepared by a variety of methods [26,27]. The reason for this phase stabilization may be due to the fact that decomposition of carboxylate ligands leads to the presence of some carbonate species on the surface that stabilize the tetragonal phase.

The crystallite size derived from the Scherrer's equation obtained by the X-ray pattern using a line broadening method showed an increase in crystallite size with an increase of the calcination temperature. Figure 2-15 shows the crystallite size distribution of zirconia deduced from zirconium propionate calcined at different temperatures. A slight increase in the average crystallite size from 3.2 nm to 6.7 nm was observed when the precursor was heated at 590 °C and 720 °C respectively. A higher average crystallite size of 18.4 nm was observed when the sample calcined at 800 °C, at which point the substance is almost completely transformed into a monoclinic phase.

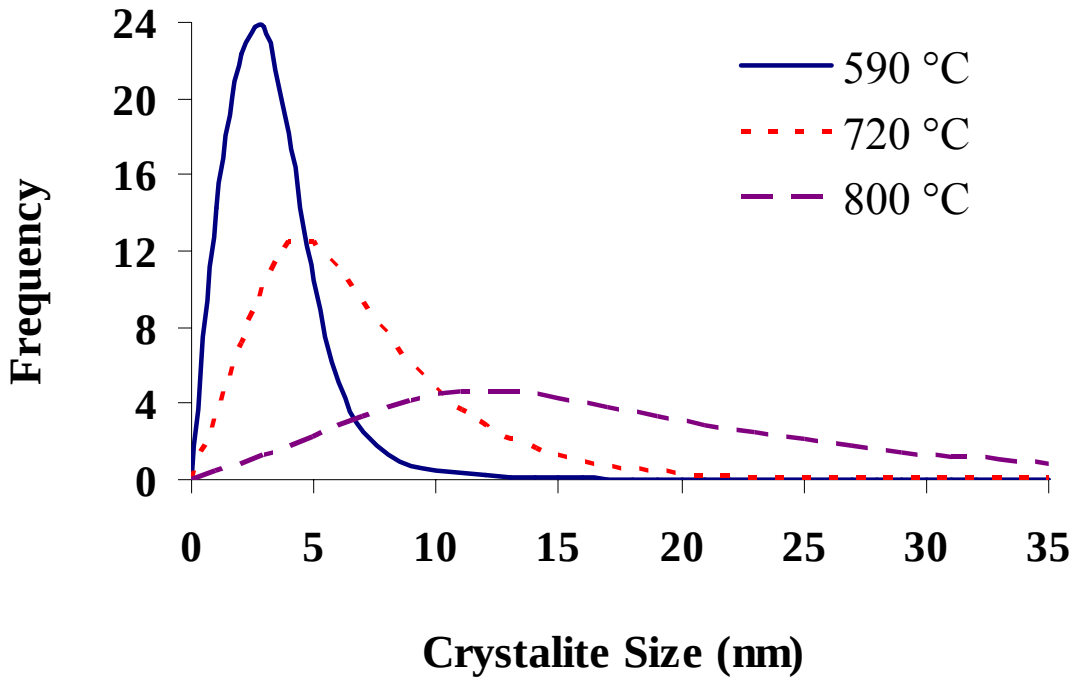


**Figure 2-15: The crystallite size distribution of the zirconium propionate calcined at different temperatures.**

The phase transformation data and the surface area values are presented in Table 2-4 and Figure 2-16. The results show that the aliphatic zirconium carboxylates undergo a

phase transformation to a monoclinic system at higher temperature (> 720 ºC) compared to the α-hydroxylcarboxylate complexes. Figure 2-16 shows that the oxides derived from the thermal calcination of zirconium mandelate and zirconium hydroxybutyrate transformed into the monoclinic phase rapidly in the temperature range of 590 °C to 720 °C. An obvious increase in the volume percentage of the monoclinic zirconium oxide occurs in this temperature region. The α-hydroxyacids can undergo a decomposition to give $ZrO_2$, CO and RCHO or $R_2CO$. When zirconium benzilate, for instance, is pyrolyzed in a sealed tube at 280 ºC for 6 hours, the major product obtained from the decomposition reaction is benzophenone. The thermal decomposition of such precursors is believed to occur according to the following pathway:

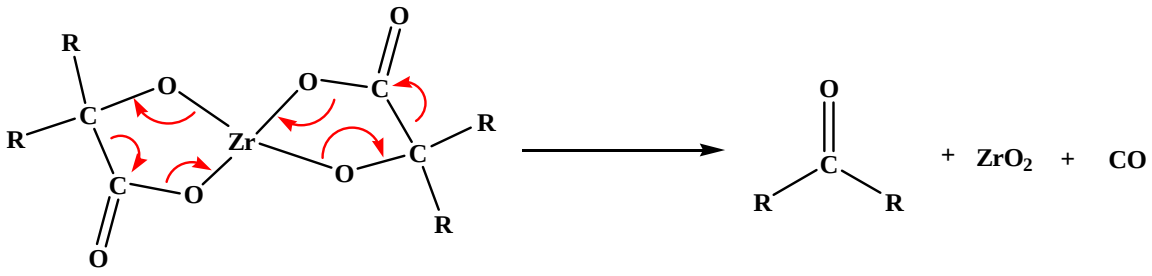


Since this pathway generates zirconia without many surface hydroxyl or carbonate species, the phase transformation to monoclinic zirconia is not retarded.

**Table 2-4: The surface area and phase composites of the zirconium oxides derived from thermal calcinations of zirconium carboxylates.**

| *Sample code | Calcination Temperature (°C) | Surface Area ($m^2/g$) | Phase (%) | |
|---|---|---|---|---|
| | | | $V_{tetragonal}$ | $V_{monoclinic}$ |
| **ZrAc(590)** | 590 | 4.60 | 35 | 65 |
| **ZrAc(720)** | 720 | 3.20 | 8.0 | 92 |
| **ZrAc(850)** | 850 | 0.32 | 0 | 100 |
| **Zr-1(590)** | 590 | 4.10 | 100 | 0 |
| **Zr-1(700)** | 700 | 0.97 | 64 | 36 |
| **Zr-1(800)** | 800 | 0.57 | --- | --- |
| **Zr-2(590)** | 590 | 2.15 | 100 | 0 |
| **Zr-2(720)** | 720 | 1.01 | 59 | 41 |
| **Zr-2(800)** | 800 | 0.83 | 2.0 | 98 |
| **Zr-2(850)** | 850 | 1.77 | 1.0 | 99 |
| **Zr-3(590)** | 590 | 8.30 | 100 | 0 |
| **Zr-3(650)** | 650 | 10.2 | 95 | 5.0 |
| **Zr-3(720)** | 720 | 9.56 | 69 | 31 |
| **Zr-3(750)** | 750 | 4.70 | 30 | 70 |
| **Zr-3(850)** | 850 | 7.20 | 8.0 | 92 |
| **Zr-4(590)** | 590 | 6.90 | 100 | 0 |
| **Zr-4(650)** | 650 | 7.20 | 94 | 6.0 |
| **Zr-4(720)** | 720 | 5.72 | 63 | 37 |
| **Zr-4(750)** | 750 | 5.60 | 26 | 74 |
| **Zr-4(850)** | 850 | 4.80 | 0 | 100 |
| **Zr-5(350)** | 350 | 14.9 | 100 | 0 |
| **Zr-5(500)** | 500 | 7.65 | 100 | 0 |
| **Zr-5(590)** | 590 | 9.30 | 96 | 4.0 |
| **Zr-5(720)** | 720 | 5.32 | 69 | 31 |
| **Zr-5(850)** | 850 | 6.30 | 15 | 85 |
| **Zr-6(590)** | 590 | 7.59 | 85 | 16 |
| **Zr-6(720)** | 720 | 6.64 | 85 | 15 |
| **Zr-6(850)** | 850 | 6.40 | 0 | 100 |
| **Zr-7(470)** | 470 | 31.6 | 100 | 0 |
| **Zr-7(600)** | 600 | 16.4 | 59 | 41 |
| **Zr-7(720)** | 720 | 8.50 | 28 | 72 |
| **Zr-7(850)** | 850 | 5.30 | 1.0 | 99 |

** The specifications correspond to each sample's code are described in Table 2-2.*

*ZrAc = Zirconium (IV) acetate hydroxide*

**Table 2-4: The surface area and phase composites of the zirconium oxides derived from thermal calcinations of zirconium carboxylates (continue).**

| *Sample code | Calcination Temperature (°C) | Surface Area ($m^2/g$) | Phase (%) | |
|---|---|---|---|---|
| | | | $V_{tetragonal}$ | $V_{monoclinic}$ |
| **Zr-8(590)** | 590 | 19.8 | 62 | 38 |
| **Zr-8(720)** | 720 | 8.30 | 25 | 75 |
| **Zr-8(850)** | 850 | 6.80 | 0 | 100 |
| **Zr-9(590)** | 590 | 3.28 | 83 | 17 |
| **Zr-9(720)** | 720 | 4.04 | 19 | 81 |
| **Zr-9(850)** | 850 | 2.70 | 0 | 100 |
| **Zr-10(500)** | 500 | 7.10 | 100 | 0 |
| **Zr-10(590)** | 590 | 6.97 | 95 | 5.0 |
| **Zr-10(720)** | 720 | 5.56 | 65 | 35 |
| **Zr-10(850)** | 850 | 2.87 | 14 | 86 |
| **Zr-11(590)** | 590 | 6.20 | 88 | 12 |
| **Zr-11(620)** | 620 | 4.30 | 66 | 34 |
| **Zr-11(720)** | 720 | 1.92 | 39 | 61 |
| **Zr-11(850)** | 850 | 0.68 | 2.0 | 98 |
| **Zr-12(590)** | 590 | 17.3 | 100 | 0 |
| **Zr-12(720)** | 720 | 15.6 | 65 | 35 |
| **Zr-12(850)** | 850 | 11.1 | 12 | 88 |
| **Zr-14(460)** | 460 | 31.6 | 100 | 0 |
| **Zr-14(590)** | 590 | 9.33 | 64 | 36 |
| **Zr-14(720)** | 720 | 1.44 | 55 | 45 |
| **Zr-14(850)** | 850 | 0.68 | 0 | 100 |

** The specifications correspond to each sample's code are described in Table 2-2.*

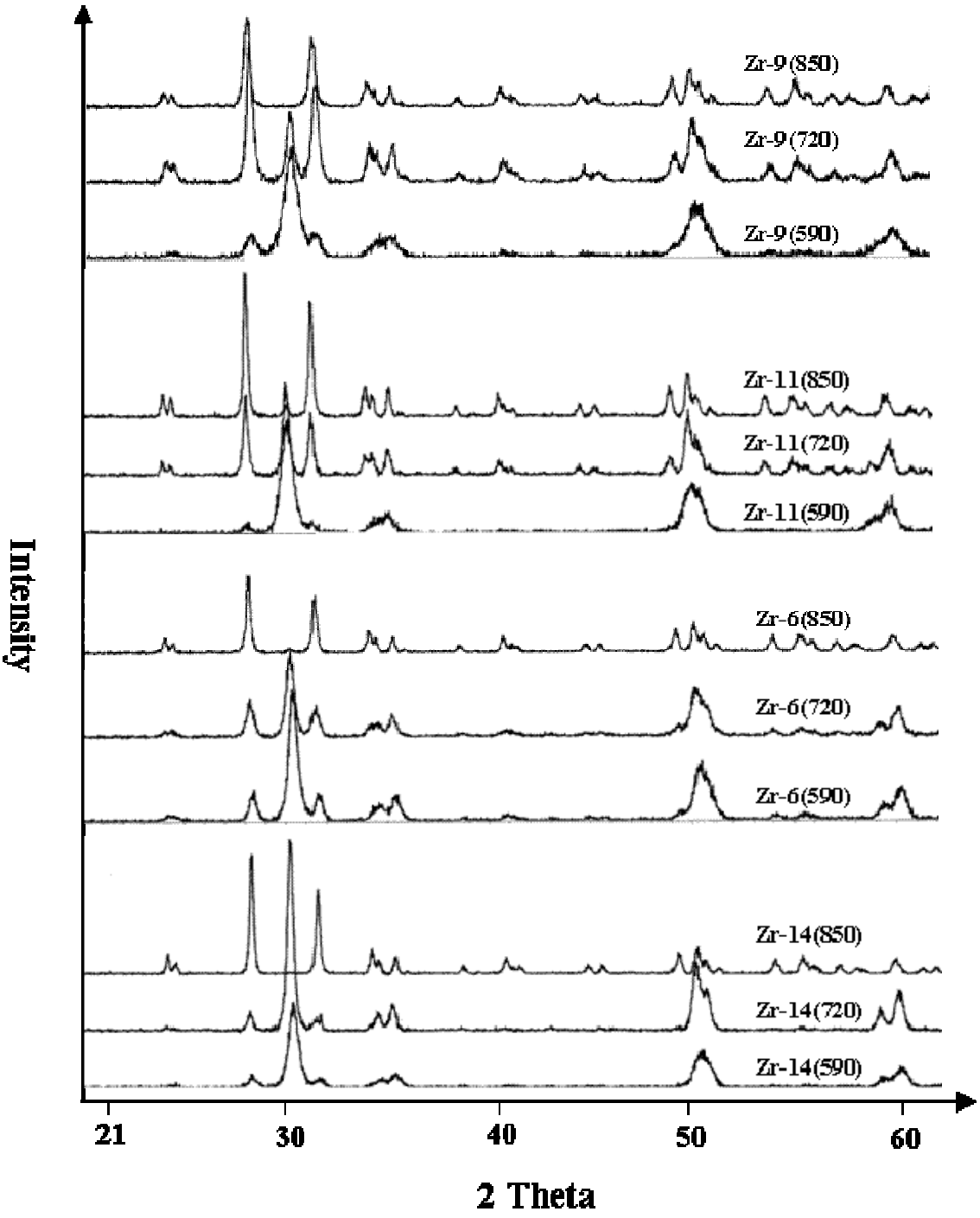


**Figure 2-16: X-ray diffraction pattern for several zirconium carboxylate precursors calcined at three different temperatures; Zr-14 (Zirconium benzilate), Zr-6 (Zirconium hydroxylpivalate), and Zr-11 (Zirconium mandelate), and Zr-9 (Zirconium hydroxylisobutyrate)**

As shown in Table 2-4 and Figure 2-17, the surface area of the zirconium precursors showed a slight increase upon calcination due to the loss of the ligand and the formation of oxides with open pores. Further heating led to the gradual sintering of the oxide particles and decrease in the surface area. The precursors that showed a long order range and very high surface areas (the zirconium benzilate and zirconium pivalate) exhibited a sharp decrease in the surface area as mentioned earlier due to the collapse of the metallo-organic framework to form oxide and then a slow decrease in the surface area due to the sintering process. Furthermore, the zirconium oxides obtained from the aliphatic carboxylates (Table 2-4) showed a dependency on the carboxylate ligands. That is, the longer the carboxylate ligand chain, the higher the surface area of the resulting zirconia. For example, zirconia obtained from zirconium ethylhexanoate showed a relatively higher surface area of 31.6 $m^2/g$ (sample calcined at 470 °C) compared to that of the zirconia prepared from the other aliphatic zirconium carboxylate complexes.

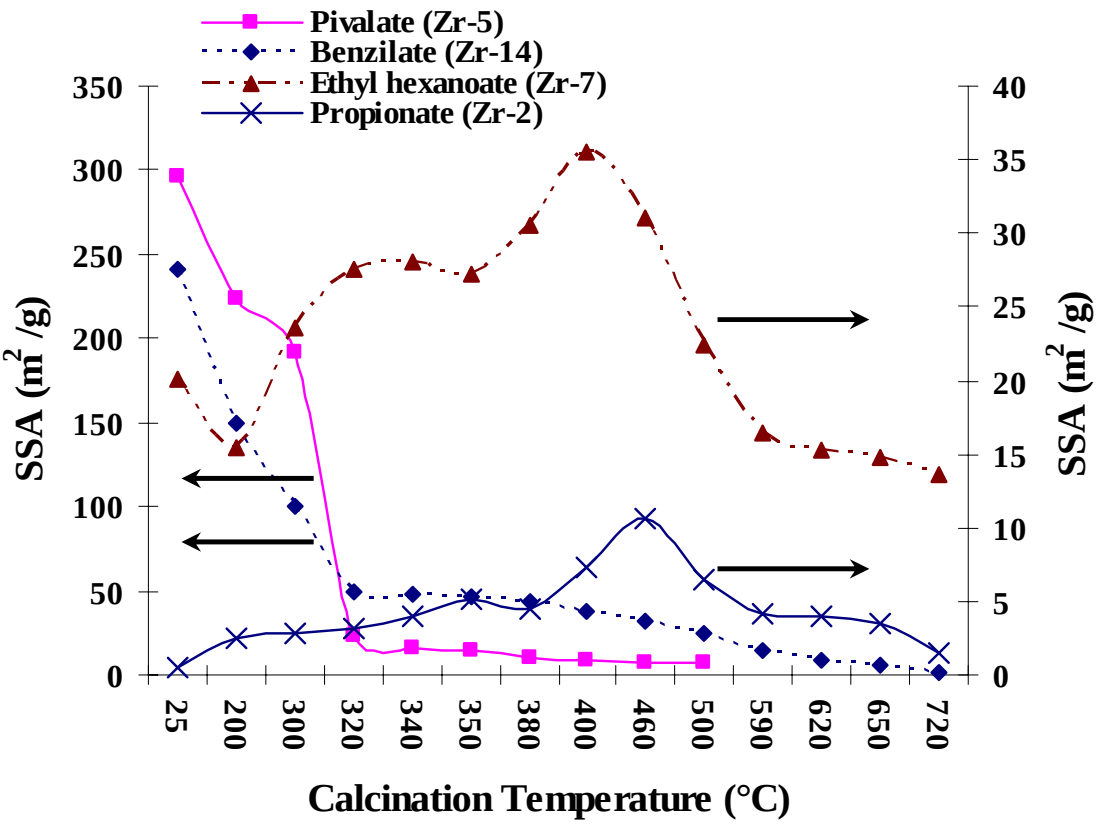


**Figure 2-17: Effect of the calcination temperature of the zirconium carboxylate precursors on the specific surface area of the pyrolysis product.**

Figure 2-18 shows the scanning electron micrographs of the zirconium oxide derived from the thermal treatment of zirconium benzilate and zirconium pivalate. The SEM showed an influence of the zirconium precursor on the morphology of the final oxide. The oxide derived from zirconium pivalate [sample Zr-3(500)] showed the formation of agglomerates containing spherical nanosize individual particles with approximate average diameter of about 100-200 nm. On the other hand, the zirconium oxide powder derived from the pyrolysis of zirconium benzilate [sample Zr-12(460)] showed a quite different morphology. Zirconium oxide derived from zirconium benzilate

complex displaced a flat smooth relief surface of a large aggregate. According to the SEM images, uniform and regular hollow cubic and regular shaped particles with different sizes and origination were adhered to the smooth aggregate surface. These uniform morphologies of both oxide powders shown in Figure 2-18 reflect the homogeneity and polymerization of the zirconium tetramers.

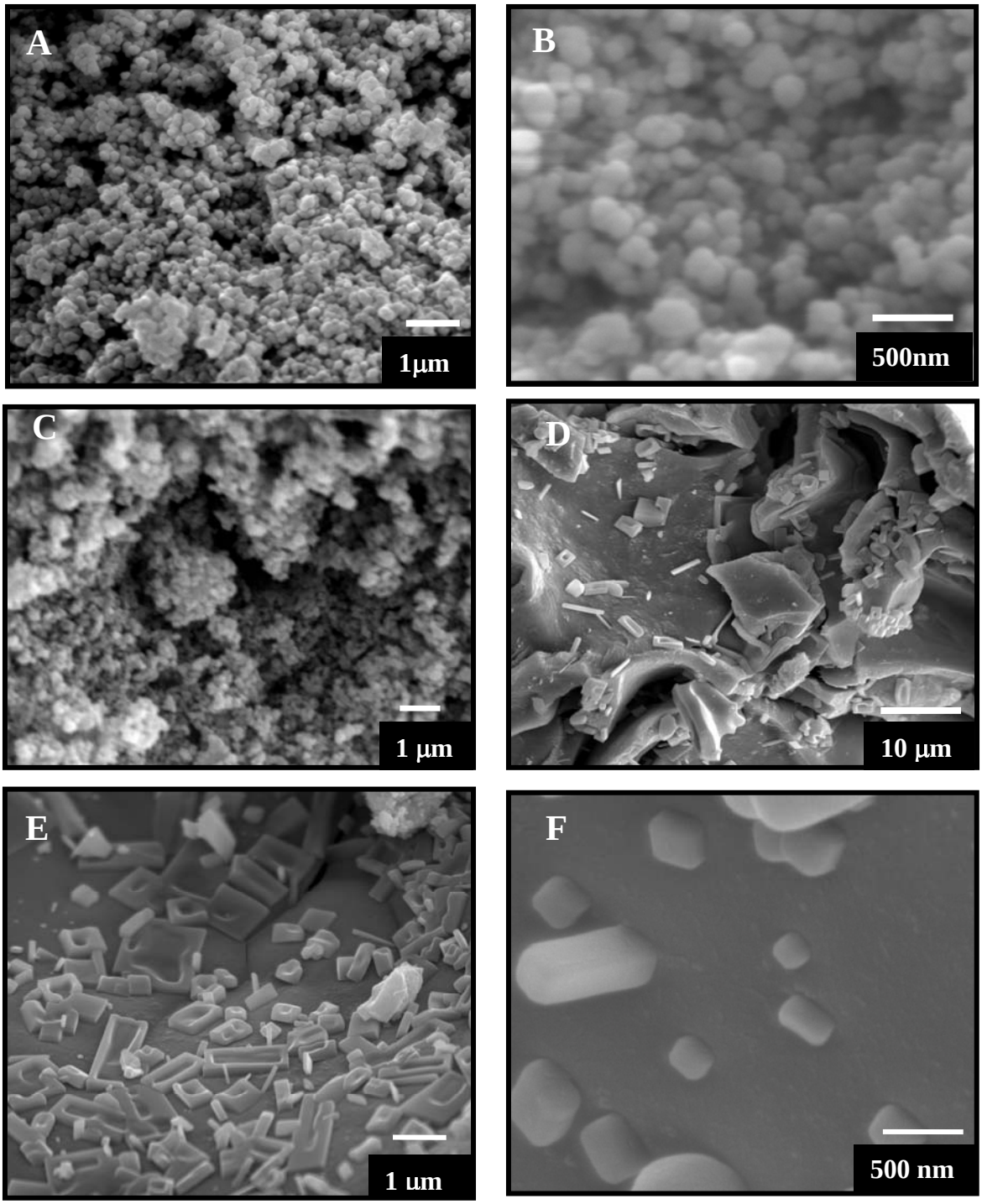


**Figure 2-18: Scanning electron micrographs for the zirconium oxide derived from thermal calcination of zirconium carboxylate precursors. $ZrO_2$ form zirconium pivalate at 400 ºC (Zr-8(400)): A(13000X), B(40,000X), C(9000X); $ZrO_2$ from zirconium benzilate at 460 ºC (Zr-14(460)): D(2000X), E(3400X), F(40,000X).**

## CONCLUSIONS AND REMARKS:

This work can be considered as a competitive alternative to the existing synthetic methods for zirconium oxide. Zirconium carboxylate complexes were synthesized by reaction of zirconium oxychloride with carboxylic acids or carboxylate salts in aqueous media. Different carboxylates were used in this study, namely propanoic acid, pivalic acid, hydroxypivalic acid, and 2-ethylhexanoic acid as aliphatic carboxylic acids, and α-hydroxyisobutyric acid, mandelic acid, and benzilic acid as an α-hydroxyl carboxylic acids. Furthermore, the characterization results showed that the aliphatic zirconium carboxylate complexes coordinate to the zirconium metal in a bridging bidentate mode while a bridging chelating bonding with incorporation of the OH in the bonding was observed with the α-hydroxylcarboxylate complexes.

All the zirconium carboxylate precursors showed a general trend for the decomposition to yield a tetragonal zirconia, which then was further transformed into a monoclinic phase. The precursors formed a tetragonal phase when they were heated in the temperature range between 400 °C–500 °C. Transformation to the more stable monoclinic phase occurred when the precursors were calcined at temperatures higher than 600 °C. The degree of the crystallization, as well as the phase composition, depends on the zirconium carboxylate starting materials. The oxides obtained from different zirconium carboxylate precursors showed different properties, such as surface morphologies, phase composition, and crystallite size. These changes implied strong dependency of the properties of the final oxide formed upon the carboxylate ligands, which coordinate to the zirconium in the precursor complexes.

**REFERENCES CITED:**


1. F. Lange, *J. Mater. Sci*. **1982**, *17,* 240.
2. W. Rhodes, *J. Amer. Ceram*. Soc. **1981**, *64*, 19.
3. A. Glushkova; A. Lapshin; A. Podzorova; V. Voglkov. *Glass Physics and Chemistry*, **2003**, *29(6)*, 613.
4. W. Blumenthal, *The Chemical Behavior of Zirconium,* Van Nostrand Company: Princeton, 1958.
5. R. Kapoor; R. Mehrotra, *Journal of the American Chemical Society* **1958**, *80* 3569.
6. R. Kapoor; R. Mehrotra, *Journal of the Chemical Society*,**1959**, *81*, 422.
7. K. Nakamoto. Infrared and Raman Spectra of the Inorganic and Coordination Compounds, Fifth Edition, Wiley: New York, 1997.
8. M. Aberg, *Acta Chemica Scandinavica*, **1977**, *B31*, 171.
9. R. Paul; Baidya, O.; Kumar, R; Kapoor, R. *Aust. J. Chem.* **1976**, *29 (7)*, 1605.
10. N. Alcock; V. Tracy; T. Waddington, *J. Chem. Soc. Dalton Transaction* **1976**, 21, 2238.
11. N. Kommisarova; *Russ. J. Inorg. Chem.* **1963**, 8(1), 56.
12. M. Balmer; F. Lange; G. Levi, *J. Am. Ceram. Soc.* **1992**, *75(4)*, 946.
13. A. Geiculescu; H. Spencer, *J. Sol-Gel Sci. Technol*. **1999**, 16(3), 243.
14. F. Berry; S. Skinner; I. Bell; R. Clark; C. Ponton, *J. Solid State Chem.* **1999**, *145 (2),* 394.

15. A. Samdi; B, Durand; M. Roubin; A. Daoudi *J. Eur. Ceram. Soc.* **1993**, *12(5)*, 353.

16. G. Gong-Yi; C. Yu-Li, *Ceramics International*, **2004**, *30*, 469.

17. A. Apblett, S. Kuriyavar and B. Kiran, *J. Mater. Chem.* **2003**,*13(5)*, 983.

18. H. Toraya, M. Masahiro and S. Somiya, *Comm. Am. Ceram. Soc.*, **1984**, C-119.

19. G. Svehla, *Vogel's Quantitative Inorganic Analysis,* Seventh Edition, Longman Group Limited: London, 1997.

20. A. Clearfield, *Reviews of Pure and Applied Chemistry*, **1964**, *14*, 91.

21. Ye, Wumao, Univ. California, Berkeley, Ph.D. Thesis, **1990**, 174 pp.

22. G. Deacon; R. Phillips, *Coord. Chem. Rev.* **1980**, *33*, 227.

23. V. Bolis; G. Magnacca; G. Cerrato; C. Morterra, *Topics in Catalysis*, **2002**, *19*, 259.

24. C. Morterra; M. Penarroya; and G. Cerrato, *Phys. Chem. Chem. Phys.* **2002**, *4*, 676.

25. V. Bolis; G. Mangnacca; G. Cerrato; C. Morterra, *Thermochimica Acta.* **2001**, *379*, 147.

26. R. Gomez; T. Lopez, *J. Sol-Gel Sci. Technol.* **1998**, *11*, 309.

27. K. Manish; T. Beena; V. Raksh, *Ind. Eng. Chem. Res.* **2003**, 42, 5727.

# CHAPTER 3

## SYNTHESIS OF SULFATED ZIRCONIA POWDERS DERIVED FROM SINGLE SOURCE ZIRCONIUM SULFONATE PRECURSORS

### INTRODUCTION:

The purpose of the research reported herein is to develop zirconium sulfonate complexes as single source precursors for sulfated zirconia. Sulfonate dyes, such as 2-hydroxy-5-methylazobenzene-4-sulfonic acid, were used extensively in the past to determine gravimetrically the contents of zirconium metal in samples [1]. This is because of a strong tendency of the dye towards formation of stable bonds with zirconium atoms. The anions of the sulfonic acid are believed to be bonded covalently with zirconium metal to form salts such as $[Zr(SO_3R)_n]^{+(4/n)}$. As a matter of fact, the chemistry of transition metal coordination by sulfonates is not as well studied or understood as that of phosphates and carboxylates. It is well known that sulfonate ions are poor ligands and they are weakly bound or non-bonded to most of the transition metals [2]. Furthermore, as in the case of carboxylates, sulfonate groups can be coordinated to the center of the transition metal in variety modes. Sulfonates can bond in a monodentate fashion, a O-O chelating bidentate fashion, or they can bridge two metal centres via two oxygen atoms or sometimes even via one oxygen atom [3,4]. Figure 3-1 shows the schematic diagram for some bonding modes of sulfonate groups.

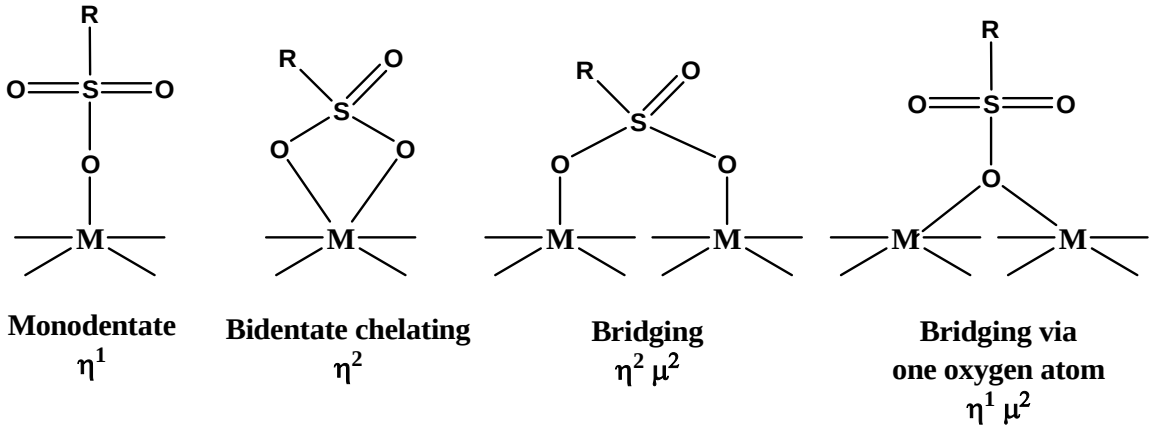


**Figure 3-1: Some coordination modes of the sulfonate groups.**

Generally, sulfated zirconias are synthesized by precipitation of zirconium hydroxide from a variety of zirconium salts by aqueous ammonia solution, followed by sulfation using ammonium sulfate or sulfuric acid solutions [5-9]. The only single precursor source utilized for the synthesis of sulfated zirconia disclosed in the literature is zirconium sulfate. Thermal decomposition of zirconium sulfate leads to the formation of zirconium oxide and sulfur trioxide, which can be retained on the zirconia surface to give sulfated zirconia [10,11]. However, the acid strength and the catalytic activity of the oxide prepared via this pathway are much lower than that of zirconia prepared by conventional procedures. This is presumably due to the decomposition mechanism, which facilitates the rapid loss of sulfur species and hence reduces the surface acidity. The physical and chemical properties such as the specific surface area, number and type of active sites, crystalline structure and phase composition are believed to be strongly influenced by several factors such as, preparation procedure, thermal treatment, nature of the starting materials, and type of sulfation agents [12,13].

At present, there are no comprehensive studies in the literature describing the synthesis and characterization of sulfated zirconia from zirconium sulfonate complexes. In this chapter of the thesis, several zirconium sulfonate complexes that were synthesized and utilized as single-source precursors for sulfated zirconia will be reported. Zirconium oxychloride and zirconium hydroxyl acetate were used as the starting reagents for preparation of zirconium complexes. Upon thermal treatment of precursors, sulfated zirconia was prepared with profoundly diverse physical and chemical properties. The effect of the starting precursor on the physical and chemical properties of the resultant sulfated zirconium oxide will be addressed in this section.

**EXPERIMENTAL:**

**Chemicals:**

All the chemicals were purchased and used without any further purification. The chemicals that used in this section were as follows; zirconium oxychloride [$ZrOCl_2 \cdot 8H_2O$, Alfa Aesar], zirconium(IV) acetate hydroxide [$(CH_3CO_2)_xZr(OH)_y$ ($X+Y \approx 4$), Aldrich], 8-hydroxyquinoline-5-sulfonic acid [$C_9H_7SO_4N$, Aldrich], 8-hydroxyquinoline [$C_9H_7ON$, Aldrich], *p*-toluenesulfonic acid monohydrate [$CH_3C_6H_4SO_3H.H_2O$, Aldrich], sodium dodecyl sulfate [$CH_3(CH_2)_{10}SO_4^-Na^+$, K & K Laboratories, INC.], ethanesulfonic acid [$CH_3CH_2SO_3H$, Aldrich], hexadecyl sulfuric acid, sodium salt (contains 40% sodium stearylsulfate) [$CH_3(CH_2)_{15}SO_4^-Na^+$, Aldrich], cyclohexane [$C_6H_{12}$, Fisher Scientific], cyclohexylamine [$C_6H_{11}NH_2$, Aldrich], trans-chalcone [$C_{15}H_{12}O_5$, Aldrich], anthraquinone [$C_{14}H_8O_2$, TCI], phenanthrene [$C_{14}H_{10}$, TCI], hexamethyl-pararosaniline chloride (crystal violet) [$C_{25}H_{30}N_3Cl$, Spectrum],

neutral red [$C_{15}H_{17}ClN_4$, TCI], dicinnamalacetone [$C_{21}H_{18}O$, TCI], 4-phenylazo-1-naphthylamine hydrochloride [$C_{16}H_{14}N_3Cl$, TCI], *p*-dimethylaminoazobenzene (methylene yellow) [$C_{14}H_{15}N_3$, TCI], acetonylacetone [$C_6H_{10}O_2$, Aldrich], 2.5-dimethylfurane [$C_6H_8O$, Aldrich], 3-methyl-2-cyclopentene-1-one [$C_6H_8O$, Aldrich] and benzene [$C_6H_6$, Fisher Scientific].

**Synthesis of the zirconium sulfonate precursors:**

Figure 3-2 showed the chemical structure of sulfonate ligands used for the synthesis of zirconium sulfonate complexes.

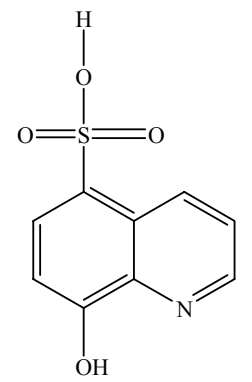

8-hydroxyquinoline-5-sulfonic

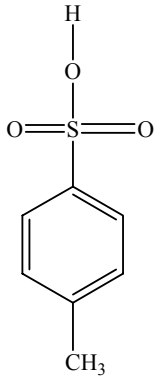

*p*-toluene sulfonic acid

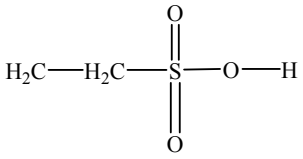

ethane sulfonic acid

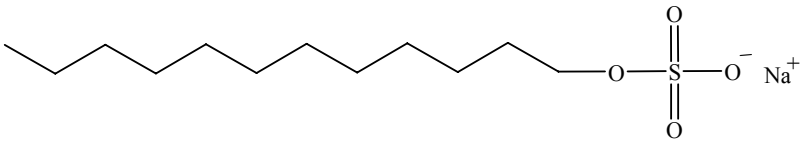

sodium dodecyl sulfate

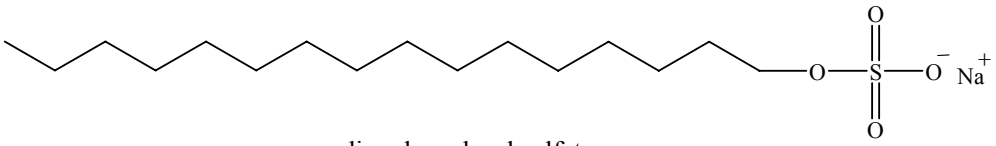

sodium hexadecyl sulfate

**Figure 3-2: The chemical structure of sulfonic acids used for the preparation of zirconium sulfonate single precursors.**

**Precursors from the reaction of zirconium salts with aqueous solutions of ethanesulfonic acid:**

Zirconium acetate and zirconium oxychloride were reacted with ethanesulfonic acid with variant mole ratios of the zirconium salt to ethanesulfonic acid followed by drying to give amorphous powders. The prepared precursors are as following:

***Reaction of zirconium acetate with ethanesulfonic acid with (1:0.25) mole ratio $[Zr(O)_{0.9}(OH)_1(OAC)_1(ESA)_{0.2}]\cdot 0.8H_2O$ (SZ-1(1:0.25)):***

A sample of 5.35 g (25 mmol) zirconium acetate was dissolved in 20 ml of distilled water in a 250ml beaker. An amount of 0.98 g (6.25 mmol) of ethanesulfonic acid (70 wt% solution in water) was dissolved in 30 ml of de-ionized water. The ethanesulfonic acid solution was added slowly to the zirconium acetate solution. Ethyl sulfonate groups replaced the acetate ligands and released acetic acid into the solution. The precursor was obtained by evaporation of water and acetic acid from the solution, followed by drying under vacuum for 12 hours. The reaction yielded 5.48 g (98% based on zirconium acetate). IR($cm^{-1}$)(KBr): 3324(s, br), 2991(s), 2948(s), 2881(m), 1578(s), 1454(s), 1342(w), 1261(m), 1193(m), 1144(m), 1042(m), 977(vw), 745(w), 654(w), 527(vw). $^{13}C$ NMR: δ 179.1, 23.6 ($CH_3COO$), 8.8, 45.7 ($CH_3CH_2SO_3$).

***Reaction of zirconium acetate with ethanesulfonic acid with (1:0.5) mole ratio $[Zr(O)_{1.25}(OAC)_1(ESA)_{0.5}]\cdot 0.5H_2O$ (SZ-1(1:0.5)):***

A sample of 5.35 g (25 mmol) zirconium acetate was dissolved in 20 ml of distilled water in a 250ml beaker. An amount of 1.95 g (12.5 mmol) of ethanesulfonic

acid (70 wt% solution in water) was dissolved in 30 ml of de-ionized water. The ethanesulfonic acid solution was added slowly to the zirconium acetate solution. The precursor was obtained by evaporation of water and acetic acid from the solution followed by drying under vacuum for 12 hours. The reaction yielded 5.95 g (97% based on zirconium acetate). IR($cm^{-1}$)(KBr): 3329(s, br), 2988(s), 2942(s), 2884(m), 1575(s), 1456(s), 1347(w), 1261(m), 1193(m), 1144(m), 1042(m), 977(vw), 745(w), 654(w), 527(vw). $^{13}C$ NMR: δ 179.1, 23.6 ($CH_3COO$), 8.8, 45.7 ($CH_3CH_2SO_3$).

***Reaction of zirconium acetate with ethanesulfonic acid with (1:1) mole ratio $[Zr(O)_{1.3}(OAC)_{0.6}(ESA)_{0.8}]\cdot 2H_2O$ (SZ-1(1:1)):***

A sample of 5.35 g (25 mmol) zirconium acetate was dissolved in 20 ml of distilled water in a 250ml beaker. Then, 3.90 g (25 mmol) of ethanesulfonic acid (70 wt% solution in water) was dissolved in 30 ml of de-ionized water. Ethanesulfonic acid solution was added slowly to the zirconium acetate solution. The precursor was obtained by evaporation of water and acetic acid from the solution, followed by drying under vacuum for 12 hours. The reaction yielded 6.83 g (98% based on zirconium acetate). IR($cm^{-1}$)(KBr): 3337(s, br), 2982(m), 2943(m), 2884(m), 1652(w), 1557(m, sh), 1455(m), 1379(vw), 1347(vw), 1275(m), 1227(m), 1186(m), 1138(m), 1041(m), 745(w), 674(w), 649(w), 518(vw). $^{13}C$ NMR: δ 179.5, 23.6 ($CH_3COO$), 8.8, 45.7 ($CH_3CH_2SO_3$).

***Reaction of zirconium acetate with ethanesulfonic acid with (1:2) mole ratio $[Zr(O)_{0.9}(OAC)_{0.4}(ESA)_{1.8}]\cdot 2.2H_2O$ (SZ-1(1:2)):***

A sample of 5.35 g (25 mmol) zirconium acetate was dissolved in 20 ml of distilled water in a 250ml beaker. Next, 7.80 g (50 mmol) of ethanesulfonic acid (70 wt% solution in water) was dissolved in 30 ml of de-ionized water. Ethanesulfonic acid solution was added slowly to the zirconium acetate solution. The precursor was obtained by evaporation of water and acetic acid from the solution followed by drying under vacuum for 12 hours. The reaction yielded 8.83 g (97% based on zirconium acetate). IR($cm^{-1}$)(KBr): 3518(s, br), 3348(s, br), 2985(s), 2946(m), 2886(m), 2047(vw), 1641(w), 1540(w), 1459(m, sh), 1416(w), 1382(vw), 1308(m, br), 1220(m), 1147(w), 1110(w), 1076(w), 981(vw), 746(w), 660(w), 596(w), 536(w). $^{13}C$ NMR: δ 179.8, 23.7 ($CH_3COO$), 8.4, 46.3 ($CH_3CH_2SO_3$).

***Reaction of zirconium acetate with ethanesulfonic acid with (1:3) mole ratio $[Zr(O)_{0.5}(ESA)_3]\cdot 3H_2O$ (SZ-1(1:3)):***

A sample of 5.35 g (25 mmol) zirconium acetate was dissolved in 20 ml of distilled water in a 250ml beaker. A sample of 11.7 g (75 mmol) of ethanesulfonic acid (70 wt% solution in water) was dissolved in 30 ml of de-ionized water. Ethanesulfonic acid solution was added slowly to the zirconium acetate solution. The precursor was obtained by evaporation of water and acetic acid from the solution followed by drying under vacuum for 12 hours. The reaction yield was 11.7 g (≈100% based on zirconium acetate). IR($cm^{-1}$)(KBr): 3348(s, br), 2983(s), 2946(s), 2885(m), 2441(w), 2201(w), 1640(m), 1459(m, sh), 1417(w), 1293(s), 1233(m), 1150 (m), 1130(m), 1048(m),

1005(m), 973(m), 748(m), 651(vw), 595(vw), 522(w). $^{13}C$ NMR: δ 8.5, 46.5 ($CH_3CH_2SO_3$).

***Reaction of zirconium oxychloride with ethanesulfonic acid with (1:2) mole ratio $[Zr(O)_{0.75}(ESA)_{1.5}(Cl)_1]\cdot 5H_2O$ (SZ-2):***

A sample of 6.44 g (20 mmol) zirconium oxychloride was dissolved in 20 ml of distilled water in a 250ml beaker. A sample of 5.70 g (150 mmol) of ethanesulfonic acid (70 wt% solution in water) was dissolved in 30 ml of de-ionized water. The ethanesulfonic acid solution was then added slowly to the zirconium oxychloride solution. The precursor was obtained by evaporation of water from the solution followed by drying under vacuum for 12 hours. The reaction yielded 6.72 g (93% based on zirconium oxychloride). IR($cm^{-1}$)(KBr): 3341(s, br), 2985(s), 2946(s), 2886(m), 1634(m), 1458(m, sh), 1417(w), 1383(vw), 1292(s), 1230(m), 1135(m), 1043(m), 976(w), 782(vw), 747(m), 642(vw), 590(vw), 531(w).

**Precursor from the reaction of zirconium salts with other sulfonate reagents:**

***Reaction of zirconium acetate with p-toluene sulfonic acid***

***$[Zr(O)_{0.8}(OH)_1(OAc)_1(PTSA)_{0.4}]\cdot 1H_2O$ (SZ-3):***

A sample of 10.6 g (50 mmol) zirconium acetate was dissolved in 40 ml of distilled water in a 250ml beaker. An amount of 9.51 g (50 mmol) of *p*-toluenesulfonic acid was dissolved in 30 ml of de-ionized water. The zirconium solution was added slowly to the acid solution. A white precipitate was formed immediately. The precipitate

was filtered, washed with distilled water and dried under vacuum for 24 hours. The reaction yield was 13.2 g (93% based on zirconium acetate). IR($cm^{-1}$)(KBr): 3487(br, m), 3062(m), 2015(vw), 1960(vw), 1695(w), 1567(m), 1522(w), 1454(m), 1378(vw), 1347(w), 1249(w), 1156(w), 1156(w), 1125(w), 1035(w, sh), 1009(w, sh), 814(w), 658(w), 570(w).

***Reaction of zirconium oxychloride with p-toluene sulfonic acid***

***$[Zr(OH)_{1.5}(PTSA)_2Cl_{0.5}]\cdot 5H_2O$ (SZ-4) :***

A sample of 25.7 g (80 mmol) of zirconium oxychloride octahydrate was dissolved in 30ml of distilled water in a 250 ml beaker. A sample of 30.4 g (160 mmol) of *p*-toluenesulfonic acid was dissolved in 30 ml of de-ionized water. The zirconium solution was added slowly to the acid solution to form a color less solution. The solution was left in the fume hood for precipitation and recrystallized for 12 days. The precipitate formed was filtered, washed with de-ionized water and dried under vacuum for 24 hours. The reaction yielded 34.0 g (84% based on zirconium oxychloride). IR($cm^{-1}$)(KBr): 3354(s, br), 3064(m), 2986(m), 2952(m), 2922(m), 1916(w), 1629(m), 1600(m), 1496(m), 1450(w), 1275(m), 1151(s), 1127(s), 1036(s), 1009(s), 813(m), 783(w), 685(m), 565(m).

***Reaction of zirconium acetate with 8-hydroxyquinoline-5-sulfonic acid***

***$[Zr(O)_{0.5}(OH)_2(OAc)_{0.7}(HQSA)_{0.3}]\cdot 1.5H_2O$ (SZ-5):***

A sample of 21.0 g (50 mmol) of 8-hydroxyquinoline-5-sulfonic acid was suspended in 200ml of distilled water in a round-bottomed flask. Then, 10.1 g (100

mmol) of zirconium acetate ($Zr(OAC)_x(OH)_y$) was dissolved in 150ml of distilled water in 250 ml beaker. This solution was added gradually to the zirconium solution. The reaction mixture was then refluxed for 60 hours. A dark yellow, gel-like precipitate was formed. The precipitate was then filtered and washed with a large amount of distilled water to remove any unreacted starting materials. Finally the precipitate was dried under vacuum for 12 hours. The purity of the product was determined by recording the X-ray pattern after washing until peaks due to the starting materials disappeared. The reaction yielded 23.8 g. (81% based on zirconium acetate). IR($cm^{-1}$)(KBr): 3419(s br), 3080(m), 1599 (m, sh), 1574(m), 1502(m, sh), 1465(m), 1373(w), 1325(m), 1236(w), 1195(w), 1159(m), 1093(vw), 1036(m), 838(w), 699(w), 613(w).

***Reaction of zirconium oxychloride with 8-hydroxyquinoline-5-sulfonic acid $[Zr(O)_{1.5}(HQSA)_1]\cdot 1H_2O$ (SZ-6):***

A sample of 20.2 g (90 mmol) of 8-hydroxyquinoline-5-sulfonic acid was added to 200ml of distilled water in a round-bottomed flask. A sample of 14.3 g (45 mmol) of zirconium oxychloride was dissolved in 150 ml of distilled water in 250ml beaker. The solution was added gradually to the former solution and refluxed for 68 hours. A yellow, gel-like, precipitate was formed. The precipitate was filtered and washed with a large amount of distilled water to remove all the unreacted starting materials. Finally, the precipitate was dried under vacuum for 12 hours. The purity of the product was determined by registering the X-ray pattern after washing until the disappearance of peaks due to the starting metal. The reaction yielded 23.8 g (71.3% based on zirconium oxychloride). IR($cm^{-1}$)(KBr): 3413 (s, br), 3080 (m), 1629 (w), 1602 (m), 1576 (m),

1501 (s, sh), 1465 (m), 137 (m), 1323 (m), 1223 (m), 1196 (m), 1161 (m), 1094 (vw), 1037 (m, sh), 965 (vw), 840 (w), 700 (w), 613 (w), 561(w), 510 (w).

***Reaction of zirconium acetate with 8-hydroxyquinoline***

***$[Zr(O)_{0.8}(OAc)_{0.6}(HQ)_{1.8}]\cdot 1H_2O$ (SZ-7):***

A sample of 13.6 g (90 mmol) of 8-hydroxyquinoline were suspended to 200 ml of distilled water in a round-bottomed flask. A sample of 9.54 g (45 mmol) of zirconium acetate was dissolved in 100ml of distilled water in 250ml beaker. The solution was added gradually to the previous solution with continuous reflux for 21 hours. During this addition the organic color of the 8-hydroxyquinoline solution faded and a yellow precipitate formed. The precipitate was then filtered and washed with distilled water to remove all the residual materials. Finally, the precipitate was dried under vacuum for 12 hours. The purity of the product was determined by recording the X-ray pattern after washing until the disappearance of starting metals peaks. The reaction yielded 10.6 g (88.5% based on zirconium acetate). IR ($cm^{-1}$)(KBr): 3412(w, br), 3045(w), 1603(m), 1574(s), 1496(s, sh), 1465(s, sh), 1424(w), 1378(s), 1320(s, sh), 1276(m), 1228(w), 1173(vw), 1109(s), 1052(w), 1029(w), 909(w), 822(m), 806(w), 785(m), 740(m), 644(w), 615(w), 515(m), 495(w).

***Reaction of zirconium oxychloride with 8-hydroxyquinoline $[Zr(O)_{1.5}(HQ)_1]\cdot 0.5H_2O$ (SZ-8):***

A sample of 13.6 g (90 mmol) of 8-hydroxyquinoline was suspended to 200ml of distilled water in a round-bottomed flask. A sample of 14.5 g (45 mmol) of zirconium

oxychloride was dissolved in 40ml of distilled water in 100ml beaker. This solution was added gradually to the previous solution. The mixture was refluxed for 21 hours. The color of the solution was changed upon addition from orange to yellow color precipitate. The precipitate was separated by centrifuge and washed with distilled water four times to remove all the unreacted starting materials. Finally it was dried under vacuum for 12 hours. The purity of the product was determined by recording the X-ray pattern after washing until disappearance of peaks due to the starting metals. The reaction yielded 8.35 g (77.39% based on zirconium oxychloride). IR($cm^{-1}$)(KBr): 3266 (m, br), 3080 (m), 1606 (m), 1578 (m), 1544 (w), 1501 (s, sh), 1470 (s), 1423(m), 1379 (m), 1321 (s), 1274 (m), 1239 (w), 1175 (w), 1109 (m), 1056 (w), 823 (m), 741(m), 643(w), 517 (w).

***Reaction of zirconium acetate with sodium dodecyl sulfate***

***$[Zr(O)_{0.5}(OH)_1(OAc)_{1.5}(SDS)_{0.5}]\cdot 1H_2O$ (SZ-9):***

A sample of 8.00 g (28 mmol) of sodium dodecyl sulfate were added to 400 ml of de-ionized water with continues stirring until all the salt dissolved in a 1 L beaker. An amount of 3.10 g (14.6 mmol) of zirconium dichloride oxide was dissolved in 50ml of deionized water in a 250ml beaker. The latter solution was added gradually to the previous solution with continues stirring at room temperature for 30 minuets to give a white precipitate. The precipitate was filtered and washed with enough distilled water to remove all the residual materials, and it was then dried under vacuum for 12 hours. The reaction yielded 8.60 g (82.6 % based on zirconium acetate). IR($cm^{-1}$)(KBr): 3525(s, br), 2978(s), 2924(s), 2853(s), 2030(w,br), 1577(m), 1459(m), 1346(w), 1280(w), 1241(w), 1195(w), 1059(w), 977(w), 687(vw).

***Reaction of zirconium oxychloride with sodium dodecyl sulfate $[Zr(O)_{1.5}(SDS)_1]\cdot 1H_2O$ (SZ-10):***

A sample of 7.20 g (26.5 mmol) of sodium dodecyl sulfate was added to 400 ml of de-ionized water with continuous stirring until all the salt dissolved in a 1 L beaker. Then, 4.03 g (12.5 mmol) of zirconium oxychloride were dissolved in 50ml of de-ionized water in 250ml beaker, the later solution was added gradually to the previous solution with continuous stirring at room temperature for 30 minutes to give a white. The precipitate was filtered and washed with enough distilled water to remove all the residual materials, finally it was dried under vacuum for 12 hours. The reaction yielded 4.49 g (97% based on zirconium oxychloride). IR($cm^{-1}$)(KBr): 3400(s, br), 2952(s), 2922(s), 2852(s, sh), 1641(m), 1467(m, sh), 1378(vw), 1287(m), 1170(m), 1063(w), 966(m), 828(w), 721(w), 576(w, br).

***Reaction of zirconium acetate with sodium hexadecyl sulfate $[Zr(O)_{0.7}(OAc)_2(HDSA)_{0.6}]\cdot 1H_2O$ (SZ-11):***

A sample of 16.3 g (47 mmol) of sodium hexadecylsulfate was dissolved in 300 ml of distilled water in a round-bottomed flask. A sample of 10.0 g (47 mmol) of zirconium acetate hydroxide was dissolved in 60ml of distilled water in 100ml beaker. This solution was added gradually to the previous solution resulting in immediate formation of a white precipitate. After stirring for three hours, the precipitate was filtered off and washed with distilled water several times to remove all the impurities and unreacted starting materials. Finally it was dried under vacuum for 12 hours. The reaction yielded 21.4 g (≈100% based on zirconium acetate). IR($cm^{-1}$)(KBr): 3450(m,

br), 2956(s), 2926(s), 2851(s), 2017(w), 1581(s), 1470(m), 1450(m), 1378(w), 1346(w), 1262(m), 1210(m), 1083(w), 998(w), 829(m), 719(m), 647(m), 493(m).

***Reaction of zirconium oxychloride with sodium hexadecyl sulfate:***

***$[Zr(O)_{1.55}(HDSA)_{0.9}]\cdot 1H_2O$ (SZ-12):***

A sample of 8.60 g (25 mmol) of sodium hexadecylsulfate was dissolved in 200 ml of distilled water in a round-bottomed flask. Next, 8.20 g (25 mmol) of zirconium oxychloride were dissolved in 40ml of distilled water in 100ml beaker. The solution was added gradually to the previous solution and a white precipitate was formed immediately. The solution was continuously stirred for three hours. The precipitate was filtered off and washed with distilled water several times to remove all the impurities and unreacted starting materials. It was then dried under vacuum for 12 hours. The reaction yielded 11.98g (≈100% based on zirconium oxychloride). IR($cm^{-1}$)(KBr): 3454(s, br), 2954(s), 2919(s), 2850(s), 1639(w), 1468(m, sh), 1392(vw), 1375(vw), 1282(m), 1173(m), 1066(w), 976(w), 722(vw).

**Characterization:**

In addition to the characterization techniques that discussed previously in detail in Chapters 2, $^{13}C$ NMR was also used for the characterization of the prepared zirconium complexes. $^{13}C$ spectra were obtained with a Chemagnetics CMX-II solid-state NMR spectrometer operating at 75.694 MHz for carbon-13 and a Chemagnetics 5mm double resonance magic-angle spinning probe. Carbon-13 cross-polarization/magic-angle spinning (CP/MAS) was carried out with a quasi-adiabatic sequence (1) using two pulse

phase modulation (TPPM) decoupling (2) at 50-75 kHz. The C-13 CP contact pulse of 1 msec length was divided into 11 steps of equal length with ascending radiofrequency field strength, while the H-1 contact pulse had constant radiofrequency field strength. At least 3600 scans were acquired with a delay of 1.0 s between scans. The MAS sample spinning frequency was 6.0 kHz, maintained to within a range of +/- 5 Hz or less with a Chemagnetics speed controller.

**Acidity measurements:**

The acidity measurements for the synthesized sulfated zirconia catalysts were conducted using three different procedures as follows:

***Acidity measurements using cyclohexylamine probe:***

The total acidity of the synthesized zirconias was determined from Langmuir adsorption isotherm using cyclohexylamine as an adsorbate (a titration agent) [14,15]. The concentration of non-adsorbed base in equilibrium with the concentration of the adsorbed base on the surface of solid (C) was determined from the difference in the UV absorption before and after the adsorption of the titrating agent on the sulfated zirconia surface. A solution of approximately 5.0 x $10^{-2}$ (moles/l) cyclohexylamine in cyclohexane ($\lambda_{max} \approx 226$ nm) was prepared. A sample of 10 ml of the cyclohexylamine solution was added to a specific amount of sulfated zirconia in a 20-ml glass vial. This mixture was then stirred for 12 hours, the mixture was filtered off and then the UV absorption was measured at the $\lambda_{max}$ of the cyclohexylamine solution to give the equilibrium concentration (C) and the amount of the base adsorbed per gram of the

zirconia (X). The number of acidic sites on the surface of the oxide expressed in μmol/g is equal to the amount of adsorbate adsorbed by the oxide to form a monolayer ($X_m$), which is equal to the reciprocal of the slope of the straight line obtained from the plot of C/X versus C according to the Langmuir equation (eq 3-1).

$$C/X = C/ X_m + b/ X_m \qquad \textbf{Eq 3-1}$$

Where *b* is a characteristic constant of the adsorbent under study state which can be determined experimentally by dividing the intercept by the slope.

***Acid strength using Hammett indicators:***

The acid strength of the prepared sulfated zirconia powders was determined using Hammett organic base indicators [16]. This determination is based on the ability of the oxide surface to change the organic base indicator into its conjugate acid due to transfer of proton from Brønsted acid site on the surface to the indicator. The lower the Ho value, the higher the acidity of the oxide surface. If the surface sites have a Ho values less than the pKa values of the indicators, the color will change as a result of the acid base reaction on the surface.

The indicator solutions were prepared in 1% wt/wt concentration by dissolving of 0.5 g of the organic indicator in 50 ml of dry benzene since water can affect the results by rapid adsorption on the surface oxide. The sample surface was cleaned prior performing the tests by heating the samples under vacuum at 80 ºC for 2 hours. The acidity strength was experimentally determined by addition of 0.1g of the solid to 2 ml of dry benzene in

20 ml test tube followed by addition of 1ml of the indicator solution. The tube was covered and left for one hour to allow equilibrium to occur before recording the color changed. The pKa values of the conjugate acid of the indicators as well as the acid-base color is shown in Table 3-1 while the chemical structure of the Hammett organic base indicators used in this study is shown in Figure 3-3.

**Table 3-1: The pKa values of Hammett indicators conjugate acids along with its acid-base colors.**

| Indicator | pKa | Wt % $H_2SO_4$ of equivalent strength | Basic color | Acid color |
|---|---|---|---|---|
| **A) neutral red** | 6.8 | - | Yellow | Red |
| **B) *p*- dimethylaminoazobenzene** | 3.3 | $3 \times 10^{-4}$ | Yellow | Red |
| **C) 4-phenylazo-1-naphthylamine hydrochloric acid** | 1.5 | - | Yellow | Purple |
| **D) hexamethyl-paraosaniline chloride (crystal violet)** | 0.8 | - | Blue | Yellow |
| **E) dicinnamalacetone** | -3.0 | 48 | Yellow | Red |
| **F) trans-chalcone** | -5.7 | 72 | Color less | Yellow |
| **G) anthraquinone** | -8.2 | 90 | Color less | Yellow |
| **H) 4-nitrotoulene** | -11.4 | 100 | Color less | Yellow |

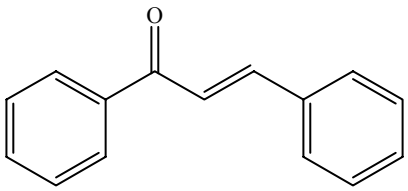

**trans- chalcone**

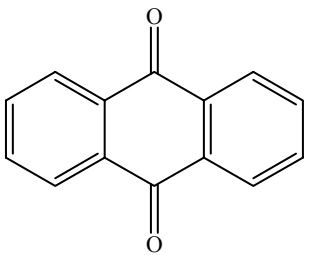

**anthraquinone**

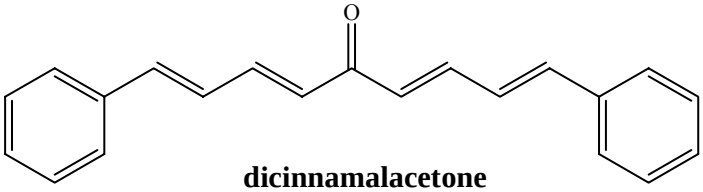

**dicinnamalacetone**

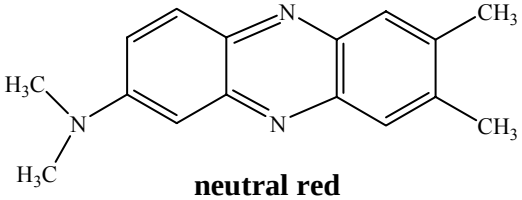

**neutral red**

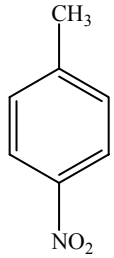

***p*-nitrotoluene**

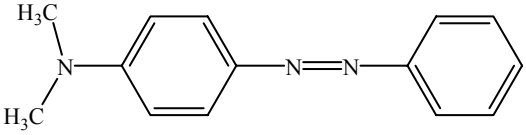

***p*-dimethylaminoazobenzene**
**(methylene yellow)**

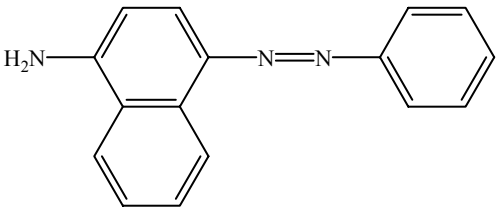

**4-phenylazo-1-naphthylamine**

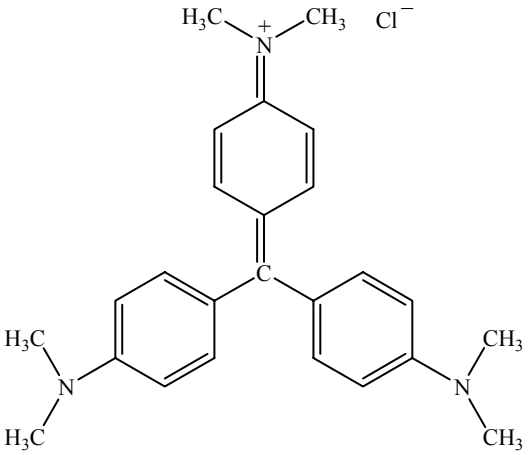

**hexamethyl-pararosaniline chloride**
**(crystal violet)**

**Figure 3-3: Hammett organic base indicators used to evaluate the acidity strength of sulfated zirconia.**

***Acidity Evaluation via acetonylacetone conversion reaction:***

Acetonylacetone can undergo an acid-base catalyzed intermolecular cyclization reaction [17]. In this part of the work, an attempt to use acetonylacetone as a probe to determine the ability of the different synthesized sulfated zirconia samples to catalyze the intermolecular cyclization reaction and to utilize this reaction to measure their acid strength was conducted. The acid-catalyzed product out of this reaction is dimethylfuran while the base-catalyzed one is methyl-cyclopentanone. The proposed mechanism for this reaction is shown in Figure 3-4. This reaction was utilized in the current research to estimate the acidity of the oxide catalyst surface. Approximately 1.0 gram of acetonylacetone was added to 0.2 g of the catalyst sample in a Teflon bomb reactor and was heated in the oven at 150 ºC for 20 hours. The acetonylacetone conversion and the dimethylfuran selectivity were obtained from GCMS analysis data.

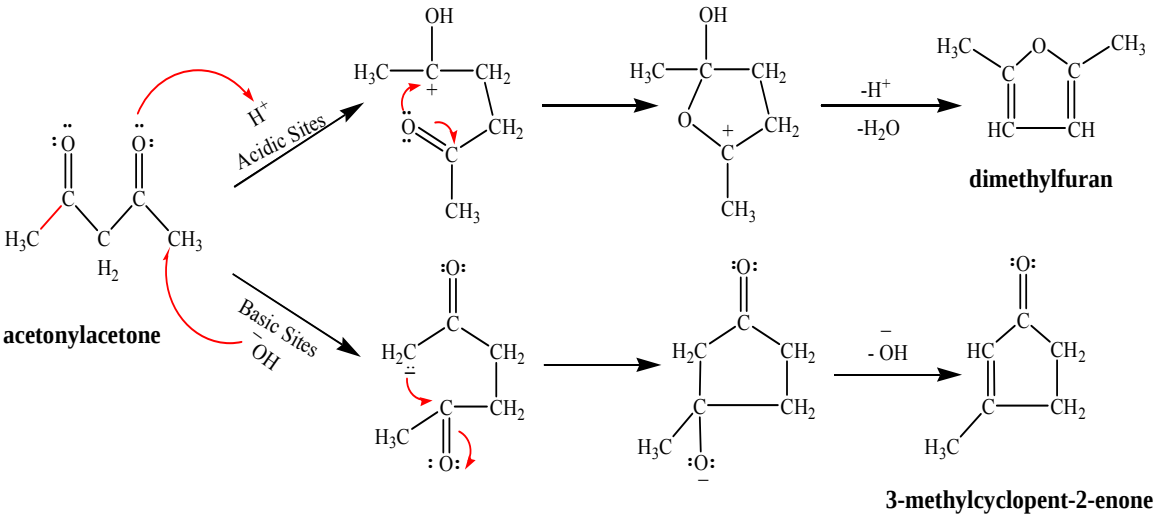


**Figure 3-4: Acid-base catalyzed cyclization of acetonylacetone**

## RESULTS AND DISCUSSIONS

### Precursors obtained from the reaction of zirconium salts with ethanesulfonic acid and its corresponding oxides:

Table 3-2 and Table 3-3 shows the C,H,S elemental analyses and the details of some precursors obtained from the reaction of zirconium acetate and zirconium oxychloride with ethanesulfonic acid in different mole ratios. The possible proposed formulas are deduced based on the elemental analyses and the TGA data.

**Table 3-2: The structures and properties of the synthesized zirconium sulfonate complexes obtained from reaction of zirconium salts with ethanesulfonic acid.**

| Sample code | ‡Initial mixture | Calcination to oxide | | *Oxide Temp. (°C) | ‡ Proposed precursor formula | Surface Area ($m^2/g$) |
|---|---|---|---|---|---|---|
| | | $ZrO_2$ (%) | Molecular weight (gm / mol) | | | |
| **SZ-1(1:0.25)** | ZA with 0.25 ESA | 55.4 | 226 | 700 | $[Zr(O)_{0.9}(OH)_1(OAC)_1(ESA)_{0.2}]\cdot 0.8H_2O$ | ---- |
| **SZ-1(1:0.5)** | ZA with 0.5 ESA | 50. 5 | 243 | 700 | $[Zr(O)_{1.25}(OAC)_1(ESA)_{0.5}]\cdot 0.5H_2O$ | 0.004 |
| **SZ-1(1:1)** | ZA with 1 ESA | 44.5 | 276 | 650 | $[Zr(O)_{1.3}(OAC)_{0.6}(ESA)_{0.8}]\cdot 2H_2O$ | 0.47 |
| **SZ-1(1:2)** | ZA with 2 ESA | 34.0 | 361 | 650 | $[Zr(O)_{0.9}(OAC)_{0.4}(ESA)_{1.8}]\cdot 2.2H_2O$ | 0.28 |
| **SZ-1(1:3)** | ZA with 3 ESA | 26.4 | 465 | 650 | $[Zr(O)_{0.6}(ESA)_{2.8}]\cdot 3H_2O$ | 0.86 |
| **SZ-2** | ZOC with 2 ESA | 31.4 | 392 | 600 | $[Zr(O)_{0.75}(ESA)_{1.5}(Cl)_1]\cdot 5H_2O$ | 0.441 |

***‡ ZA = Zirconium acetate hydroxide; ZOC = zirconium oxychloride; ESA= Ethanesulfonic acid, and OAc = acetate group.***

**** The minimum temperature required for the combustion of precursor to zirconium oxide.***

**Table 3-3: The elemental analysis results for the synthesized zirconium sulfonate complexes obtained from reaction of zirconium salts with ethanesulfonic acid.**

| Sample code | Elemental analysis (%) | | | Product proposed formula | *Expt. Fwt (g/mol) | **Theor. Fwt (g/mol) |
|---|---|---|---|---|---|---|
| | C | H | S | | | |
| **SZ-1(1:0.25)** | 12.3 | 3.29 | 2.62 | $[Zr(O)_{0.9}(OH)_1(OAC)_1(ESA)_{0.2}]\cdot 0.8H_2O$ | 222 | 219 |
| **SZ-1(1:0.5)** | 13.5 | 3.40 | 6.33 | $[Zr(O)_{0.7}(OH)_{1.25}(OAC)_{0.85}(ESA)_{0.5}]\cdot 1H_2O$ | 243 | 247 |
| **SZ-1(1:1)** | 12.1 | 3.54 | 9.52 | $[Zr(O)_{1.3}(OAC)_{0.6}(ESA)_{0.8}]\cdot 2H_2O$ | 276 | 272 |
| **SZ-1(1:2)** | 14.6 | 3.61 | 16.91 | $[Zr(O)_{0.9}(OAC)_{0.4}(ESA)_{1.8}]\cdot 2.2H_2O$ | 361 | 367 |
| **SZ-1(1:3)** | 15.7 | 3.49 | 18.5 | $[Zr(O)_{0.6}(ESA)_{2.8}]\cdot 3H_2O$ | 465 | 464 |
| **SZ-2** | 9.24 | 4.98 | 10.41 | $[Zr(O)_{0.75}(ESA)_{1.5}(Cl)_1]\cdot 5H_2O$ | 392 | 394 |

** from TGA and thermal analysis*

*** from proposed formula*

The TGA profiles of the zirconium sulfonate precursors derived from the reaction of zirconium salts with different concentrations of ethanesulfonic acid are shown in Figure 3-5. The TGA curve of the SZ-1(1:1) sample was slightly different from the SZ-1(1:2) sample. The TGA profile of SZ-1(1:1) exhibited a stepwise thermal decomposition with three distinct regions. A weight loss observed between room temperature and 150 °C is due to evolution of the coordinated water molecules. A gradual decomposition was observed between 150 °C and 350 °C, which can be attributed to the decomposition of the organic sulfate ligands and hydroxy groups. The weight loss between 350 °C and 600 °C is attributed to the decomposition of the acetate ligands. The TGA curve for the SZ-1(1:2) sample, however, showed a sharp weigh loss between 350 °C and 450 °C due to the loss of the additional ethane sulfonate ligands.

The SZ-2 sample has a more significant weight loss before 250 °C. However, chlorine analysis showed that the SZ-2 precursor contains 16% chloride ions. Upon thermal drying at 130 ºC, the chloride content drops to 8%. This implies that the weight loss shown in the TGA profile of the sample SZ-2 (Figure 3-5) in the temperature region from 25 ºC to 250 ºC is attributed to both the loss of water molecules and the loss of chloride ions probably as HCl.

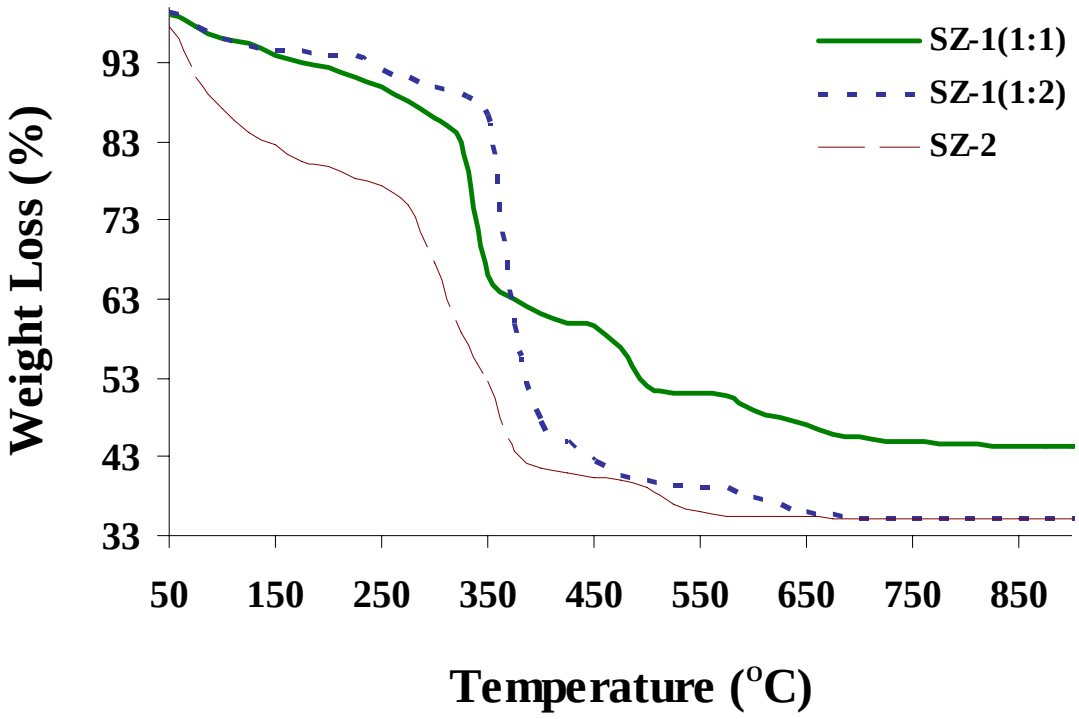


**Figure 3-5: The thermogravimetric analysis (TGA) graphs for the prepared zirconium ethane sulfonate hydroxide precursors: (SZ-1(1:1)): zirconium acetate with 1 mole of ethanesulfonic acid; (SZ-1(1:2)): zirconium acetate with 2 moles of ethanesulfonic acid; (SZ-2): zirconium oxychloride with 2 moles of ethanesulfonic acid.**

The carboxylate stretching frequencies of zirconium acetate complexes occur between 1400 $cm^{-1}$ and 1700 $cm^{-1}$. Table 3-4 and Figure 3-6 list the stretching frequencies of the carboxylate carbonyl group $\nu_{COO(symm)}$ and $\nu_{COO(asymm)}$ and the splitting ($\Delta\nu$) between the asymmetric and symmetric carbonyl stretching frequencies of several synthesized zirconium acetate ethyl sulfonate complexes, which were prepared by the reaction of zirconium acetate with variant amounts of ethanesulfonic acid. The results show clearly that the asymmetric carboxylate absorption stretching frequencies $\nu_{COO(asymm)}$ and the $\Delta\nu$ values decrease dramatically with an increase of the number of ethylsulfonates on the precursors. This is indicative of a change in the mode of coordination of the bridging acetate groups to either wider angle or higher delocalization to the double bond. Additionally, the $^{13}C$ NMR spectra of the zirconium sulfonate precursors obtained from the reaction of zirconium acetate with different mole ratio of ethanesulfonic acid are shown in Figure 3-7. The NMR spectra show that the intensity of the $^{13}C$ acetate peaks at 24 ppm and 178 ppm decreased while the intensity of the $^{13}C$ of the ethylsulfonate at 8.8 ppm and 45.7 ppm increased with an increasing amount of ethylsulfonate until the point at which the acetate peaks disappear completely. These results confirmed the results observed by the IR spectroscopy and clearly suggest that the ethane sulfonate gradually replace the acetate ligands. The complete replacement was observed when the zirconium acetate precursor reacts with three mole equivalents of ethanesulfonic acid.

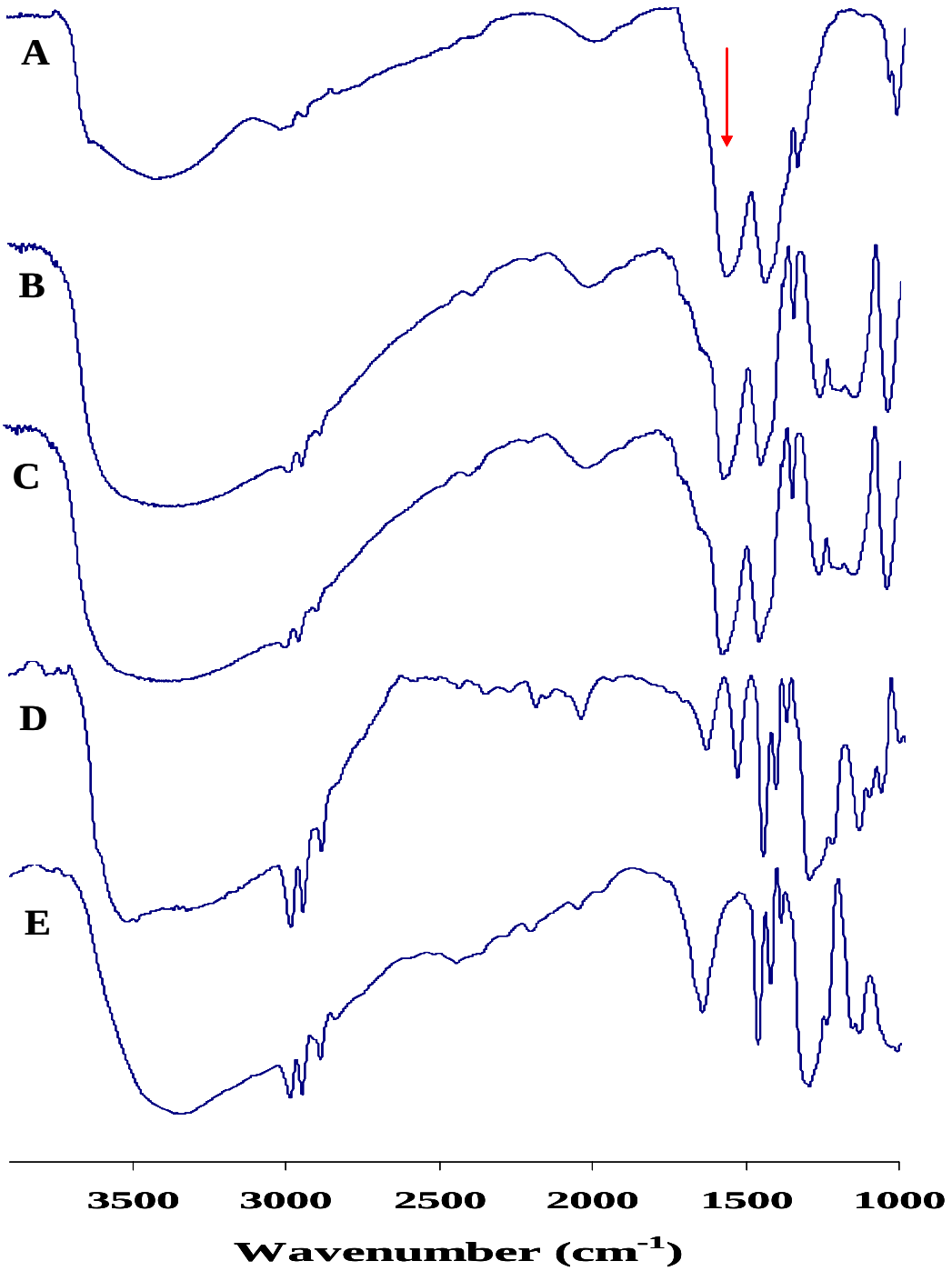


**Figure 3-6: The IR spectra of the zirconium sulfonate precursors obtained from the reaction of 1 mole of zirconium acetate with different mole ratio of ethanesulfonic acid (ESA): A: zirconium acetate; B: with 0.5 ESA; C: with 1 ESA; D: with 2 ESA; and E: with 3 ESA.**

**Table 3-4: IR stretching frequencies of the asymmetric and symmetric carbonyl groups in the synthesized zirconium acetate ethyl sulfonate complexes containing different amount of ethanesulfonic acid.**

| Sample Code | Precursor | pH | $\nu_{COO}$ ($cm^{-1}$) | | Complex $\Delta\nu$ ($cm^{-1}$) |
|---|---|---|---|---|---|
| | | | Asymmetric | Symmetric | |
| *** ZrA** | ZrA | 4.45 | 1573 | 1450 | 123 |
| **SZ-1(1:0.1)** | ZrA with 0.1ESA | 3.70 | 1573 | 1445 | 128 |
| **SZ-1(1:0.5)** | ZrA with 0.5ESA | 2.30 | 1575 | 1456 | 119 |
| **SZ-1(1:1)** | ZrA with 1ESA | 0.56 | 1557 | 1455 | 102 |
| **SZ-1(1:2)** | ZrA with 2 ESA | ≈ 0 | 1540 | 1459 | 81 |

** ZrA = zirconium acetate hydroxide; ESA=ethanesulfonic acid*

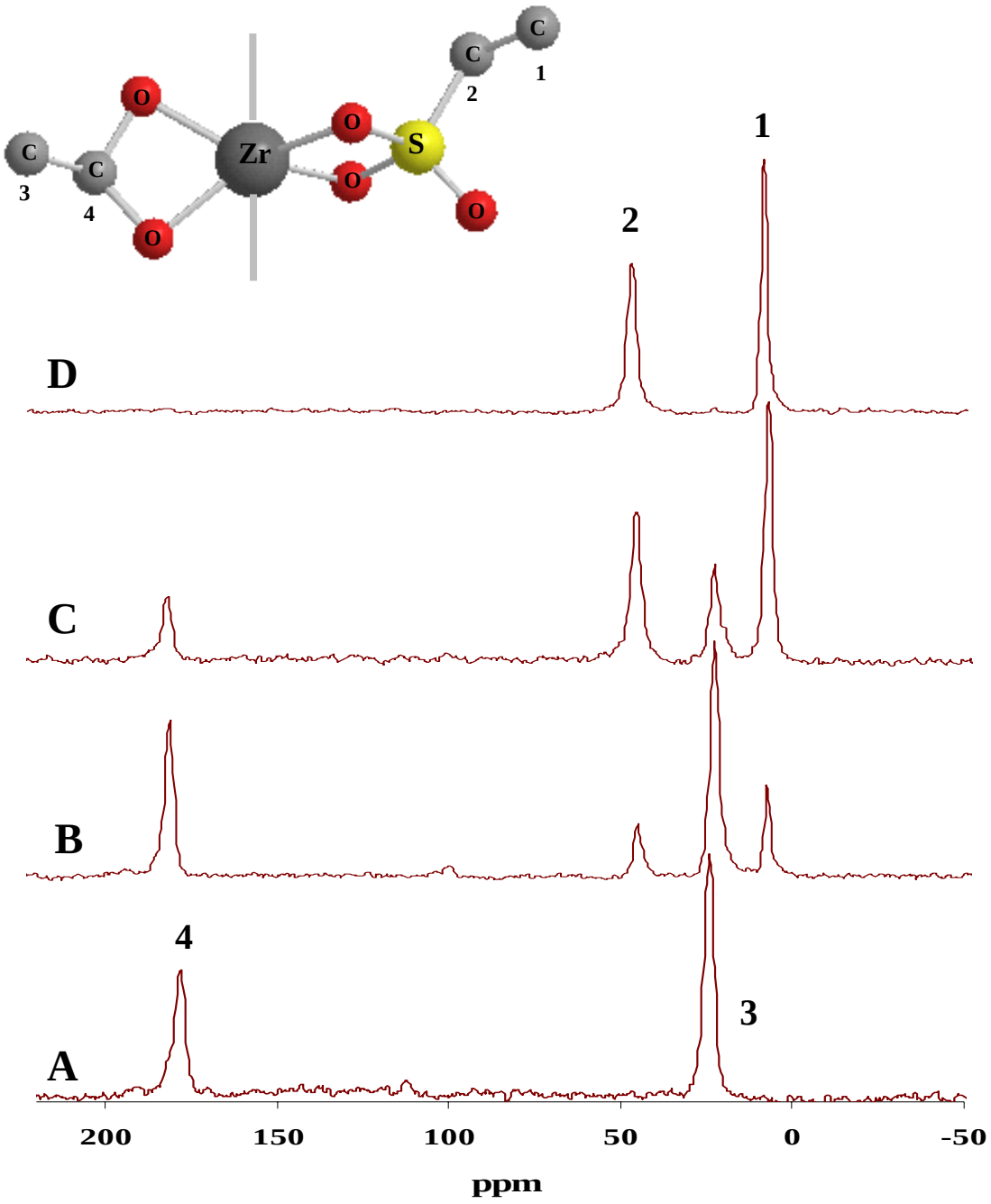


**Figure 3-7: The $^{13}$C NMR spectra of the zirconium precursors obtained from the reaction of 1 mole of zirconium acetate with different mole ratios of ethanesulfonic acid (ESA): A: zirconium acetate; B: with 0.5 ESA; C: with 1ESA; and D: with 3ESA.**

The XRD pattern of the precursor derived from the reaction of zirconium acetate with one mole equivalent of ethanesulfonic acid calcined at different temperatures is shown in Figure 3-8. It is known, that the hydroxyl ions available on the surface of zirconium oxide stabilize the tetragonal phase and delay the transformation to the monoclinic phase [18]. As shown in Figure 3-8, the tetragonal phase started to appear at approximately 500°C. With an increase of the temperature, more crystalline tetragonal phases develop without the appearance of the monoclinic phase until about 950 °C. Comparison of these data with that of zirconium oxide derived from thermal treatment of zirconium carboxylate complexes (discussed in Chapter 2) and with that from zirconium acetate shown in Figure 3-8F revealed that the zirconium sulfonate precursors produce a highly thermally stabile tetragonal phase due to the presence of the sulfate ions. Sulfate ions are believed to increase the thermal energy required to remove the hydroxyl ions during the thermal dehydroxylation process [19]. The phase composition results also show a degree of dependency on the nature of the sulfated zirconia single precursor and on the amount of sulfur species available in the surface.

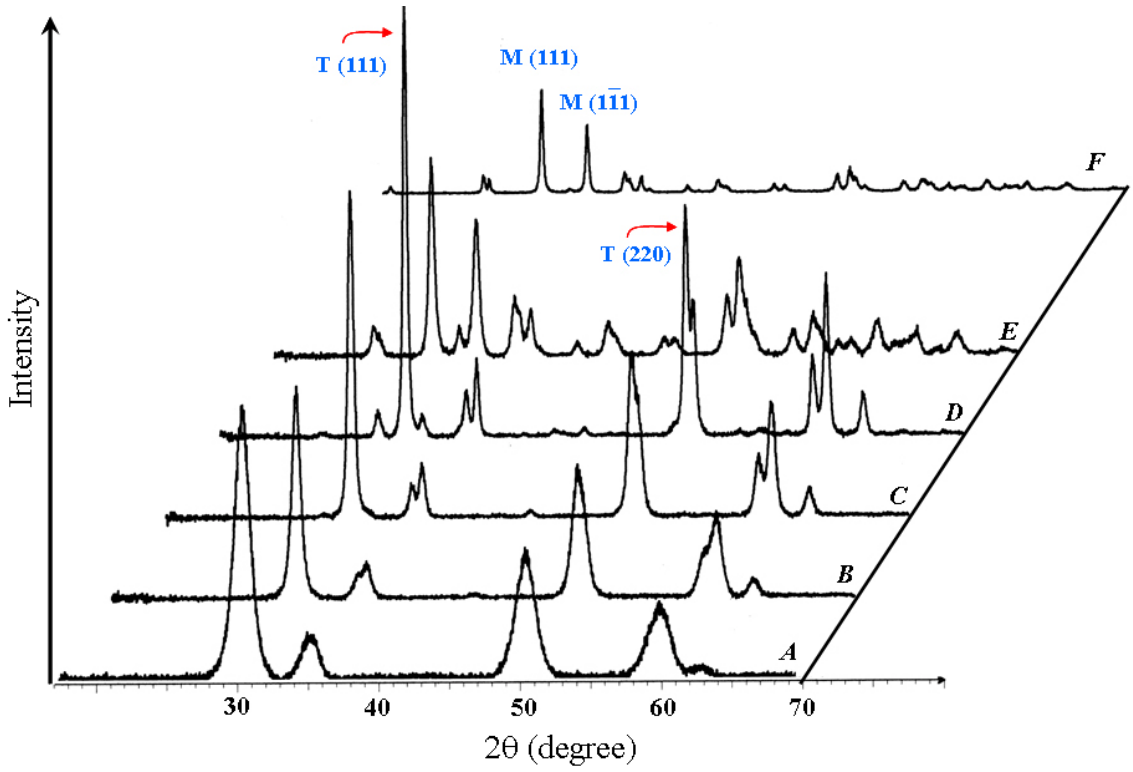


**Figure 3-8: X-ray diffraction pattern for the zirconium sulfonate single precursor derived from reaction of 1 mole of zirconium acetate with 1 mole of ethanesulfonic acid (SZ-1(1:1)). A; at 550 °C; at B: 700 °C; C: at 850 °C; D: at 950 °C; E: at 1050 °C; and F: zirconium acetate at 800 °C.**

The crystallite size measurements obtained from the X-ray diffraction for the thermally treated single precursor (SZ-1(1:3)) at different calcination temperatures are shown in Figure 3-9. A small average crystallite size of about 4 nm was observed for the sample calcined at 550 °C. The crystallite size increased with an increase in the temperature and reached a 12 nm average size when the sample was calcined at 850 °C. This increase in the crystallite size is presumably due to the sintering and agglomeration of the particles during thermal treatment. By comparison, the crystallite size of zirconia derived fro, zirconium carboxylates, displaced markedly higher increases upon

calcinations at similar temperatures. This clearly indicates that the sintering of zirconia crystallites during calcination process is delayed by the presence of sulfate ions on the oxide surface resulting in smaller crystallite size.

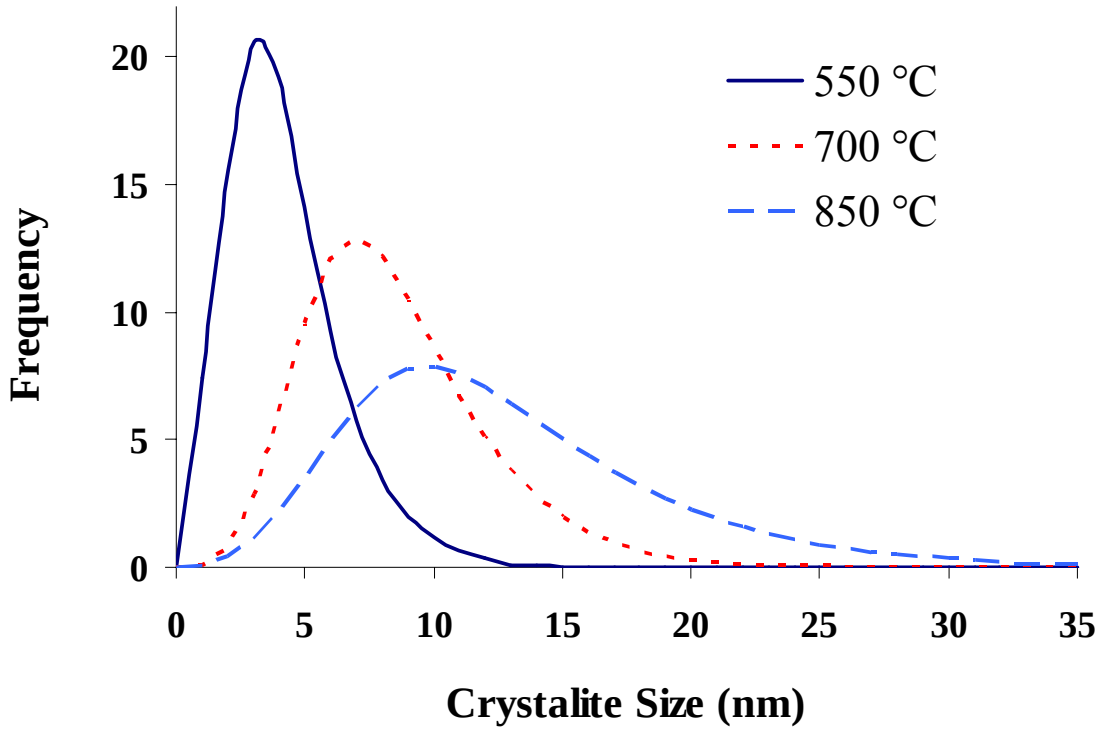


**Figure 3-9: The average crystallite size of the SZ-1(1:3) precursor calcined at different temperature.**

The infrared spectrum of the oxide obtained from thermal decomposition of the precursor SZ-1(1:3) at 650 °C is shown in Figure 3-10. Three peaks in the IR region from 1000 $cm^{-1}$ to 1250 $cm^{-1}$ were observed, specifically, 1029 $cm^{-1}$ - 1069 $cm^{-1}$, 1143 $cm^{-1}$, and 1222 $cm^{-1}$ - 1243 $cm^{-1}$. These bands are considered as characteristic peaks for the S-O stretching modes of vibration of the coordinated $SO_4^{2-}$ species on the surface. They are typical of the chelating bidentate sulfate species coordinated to the zirconium

metal ion [20]. Furthermore, the peak that was observed at about 1389 $cm^{-1}$ is believed to correspond to the S=O stretching frequency of sulfate adsorbed on the metal oxide surface [20,21]. The broad peak observed at 3375 $cm^{-1}$ is attributed to the hydrogen bonding OH stretching mode of the adsorbed water on the surface of the zirconia [22]. Additionally, the peak appearing at 1627 $cm^{-1}$ was attributed to the δ OH bending mode of the adsorbed water molecules on the surface [22]. It is obvious from Figure 3-10 that the oxide obtained form the SZ-1(1:1) and SZ-1(1:2) precursors are similar to each other with slight differences in the relative intensities of the peaks. This implies that the sulfate groups adsorbed on the surface have similar structures. The characteristic peak for the $\nu_{S=O}$ with the zirconia sample SZ-1(1:1) was observed at frequency of 1376 $cm^{-1}$ but it is shifted to higher position (1389 $cm^{-1}$) for the zirconia sample SZ-1(1:2). This increase in the band absorption frequency presumably occurs due to the increase of the surface sulfate groups concentration. As shown in Figure 3-10, the oxide with high sulfate contents (SZ-1(1:3) sample) has a different IR spectrum in the $\nu_{S-O}$ region with appearance of new strong bands at about 1065 $cm^{-1}$ and 900-1000 $cm^{-1}$. This change is presumably due to the formation of polynuclear sulfate compounds [21,23]. Furthermore, the degree of hydration of the crystalline sulfate groups maybe also influence the structure of the adsorbed sulfate groups on the surface [21].

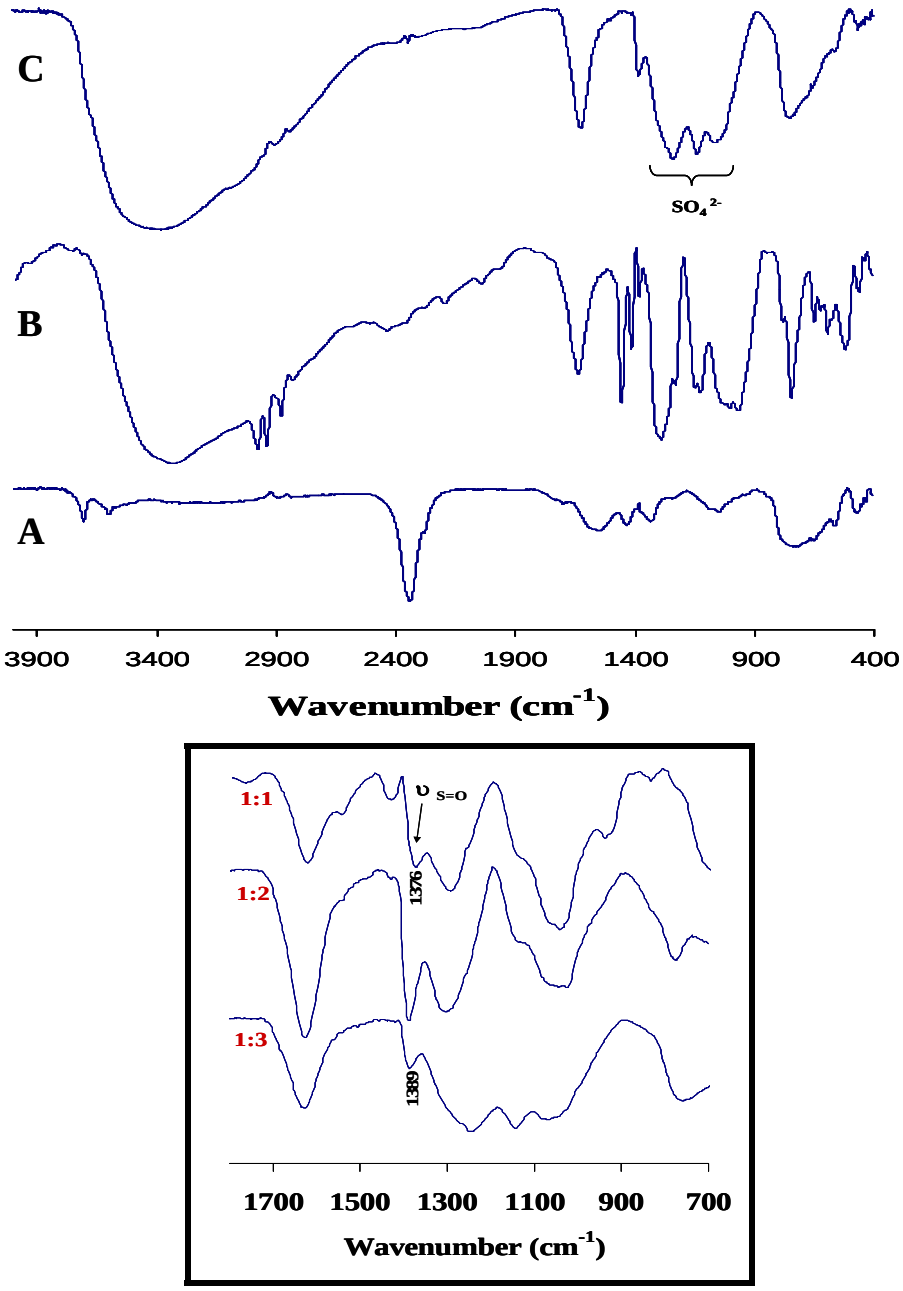


**Figure 3-10: (Upper spectra), the IR of the (A) zirconia obtained from zirconium acetate heated at 720 °C; (B) zirconium sulfonate precursor SZ-1(1:3) dried at 100 °C; (C) sulfated zirconium oxide obtained from calcination of SZ-1(1:3) at 650 °C. (Lower spectra); sulfated zirconia obtained from pyrolysis of zirconium sulfonate precursors at 650 °C; (1:1): oxide from SZ-1(1:1); (1:2) : oxide from SZ-1(1:2); and (1:3): oxide from SZ-1(1:3). *(The precursor details are summarized in Table 3-2)***

Figure 3-11 shows the influence of the sulfate concentration on the phase composition and thermal stability. All the samples were calcined at 950 °C for 8 hours. It was previously reported that the acetate to the zirconium stoichiometry in the zirconium acetate complex precursors had only a negligible effect on the crystallite phase and the crystallization temperature [24]. Therefore, the observed variation in the phase composition can be directly attributed to the presence of the sulfate groups on the final oxide surface. Zirconium acetate itself showed a complete transformation of the tetragonal phase to the monoclinic phase at this temperature. However, the results showed that with addition of 0.1 mole ratio of ethanesulfonic acid (ESA) to zirconium acetate, the tetragonal phase was highly stable and resisted the transformation into a monoclinic phase. The presence of the tetragonal phase was about 56%. It seems that even a small amount of sulfate introduced into the defect sites of the zirconium oxide crystals is capable of stability of the tetragonal phase. With an increase in the mole ratio of ESA, the structure retained more of the tetragonal phase at high calcination temperature. At 1 mole ratio of ESA, the structure almost completely retains its tetragonal phase at 950 °C.

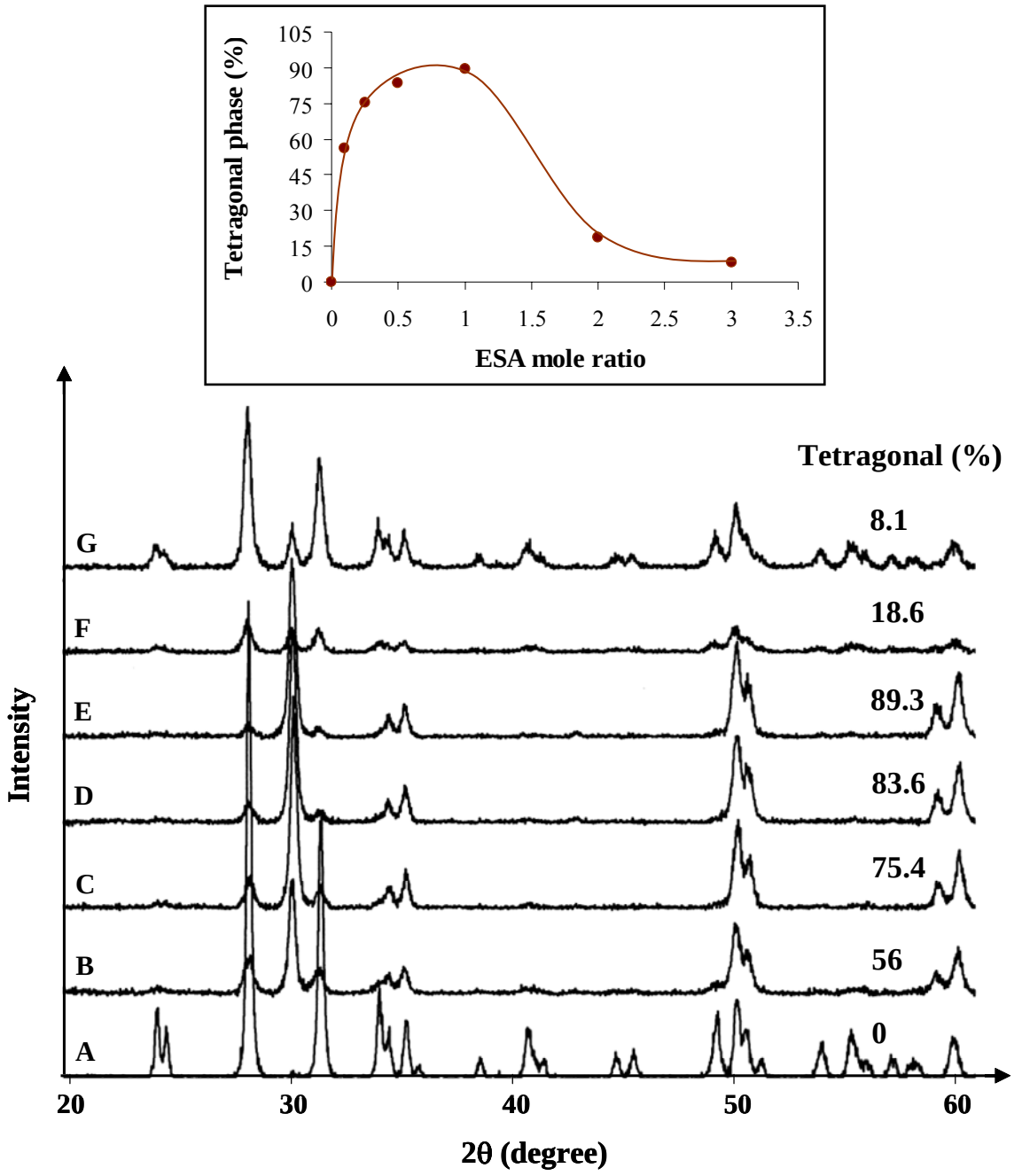


**Figure 3-11: Effect of the ethanesulfonic acid (ESA): zirconium acetate (ZrAc) mole ratio on the phase composition of the sulfated zirconium oxide calcined at 950 °C; A: zirconium acetate; B: with 0.1 ESA; C: with 0.25 ESA; D: with 0.5 ESA; E: with 1 ESA; F: with 2ESA; and G: with 3 ESA.**

It has been reported that sulfates stabilized the tetragonal phase by contribution to the rigidity of the structure and increasing the Zr-Zr bond separation [12]. However, there is another reason that is believed to influence the structure stability by sulfate ions. It is expected that the zirconium oxide surface has some sites and vacancies that can adsorb oxygen and hence inspire the phase transformation from tetragonal to monoclinic [9]. However, the sulfate ions, coordinated to the surface, cover such sites and delay the phase development from both amorphous to crystalline phase and from tetragonal to monoclinic phase.

Interestingly, beyond a 1:1 mole ratio of zirconium acetate to the ESA (Figure 3-11), a decrease in the stability of the tetragonal phase was observed. The cause of this is not understood, but it may reflect a very different decomposition pathway leading to sulfated zirconia particles with varying microstructures and hence the tetragonal to monoclinic transformation. Additionally, this may be due to the observed change in the nature of the sulfate groups coordinated to the surface of the zirconium. For example, a zirconia with 91.9% monoclinic phase was obtained from the three mole equivalents of ethanesulfonic acid precursor. Figure 3-12 shows also the effect of the sulfur contents on the development and the initial formation of the tetragonal phase. When the precursor (SZ-1(1:1)) is calcined at 550 °C for 6 hours, most of the sample mainly remains amorphous. However, calcination of the (SZ-1(1:3)) precursor at the same temperature results in the formation of a more crystalline tetragonal phase.

Apparently, one can conclude from all the characterization results that there is a maximum in the amount of sulfate groups necessarily for the stabilization of the tetragonal phase at high temperature and the maximum phase stability is obtained when

the oxide surface has a certain ratio of $SO_4^{2-}/OH^-$. Beyond that ratio, the sulfate groups replace large amounts of the hydroxyl groups from the surface and appear to be crowded on the surface, which affects its coordination nature and hence facilitates the evolution of sulfate species in the form of $SO_3$ gas at elevated temperature.

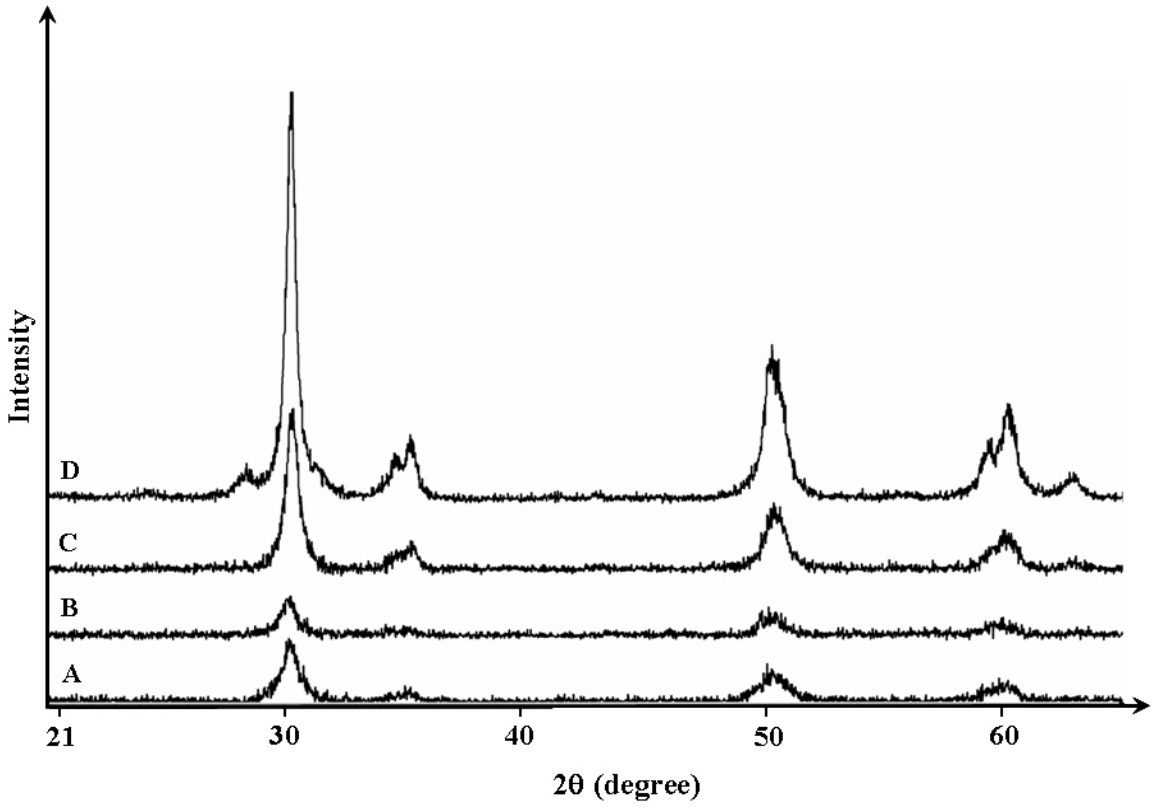


**Figure 3-12: Effect of the ethanesulfonic acid (ESA) concentration in the initial crystallization of the tetragonal sulfated zirconia. Samples were calcined at 550 °C for 6 hours. A: with 0.5 ESA; B: with 1 ESA; C: with 2 ESA; D: with 3 ESA.**

Figure 3-13 showed the relationship between the specific surface area and the mole ratio of the zirconium acetate to the ethanesulfonic acid in the single precursor series (SZ-1). The mole ratio of the ethanesulfonic acid is believed to be proportional to

the amount of the sulfate groups on the surface area of the final oxides. All the samples were calcined at 650 °C for 8 hours. The results show a dramatic increase in the oxide surface area with an increase of the sulfur content. This can be attributed to the interaction of the sulfate groups on the oxide surface. The reason behind the growth in the surface area maybe attributed to the presence of bridging sulfate $SO_4^{2-}$ ions on the surface. Apparently, the bridging sulfate ions replace the hydroxyl groups present on the surface resulting in a more rigid and stable structure. Furthermore, the bridging sulfate ions caused an increase the Zr-Zr separation from about 3.4 A° to 4.3 A° [12,25] which also appears to facilitate the dispersion of the oxide particles and hence increases the surface area.

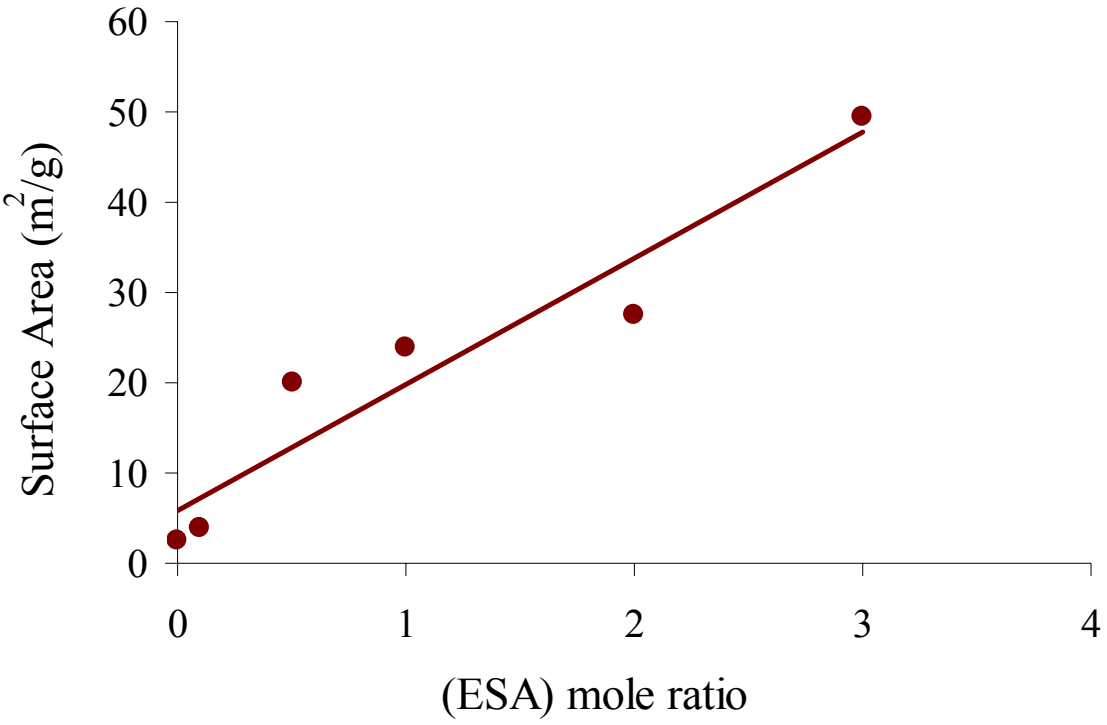


**Figure 3-13: Effect of the ethanesulfonic acid (ESA) mole ratio in the surface area of the sulfated zirconium oxide calcined at 650 °C.**

The general proposed pathway for the thermal decomposition of the zirconium sulfonate precursors to form sulfated zirconium oxide is shown in the following scheme:

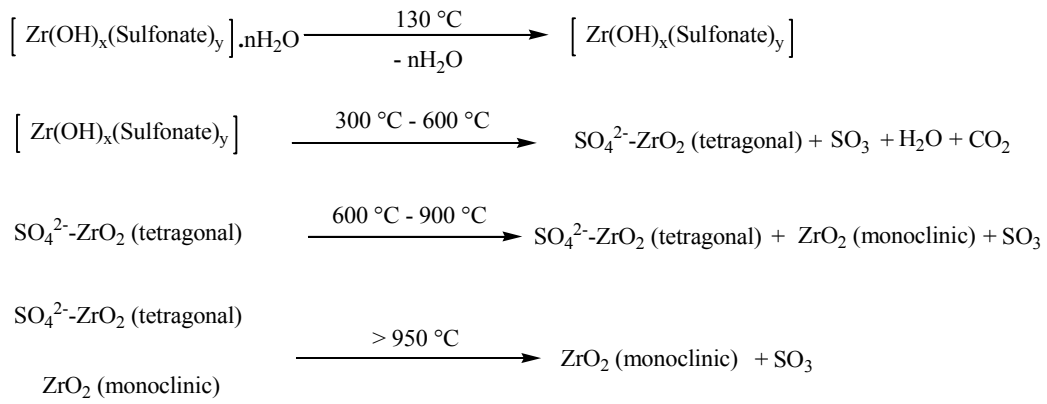


The SEM micrograph of the zirconium acetate starting material and the zirconium ethyl sulfonate precursor (SZ-1(1:3)) are shown in Figure 3-14. The SEM was recorded for both, the precursor itself and the oxide obtained from the pyrolysis of the precursor. The micrographs of the zirconium acetate (Figure 3-14 A,B) show smooth spherical particles with uniform holes on the walls of the particles. The size of these particles lay in the range from 2 μm to about 20 μm. When the zirconium acetate was heated to 700 °C to yield zirconium oxide (Figure 3-14 C,D), the SEM of the resulting oxide showed that it maintained the morphology of the precursor with more polished spherical particles. The morphology of the zirconium sulfonate precursor (SZ-1(1:3)) showed uniformly shaped crystals stuck together with average diameters of about 0.5μm. Upon calcination, the morphology completely changed to form rod-like zirconia with an average diameter of about 200 to 500 nm with several microns in length. This apparently occurred due to the sintering of the particles during the thermal transformation of the precursor to the oxide. The uniaxial growth may be a reflection of the formation of the tetragonal phase with preferred growth in the C axis.

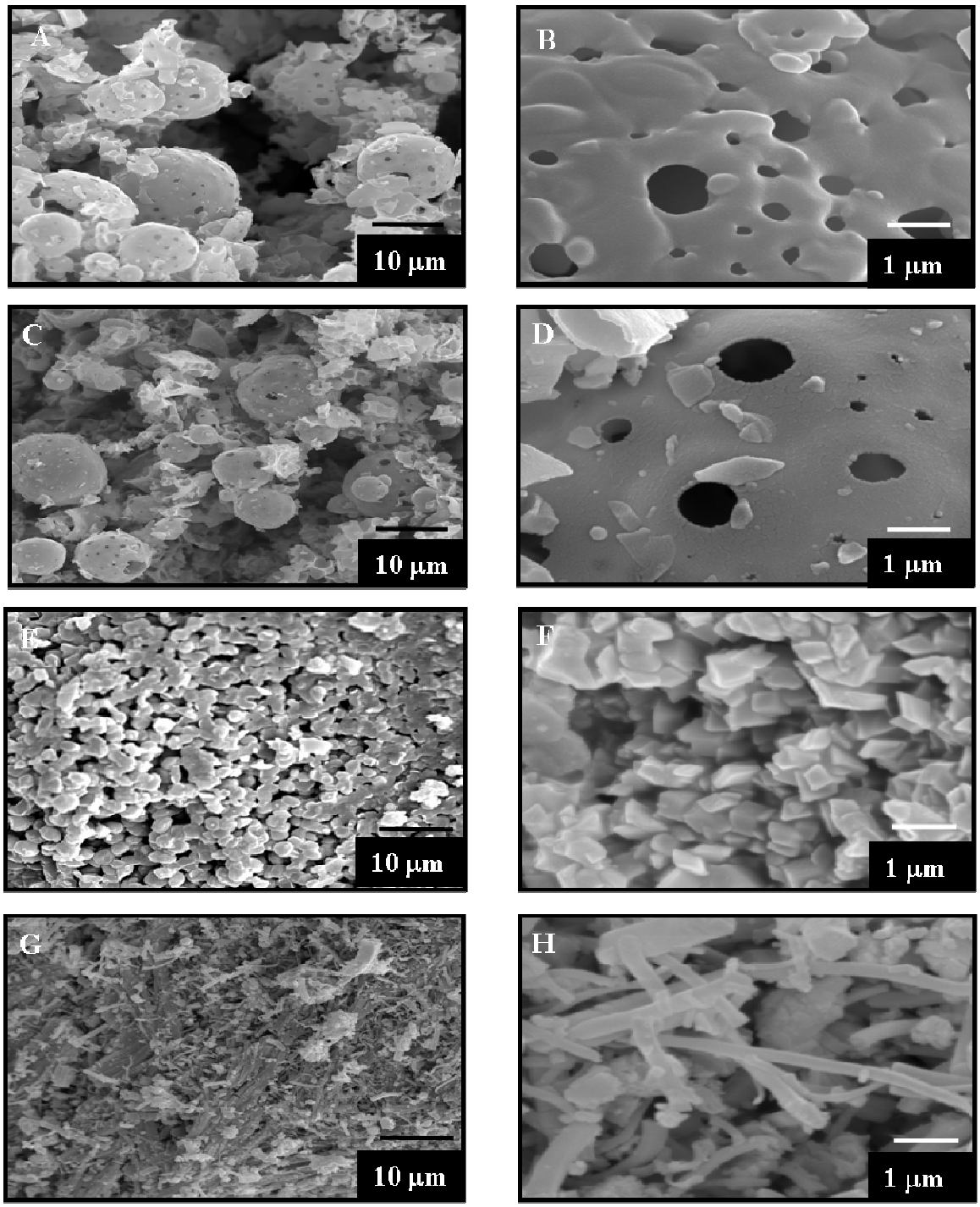


**Figure 3-14: Scanning electron micrographs of the zirconium acetate [(A(1500X) and B(13000X)]; zirconium acetate at 700 °C [C(1500X) and D(13000X)]; zirconium ethane sulfonate (SZ-1(1:3)) [E(1500X) and F(13000X)]; and zirconium ethane sulfonate (SZ-1(1:3)) at 650 °C [G(1500X) and H(13000X)].**

**Other synthesized zirconium sulfonate precursors and their corresponding oxides:**

Single source precursors synthesized in the current research work were obtained from the reaction of zirconium salts with a variety other sulfonic acids or sulfonic acid salts. Zirconium sulfonate precursors prepared by these methods were obtained generally with about 80% yield. Table 3-5 showed the details of these precursors with its proposed chemical formula while Table 3-6 shows the C,H,S,N elemental analysis results. The TGA profiles of some zirconium sulfonate precursors obtained from the reaction of zirconium salts with different sulfonate reagents are shown in Figure 3-15.

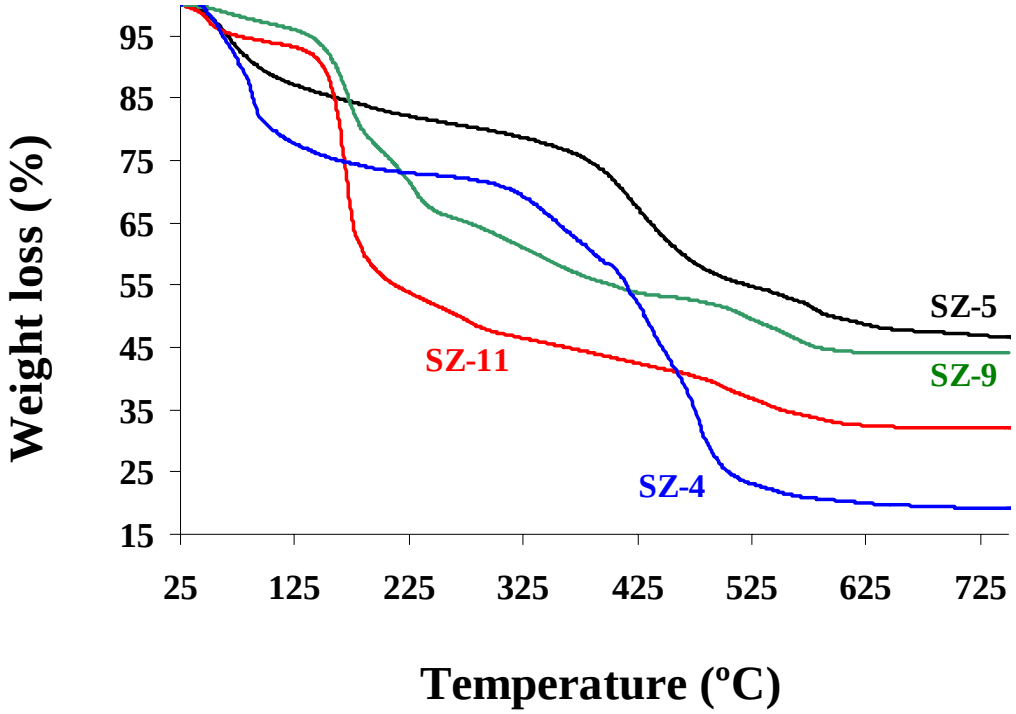


**Figure 3-15: TGA profiles of some zirconium sulfonate precursors; (SZ-4): zirconium oxychloride with *p*-toluene sulfonic acid; (SZ-5): zirconium acetate with 8-hydroxyquinoline sulfonic acid; (SZ-9): zirconium acetate with sodium dodecyl sulfate; and (SZ-11): zirconium acetate with sodium hexadecyl sulfate.**

**Table 3-5: The chemical formulas and properties of the synthesized zirconium sulfonate complexes.**

| Sample code | ‡Initial components | Calcination to oxide | | *Oxide Temperature (°C) | Product proposed Structure | Surface Area ($m^2/g$) | Product yield (%) | Crystal phase |
|---|---|---|---|---|---|---|---|---|
| | | $ZrO_2$ (%) | Molecular weight (gm / mol) | | | | | |
| **SZ-3** | ZA with PTSA | 42.8 | 274 | 630 | $[Zr(O)_{0.8}(OH)_1(OAc)_1(PTSA)_{0.4}]1H_2O$ | 0.44 | 93 | Amorphous |
| **SZ-4** | ZOC with PTSA | 21.8 | 564 | 580 | $[Zr(OH)_{1.5}(PTSA)_2Cl_{0.5}]5H_2O$ | 0.92 | 84 | Amorphous |
| **SZ-5** | ZA with HQSA | 45.8 | 269 | 650 | $[Zr(O)_{0.5}(OH)_2(OAc)_{0.7}(HQSA)_{0.3}]1.5H_2O$ | 20.1 | 81 | Amorphous |
| **SZ-6** | ZOC with HQSA | 39.5 | 311 | 620 | $[Zr(O)_{1.6}(HQSA)_{0.8}]1H_2O$ | 2.54 | 71.3 | Crystalline |
| **Zr-7** | ZA with HQ | 29.0 | 424 | 420 | $[Zr(O)_{0.8}(OAc)_{0.6}(HQ)_{1.8}]1H_2O$ | 41.8 | 88.5 | Crystalline |
| **Zr-8** | ZOC with HQ | 50.4 | 267 | 480 | $[Zr(O)_{1.5}(HQ)_{0.75}(Cl)_{0.25}]1H_2O$ | 0.78 | 77.4 | Crystalline |
| **SZ-9** | ZA with SDS | 44.3 | 345 | 620 | $[Zr(O)_{0.5}(OH)_1(OAc)_{1.5}(SDS)_{0.5}]1H_2O$ | 0.96 | 82.6 | Amorphous |
| **SZ-10** | ZOC with SDS | 30.8 | 399 | 620 | $[Zr(O)_{1.5}(SDS)_1]1H_2O$ | 0.84 | 98.3 | Amorphous |
| **SZ-11** | ZA with HDSA | 28.9 | 426 | 600 | $[Zr(O)_{0.7}(OAc)_2(HDSA)_{0.6}]1H_2O$ | 33.5 | 100 | Amorphous |
| **SZ-12** | ZOC with HDSA | 29.1 | 423 | 500 | $[Zr(O)_{1.55}(HDSA)_{0.9}]1H_2O$ | 3.50 | 100 | Amorphous |

***‡ ZA = zirconium acetate hydroxide; ZOC = Zirconium oxychloride; PTSA = p-toluene sulfonate; SDS = sodium dodecyl sulfate; HDSA= sodium hexadecyl sulfate; HQ= 8-hydroxy quinolate; HQSA = 8-hydroxy quinoline-5-sulfate; OAc = acetate.***

**** The minimum temperature for the complete conversion of precursor to zirconium oxide.***

**Table 3-6: The elemental analysis results for the synthesized zirconium sulfonate complexes.**

| Sample code | Elemental analysis (%) | | | | Product proposed formula | *Expt. Fwt (g/mol) | **Theor. Fwt (g/mol) |
|---|---|---|---|---|---|---|---|
| | S | C | H | N | | | |
| **SZ-3** | 5.08 | 21.4 | 3.11 | --- | $[Zr(O)_{0.8}(OH)_1(OAc)_1(PTSA)_{0.4}]\cdot 1H_2O$ | 274 | 268 |
| **SZ-4** | 11.4 | 29.7 | 4.68 | --- | $[Zr(OH)_{1.5}(PTSA)_2Cl_{0.5}]\cdot 5H_2O$ | 564 | 567 |
| **SZ-5** | 3.51 | 18.3 | 3.44 | 1.89 | $[Zr(O)_{0.5}(OH)_2(OAc)_{0.7}(HQSA)_{0.3}]\cdot 1.5H_2O$ | 269 | 269 |
| **SZ-6** | 9.26 | 32.4 | 4.16 | 3.62 | $[Zr(O)_{1.5}(HQSA)_1]\cdot 1H_2O$ | 349 | 358 |
| **Zr-7** | --- | 48.4 | 3.77 | 5.80 | $[Zr(O)_{0.8}(OAc)_{0.6}(HQ)_{1.8}]\cdot 1H_2O$ | 424 | 419 |
| **Zr-8** | --- | 40.0 | 2.46 | 4.93 | $[Zr(O)_{1.5}(HQ)_{0.75}(Cl)_{0.25}]\cdot 1H_2O$ | 267 | 252 |
| **SZ-9** | 4.30 | 30.6 | 5.74 | --- | $[Zr(O)_{1.5}(HQ)_1]\cdot 0.5H_2O$ | 345 | 356 |
| **SZ-10** | 8.16 | 40.6 | 6.84 | --- | $[Zr(O)_{1.5}(SDS)_1]\cdot 1H_2O$ | 399 | 399 |
| **SZ-11** | 4.73 | 38.1 | 5.83 | --- | $[Zr(O)_{0.7}(OAc)_2(HDSA)_{0.6}]\cdot 1H_2O$ | 426 | 431 |
| **SZ-12** | 5.74 | 40.4 | 7.45 | --- | $[Zr(O)_{1.55}(HDSA)_{0.9}]\cdot 1H_2O$ | 423 | 424 |

** from TGA and thermal analysis*

*** from proposed formula*

The TGA profiles of the zirconium sulfonate showed a decomposition profile similar to that of the SZ-1 precursor series which obtained from the reaction of zirconium acetate with ethanesulfonic acid. The thermal decomposition of precursors occurs in a stepwise manner with the loss of water molecules at the beginning followed by the decomposition of sulfonate ligands. The degree of the decomposition depends on the nature of the zirconium sulfonate precursor. However, most of precursors show the formation of the oxide at about 600 ºC. Sulfated zirconium oxides were obtained by pyrolysis of synthesized zirconium sulfonate precursors at different calcination

temperatures. The synthesized oxides are listed in Table 3-7 along with their specific surface areas and phase compositions.

**Table 3-7: The surface areas and the phase composites of the sulfated zirconium oxides derived from calcination of zirconium sulfonate complexes.**

| *Sample code | Calcination Temperature (°C) | Surface Area ($m^2/g$) | Phase (%) | |
|---|---|---|---|---|
| | | | $V_{Tetragonal}$ | $V_{Monoclinic}$ |
| **SZ-3(580)** | 580 | 49.5 | 100 | 0 |
| **SZ-3(650)** | 650 | 25.4 | 100 | 0 |
| **SZ-3(680)** | 680 | 20.9 | 100 | 0 |
| **SZ-3(750)** | 750 | 12.3 | 100 | 0 |
| **SZ-3(850)** | 850 | 7.40 | 100 | 0 |
| **SZ-4(500)** | 500 | 9.94 | 100 | 0 |
| **SZ-4(580)** | 580 | 32.9 | 100 | 0 |
| **SZ-4(650)** | 650 | 16.4 | 97 | 3 |
| **SZ-4(750)** | 750 | 2.90 | 96 | 4.0 |
| **SZ-4(850)** | 850 | 1.30 | 68 | 32 |
| **SZ-5(580)** | 580 | 16.2 | 100 | 0 |
| **SZ-5(650)** | 650 | 63.6 | 100 | 0 |
| **SZ-5(750)** | 750 | 36.3 | 100 | 0 |
| **SZ-5(850)** | 850 | 15.5 | 100 | 0 |
| **SZ-6(580)** | 580 | 32.6 | 100 | 0 |
| **SZ-6(620)** | 620 | 17.2 | 100 | 0 |
| **SZ-6(650)** | 650 | 15.8 | 100 | 0 |
| **SZ-6(680)** | 680 | 13.2 | 100 | 0 |
| **SZ-6(750)** | 750 | 12.7 | 100 | 0 |
| **SZ-6(850)** | 850 | 6.30 | 7.0 | 93 |
| **Zr-7(460)** | 460 | 22.3 | 100 | 0 |
| **Zr-7(580)** | 580 | 15.2 | 100 | 0 |
| **Zr-7(650)** | 650 | 12.8 | 77 | 23 |
| **Zr-7(750)** | 750 | 18.0 | 73 | 27 |
| **Zr-7(850)** | 850 | 8.60 | 55 | 45 |
| **Zr-8(590)** | 590 | 23.2 | 100 | 0 |
| **Zr-8(650)** | 650 | 7.50 | 47 | 53 |
| **Zr-8(750)** | 750 | 2.80 | 0 | 100 |
| **Zr-8(850)** | 850 | 1.32 | 0 | 100 |

** The samples specifications correspond to each samples code was described in Table 3-5.*

**Table 3-7: The surface areas and phase composites of sulfated zirconium oxides derived from calcination of zirconium sulfonate complexes (continue).**

| *Sample code | Calcination Temperature (°C) | Surface Area ($m^2/g$) | Phase (%) | |
|---|---|---|---|---|
| | | | $V_{Tetragonal}$ | $V_{Monoclinic}$ |
| **SZ-9(610)** | 610 | 34.3 | 100 | 0 |
| **SZ-9(650)** | 650 | 28.9 | 100 | 0 |
| **SZ-9(720)** | 720 | 22.5 | 86 | 14 |
| **SZ-9(750)** | 750 | 21.7 | 84 | 16 |
| **SZ-9(800)** | 800 | 14.5 | 70 | 30 |
| **SZ-9(850)** | 850 | 12.2 | 64 | 36 |
| **SZ-9(900)** | 900 | 7.20 | 40 | 60 |
| **SZ-9(950)** | 950 | 4.90 | 22 | 78 |
| **SZ-10(610)** | 610 | 20.8 | 100 | 0 |
| **SZ-10(650)** | 650 | 18.7 | 100 | 0 |
| **SZ-10(720)** | 750 | 12.4 | 49 | 51 |
| **SZ-10(750)** | 750 | 9.97 | 77 | 23 |
| **SZ-10(800)** | 800 | 3.70 | 26 | 74 |
| **SZ-10(850)** | 850 | 3.10 | 15 | 85 |
| **SZ-10(900)** | 900 | 1.20 | 11 | 89 |
| **SZ-11(600)** | 600 | 34.3 | 100 | 0 |
| **SZ-11(650)** | 650 | 45.6 | 100 | 0 |
| **SZ-11(750)** | 750 | 20.4 | 78 | 22 |
| **SZ-11(850)** | 850 | 5.90 | 8.0 | 92 |
| **SZ-12(500)** | 500 | 31.7 | 100 | 0 |
| **SZ-12(600)** | 600 | 75.4 | 100 | 0 |
| **SZ-12(650)** | 650 | 52.2 | 90 | 10 |
| **SZ-12(720)** | 720 | 41.0 | 23 | 77 |
| **SZ-12(750)** | 750 | 36.3 | 10 | 90 |
| **SZ-12(850)** | 850 | 16.5 | 4.0 | 96 |

** The samples specifications correspond to each samples code was described in Table 3-5.*

The surface area of the resulting oxide showed also a kind of dependency on the single source zirconium sulfonate precursor itself. The higher surface area was observed with the oxide obtained from calcination of SZ-12 precursor (zirconium oxychloride with sodium hexadecyl sulfate) at 600 °C. Additionally, as we have seen in the case of the sulfated zirconia obtained for the precursors SZ-1 and SZ-2, the oxides showed a high

stability of the tetragonal phase over the monoclinic phase due to the presence of surface sulfate groups. Figure 3-16 shows the X-ray diffraction pattern for the sulfated zirconia obtained from different synthesized precursors utilizing both zirconium oxychloride and zirconium acetate as starting zirconium salts. The influence of the sulfate ions on the surface of the final oxide can be observed from Figure 3-16(a, and b). The oxide obtained from zirconium quinoline (Zr-7, and Zr-8) showed a much low stability of the tetragonal phase than the oxide obtained from the pyrolysis of zirconium quinoline sulfonic acid (SZ-5 and SZ-6). This is probably due to the presence of adsorbed sulfate groups on the surface of the latter oxide.

Furthermore, as in case of oxides derived from zirconium carboxylate precursors discussed in Chapter 2, the results demonstrated in Table 3-7 and Figure 3-16 showed that the phase stability have some kind of dependency on the chain length of the alkyl ligands. The oxide obtained from (SZ-12) precursor at 850 °C showed a complete transformation to the monoclinic phase. With smaller alkyl group ligands, as in case of sodium dodecyl sulfate (SZ-9 and SZ-10), the percent volume of the tetragonal phase was higher at the same calcination temperature. The oxide obtained from the reaction of zirconium salts with ethanesulfonic acid (SZ-1) showed the highest tetragonal phase stability even at high temperature.

In general, as can be seen from Figure 3-16 and Table 3-7, one can say that the nature of zirconium precursors strongly influence the phase composition of the resulting sulfated zirconia hence it can effect the concentration and structure of sulfate ions and hydroxyl groups on the surface of the sulfated zirconia.

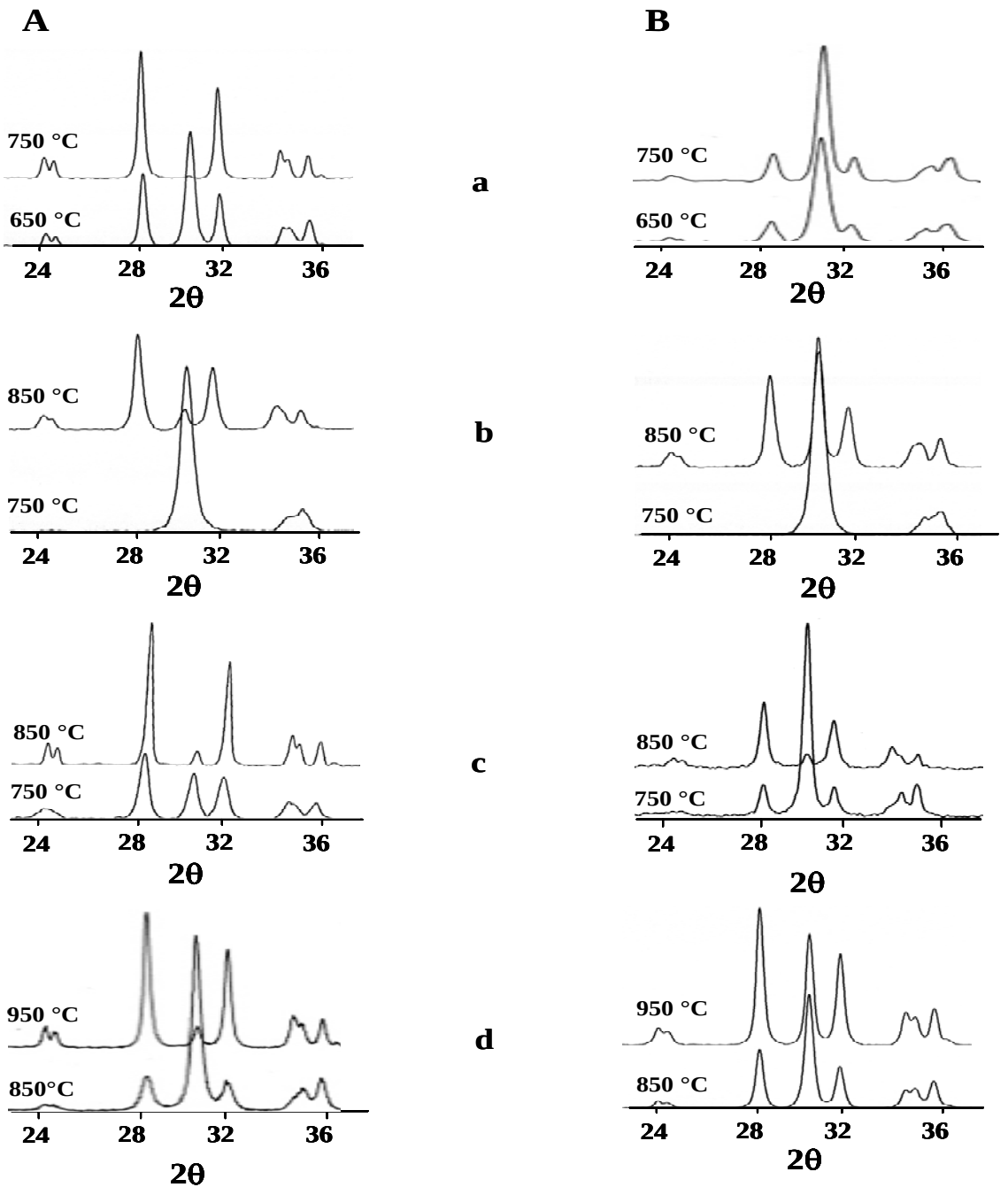


**Figure 3-16: Sulfated zirconia obtained from the reaction of A: zirconium oxychloride and B: zirconium acetate with: a) 8-hydroxyquinoline; b) 8-hydroxyquinoline sulfonic acid; c) sodium hexadecyl sulfate and d) sodium lauryl sulfate.**

Once again, one can see the influence of the sulfate groups on the morphology of the final zirconium oxide. Figure 3-17 shows the SEM micrographs of the precursor and the oxide obtained from the reaction of zirconium acetate with 8-hydroxyquinoline (SZ-7) and the oxide obtained from the reaction of zirconium acetate with 8-hydroxyquinoline-5-sulfonic acid (SZ-5). The morphology of the two precursor (SZ-7) consisted of similar uniform spherical particles. Upon thermal heating at 460 ºC, however, two remarkably different microstructures resulted from the two precursors. A smooth glassy surface with few small particles deposited on this surface (Figure 3-17B) resulted from firing of the 8-hydroxyquinolene precursor (Zr-7). This implies that zirconium particles undergo some sort of melting and aggregation. On the other hand, the SZ-5 precursor produced an oxide consisted of spherical particles with an average particle size of 50-200 nm. This is quite similar to the oxide obtained from the precursor Zr-7, implying that there was no sintering or major aggregation occurring. The preservation of the spherical particles after heating apparently reflects the influence of the surface sulfate groups on the sintering resistance.

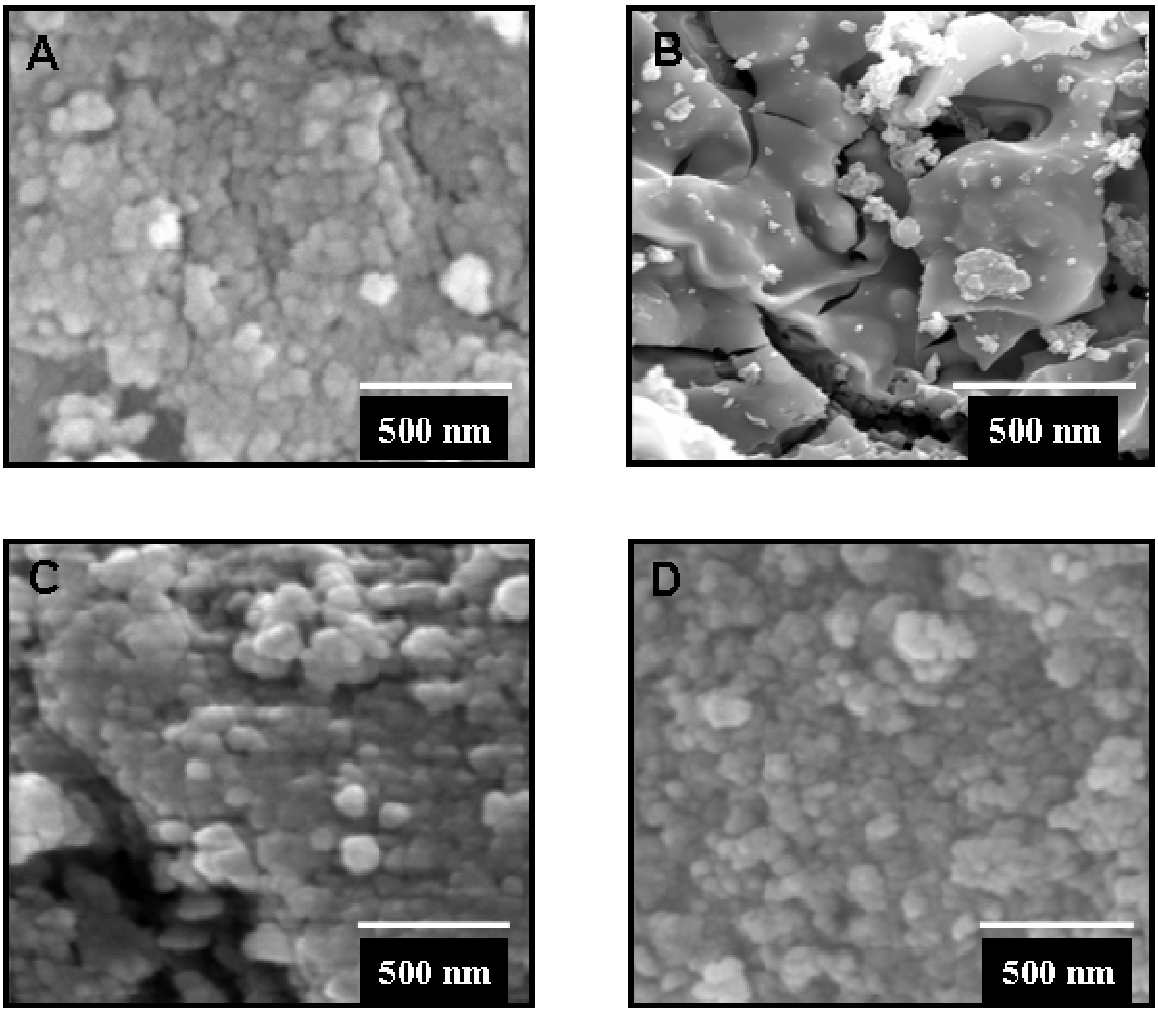


**Figure 3-17: Scanning electron micrographs of: (A) zirconium acetate hydroxyquinolate (SZ-7) (A (40000X); (B) zirconium acetate hydroxyquinolate at 460 °C (SZ-7(460)) (B (50000X); (C) zirconium acetate hydroxyquinolate sulfonate (SZ-5) (C (40000X) and (D) zirconium acetate hydroxyquinolate sulfonate at 650 °C (SZ-5(650)) (D (40000X).**

**Surface acidity:**

The total acidity measurements of several sulfated zirconium oxides obtained from different zirconium sulfonate precursors are listed in Table 3-8. The listed values were obtained from the intramolecular cyclization of acetonylacetone and adsorption of cyclohexylamine. The acid strength data (Table 3-9) was estimated using different Hammett indicators. The data in Tables 3-8 and 3-9, indicate that the surface acidity of the sulfated zirconia obtained from different precursors have widely verity total acidities and acid strengths. These dissimilar acidic properties can be mainly attributed to the both variations in specific surface area of the oxide and the availability and concentration of the active sites, and the structure of sulfate species on the surface. Table 3-9 shows that the acid site density of the sulfated zirconia samples is higher than that of the pure zirconium oxide by a factor of 3-5 times. This confirms that the coordinated surface sulfate groups create the strong acidity. Moreover, the acidity measurements of the oxide series obtained from the reaction of zirconium acetate with different mole ratios of ethanesulfonic acid demonstrated that the acidity increased with the increase of the sulfate concentration on the surface.

As shown in Tables 3-8 and 3-9, the total acidity and the acid strength of the pure zirconium oxide prepared from pyrolysis of zirconium acetate or zirconium hydroxyquinolate (SZ-7 and SZ-8) was very low with no significant values compare to that of sulfated zirconia. Furthermore, the intermolecular cyclization of acetonylacetone over pure zirconia showed no selectivity towards the production of dimethylfuran which is the product obtained from the reaction over acid sites.

**Table 3-8: Acidity measurement of the synthesized sulfated zirconia obtained from the pyrolysis of the prepared single source precursors.**

| *Sample code (Temperature °C) | $S_{BET}$ ($m^2/g$) | Acidity Measurements | | | |
|---|---|---|---|---|---|
| | | Cyclohexylamine adsorption | | Acetonylacetone cyclization reaction | |
| | | Acidity μmol/g | Site density μmol/$m^2$ | Acetonylacetone conversion (%) | Dimethylfuran selectivity (%) |
| **Zirconium acetate (650)** | 2.58 | 2.10 | 0.81 | 3.23 | 0 |
| **SZ-1(1:0.1)(650)** | 3.85 | --- | --- | 24.0 | 31.0 |
| **SZ-1(1:0.5)(650)** | 20.1 | 65.3 | 3.24 | 37.0 | 72.0 |
| **SZ-1(1:1)(650)** | 23.9 | 109 | 4.50 | --- | --- |
| **SZ-1(1:2)(650)** | 27.5 | 139 | 5.08 | 15.5 | 81.0 |
| **SZ-1(1:3)(650)** | 49.6 | 278 | 5.67 | 28.4 | 89.0 |
| **SZ-2(700)** | 14.0 | 77.2 | 5.50 | --- | --- |
| **SZ-3(680)** | 20.9 | 122 | 5.80 | --- | --- |
| **SZ-5(650)** | 63.6 | 305 | 4.80 | 32.2 | 91.1 |
| **SZ-6(650)** | 13.2 | 41.1 | 3.11 | 28.4 | 96.4 |
| **SZ-7(650)** | 12.8 | 12.3 | 0.96 | 14.7 | 11.3 |
| **SZ-8(650)** | 7.50 | 1.63 | 0.22 | --- | --- |
| **SZ-10(610)** | 25.7 | 146 | 5.60 | 14.5 | 0 |

**All the samples details are summarized in Table 3-2 and Table 3-5.*

**Table 3-9: Acidity strength estimation of the sulfated zirconia obtained from the pyrolysis of synthesized single source precursors using Hammett indicator.**

| ‡Sample code | *Color Indicator / (pKa) | | | | | | |
|---|---|---|---|---|---|---|---|
| | **B(+3.3)** | **C(+1.5)** | **D(+0.8)** | **E(-3)** | **F(-5.7)** | **G(-8.2)** | **H(-11.4)** |
| **ZrAc(650)** | L. orange | Yellow | Green | L. yellow | Colorless | Colorless | Colorless |
| **SZ-1(1:0.5)(650)** | D. red | D. purple | Yellow | D. orange | L. yellow | Colorless | Colorless |
| **SZ-1(1:1)(650)** | D. orange | Purple | Yellow | D. Red | Yellow | L. yellow | Colorless |
| **SZ-1(1:2)(650)** | Red | D. purple | Yellow | Red | Yellow | L. yellow | Yellow |
| **SZ-1(1:3)(650)** | D. red | Purple | Yellow | Red | Yellow | Yellow | L. yellow |
| **SZ-2(700)** | Red | L. purple | Yellow | D. red | Yellow | Colorless | Colorless |
| **SZ-5(650)** | D. red | Purple | Yellow | D. red | Yellow | Pink | L. yellow |
| **SZ-6(650)** | D. orange | Purple | Yellow | D. red | Yellow | L. pink | Colorless |
| **SZ-7(650)** | Red | L. purple | L. green | L. orange | Colorless | Colorless | Colorless |
| **SZ-8(650)** | L. yellow | L. purple | L. green | L. orange | Colorless | Colorless | Colorless |
| **SZ-9(610)** | Red | Purple | L. green | D. orange | L. yellow | Colorless | Colorless |
| **SZ-10(610)** | Red | Purple | L. green | Orange | L. yellow | Colorless | Colorless |
| **SZ-11(650)** | Red | Purple | L. green | Orange | Colorless | Colorless | Colorless |
| **SZ-12650)** | Red | Purple | L. green | Orange | Colorless | Colorless | Colorless |

*‡ All the samples details are summarized in Table 3-2 and Table 3-5.*

** All the indicators detailed are summarized in Table 3-1 and Figure 3-3.*

The acidity measurement results, particularly those for the oxide obtained from the series of precursors obtained from the reaction of zirconium acetate with ethanesulfonic acid, show that the acidity increases with an increase of the sulfate concentration. This may be attributed to the generation of more Brønsted acid sites. It is expected that the initial decomposition of the zirconium sulfonate precursor during the thermal treatment in air at low temperature may proceed by $\beta$-hydride elimination to give ethylene and water. Adsorbed water may then react with the adjacent sulfate groups to

yield adsorbed bisulfates ($HSO_4^-$) and hydroxyl groups. In a similar manner to that which was proposed by Muriel et al. [26] at low sulfate concentration, the surface presumably is rich with the hydroxyl and bridging hydroxyl groups along with bisulfate groups. Upon further heating to higher temperature (above 600 °C), the bisulfate undergoes a kind of condensation reaction with the adjacent hydroxyl groups to evolve water and forms a bridging bidentate sulfate group on the surface with concurrent formation of week and strong Lewis acid sites. Water molecules were evolved during the thermal decomposition of the precursor or it can be re-adsorbed on Lewis acid sites to form weak Brønsted acid sites. The delay of the formation of the tetragonal phase with low sulfate concentration as well as the thermal stability of this phase at higher temperature may be emphasized the presence of a high concentration of stabilized hydroxyl groups on the surface. Figure 3-18 presents a schematic diagram of the proposed low and high sulfate load surface structures with showing both, the Brønsted and Lewis acid sites.

Additionally, with further increase in the concentration of the sulfur species, the bisulfate groups on the oxide surface will increase and presumably some polynuclear sulfate compound such as pyrosulfate may be formed. As shown earlier, the X-ray diffraction data showed that the sample with high sulfur species undergoes a rapid transformation of the tetragonal phase to monoclinic upon calcination at higher temperature. Presumably, this is due either to the different microstructure (nanocrystalline) of the zirconia and/or a none facile loss of sulfate due to the different mode of coordination.

**A: Low sulfate load structure**

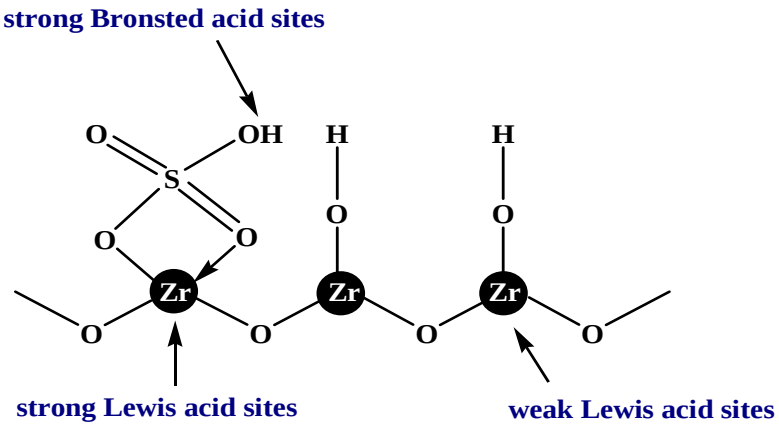


**B: High sulfate load structure**

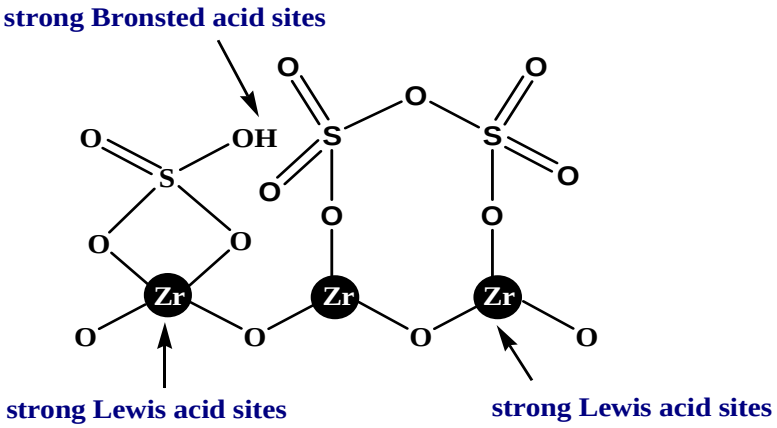


**Figure 3-18: Proposed structure of the synthesized sulfated zirconia with low and high sulfur concentrations [21, 26].**

In fact, it was observed that sulfated zirconium oxides obtained from the zirconium acetate starting material exhibited more surface acidity and higher surface area

than that derived from zirconium oxychloride when prepared and treated at the same conditions. We can also conclude, as seen from the TGA profile of zirconium ethane sulfonate (Figure 3-5), that the zirconium sulfonate precursors obtained from zirconium acetate required a higher temperature for the removal of the $SO_4^{2-}$ compared to that the precursor obtained from the reaction of zirconium oxychloride with sulfonic acids. This higher temperature implies that there is a strong interaction between the zirconium acetate-derived zirconia particles and sulfonate ions. Additionally, in order to investigate the influence of the zirconium salts on the phase composition of the final zirconium oxide, the two starting zirconium salt precursors were dissolved in water, then dried and calcined at 600 °C in order to mimic the preparation and firing of the sulfonate precursors. The XRD patterns for these samples are shown in Figure 3-19. The XRD pattern shows that the zirconium acetate sample retained the tetragonal structure of the oxide while the zirconium oxide derived from zirconium oxychloride undergoes almost a complete transformation from a tetragonal to monoclinic zirconia phase (≈ 78% of monoclinic). This indicates that the zirconium acetate sample may be preserve more hydroxyl groups on the surface of the final oxide, as well as some carbonate species, which interact easily with the sulfate species to form stable $SO_4^{2-}$ anions on the surface resulting in more phase stability. These results also indicate that the dehydroxylation process is delayed in zirconia derived from decomposition of acetate groups.

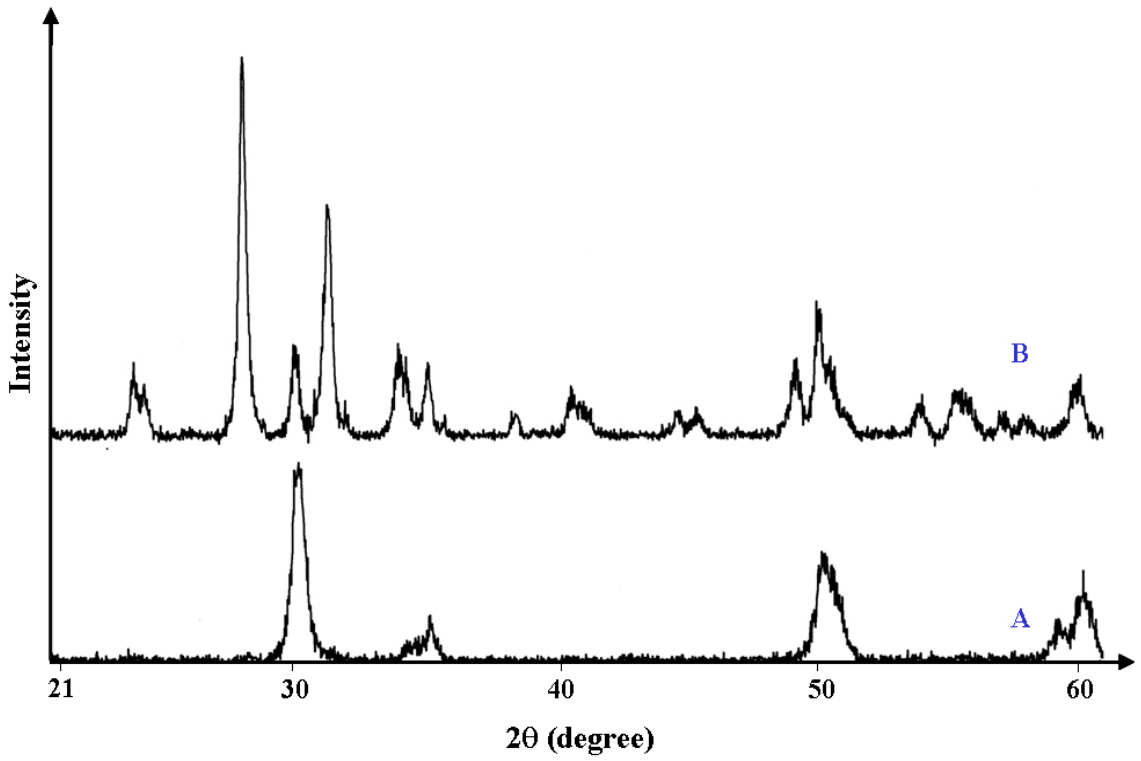


**Figure 3-19: X-ray diffraction pattern of zirconium precursors pyrolyzed at 600 °C for 4 hours. A: zirconium acetate, B: zirconium oxychloride.**

**Thermal decomposition of the sulfated zirconia precursors:**

The precursor, derived from the reaction of zirconium acetate with ethanesulfonic acid, was heated in a sealed glass tube using a tube furnace at various temperatures in the range of 250 °C to 450 °C. The decomposition process initiated at about 200 °C -300 °C by $\beta$-hydride elimination reaction to evolve ethylene gas. The ethylene gas presumably further undergoes dimerization and trimerization over the acid surface at high temperatures to yield a mixture of $C_4$-$C_6$ olefins. Sulfur dioxide was also formed at this stage. Hydrogen sulfide and more sulfur dioxide were also released as byproducts at higher decomposition temperatures (above 350 °C). The $C_4$ and $C_6$ olefins directly

reacted with hydrogen sulfide via cyclization to give a mixture of thiophenes. It is well established that one potential pathway for the synthesis of thiophenes is from the reaction of alkanes or olefins with sulfur dioxide or hydrogen sulfide at high temperature in an inert gas environment [27,28]. In our experiments, the formation of thiophene and hydrogen sulfide started at about 400 °C. At lower than 400 °C, the reaction mainly produced $SO_2$, water, and ethylene. Figure 3-20 showed a schematic diagram for the possible products formed from the thermal decomposition of the zirconium sulfonate single-source precursor SZ-1(1:3). Notably, thiophenes were produced in substantial amounts when a larger amount of sample was placed in the sealed tube due to the presence of less oxygen gas. Thiophene compounds may also be formed as a result of the reaction of sulfur with ethylene to form a conjugated thiodiethylene intermediate, which further reacts with another ethylene molecule followed by intramolecular cyclization. The formation of diethyl sulfide and dithiolanes also suggest that the reaction follows a free radical mechanism.

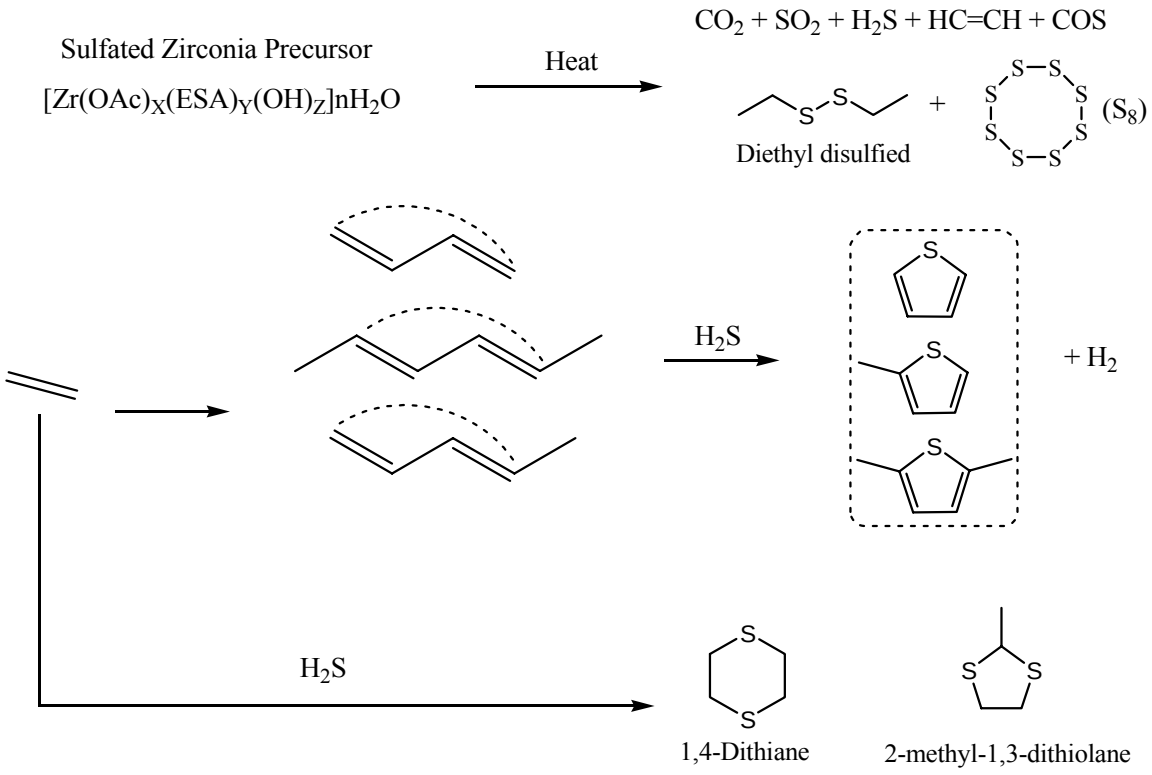


**Figure 3-20: Schematic diagram for the possible products obtained from the thermal decomposition of the sulfated zirconia single-source precursor (SZ-1).**

Other products obtained, such as elemental sulfur ($S_8$), carbonyl sulfide (COS), diethyl disulfide, 1,4-dithiane, and 2-methyl-1,3-dithiolane were also detected as a result of the reduction pyrolysis of the precursor. Elemental sulfur, which was observed at a high decomposition temperature (above 450 °C), apparently was formed as a result of the decomposition of hydrogen sulfide or thiophene under the reduction conditions. The sulfur then was deposited on the surface of the decomposed precursor. When the pyrolysis was conducted in a larger volume sealed tube with more oxygen concentration, the reaction produced $CO_2$ and $SO_2$ at higher yield than the thiophene and other products.

This implies that the thiophene, alkylated thiophene products, and other possible aromatic products are oxidized to sulfur dioxide and carbon dioxide gases. When the precursor was pyrolyzed in oxygen rich environment in an open vessel at 450 °C followed by extraction with methylene chloride, no elemental sulfur ($S_8$) was deposited indicating that all the sulfur species are oxidized to sulfur dioxide gas or surface sulfate groups.

When the long chain zirconium precursor was pyrolyzed at high temperature in a sealed tube, no elemental sulfur was produced. Zirconium hexadecylsulfonate complexes (SZ-11), for example, produced mainly the $\beta$-hydride elimination products, other products due to elimination reaction and cyclization of the long chain hydrocarbons products, and sulfur dioxide. The structures of the long chain hydrocarbon products are shown in Figure 3-21. Apparently, 3-Octadecene was produced due to the large presence of sodium stearylsulfate on the sodium hexadecyl sulfate starting material.

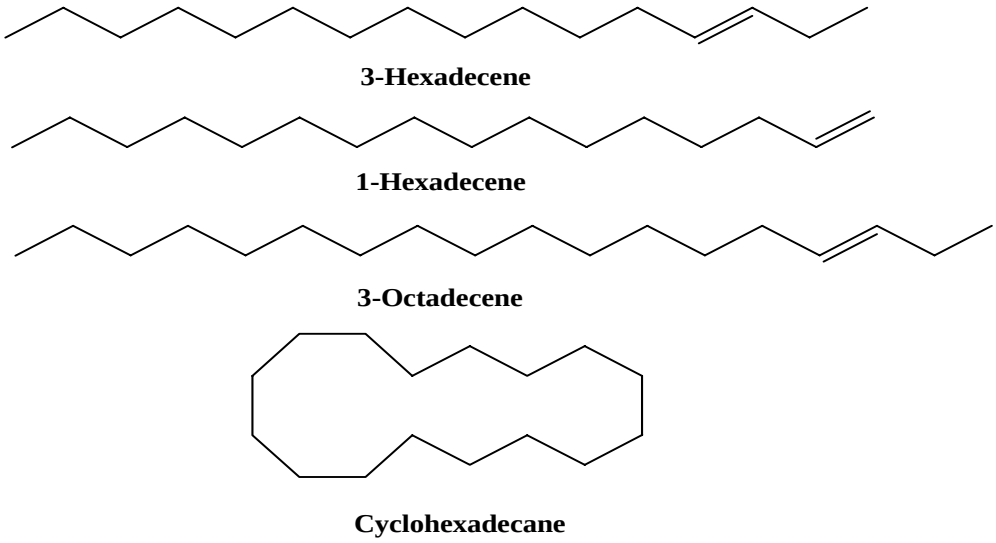


**Figure 3-21: Schematic diagram for the long chain hydrocarbon products obtained from the thermal decomposition of the sulfated zirconium hexadecyl sulfate precursor (SZ-11).**

The yield of the thiophene products and other heterocyclic products were very low in this case. This is due to the formation of long chain hydrocarbons which tend to form dehydrocyclization products rather than react with sulfur to form the heterocyclic products. This conclusion is supported by the results obtained from the reaction of the hydrocarbons of different length ($C_4$-$C_8$) with hydrogen sulfide [27]. Other precursors, such as $[Zr(O)_{0.5}(OH)_2(OAc)_{0.7}(HQSA)_{0.3}]1.5H_2O$ (SZ-5 sample), did not produce thiophene upon thermal decomposition in a sealed tube at 500 °C, which implies that the thiophene is only produced upon the reaction of the unsaturated hydrocarbons with the sulfur or hydrogen sulfide.

In conclusion, three main processes during the thermal decomposition of the precursor in a sealed tube were observed. First, the evolution of $SO_2$ gas at a temperature below 300 °C. Second, the evolution of the $H_2S$ and thiophenes at a temperature range between 300 °C - 450 °C. And third, the formation of elemental sulfur at a temperature above 450 °C. The amount of $SO_2$, $S_8$, and $H_2S$ depend on the pyrolyzed precursor. This clearly implies that upon the formation of the zirconia lattices as a result of the thermal treatment, different sulfate group structures are presented on the surface and these decompose at different temperatures. The preparation methods and the nature of the zirconium sulfonate precursor strongly influence the sulfate contents, the nature and the structure of the sulfate groups on the surface. Therefore, sulfated zirconium oxides obtained from the thermal decomposition of the synthesized zirconium sulfonate precursors are expected to have variable catalytic properties and surface acidity.

**CONCLUSIONS AND REMARKS:**

The zirconium sulfonate complexes used in this study yield highly stabilized tetragonal phase sulfated zirconia with small crystallite size after pyrolysis. The tetragonal phase was stabilized by the sulfate ions to a relatively high temperature. The crystallite size and the phase composition showed a strong dependency on the zirconium sulfonate single precursor employed. The ratio of the tetragonal to the monoclinic phase is strongly influence by the surface structure and the amount of sulfate groups coordinated to the oxide surface.

The reaction of zirconium acetate with different concentrations of ethanesulfonic acid provides a successful method for controlling of sulfur content on the surface of the final sulfated zirconium oxide obtained after the pyrolysis of single precursors. This was achieved by the gradual displacement of the acetate ligands by the sulfonate ions sequentially. Sulfated zirconium oxide powders prepared by the thermal treatment of the zirconium sulfonate single source precursors exhibited a strong surface acidity and relatively high surface areas. The results obtained from different characterization techniques demonstrated that the surface sulfate structure and the surface acidity strongly depend on the concentration of the sulfate on the surface. The total surface acidity, acid strength and surface area showed an increase with an increase of the amount of sulfate groups on the surface.

The thermal decomposition of zirconium ethane sulfonate complexes showed that the initial step in the precursor complex decomposition is probably the evolution of ethylene gas as a result of $\beta$-hydride elimination, which further oligomerizes to higher molecular weight olefins. Thiophenes were produced when the precursor is pyrolyzed

above 400 °C. $SO_2$, $CO_2$, COS and $H_2S$ gases as well as $S_8$ (elemental sulfur) were also observed among the pyrolysis product mixture. The product distribution obtained by pyrolysis showed a dependency on the sample to oxygen ratio available.

**REFERENCES CITED:**


1. V. Kuznetsov, *J. Appl. Chem.* **1940**, *13*, 1257.
2. J. Davies, C. Hockensmith; V. Kukushkin; and Y. Kukushkin, *Synthetic Coordination Chemistry: Principles and Practices*, World Scientifics, London, 1996, p. 58.
3. A. Cote, G. Shimizu, *Coordination Chemistry Reviews*, **2003**, *245*, 49.
4. G. Shimizu, G. Enright, C. Ratciffe, K. Preston; J. Reid, and J. Ripmeester, *Chem. Commun.* **1999**, 1485.
5. M. Hino, S. Kobayashi and K. Arata, *J. Am. Chem. Soc.*, 101, 6439, 1979.
6. M. Hino and K. Arata, *J. Chem. Soc., Chem. Commun.*, **1980**, 851.
7. K. Arata, *Adv. Catal.* **1990**, *37*, 165.
8. R. Gillespie and T. Peel, *Adv. Phys. Org. Chem.*, **1972**, *9*,1
9. B. Davis, R. Keogh and R. Srinivasan, *Catal. Today*, **1994**, *20,* 219.
10. K. Arata, M. Hino and N. Yamagata, *Bull. Chem. Soc. Jpn*. **1990**, *63*, 244,.
11. E. Escalona and M. Penarroga, *Catal. Lett.*, **1995**, *30*, 31.
12. S. Song and A. Sayari. *Cat. Rev.Sci. Eng.*, **1996**, *38(3)*, 329.
13. G. Yadav and J. Nair, *Micro. Meso. Mat.*, **1999**, *33*, 1.
14. C. Breen, *Clay Minerals*, **1991**, *26*, 487.
15. F. Kooli, T. Sasaki and M. Watanabe, *Langmuir*, **1999**, *15*, 1090.
16. L. Hammett and A. Deyrap, *J. Am. Chem. Soc.*, **1932**, *54*, 2721.
17. R. Dessau, *Zeolites*, **1990**, *10*, 205.
18. R. Gomez and T. Lopez, *J. Sol-Gel Sci. Technol*. **1998**, *11*, 309.

19. J. Wang, M. Valenzyela, J. Salmon, A. Vazquez, A. Garcia-Ruiz and X. Boxhimi, *Catal. Today*, **2001**, *68*, 21.

20. D. Ganapathy and J. Jayeshi, *Microporous Mesoporous Materials,* **1999**, *33*, 1.

21. C. Morterra, G. Cerrato, C. Emanule and V. Bolis, *J. Catal.* **1993**, *142*, 349.

22. D. Ward, and E. Ko, *J. Catal.***1994**,*150*, 18.

23. M. Bensitel, O. Saur; J. Lavally and B. Morrow. *Mater. Chem. Phys.***1988**, *19*, 147.

24. A. Geiculescu and H. Specncer. *J. Sol-Gel Sci. Tech.* **1999**, *16*, 243.

25. W. Aiken and E. Matijevic, *J. Mater. Sci.* **1996**, *38(3)*, 329.

26. M. Ecormier, K. Wilson and A. Lee, *J. Catal.* **2003**, *215*, 57.

27. M. Ryashentseva, *Rev. Heter. Chem.*, **1994**, *10*, 23.

28. M. Ryashentseva, Kh. Minacher and Ya. Afanas'eva: USSR Patent 165425(1964). Chem. Abst. **62** 5256e (1965).

# CHAPTER 4

## SYNTHESIS AND CHARACTERIZATION OF SUPPORTED SULFATED ZIRCONIA OVER MESOPOROUS MOBIL CRYSTALLINE MATERIALS (MCM-41)

### INTRODUCTION:

Although sulfated zirconia is considered to be one of the important superacid catalysts, it has not achieved industrial and commercial applications due to its low surface area and short life time in catalytic reactions. There are several possible reasons responsible for the deactivation of sulfated zirconia, such as sintering, sulfur migration into the bulk metal oxide, and coke formation [1]. Another possible route for deactivation is that the sulfur is further reduced to a lower oxidation state in the form of $SO_2$ or $H_2S$. This process was interpreted by Lee et al. based on temperature programmed desorption TPD analysis [2,3], and was also confirmed by Arata and co-authors [4,5]. They demonstrated that when a reactant such as 1-butene adsorb and interact with the sulfate groups in the surface at relatively high temperature, a kind of redox reaction between sulfate group and adsorbate reactant take place leading to formation of oxidized species and loss of $SO_2$ gas.

In order to overcome such problems, sulfated zirconia can be supported over high surface area support. Supporting of zirconia over a proper support will prevent the sintering of the zirconia particles to form large particles, provide a high surface area, and facilitate the formation of the tetragonal active zirconia phase. Therefore, a better solution to overcome the problems associated with catalysis using sulfated zirconia is to find unique pore materials with uniform pores size and higher specific surface area. Porous materials have been extensively utilized in many catalysis and industrial applications. Depending on their microstructure, porous materials are classified into three categories according to the International Union of Pure and Applied Chemistry (IUPAC), microporous ($\leq$ 2nm) such as zeolites and related materials, mesoporous (2-50 nm) such as MCM and silica gel, and macroporous ($\geq$ 50nm) such as porous glasses and alumina membranes. Ishida et al. [5] synthesized supported sulfated zirconia on silica and studied its applications for the cyclopropane ring-opening isomerization reaction. A family of high surface area mesoporous silica materials MCM (Mobil Crystalline Materials ) was discovered for the first time in the early 1990's by research group in Mobile Corporation [6,7]. Upon this discovery, MCM was found effective in application as a support material in the petroleum refining industries. It has a unique ordered structure with uniform mesopores arranged into a hexagonal lattice. This is illustrated in the high resolution transmission electron microscopy picture shown in Figure 4-1. It exhibits narrow pore-size distribution, high thermal stability, and a large surface area of about 1000 $m^2/g$ with low density. The pore size of these materials varied between 2 nm and 10 nm depending on the surfactant chain length used. This pore size is much higher than the pore size of other porous materials such as conventional zeolites and aluminum phosphates.

However, these materials themselves are not very active in catalytic processes due to weak acidity that results from the amorphous structure of the silicate mesoporous materials.

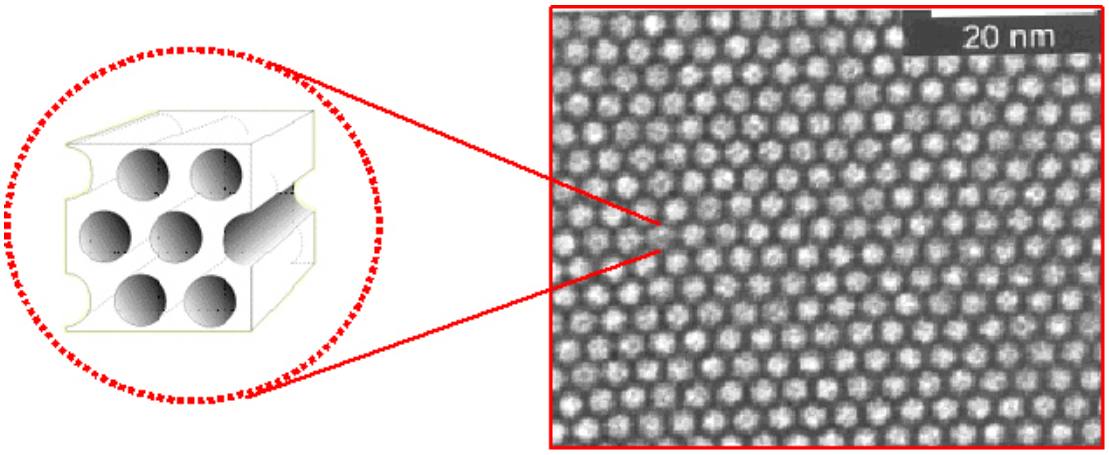


**Figure 4-1: Transmission Electron Micrograph of MCM-41. The mesoporous arrange in honeycomb-like structure, the black walls are thin amorphous silica [8].**

MCM-41 is usually synthesized by hydrothermal reaction using a suitable surfactant [6,7] to form a precipitate which can be filtered out, washed and calcined. Several factors are found to influence the resultant product such as solvent, source of silica, surfactant used, and thermal treatment. Mobil researchers have proposed two possible pathway for the formation of such mesoporous materials. This mechanism is called "liquid crystal templating" (LCT). The mechanism was proposed based on the fact that the pore size is dependant on the surfactant chain length and the close similarity of the morphology of the silicate mesophase and the structure of surfactant micelles in liquids. The mechanism is shown in Figure 4-2. In the first pathway, the template

organizes itself in the solution to form the hexagonal liquid crystal phase. The addition of silicate inorganic species then results in precipitation of these species on the hydrophilic surfaces of the micelles to form the MCM-41 framework. In the second pathway, it is proposed that the silicate inorganic species contribute to the formation of the liquid crystals by combination with the surfactant which results in the formation of the micellar rods. The micellar rods are further arranged by the inorganic phase to form the ordered hexagonal structure.

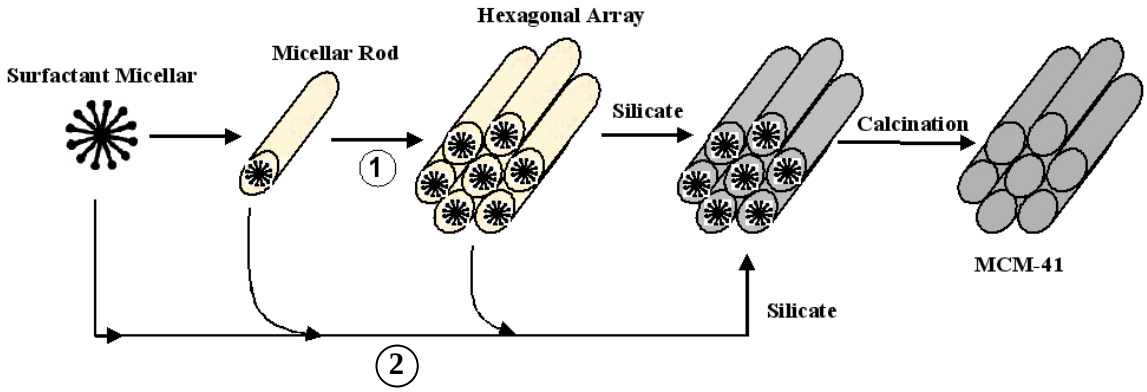


**Figure 4-2: Possible liquid crystal templating mechanism pathways for the formation of MCM-41.**

Gao et al. [9] have synthesized supported sulfated zirconia over MCM-41 by two-step impregnation methods. They reported that the acidity increased with increasing of the zirconium oxide content over the support. With this method, they claimed that the mesoporous frame work was destroyed by supporting more than 30% wt/wt $ZrO_2$. Xia et al. [10] prepared supported sulfated zirconia over MCM by chemical deposition of zirconium propoxide in hexane, followed by hydrolysis in an aqueous solution of sodium chloride and sulfation using sulfuric acid. They achieved highly acidic supported

catalysts which exhibited high catalytic activity for the isomerization of *n*-pentane and for the gas phase synthesis of methyl tertiary butyl ether (MTBE). However, their method of preparation was complicated and quite costly, and only one zirconia concentration was reported.

Despite the high thermal stability of the MCM materials, it has a limited stability due to the reactivity of the silica walls toward several reagents such as steam, and hydrolysis by materials such as hydroxide and flouride which results in collapse of the thin walls. Therefore, the stability of MCM in an aqueous solution is limited to a pH of 7 or less. In this chapter, we reported a new method for the synthesis and characterization of the several supported sulfated zirconia over MCM-41 composites by the preparation of a single precursor exploiting zirconium acetate and ethanesulfonic acid as starting reagents.

## EXPERIMENTS:

### Chemicals:

All the starting materials were purchased and used without any further purification. These were zirconium (IV) acetate hydroxide [$(CH_3CO_2)xZr(OH)y$ X+Y~ 4, Aldrich], ethanesulfonic acid [$(CH_3CH_2SO_3H)$, Aldrich], tetraethyl orthosilicate [$Si(OCH_2CH_3)_4$, Aldrich]; ethanol [$(C_2H_5OH)$, Aldrich]; iso-propanol [$(C_3H_9OH)$, Fisher-Scientific]; and hexadecylamine ($CH_3(CH_2)_{15}NH_3$), Aldrich].

**Synthesis:**

The MCM-41 support was synthesized in a manner similar to that described by Tuel et al [11]. First, a tetraethyl orthosilicate (TEOS) solution (250 mmole) in ethanol and iso-propanol was prepared with mole ratio of 1:6:1 TEOS, ethanol, and iso-propanol, respectively. A solution of hexadecylamine (75 mmoles) in 9000 mmoles of distilled water was added to the TEOS solution, and the resulting mixture was stirred continuously for 1 hour and then left for 12 hours without stirring at room temperature. The resulting solid was filtered off and washed with 300 ml of distilled water to remove all of the residual template and solvents. The solid was dried under vacuum at room temperature and calcined at 500°C for 12 hours to produce a mesoporous silica material. The supported sulfated zirconia was synthesized by addition of the required amount of MCM-41 support to an aqueous solution of 0.303 g (1.43 mmole) of zirconium (IV) acetate hydroxide [$Zr(OAc)_x(OH)_y$] and 0.312 g (2.86 mmole) of ethanesulfonic acid with stirring for 3 hours at room temperature to insure the impregnation of the zirconium salt into the pores of the silica support. The water in the solution was evaporated by rotary evaporation, and the samples were dried under vacuum. The supported sulfated zirconia was obtained by calcination of the supported precursors at 650 °C according to the thermogravimetric analysis data. The unsupported sulfated zirconia sample [SZ-(1:3)(650 °C)] was prepared according to the procedure that described earlier in Chapter 3.

**Characterization:**

In addition to the characterization techniques that pointed out in Chapters 2 and 3, three other analytical techniques were used for the characterization of the supported sulfated zirconia samples. These were X-ray photoelectron spectroscopy (XPS), carbon nitrogen sulfur microanalysis (CNS) and X-ray flourescence analysis.

The XPS measurements were performed by the Dr. Resasco research group at the University of Oklahoma. The XPS data were recorded on a Physical Electronics PHI 5800 ESCA System with a background pressure of approximately 3.0X $10^{-9}$ Torr. The electron takeoff angle was $45^{o}$ with respect to the sample surface. A 800-um spot size and 23 eV pass energy were typically used for the analysis. The Binding energies were corrected by reference to the C1s line at 284.8 eV for hydrocarbon. Quantification of the surface composition was carried out by integrating the peaks corresponding to each element with aid of the Shirley background subtraction algorithm, and then converting these peak areas to atomic composition by using the sensitivity factors provided for the each element by the PHI 5800 system software.

Carbon hydrogen nitrogen sulfur analysis were performed using (CHNS) Elemental Analyzer, model Vario ELMake: Elementar Germany. Simply, the sample was weighed in a tin capsule with continuous purging with oxygen on top of the capsule to free it from atmospheric nitrogen. The capsule was sealed with a specially designed capsule press. Samples were then transferred, by a sampling device, to the combustion tube heated at 1200ºC in an oxygenated helium atmosphere. The combustion of CHNS sample produces $CO_2$, $H_2O$, $SO_2$, $N_2$, NO, and $NO_2$. The oxygenated products are passed through a reduction tube containing copper at 850 ºC which quantitatively reduces the

nitrogen and sulfur oxides to molecular nitrogen and sulfur dioxide and binds excess oxygen as copper oxide. The remaining gas mixture of helium, $CO_2$, $H_2O$, $N_2$ and $SO_2$ is subsequently guided to a separation and measuring system. A thermal conductivity detector (TCD) is used for the detection of each component which is diverted to the detector sequentially by the adsorption and desorption columns.

Elemental analysis was determined using Siemens model *SRS 3000* wavelength dispersive X-ray fluorescence (WDXRF). The instrument uses X-ray energy as an excitation source for elemental lines emissions and characterizes elements according to their differing fluorescent wavelengths.

## RESULTS AND DISCUSSION:

### Thermogravimetric Analysis and Infrared Spectroscopy*:*

TG analysis was performed on the samples in order to estimate the suitable calcination temperature for preparation of the supported zirconium oxide from the precursors. Figure 4-3 shows the TGA profiles for the unsupported and the supported precursors. The profiles suggest that the precursor thermally decomposed in stepwise manner. In the first step, the weakly bonded water molecules were lost, and with further heating, a decomposition of the coordinated ligands occurred to give a volatile organic byproducts, carbon dioxide, and water. According to Davis and associates [12], the weight loss observed above 650 ºC is probably due to the loss of sulfur in the form of sulfur dioxide and oxygen. Figure 4-4 showed the IR spectras for the supported samples taken in the region from 3500 $cm^{-1}$ to 4000 $cm^{-1}$ after calcination to 650 °C. The MCM support showed a sharp peak with medium intensity at about 3750 $cm^{-1}$ corresponding to

the O-H bond vibration of the free Si-O-H groups on the support surface. The intensity of this peak was obviously reduced with the increase of the amount of the sulfated zirconia on the support surface. These results confirm that the MCM-41 support surface is covered by a layer of the sulfated zirconia in the supported samples and the covering degree increases with increase of the sulfated zirconia on the surface.

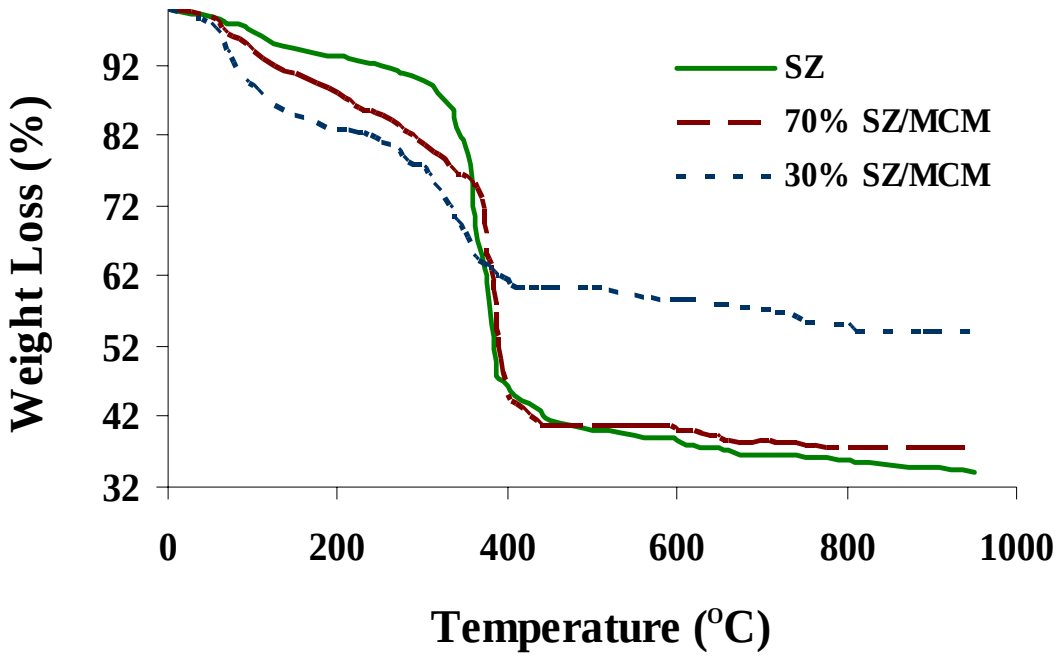


**Figure 4-3: Thermogravimetric analysis profiles for the supported sulfated zirconia with different zirconia concentrations.**

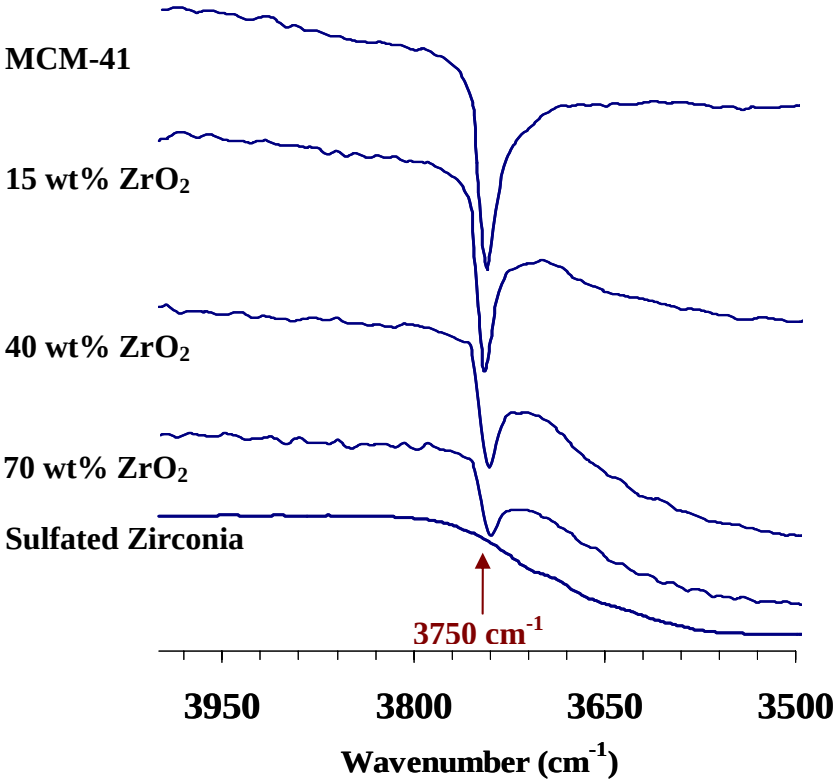


**Figure 4-4: The IR spectra for the supported samples, the stretching frequencies of the Si-OH groups of the MCM support are shown.**

**X-ray Diffraction (XRD):**

The XRD pattern for the supported samples gives an indication of the dispersion of the sulfated zirconia over the MCM-41 support surface. Figure 4-5 shows that there are no diffraction peaks corresponding to the tetragonal zirconia when the zirconia contents reached 30%. At about 40% zirconia load over the support, a weak tetragonal phase was observed indicating, that up to 40% $ZrO_2$ load, the zirconia is still well-dispersed in the pores of the silica. Above that concentration (about 70% $ZrO_2$ / MCM) a strong tetragonal phase peak at $2\theta = 30°$ was observed, which indicated that the support pores were packed and the zirconia started to build on the exterior of the MCM-

41 particles. The uniform decrease of the surface area with increasing the $ZrO_2$ content (Table 4-1) also confirmed the blockage of the pores with zirconia. It was theoretically calculated that the required amount of zirconium oxide for the formation of a monolayer over the support surface is 2.57 grams for each gram of the MCM support. This demonstrates that the zirconium oxide monolayer formed after covering about 72% of the support surface. These calculations achieved using the unit cell dimensions of the tetragonal zirconia model shown in Figure 4-6. Additionally, Figure 4-5 showed that the tetragonal phase, which is known to be the more catalytically active phase [13,14], was the only phase observed for the supported samples when calcined at 750 ºC. However, the XRD profile for the unsupported calcined precursor showed the appearance of the monoclinic phase along with the dominant tetragonal phase. These results are identical to that obtained by Huang [15] for the zirconium sulfate supported over silica gel.

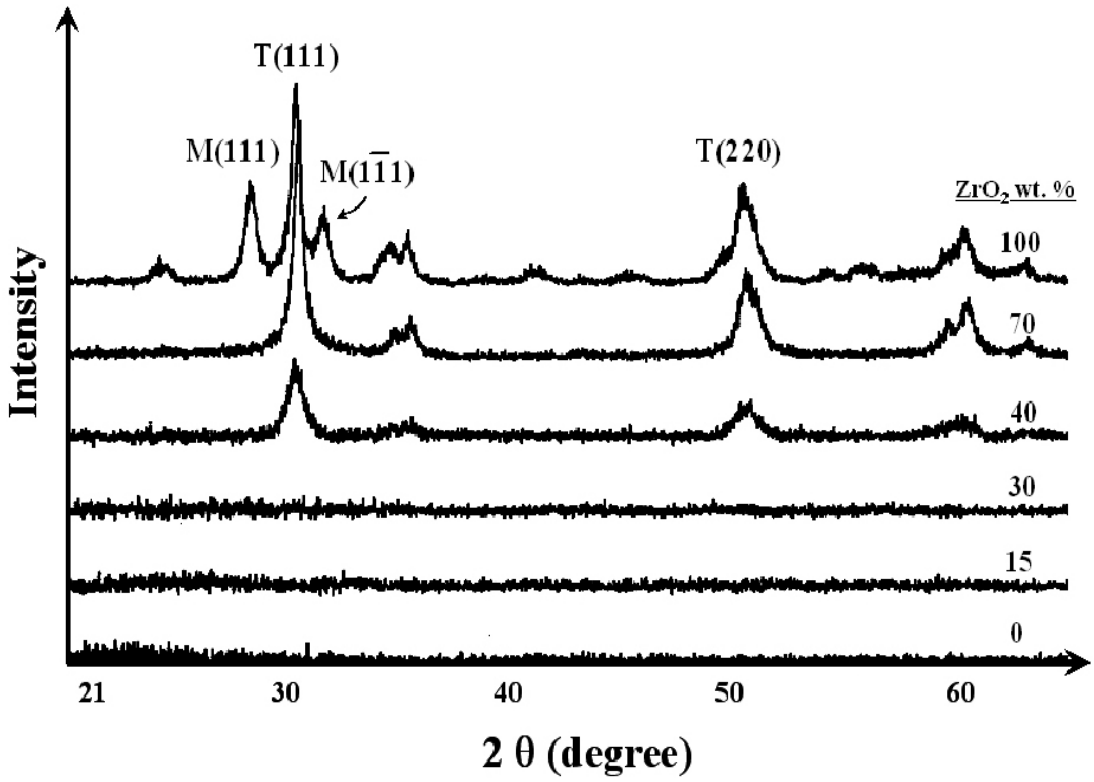


**Figure 4-5: X-ray diffraction pattern for the supported samples with different zirconia contents calcined at 750 ºC.**

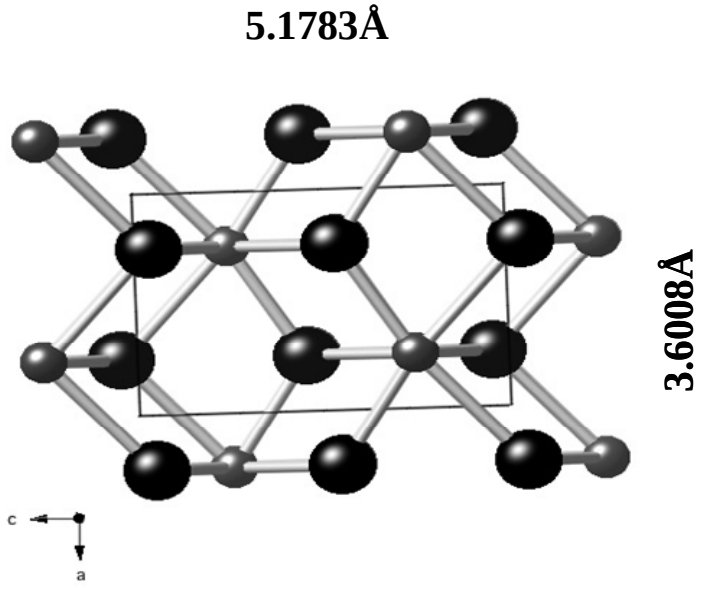


**Figure 4-6: Crystal structure and unite cell dimensions of the tetragonal zirconia.**

The average crystallite sizes obtained by Scherer's method (Figure 4-7) were 4.3 nm and 7.7 nm for the supported samples contains 40% and 70% zirconia, respectively. The average crystallite size for the unsupported zirconia was about 14 nm. This clearly implies that the crystallite size was increasing with increasing the zirconia content. The small crystallite size and the stability of the active metastable tetragonal phase was a result of supporting the sulfated zirconia on the silica MCM. Supporting of sulfated zirconium oxide on the mesoporous MCM-41 materials results in a decrease of the crystallite size by inhibiting the growth of the zirconium particles.

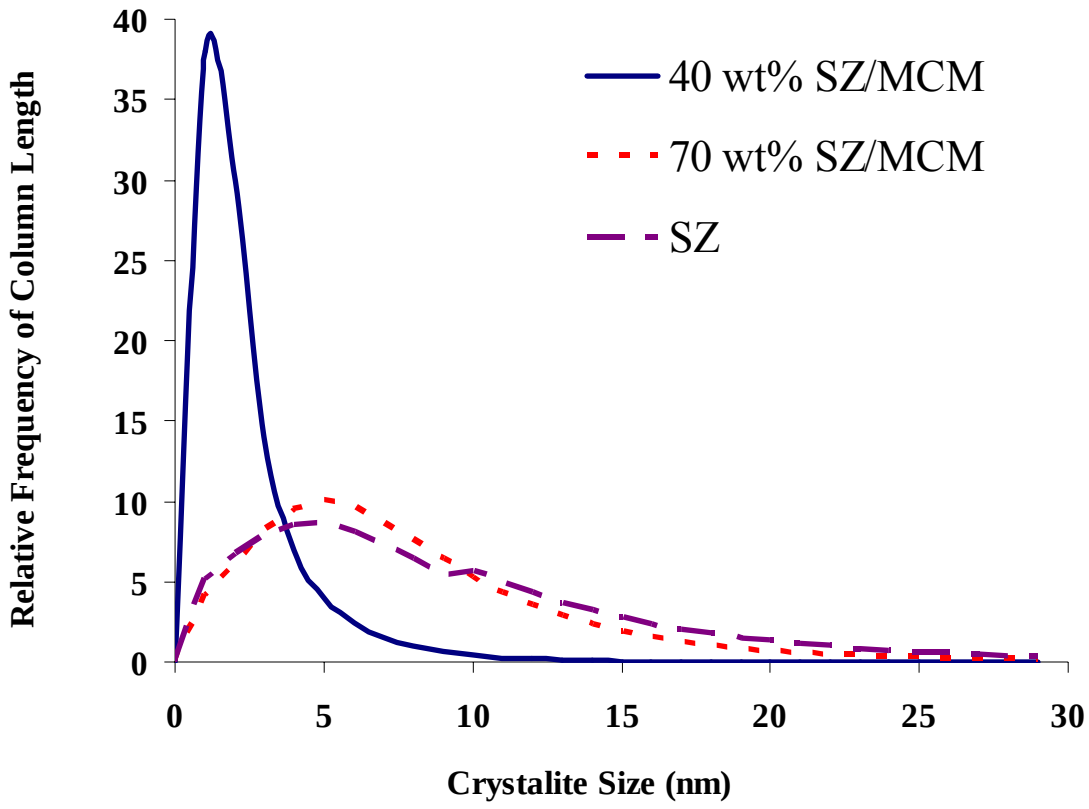


**Figure 4-7: The crystallite size distribution derived from the XRD for the supported sulfated zirconia samples over MCM, the samples calcined at 650 °C.**

**Elemental analysis and pore volume:**

The bulk elemental analysis using XRF and pore volume results of the synthesized supported catalytic systems are summarized in Table 4-1. The elemental analysis showed that the sulfur contents of the supported samples are higher than the sulfur contents of the bulk sulfated zirconia. The maximum sulfur content as observed for 40% SZ/MCM sample. This indicates that the support stabilized the coordinated sulfate groups in the surface.

Additionally, the pore volume and specific surface area data are shown in Table (4-1). The results showed a slight and uniform decrease on both the surface area and the pore volume with an increase of the zirconium oxide contents over the MCM support surface. At higher than 40% SZ/MCM composites, sharper decrease on the pore volume and surface area occurred. These results showed that most of the $ZrO_2$ contents are available inside the pores and well dispersed on the surface. However at a load higher than 40% SZ/MCM the decrease in the pore volume was observed markedly and the sulfur contents as well decreased. This decreased in the sulfur contents maybe attributed to the migration of most of the sulfate groups from the MCM pores to the surface which facilitate the decomposition during thermal calcination. This strongly implies that the support stabilized the coordinated sulfated groups to the zirconia. In this research work, the 40% SZ/MCM appear to be the dispersion threshold of sulfate zirconia on the surface.

**Table 4-1: The pore volume and elemental analysis results for the supported sulfated zirconia samples.**

| Catalyst Sample | $S_{BET}$ ($m^2/g$) | **Pore volume (ml/g) | Elemental Analysis by ‡XRF (%) | | | | Sulfur Contents by ‡‡CHNS analyzer (%) |
|---|---|---|---|---|---|---|---|
| | | | Zr | Si | S | O | |
| **MCM-41** | 1175 | 1.1 | ---- | 45.3 | ---- | 52.4 | ---- |
| ***SZ** | 49.5 | 0.08 | 73.1 | ---- | 0.41 | 26.4 | 0.38 |
| **15% SZ/MCM** | 1037 | 1.03 | 16.6 | 35.1 | 0.95 | 47.35 | 0.633 |
| **30% SZr/MCM** | 714 | 0.92 | 32.2 | 25.1 | 1.08 | 41.6 | 0.754 |
| **40% SZ/MCM** | 545 | 0.75 | 43.9 | 16.3 | 2.28 | 37.5 | 1.76 |
| **70% SZ/MCM** | 274 | 0.35 | 61.1 | 7.14 | 0.78 | 30.8 | 0.979 |

* *SZ = unsupported sulfated zirconia*
** *Total pore volume was measured at P/Po = 0.9929*
‡ *CHNS = Carbon hydrogen nitrogen sulfur*
‡‡ *XRF = X-ray Florescence*

**XPS Analysis:**

The XPS data show a strong influence of the support on the surface chemistry of the zirconia. Below the maximum loading (where crystalline $ZrO_2$ forms) the surface is rich in sulfate while once the $ZrO_2$ starts to crystallize, the surface sulfur concentration drops. The XPS surface analysis results (Table 4-2) showed that the Zr and S atomic percentage on the surface increased with increasing of the sulfated zirconia content on the MCM support. However, the results showed that the S/Zr atomic ratio on the surface decreased with increasing zirconium content. For 15 wt% SZ/MCM, the surface atomic ratio of S/Zr was higher than the ratio of Zr:S in the precursor. With further increasing the amount of sulfated zirconia on the support more than 40 wt%, the atomic ratio of S/Zr

the surface decreases remarkably. This is may be due to incorporation of the sulfur species into the catalyst bulk.

**Table 4-2: Surface atomic percentage extracted from XPS analysis.**

| Sample | Atomic % | | | | Bulk S/Zr | XPS S/Zr |
|---|---|---|---|---|---|---|
| | C | Zr | S | O | Ratio | Atomic Ratio |
| **15 wt% SZ/MCM** | 6.2 | 4.39 | 4.21 | 85.16 | 0.057 | 0.959 |
| **40 wt% SZ/MCM** | 8.7 | 8.89 | 6.25 | 76.19 | 0.05 | 0.703 |
| **70 wt% SZ/MCM** | 15.4 | 17.35 | 8.38 | 58.84 | 0.013 | 0.453 |
| **SZ** | 14.8 | 27.87 | 1.33 | 56.25 | 0.0056 | 0.05 |

** SZ = unsupported sulfated zirconia; surface area data and bulk elemental analysis are presented in Table 4-1.*

The results in Table 4-2 showed also the S/Zr ratio obtained form the XRF bulk elemental analysis. The S/Zr ratio was decreases with increases of the amount of sulfated zirconia on the MCM-41 support. These results are similar to the results obtained from the XPS analysis. However, the S/Zr ratio obtained from bulk analysis is much low (10-15 times lower) than that derived from the XPS surface analysis. These results strongly support a very important conclusion that the sulfur species are mostly available on the surface of the oxide rather than in the bulk.

It was determined by XPS that the MCM-41 silica was treated with ethanesulfonic acid followed by calcination at 650 °C did not contain a considerable amount of sulfate

species on the surface. This clearly demonstrates that the sulfate groups are strongly coordinated to the zirconium metal centers not to the silica of the MCM-41 support (Si : S atomic ratio = 200:1). Therefore, it can be concluded that the zirconium oxide attaches to the surface of the MCM-41 support by condensation with reactive silanol groups and the silicate groups are bonded to the surface of the zirconia. The proposed structure is shown in Figure 4-8.

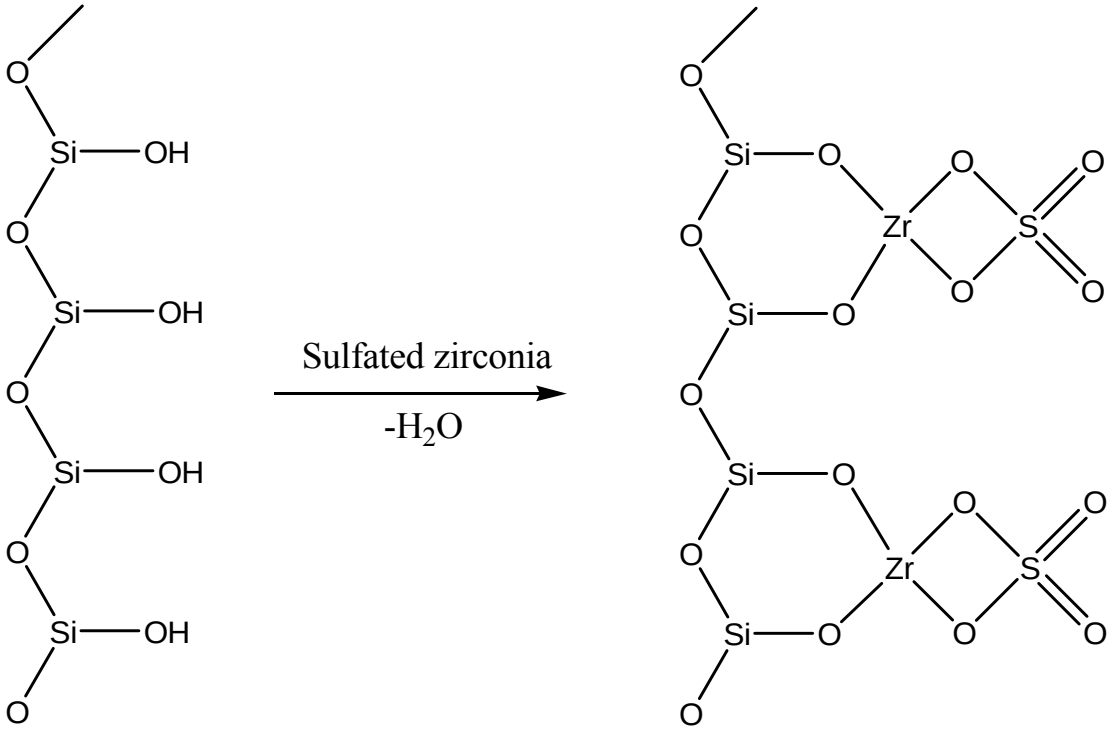


**Figure 4-8: Proposed structure of sulfated zirconia over MCM-41.**

**Scanning Electron Microscopy:**

The SEM data for the supported catalyst with 15% and 70% zirconia contents are shown in Figure 4-9. The sample with the higher concentration of zirconia contained particles similar to the support along with tubules that can be presumed to be zirconia.

The tubes have an approximate diameter between 70 nm and 120 nm. Firing of the sulfated zirconia without the MCM-41 present did not produce any zirconia nanotubes. This suggests that the MCM-41 catalyzed the crystallization of zirconia. This could occur by initial crystallization of zirconia within the pores of the MCM followed by elongation of the crystal out of the pores. However, the average width of the tubes is 7-10 times larger than the pores of the MCM (≈10nm). Thus, if this crystallization mechanism does occur the zirconia tubules would likely be bindles of several nanowires.

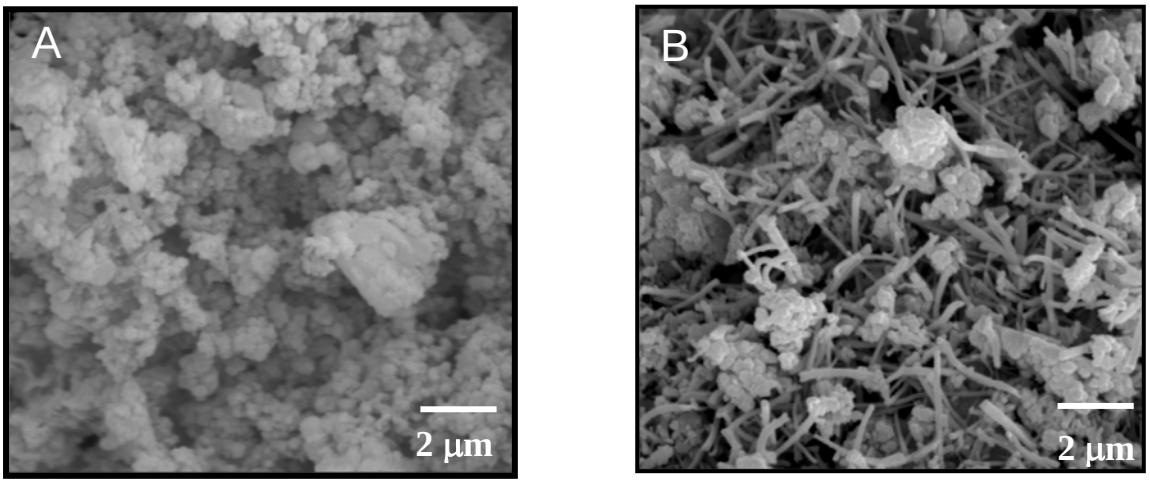


**Figure 4-9: Scanning Electron Micrographs for the supported sulfated zirconia, A: with 16% zirconia, B: with 70% zirconia.**

**Surface Acidity of the Supported Sulfated Zirconia:**

Table 4-3 showed the acidity strength measurements results using Hammett indicators. Generally, the results showed that the acidity strength increased with an increase of the amount of sulfated zirconia over the MCM-41 support surface.

**Table 4-3: Acid strength measurement of the supported sulfated zirconia using Hammett indicator**

| Sample code | *Color Indicator / (pKa) | | | | | | |
|---|---|---|---|---|---|---|---|
| | **B(+3.3)** | **C(+1.5)** | **D(+0.8)** | **E(-3)** | **F(-5.7)** | **G(-8.2)** | **H(-11.4)** |
| **MCM-41** | ---- | D. yellow | Blue | Yellow | Colorless | Colorless | Colorless |
| **SZ** | D. Red | Purple | Yellow | D. red | Yellow | Yellow | Yellow |
| **‡SZ** | L. Red | L. Purple | Green | L. orange | Colorless | Colorless | Colorless |
| **15% SZ/ MCM** | Red | D. purple | Yellow | Red | L. yellow | Colorless | Colorless |
| **30% SZ/ MCM** | D. red | Purple | Yellow | Red | L. yellow | Colorless | Colorless |
| **40% SZ/ MCM** | Red | Purple | D. yellow | D. red | Yellow | Yellow | L. yellow |
| **‡40% SZ/ MCM** | Red | Purple | Yellow | Red | Yellow | L. Yellow | L. yellow |
| **70% SZ/ MCM** | Red | Purple | Yellow | D. red | Yellow | Yellow | L. yellow |

**All the indicators detailed are summarized in Table 3-2 in Chapter 3.*
*All the samples were calcined at 650 °C.*
*‡ Samples were calcined at 950 °C*

The acid strength measurement using the Hammett indicators method showed that the supported sulfated zirconia samples exhibited high acid strength. The 40 wt% SZ/ MCM protonated *p*-nitrotoluene (pKa = -11.4) causing the indicator to change from colorless to yellow. The zirconias failed to react with 2,4-dinitrotoluene which has a pKa of -13.75 demonstrated that their pKas are in the range of -11.4 to -13.75. In order to test the influence of the support, both the supported (40 wt% SZ/MCM) and unsupported precursor were calcined at 950 °C for 8 hours. In contrast to the unsupported precursor, the supported samples calcined at high temperature retained their acid strength. The supported sample gave a yellow coloration with both anthraquinone (pKa = -8.2) and *p*-nitrotoluene (pKa= -11.4), while no color change occurred when either indicator was exposed to the unsupported samples. Additionally, supported sample calcined at high temperature gave a dark red coloration with dicinnamalacetone (pKa= -3), while a very

light orange color was noted with the unsupported sample calcined at 950°C. It is known that the acid-form color of dicinnamalacetone is red and the base-form color is yellow [16]. Therefore, the results clearly indicate that the acid strength and number of acid sites of the unsupported oxide drops when heated to high temperature, presumably due to the loss of the active sites in the form of $SO_2$ or $SO_3$. However, the supported sample retained acidity due to strong support / catalyst interaction which plays an important role in the delay of decomposition and loss of sulfur. The XRD results for the samples calcined at high temperature (Figure 4-10) showed that the phase transformation from tetragonal to monoclinic phase was delayed with the supported sample compared to that of unsupported sulfated zirconia. Not only does sulfonation stabilize the tetragonal phase, but stabilization of the tetragonal phase by interaction with the support also stabilizes the sulfonated surface. Thus, it would appear that the primary loss of acidity of sulfonated zirconias during calcination is due to surface reconstruction as the tetragonal to monoclinic phase change takes place.

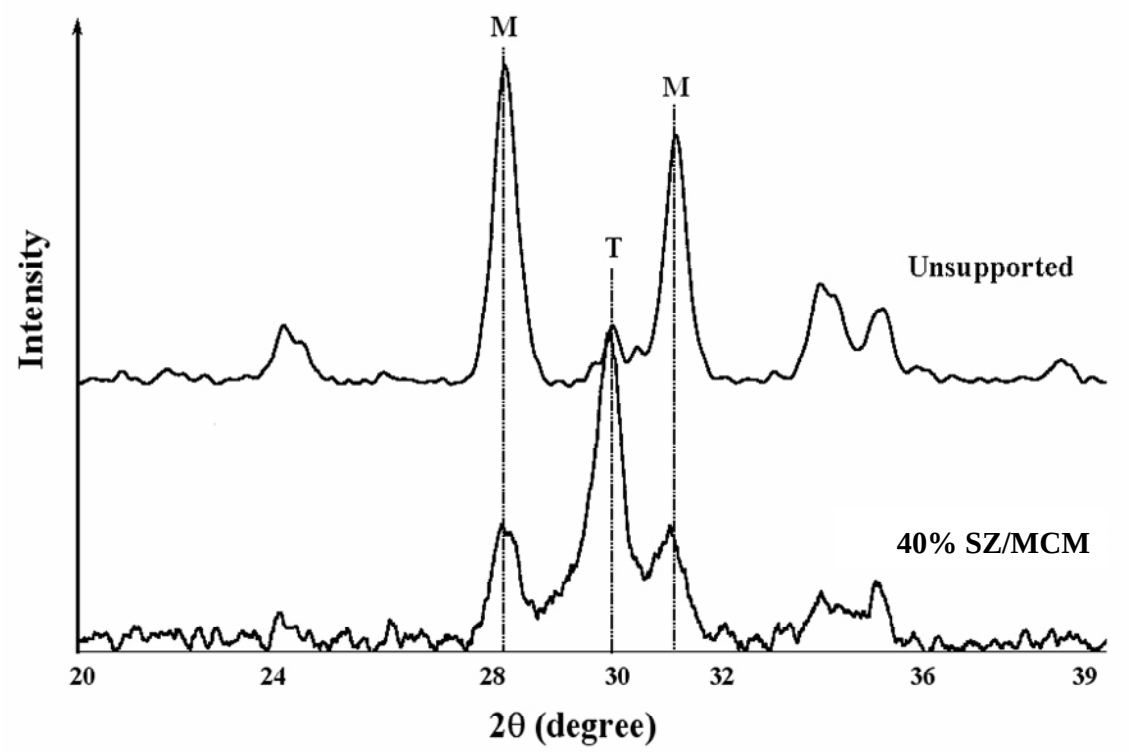


**Figure 4-10: X-ray diffraction pattern for the supported and unsupported sulfated zirconia calcined at 950 °C for 8 hours.**

The total acidity measurements were performed using cyclohexylamine as a titrant. Also, intermolecular cyclization of acetonylacetone was used as a probe reaction. The detailed of methodology of the acidity measurements using cyclohexylamine and acetonylacetone was extensively discussed earlier in Chapter 3. The results of these tests are shown in Table 4-4. The cyclohexylamine adsorption showed that the number of acid sites per square meter of the sulfated zirconia increased with increasing amount of sulfated zirconia on the MCM support. The acetonylacetone conversion and selectivity towards dimethylfuran also increased with increasing the amount of sulfated zirconia to maximum at 40% SZ/MCM, beyond which the activity and selectivity began to

decreases. The highest acetonylacetone conversion and dimethylfuran selectivity was obtained with the 40% sulfated zirconium oxide over MCM composite. This reflects the optimum combination of high specific surface area and high coverage with available active acid sites on the surface. Additionally, the cyclohexylamine adsorption on silica support showed that its acidity at 1.73 mmol/g was relatively high due to the fact that cyclohexylamine is a relatively strong base (pKa of 10.6) [17] and can be adsorbed on the weakly acidic sites of the MCM. However, no dimethylfuran product was detected from reaction of acetonylacetone over pure MCM implying that the acid sites of MCM were not strong enough to perform such reactions. Surface acidity strength measurements of the MCM confirmed this hypothesis since its pKa value was found to be higher than + 3.3.

**Table 4-4: Acidity measurement for the supported sulfated zirconia**

| Catalyst Sample | $S_{BET}$ ($m^2/g$) | Acidity Measurements | | | |
|---|---|---|---|---|---|
| | | Cyclohexylamine adsorption | | Acetonylacetone Cyclization Reaction | |
| | | μmol/g | μmol/$m^2$ | Acetonylacetone Conversion (%) | Dimethylfuran Selectivity (%) |
| **MCM-41** | 1175 | 1733 | 1.47 | 11.5 | 0 |
| **SZ** | 49.5 | 277 | 5.60 | 28.4 | 89.6 |
| **15% SZ/MCM** | 1037 | 1737 | 1.68 | 31.3 | 87.9 |
| **30% SZ/MCM** | 714 | 1469 | 2.06 | 36.0 | 95.2 |
| **40% SZ/MCM** | 545 | 1213 | 2.23 | 41.6 | 98.4 |
| **70% SZ/MCM** | 274 | 1464 | 5.34 | 35.8 | 92.3 |

*SZ = Unsupported sulfated zirconia.*

**CONCLUSIONS AND REMARKS:**

Supported samples were successfully synthesized by the impregnation of sulfated zirconia precursor over calcined MCM-41samples. This method provides a suitable route for obtaining a well dispersed, highly sulfated tetragonal zirconia content on the internal surface of the silica support with a small crystallite size without major blockage of the support pores. The supported samples showed an extremely high thermal stability with suppression of the tetragonal phase transformation to the monoclinic phase. The S/Zr ratio on the surface decreased with an increase the amount of the sulfated zirconia on the support. The XPS results also demonstrated that the surface sulfate groups strongly coordinate to the zirconium atoms but not to the silicon atoms. Furthermore, the XPS results along with the elemental analysis showed that most of the sulfur is available in the surface rather than in the catalyst bulk. Supported sulfated zirconia samples exhibited high acidity strength that was retained even when the supported samples calcined at high temperature presumably due to the availability of the acid sites inside the MCM-41 pores. These supported catalysts showed a remarkable and promising activity for alkylation and condensation reactions that will be discussed in the next chapters of this thesis.

**REFERENCES CITED:**


1 M. Lakshmi, A. Rahman, T. Bandyop and Y. Haritha, S*ynth. Comm.*, **1999**, *29(4)*, 691.

2 J. Lee and D. Park, *J. Catal*., **1990**, *126*, 361.

3 J. Lee, M. Yeom and D. Park, *J. Catal. Lett*., **1989**, *40*, 101.

4 M. Hino, S. Kobayashi and K. Arata, *Recat. Kinet Catal. Lett*., **1981**, *18*, 491.

5 H. Matsuhashi, M. Hino and K. Arata*, Appl. Catal*., **1990**, *59*, 205.

6 C. Kresge, M. Leonowiez, W. Roth, J. Vartudi, and J. Beck, *Nature*, **1992**, *359*, 710.

7 J. Beck, J. Vartuli, W. Roth, M. Leonowicz, C. Krsge, K. Schmitt, C. Chu, D. Olson, S. Sheppard, S. McCullen, J. Higgins and J. Schlenker, *J. Am. Chem. Soc.*, **1992**, *114*, 10834.

8. K. de Jong and A. Koster, *Chemphyschem*, **2002**, *3*, 776.

9 Lei, T.; Hua, M.; Tang, Y.; Yue, Y.; and Gao, Z., *Chem. J. Chin Univ.* **2000**, *21*, 1240.

10 O. Xia, K. Hidajat and S. Kawi, *Chem. Comm.*, **2000**, *22*, 2229.

11 V. Adeeva, J. Dehaan, J. Janchen, G. Leb, V. Schunemann, L. Van de ven, W. Schtler and R. Van Santen, *J. Catal.*, **1995**, *151*, 364.

12 B. Davis, R. Keogh, and R. Srinilasan, *Catal. Today*, **1994**, *20*, 219.

13 C. Morterra, G. Cerrato, F. Pinna and M. Signoretto, *J. Catal.*, **1995**, *157*, 109.

14 R. White, E. Sikabwe, M. Coelho and P. Resasco, *J. Catal.*, **1995**, *157*, 755.

15 Y. Huang, B. Zhao and Y. Xie, *App.Catal. A*, **1998**, *173*, 27.

16 K. Tanabe, M. Misono, Y. Ono and H. Hattori, *New Solid Acids and Bases, Their Catalytic Properties*. Elsevier, Tokyo, 1989.

17 F. Alvarez and S. Yalkowsky, *Inter. J. Pharm*. **1997**, *151*, 193.

# CHAPTER 5

## ALKYLATION OF BENZENE OVER SULFATED ZIRCONIA USING ETHERS AS ALKYLATING AGENTS

### INTRODUCTION:

Friedel-Crafts alkylation is a vitally important reaction for the production of fine chemicals and for petrochemical refining. Commercially, a high yield of alkylated products is usually achieved using a homogenous Lewis acid such as aluminum chloride, iron chloride, and boron fluoride or protonic acids such as sulfuric acid as catalysts [1,2]. However, there are problems associated with the technologies that utilize liquid-soluble, acid catalysts such as difficultly of separation of the spent catalysts, corrosion, and some environmental problems involving toxicity. These issues encourage the development solid acid catalysts which are suitable for alkylation reactions.

Sulfated zirconia is an environmental-friendly solid acid with numerous applications in alkylation reactions such as benzylation of benzene and benzene derivatives [3,4], alkylation of cresols with isobutylene [5], alkylation of phenol with methyl tertiary butyl ether to produce tert-butyl phenols [6], and alkylation of diphenyl oxide with olefins [7]. A variety of organic species such as alcohols, alkyl chlorides, ethers, and olefins can be used as alkylating agents in conjunction with sulfated zirconia.

In this section, the alkylation of benzene reaction over sulfated zirconia will be performing and discussed utilizing several ethers as alkylation agents to produce alkylated benzene derivatives. The ethers exploited are anisole, diethyl ether, dibenzyl ether, benzyl methyl ether, and n-butyl ether.

**EXPERIMENTAL*:***

**Chemicals:**

All the starting materials were purchased and used without any further purification. These were dibenzylether [($C_{14}H_{14}O$), Aldrich], methyl benzylether [($C_8H_{10}O$), Aldrich], n-butylether [($C_8H_{18}O$), Aldrich], benzyl alcohol [($C_7H_8O$), Aldrich], and benzene [($C_6H_6$), Fisher].

**Procedure:**

The alkylation reactions were carried out in a 30-ml Teflon bomb reactor at a variety of reaction temperatures. An appropriate amount of dibenzylether or other desired ether was mixed with an excess of benzene with a desired catalyst loading of wt% with respect to the total weight of the reactants. Samples were collected from the reactor at different reaction times and diluted with methylene chloride for analysis. (GC/MS) was performed on a Hewlett Packard G1800A instrument equipped with 30 m x 0.25 mm HP5 column (Crosslinked 5% PhME silicone). The temperature program used was an initial hold of 2 min at 35 °C, a ramp of 5°C/min to 170 °C, and a final hold of 5 min. The helium flow rate was 1 ml/min and the injection port was set at 250 °C. The ether

conversion was calculated as follows: Ether conversion (%) = (Cn/Co) X 100, where Cn and Co are the moles of ether reactant converted, and moles of ether in feed, respectively.

## RESULTS AND DISCUSSIONS:

### Effect of the catalyst concentration on alkylation reaction:

The effect of the catalyst loading on the alkylation reaction of benzene with dibenzyl ether was investigated by varying of the ratio of the unsupported sulfated zirconia catalyst to the total weight of the reactant. It was found that the rate of the dibenzyl ether conversion and the yield of diphenylmethane increased with increasing of the amount of the catalyst used (Figure 5-1). When the reaction was run for 2 hours at 150 °C, the conversion of dibenzyl ether increased from 6% to 59% with increasing of the catalyst weight percent with respect to the reactant from 10% to 50%. The slope of the plot of the natural logarithm of the catalyst concentration versus natural logarithm of the initial rate contestant $k_{obs}$ (slope = 1.06) indicate a first order reaction with respect to the catalyst concentration (Figure 5-2).

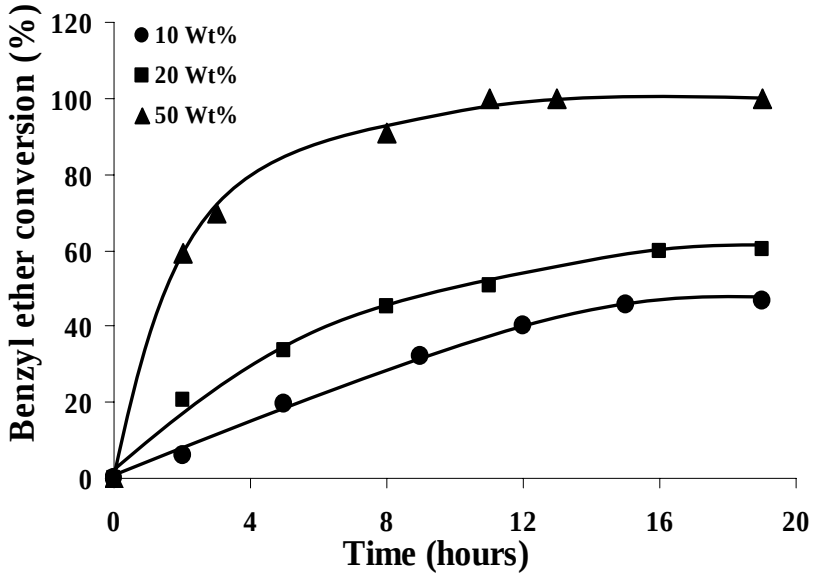


**Figure 5-1: Effect of the catalyst loading on the benzyl ether conversion in the alkylation reaction of benzene over SZ sample at 150 °C, (The weight percent is with respect to the total reactants weight).**

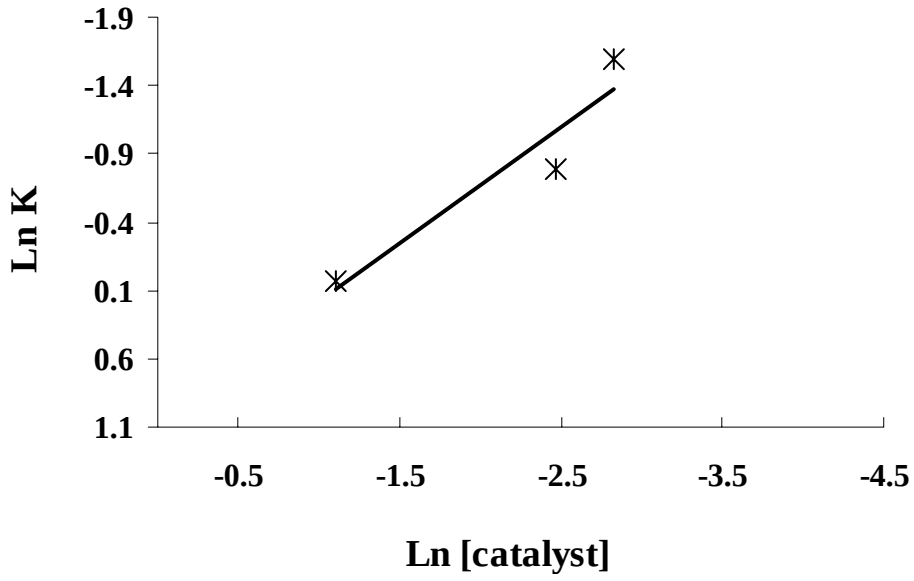


**Figure 5-2: A plot of the natural logarithm of the rate constant versus the natural logarithm of the catalyst concentration. (Slope =1.06 ( ± 0.35 within a 90% C.L.)).**

**Effect of the Reaction Temperature:**

The effect of the reaction temperature on the rate alkylation of benzene reaction was investigated by conducting the reaction at three different temperatures, mainly at 100 ºC, 150 ºC, and 180 ºC, under fixed reaction conditions (10 wt% catalyst with respect to reactants with dibenzylether : benzene mole ration of 1:10). Figure 5-3 shows a plot of the dibenzyl ether conversion versus time at different reaction temperatures. The results demonstrate that the reaction rate strongly depends on the reaction temperature.

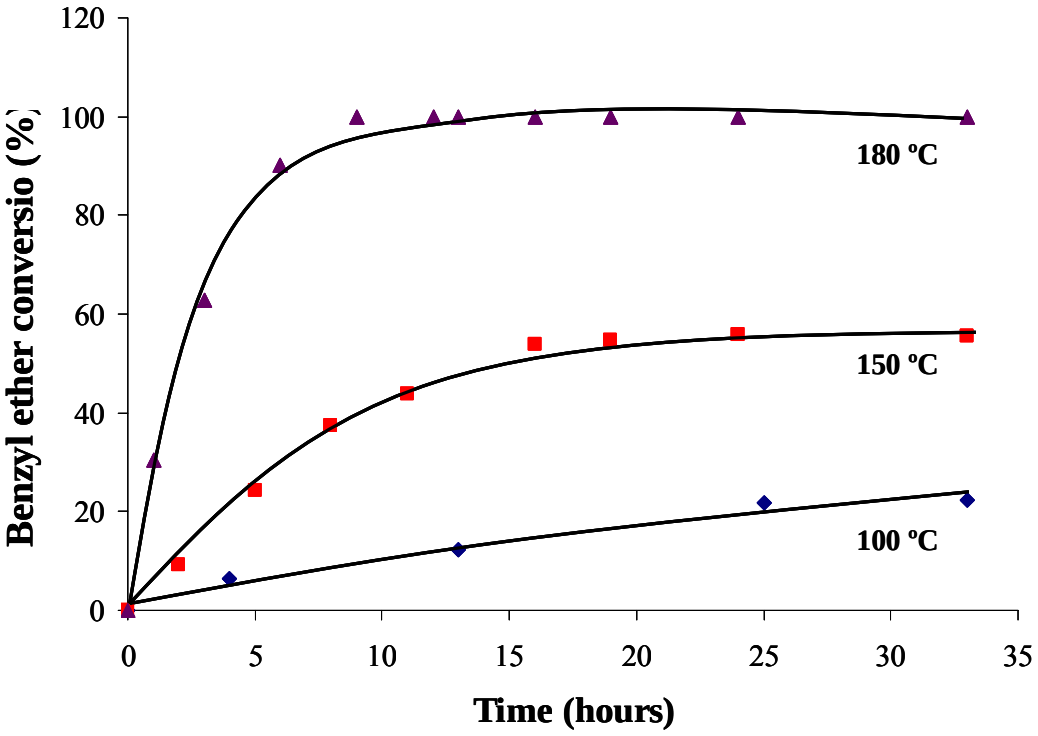


**Figure 5-3: Alkylation of benzene with benzyl ether at different reaction temperatures. (Reaction conditions: catalyst load of 10 wt% with respect to reactants; Benzyl ether: Benzene mole ratio of 1:10)**

When the reaction proceeds for 5 hours at low temperature (100 °C), the dibenzyl ether conversion was only about 7%. The diphenyl methane selectivity at this point was 65.3 % due to the formation of other products such as benzaldehyde and benzyl alcohol which is unreactive at this temperature. When the reaction temperature is elevated to 150 °C, the dibenzyl ether conversion was increased to about 25% after 5 hours with increasing of the diphenyl methane selectivity to 88%. When the reaction was conducted at higher temperature (180 °C) for 6 hours, the dibenzyl ether conversion further increased to 80% and the selectivity of the diphenyl methane increased to 93%. Apparently, the reaction is controlled by the kinetics and requires high activation energy. Even when the reaction time was prolonged to 24 hours at 180 °C and the conversion of dibenzyl ether is almost completed, high selectivity towards diphenylmethane was maintained. However, there was some formation of over-alkylation products such as benzyl diphenyl methane (BDPM) and dibenzyl diphenyl methane (DBDPM). Figure 5-4 illustrated the effect of the reaction temperature on the product distribution.

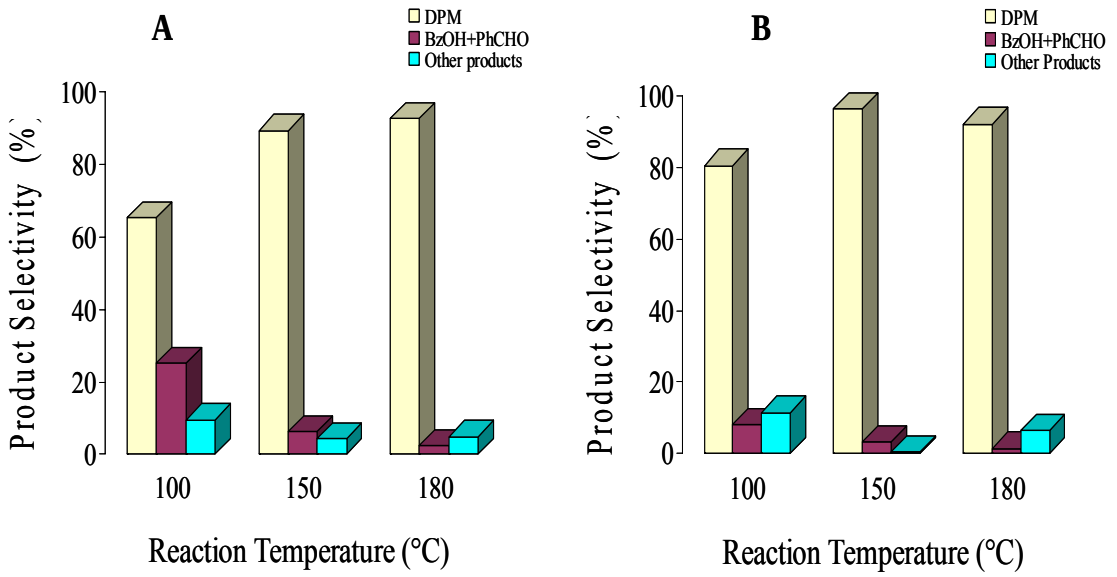


**Figure 5-4: Effect of the reaction temperature on the product selectivities of the alkylation of benzene reaction with benzyl ether. A: the reaction was performed for 5 hours, B: the reaction was performed for 24 hours. (Reaction conditions: catalyst load of 10 wt% with respect to reactants; Benzylether: Benzene mole ration of 1:10).**

** BzOH and PhCHO are benzyl alcohol and benzaldehyde respectively and DPM is diphenylmethane.*

Figure 5-5 shows a plot of the natural logarithm of the dibenzyl ether concentration versus time. The activation energy of the reaction was determined from a slope of the plot of the natural logarithm of ether conversion rate versus the inverse of the temperature according to Arrhenius equations (Figure 5-6). The resulting activation energy was 62 kJ/mole.

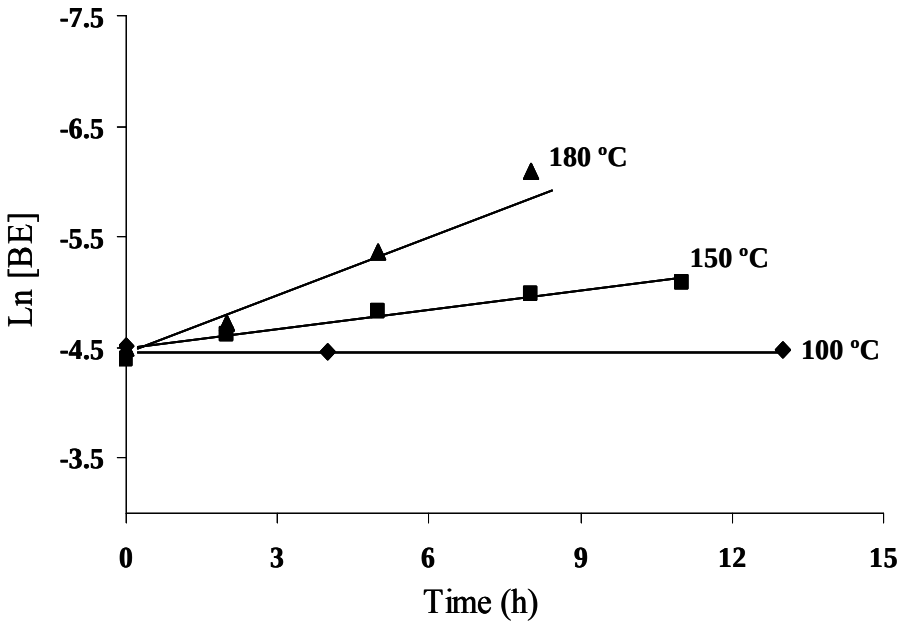


**Figure 5-5: A plot of the natural logarithm of benzyl ether concentration versus time at different reaction temperatures.**

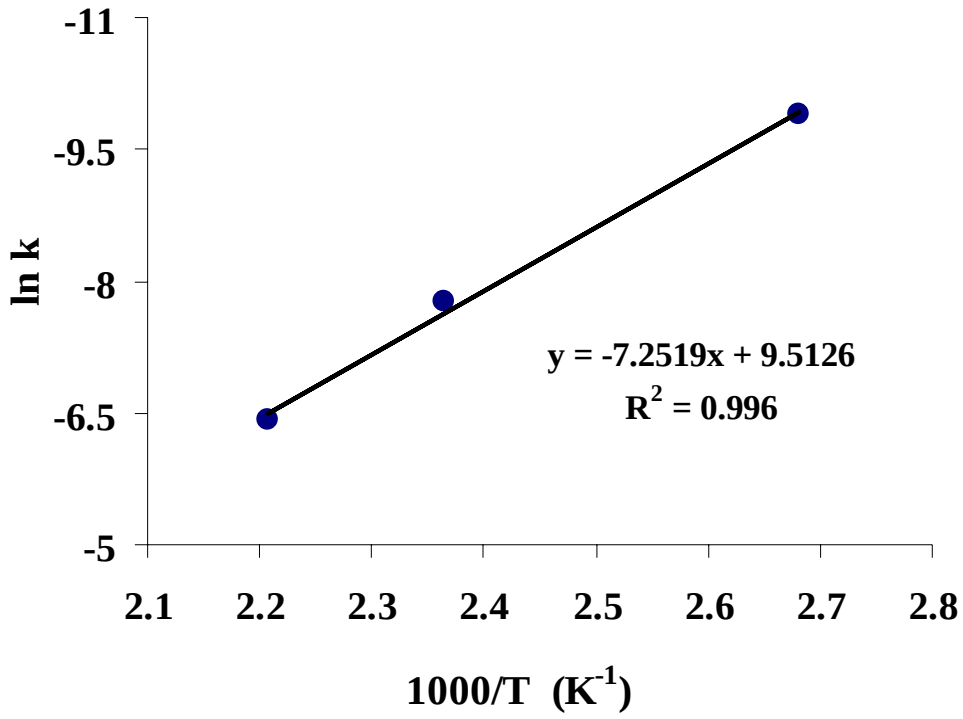


**Figure 5-6: An Arrhenius plot of ln k versus 1/T.**

**Effect of the reactant mole ratio:**

The influence of the mole ratio of the reactants on the catalytic activity and product selectivities was investigated by varying the ratio of dibenzylether to benzene while maintaining a fixed total reactant weight and catalyst concentration. The results, summarized in Table 5-1, showed that the dibenzylether conversion increased with increasing the mole ratio of dibenzyl ether to benzene. An excess of benzene reactant favored the formation of the monoalkylated product (diphenylmethane) even with prolonged reaction times. When the mole ratio of dibenzylether to benzene was decreased, the production of dialkylated products increased but these were formed at a slower rate than diphenylmethane. In addition, other products such as toluene, benzyl alcohol and benzaldehyde formed when dibenzylether was present in high concentration in the reaction media. Such products are likely formed via a disproportionation reaction that occurs between two adjacent benzyloxy groups adsorbed on the surface via direct hydrogen transfer from one surface molecule to the other to yield toluene and benzaldehyde. This is analogous to the mechanism of the disproportionation of benzyl alcohol over acidic alumina [8]. Part of the benzyl alcohol is oxidized to benzaldehyde and most of the toluene formed was alkylated by dibenzyl ether to give 2-methyldiphenyl methane (2-MDPM) and 4-methyldiphenyl methane (4-MDPM) which are shown in Figure 5-7. It is apparent that the interaction of dibenzyl ether with the sulfated zirconia catalyst generates a powerful alkylating agent that is non-selective. Thus, a large excess of the substrates is required to yield the desired reaction product cleanly.

**Table 5-1: Effect of reactant mole ratio on the alkylation reaction**

| BE : Bz mole ratio | Reaction time(h) | %BE Conversion | * % Products Selectivity | | | |
|---|---|---|---|---|---|---|
| | | | BzOH + PhCHO | DPM | BDPM + DBDPM | Others |
| **1:20** | 15 | 24.9 | 0 | 100 | 0 | 0 |
| | 35 | 47.4 | 5 | 95 | 0 | 0 |
| **1:15** | 15 | 25.5 | 8.1 | 90.2 | 1.1 | 0.6 |
| | 35 | 40.7 | 6.2 | 91.8 | 1.3 | 0.7 |
| **1:10** | 15 | 59.7 | 2.5 | 96.8 | 0 | 0.64 |
| | 35 | 61.1 | 4.1 | 91.9 | 3.42 | 0.61 |
| **1:0.2** | 15 | 16.1 | 28.4 | 6.9 | 64.7 | 1.6 |
| | 35 | 23.4 | 22.6 | 4.3 | 67.9 | 5.2 |
| **1:0.1** | 15 | 4.63 | 35.9 | 3.17 | 59.3 | 1.58 |
| | 35 | 10.6 | 19.9 | 2.02 | 75.3 | 2.78 |
| **1:0** | 45 | < 3.0 | 20.0 | 11.8 | 40.1 | 28.1 |

*Reaction conditions: catalyst load of 10 wt% with respect to reactants, reaction temperature 150 °C.*

***** *BE and Bz are dibenzyl ether and benzene respectively; BzOH and PhCHO are benzyl alcohol and benzaldehyde respectively; DPM is diphenylmethane; BDPM and DBDPM are benzyl diphenylmethane and dibenzyl diphenylmethane, respectively).*

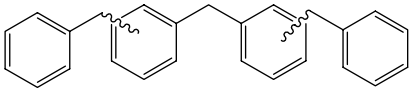

**1**
Dibenzyldiphenyl methane (DBDPM)

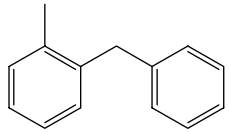

**3**
2-methyldiphenyl methane (2-MDPM)

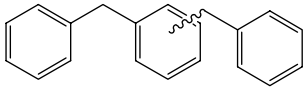

**2**
Benzyldiphenyl methane (BDPM)

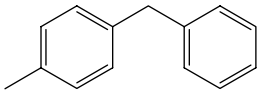

**4**
4-methyldiphenyl methane (4-MDPM)

**Figure 5-7: Possible secondary products formed from alkylation reaction of benzene with benzyl ether.**

In the kinetic experiments described above, benzene was present in a 20-fold excess. The reaction followed pseudo first order kinetics with respect to dibenzyl ether. When the benzene ratio was varied, the rate of dibenzylether reactant conversion followed a "volcano plot" curve with a maximum benzene mole fraction observed at 0.9 (Figure 5-8). This indicates that dibenzyl ether and benzene compete for similar active sites on the catalyst surface. Therefore, the reaction mechanism likely includes adsorption of the reactants on adjacent active sites of the catalyst surface, followed by a surface reaction of the two adsorbed species leading to the formation of DPM. This implies that the chemical process follows the Langmuir-Hinshelwood mechanistic kinetic model as in case of alkylation of aromatics over zeolites or other solid acid type catalyst [9-12]. The alkylation reaction mechanism can simply be described as follows; the sulfated zirconia first protonates the dibenzyl ether leading to chemisorption of the latter onto acid sites. As a result, polarization of the C-O bond of the ether will occur to give an adsorbed benzyloxy species on the catalyst surface with concomitant formation of a benzyl carbocation. An electron pair from benzene ring subsequently attacks the carbocation forming a C-C bond. The resulting cationic intermediate undergoes proton transfer to give a neutral alkylated substitution product and regenerates the catalyst. The proposed mechanism for the alkylation reaction of benzene with dibenzyl ether is shown in Figure 5-9.

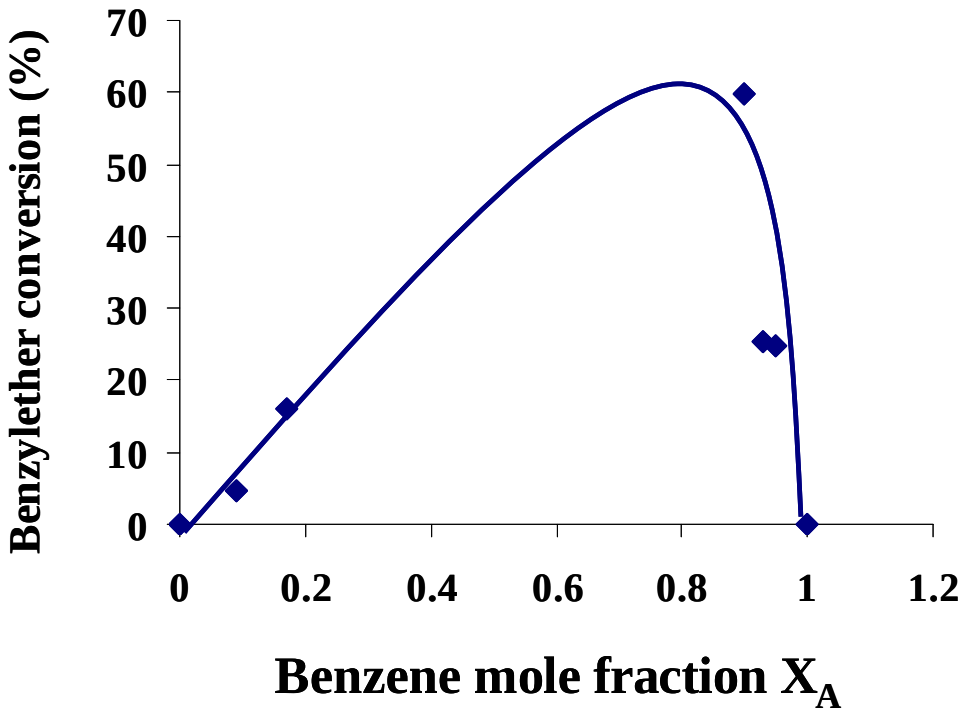


**Figure 5-8: A plot of benzyl ether conversion versus mole fraction of benzene.**

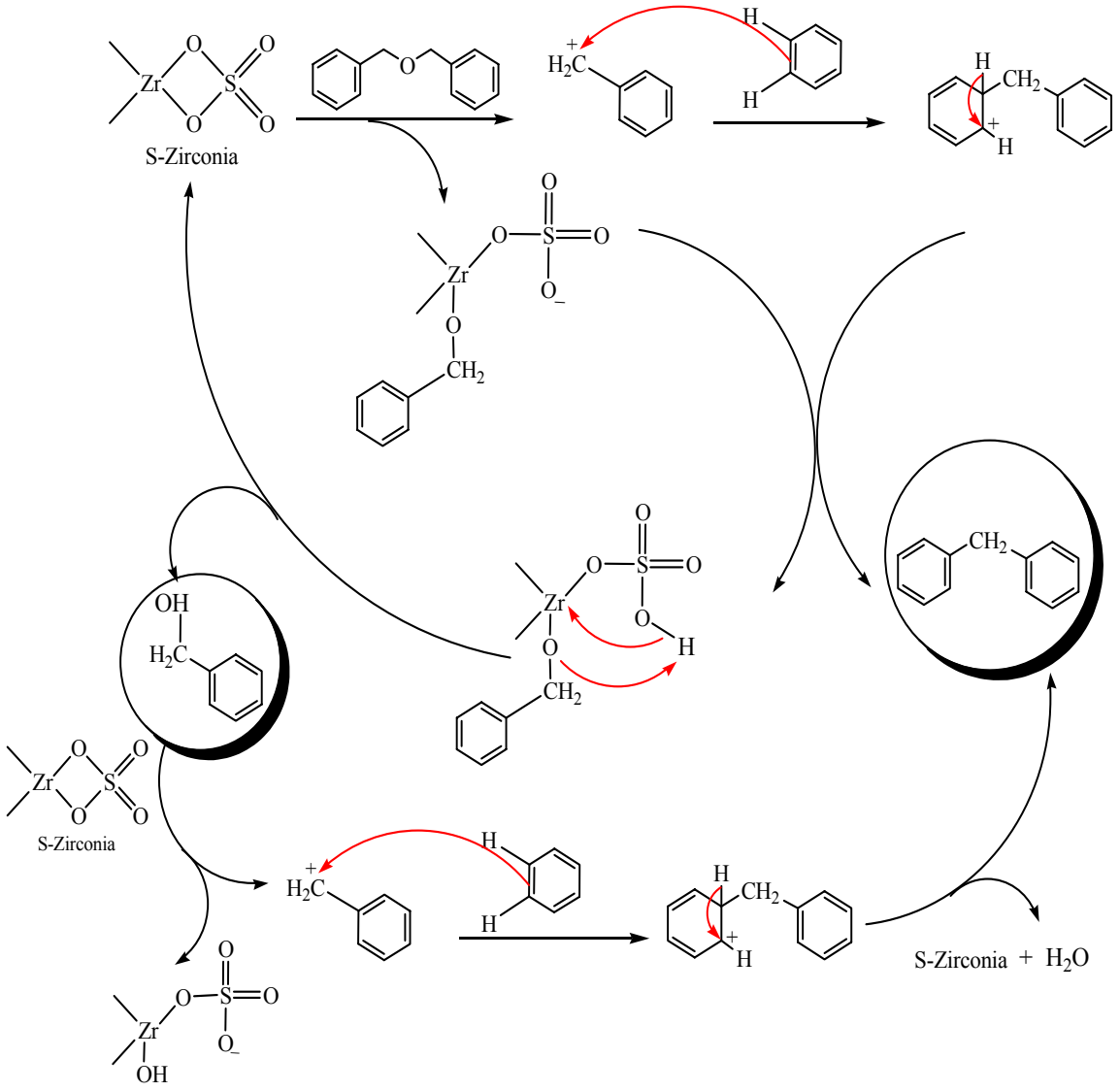


**Figure 5-9: Proposed mechanism of alkylation of benzene reaction with benzyl ether.**

**Effect of the support:**

A control reaction of benzene with dibenzyl ether was performed over pure MCM-41 support for more than 40 hours at 150 ºC. No reaction took place, indicating that the acid sites of the support were not capable of performing the alkylation reaction.

The reaction was performed using several MCM-41 supported catalyst with sulfated zirconia ranging from 15 wt% to 100 w%. Figure 5-10 shows a plot of the natural logarithm of the dibenzyl ether concentration versus time. The slopes of the resulting straight lines gave the rate of the alkylation reaction. Figure 5-11 shows a plot of the rate of reaction versus the amount of zirconia. The experimental results obtained revealed that the alkylation activities increased with increasing sulfated zirconia content on the support to a maximum at 40 wt% SZ/MCM-41 where the reaction was almost three times greater compared to the unsupported sulfated zirconia. This is in agreement with the results obtained using acetonylacetone reaction and the acidity measurements. It appears that the optimum activity is obtained with 40 wt% SZ/MCM-41 which reflects the most useful combination between the available active acid sites and the specific surface area.

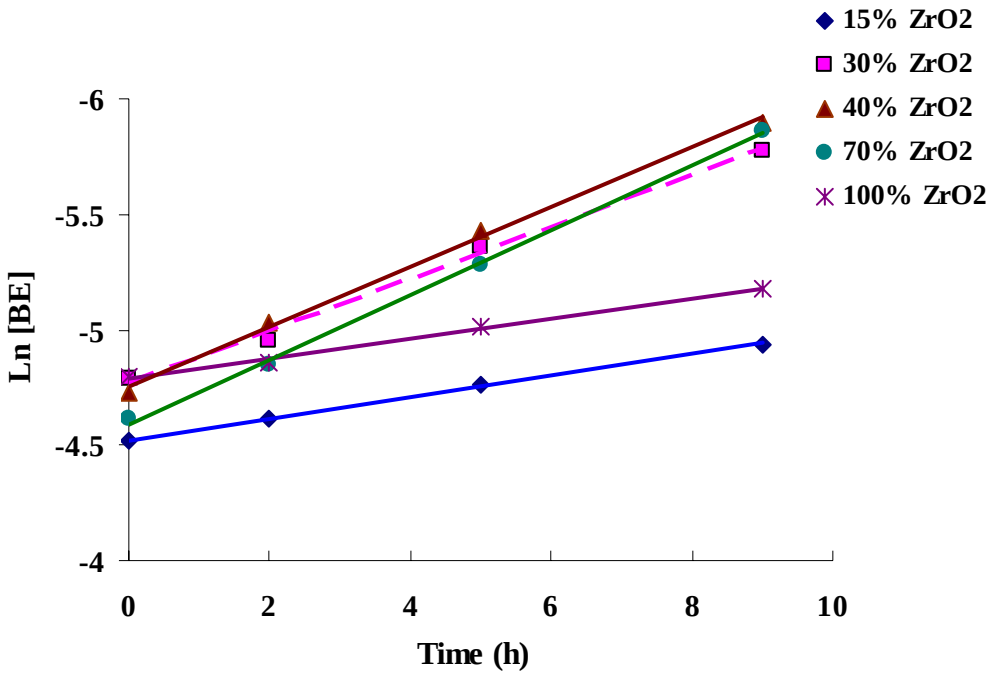


**Figure 5-10: Effect of the sulfated zirconia concentration over MCM-41 on the rate of the alkylation reaction of benzene with benzyl ether.**

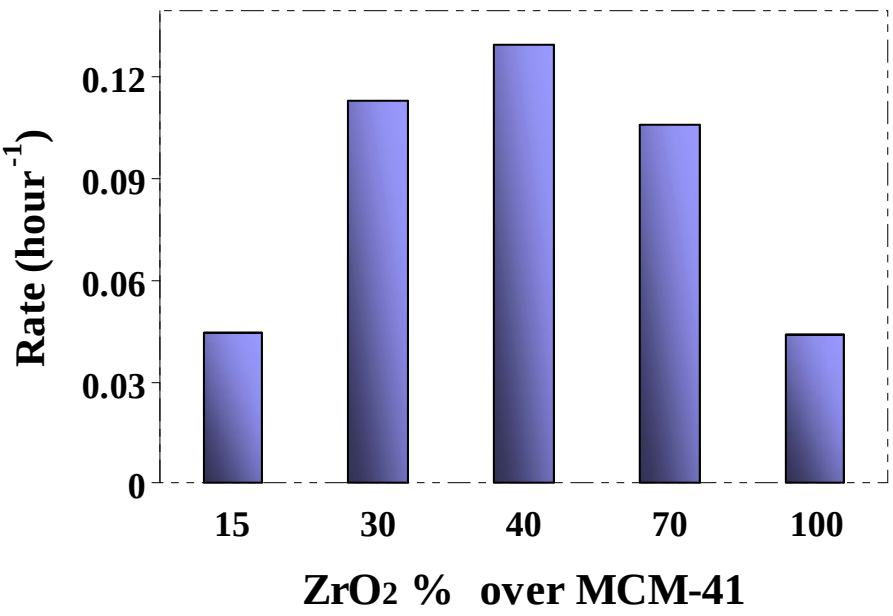


**Figure 5-11: A plot of the rate of alkylation reaction versus the zirconia content over the MCM-41. (Reaction conditions: sulfated zirconia loading = 10% w/w; benzyl ether: benzene mole ratio = 1:10; reaction temperature: 150 °C).**

**Catalyst Regeneration:**

The catalyst was deactivated when it was used for several hours during the alkylation reaction of benzene with dibenzyl ether. The deactivation was presumably due to the adsorption of benzyloxy groups which cover the active sites on the surface. Figure 5-12 shows the IR spectra for both fresh and used unsupported catalyst samples dried at 170 ºC under vacuum. The carbon-carbon double bonds stretching frequencies at 1600 $cm^{-1}$, as well as the $sp^2$ C-H stretching frequency in the range between 3000 $cm^{-1}$ and 3100 $cm^{-1}$, clearly indicate that some organic and aromatic species are adsorbed on the catalyst surface, probably benzyloxy and other aromatic species.

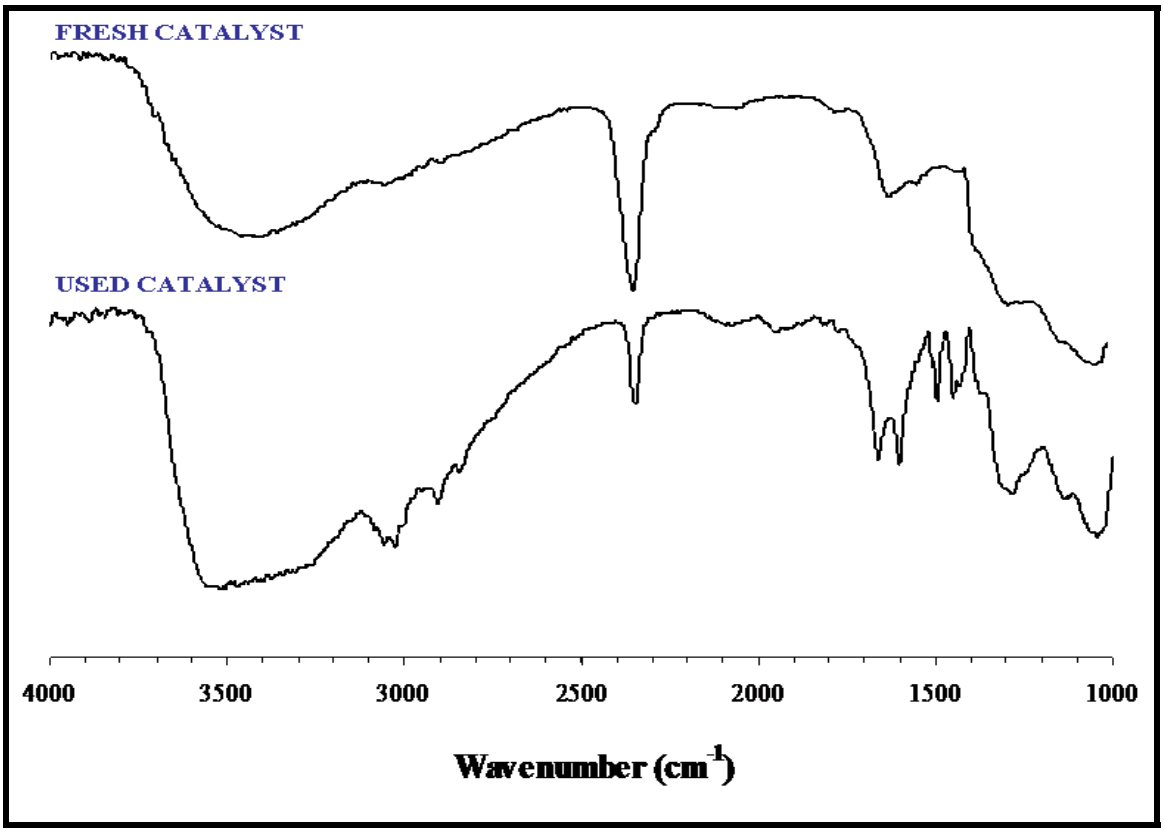


**Figure 5-12: Infrared spectra for the fresh and used catalyst.**

The used catalyst was recycled several times by heating at 500 ºC for 4 hours in flowing of air (Figure 5-13). The results showed that the catalyst completely retained its activity after the first regeneration. This implies that the deactivation is mainly due to hydrocarbon deposition, and the loss of sulfur during the reaction is ruled out. A modest loss in the activity was observed after the second and third regenerations. The conversion of dibenzyl ethers dropped from 81% for the fresh sample to 60% after the third recycling. This drop in conversion after several regenerations may be due to either the loss of the very small amount of active sites in a form of $SO_2$ or from migration of the sulfur into the bulk of the zirconium oxide. Notably, benzaldehyde formation is observed

during the catalytic reactions. This could be due to oxidation of the benzyl alcohol byproduct by dioxygen or it could be due to reduction of the sulfate group.

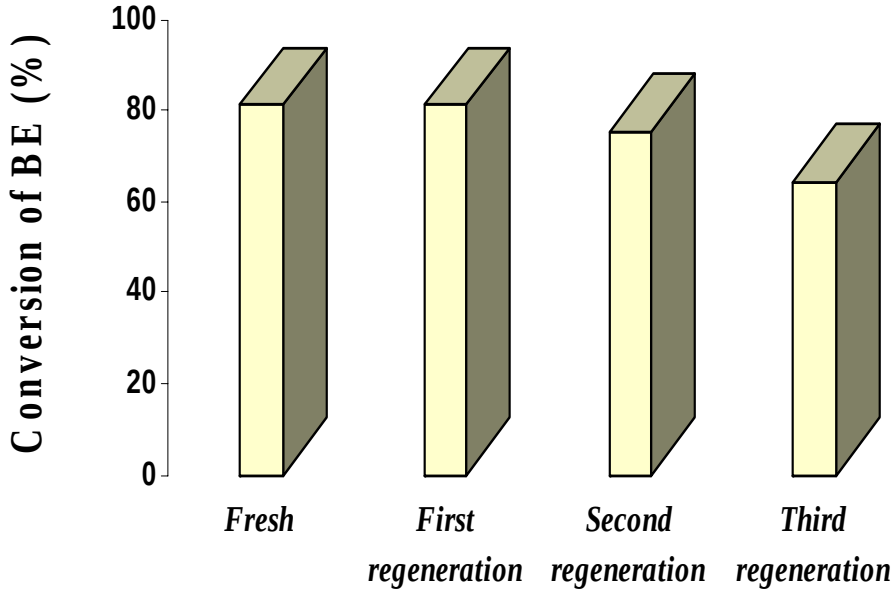


**Figure 5-13: regeneration of the used samples at 500 °C in air for 4 hours. (Reaction conditions: sulfated zirconia loading = 20% w/w; Benzylether: Benzene mole ratio = 1:10; reaction temperature: 150 °C).**

Another suggestion for the loss of sulfur is during the regeneration process rather than during the reaction. Li and associates [13-14] observed a loss in activity of sulfated catalyst towards isomersation of *n*-butane reaction when the used catalyst was regenerated in a nitrogen environment, this quite likely due to redox reactions between coke and the sulfate groups. In this work, the regeneration process was performed in a flow of air in order to minimize such reactions.

**Alkylation of Benzene with Other Ethers:**

Three different ethers were utilized for the alkylation of benzene. Figure 5-14 shows the conversion of different ethers versus the reaction time. The *n*-butyl ether conversion rate is the slowest among the three ethers. This may be attributed to the low stability of the rearranged secondary butyl carbocation which further reacts with benzene to give 2-phenylbutane. Only traces of 1-phenylbutane were formed as a result of the alkylation of benzene with the *n*-butyl carbocation before rearrangement took place. The reaction rate of methyl benzylether and dibenzylether are similar to each other. However, the catalyst seems to be deactivated faster in case of dibenzyl ether. Presumably this is due to less hindrance of the reactive sites by the smaller methoxy groups as compared to adsorbed benzyloxy groups. This will eventually make the catalyst deactivation process slower in case of benzene alkylation with MBE.

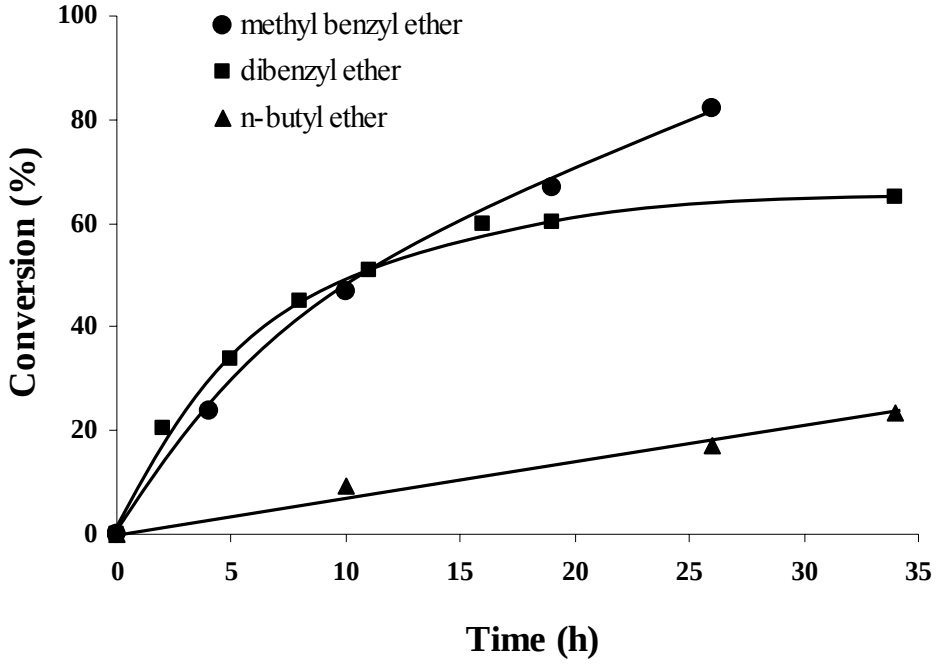


**Figure 5-14: Alkylation of benzene with different ethers over sulfated zirconia.**

**CONCLUSIONS AND REMARKS:**

Sulfated zirconia and modified sulfated zirconia were utilized for the Friedel-Crafts alkylation of benzene with ethers. The synthesized sulfated zirconia samples showed a remarkable activity in the alkylation reaction of benzene using different ethers as alkylating agents. The effects of various parameters on the reaction rates, such as reaction temperature, catalyst load, support influence and molar ratio of reactants, were studied under similar reaction conditions. The supported samples with 40% Zirconia/MCM-41 showed a three times higher activity than the bulk unsupported sample. The rate of the deactivation is decreased with supporting of sulfated zirconia over Si-MCM type of support. The reaction appears to be influenced by the reaction temperature and the catalyst concentration, and the prepared catalyst can be regenerated several times without major decrease or loss of its activity and selectivity. The chemisorbed benzyloxy and other aromatic compounds are considered to be the responsible for the initiation of the deactivation process. The sulfated zirconia catalysts can be regenerated several times without major decrease in the catalytic activity and selectivity.

**REFERENCES CITED:**


1 G. Olah, *Friedel-Crafts and Related Reactions*, Wiley-Interscience: New York, 1964.

2 G. Olah, *Friedel-Crafts Chemistry*, Wiley-Interscience,: New York, 1973.

3 P. Kumbhar, V. Yadav, G. and Yadav, *Chemically Modified Surfaces*, **1990**, *3*, 81.

4 G. Yadav, and T. Thprat, *Tetrahedron Letters*, **1996,** *37(30),* 5405.

5 G. Yadav. and J. Kirthivasan, *J. of Chem. Soc.: Chem. Comm.*, **1995**, *2*, 203.

6 G. Yadav. and N. Doshi, *Catalyst Today*, **2000**, *60(3-4)*, 263.

7 B. Giganet, M. Prazeres, C. Marcelo , A. Cornelis and P. Laszlos, *J. Amer. Chem. Soc.*, **1995**, *60*, 3445.

8 M. Jayamani, N. Murugasen, and C. Pillai, *J. Catal.*, **1984**, *85(2)*, 527.

9 G. Yadav, and S. Sengupta, *Org. Proc. Res. Dev.* **2002**, *6*, 256.

10 S. Koyande, R. Jaisral and R. Jayarm, *Ind. Eng. Chem. Res.* **1998**, *37*, 908.

11 P. Venuto and P. Landis, *Advanced Catalysis*. **1968**, *18*, 259.

12 J. Weitkamp, *Acta Phys. Chem*. **1985**, *31*, 271.

13 B. Li and R. Gonzalez, *Appl. Catal*. **1998**, *174*, 109.

14 B. Li and R. Gonzalez, *Catal. Today*. **1998**, *46*, 55.

# CHAPTER 6

## ALDOL CONDENSATION REACTION OF KETONES OVER SULFATED ZIRCONIA

### INTRODUCTION:

The aldol condensation is considered an important reaction in organic synthetic industrial chemistry [1-3]. It involves the production of $\beta$-hydroxy aldehydes or $\beta$-hydroxy ketones by condensation of two aldehydes or ketones. Self condensation of ketones, is a well established process that is important for production of $\alpha,\beta$-unsaturated carbonyl compounds [4]. Usually, such reactions are performed homogenously over a liquid base catalyst such as soda or potash [5-7] or liquid acid catalysts such as sulfuric acid [8]. These reactions ordinarily require very long, complicated, and hazardous procedures. Recently, efforts have been directed toward replacing the catalyst systems with more environmental friendly heterogonous solid catalysts. For example, solid basic catalysts such as MgO and CaO have been utilized for such reactions [9]. Other conventional solid acid catalysts used for the aldol condensation reaction include aluminum oxide [10], aluminum alkoxides [11] and zeolites [12]. The aldol condensation of ketones is a complex reaction which leads to many products via self condensation of two ketone molecules or cross condensation of one ketone with other ketone products that are formed. The reaction network and product distribution is controlled by the

catalyst properties, reaction conditions, and chemical nature of the ketones. Acetone condensation, for example, has been studied over several solid acid catalysts using many characterization techniques such as $^{13}C$ NMR and IR spectroscopies [13-15]. The results obtained from the condensation reaction of acetone over zeolites and alumina indicated that the Lewis acid sites are mainly the responsible active sites for the initial activation of acetone. The secondary side reactions which involved double bond migration, hydride transfer, oligomerization, and cracking can occur on the catalyst surface. In this chapter, a detailed investigation of liquid phase self aldol condensation reaction of four different ketones, namely, acetone, cyclopentanone, acetophenone, and methyl isopropyl ketone, was performed over sulfated zirconia sample prepared from single source precursors. These ketones were converted on the surface of sulfated zirconia to more useful aromatic compounds that have potential applications as diesel fuel and other industrial applications. The effect of several factors such as preparation method, surface acidity, and physico-chemical properties of the sulfated zirconia, on the catalytic activity and productivity was addressed.

## EXPERIMENTAL:

### Chemicals:

The reagents were used as purchased without further purification. The chemicals used in this investigation were: acetone-2-$^{13}C$ (99%$^{13}C$) [($C_3H_6O$), Aldrich], mesityl oxide [($C_6H_{10}O$), Aldrich], cyclopentanone [($C_3H_6O$), Aldrich], methyl isopropyl ketones [($C_4H_{10}O$), Aldrich], dypnone [($C_{16}H_{14}O$), Chem. Tech.] and acetophenone [($C_8H_8O$), Aldrich].

**Procedure:**

The catalysts used in this study were; SZ-1(1:3) (sulfated zirconia obtained from the reaction of zirconium acetate with three equivalents of ethanesulfonic acid), SZ-4 (sulfated zirconia produced from the reaction of zirconium acetate with 8-hydroxyquinoline-5-sulfonic acid), 15% SZ/MCM (supported sulfated zirconia with 15% sulfated zirconia over MCM-41), and 40% SZ/MCM (supported sulfated zirconia with 40% sulfated zirconia over MCM-41). The methods of preparation and characterization of the catalysts utilized in this work were described in detail previously in Chapters 2, 3, and 4. The description and properties of these samples are shown in Table 6-1. The liquid phase condensation reaction of the ketones was carried out at 150 °C in the presence of the catalysts in a Teflon-lined bomb reactor. Typically, 0.2 grams of the sulfated zirconia catalyst was added to one gram of the desired ketone. Samples from the reaction media were continuously taken at different reaction periods and diluted with pure methylene chloride before they were analyzed by the gas chromatography/mass spectrometer (GCMS).

**Table 6-1: Catalyst properties for the samples utilized for ketones condensation.**

| Catalyst code | *Description of the oxide | $S_{BET}$ ($m^2/g$) | Pore volume (ml/g) | Total Acidity | |
|---|---|---|---|---|---|
| | | | | μmol/g | μmol/$m^2$ |
| **SZ-1(1:3)** | Zirconium acetate with three equivalents of ethanesulfonic acid | 49 | 0.077 | 227 | 4.6 |
| **15% SZ/MCM** | 15% sulfated zirconia supported over MCM-41 | 1037 | 1.03 | 1737 | 2.44 |
| **40% SZ/MCM** | 40% sulfated zirconia supported over MCM-41 | 545 | 0.74 | 1213 | 2.954 |
| **SZ-4** | Zirconium acetate with 8-hydroxiquinolene sulfonic acid | 48.3 | ___ | 223 | 4.6 |

** All the samples were calcined at 650 °C*

## RESULTS AND DISCUSSION:

### Acetone condensation:

The reaction of acetone over the solid acids follows several pathways leading to numerous products. The acetone condensation reaction was performed over two different synthesized sulfated zirconias, 40% SZ/MCM, and SZ-4. The reaction was performed at 150 °C with 20 wt/wt % catalyst/ketone. Figure 6-1 summarizes all the possible reaction pathways for the acetone condensation. In the first step, protonation of acetone over the solid surface take place to form the conjugate acid. The next step involves the electrophilic addition of carbonium ion of the conjugate acid with the enol form of another acetone molecule via well known aldol reaction to yield diacetone alcohol (DAA) **1**. Dehydration of diacetone alcohol **1** occurs readily over acid sites to form mesityl oxide (MO) **2**. Another acetone enol reacts further with the mesityl oxide following the similar mechanism mentioned above to give linear phorone **3**. Cyclization of phorone to

isophorone **4** presumably mainly arises through a 1,6 Michael addition mechanism which involve the conjugate addition of the enolate nucleophile anion to the $\beta$-carbon of an $\alpha,\beta$-unsaturated carbonyl electrophile double bond [16,17]. Mesitylene **5** may be formed as a result of dehydration and rearrangement of isophorone over acid sites. Additionally, another likely possible route for formation of mesitylene is the condensation of three acetone enol form molecules to produce the trialcohol intermediate product **6** followed by rapid dehydration on the acid sites to release three water molecules and mesitylene. Among all these products, mesityl oxide, isophorone, and mesitylene are commercially the most important products obtained from acetone condensation [18,19]. These products are mainly applicable in polymerization and separation of heavy metals.

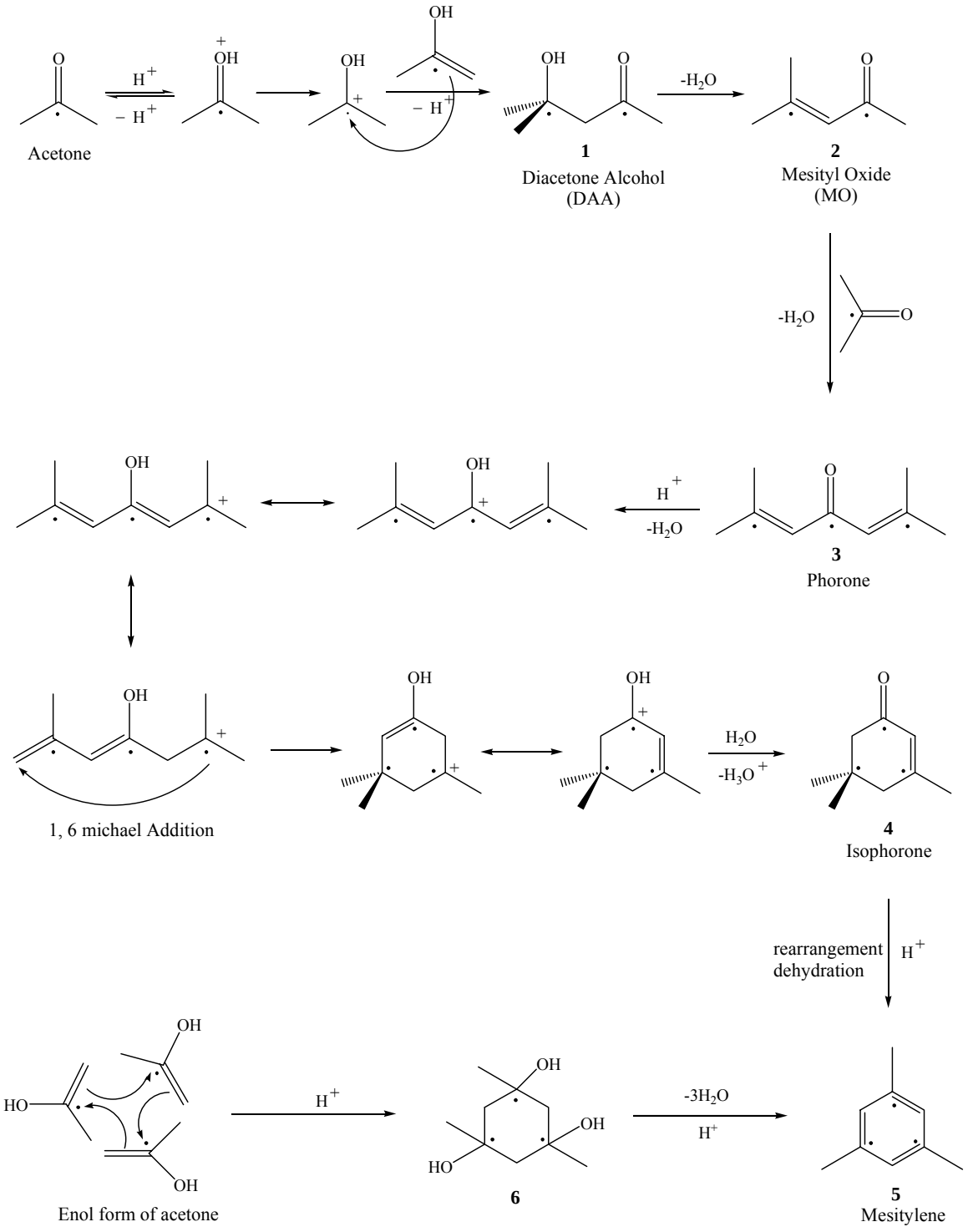


**Figure 6-1: Schematic reaction network for self acetone condensation.**

Products such as pentamers **8** or **9** are also formed in considerable amount via a proposed mechanism shown in Figure 6-2. The pentamer was identified using mass spectrometry, which indicated a molecular mass fragmentation of m/e 200 involving five $^{13}C$ atoms suggesting that it formed as a result of condensation of five acetone molecules. Most likely, this product formed directly from the reaction of isophorone with mesityl oxide to give an intermediate structure **7** followed by rapid dehydration to evolve two water molecules and products **8** and/or **9**.

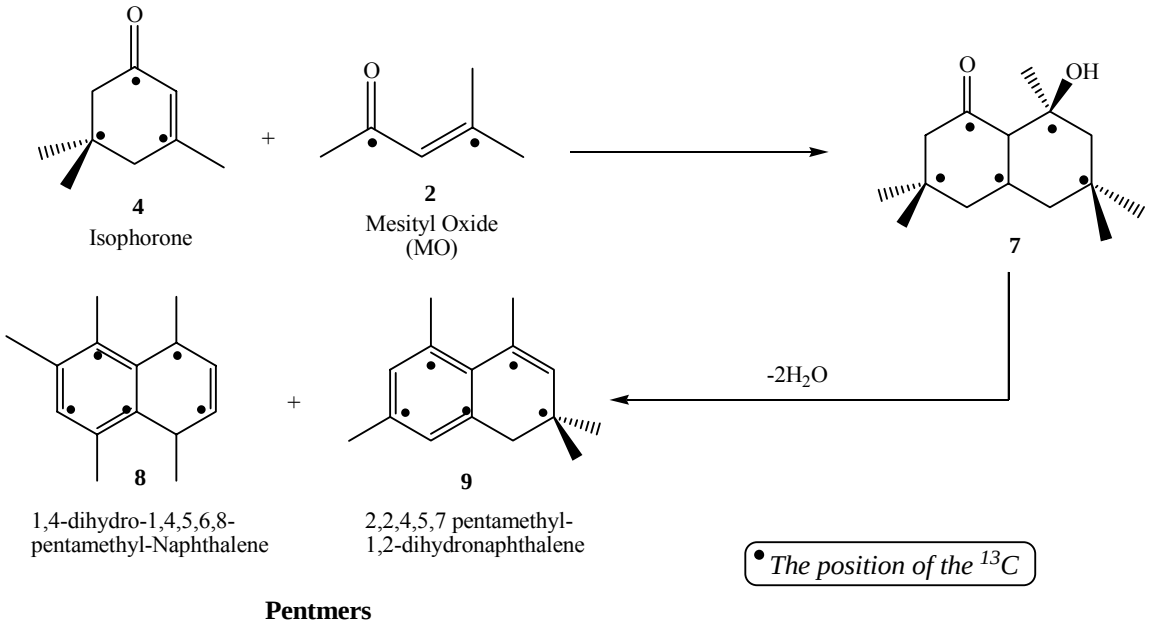


**Figure 6-2: Schematic diagram for the formation of pentmer product from acetone.**

Furthermore, the headspace analysis of the reaction mixture showed that isopropyl alcohol is produced in low concentration, this is apparently produced as a result of the reduction of acetone by protonation over the sulfated zirconia surface. Figure 6-3 shows the conversion of the acetone versus reaction time over the sulfated zirconia

samples, supported sample 40% SZ/MCM, and unsupported sample SZ-4. As shown in the Figure 6-3, the conversion over the supported samples increased rapidly to its maximum after only three hours of reaction time with about 80% conversion. Beyond that, the conversion appears to be constant without significant change. On the other hand, when the reaction of acetone was performed over SZ-4 sample, the conversion increased with a slower rate compared to 40% the SZ/MCM sample to reach a maximum conversion after about 12 hours. Obviously, this high initial activity of the supported sample is attributed to the high surface area and dispersion of the active sites on the surface. The product distribution results are summarized in Figures 6-4 and 6-5.

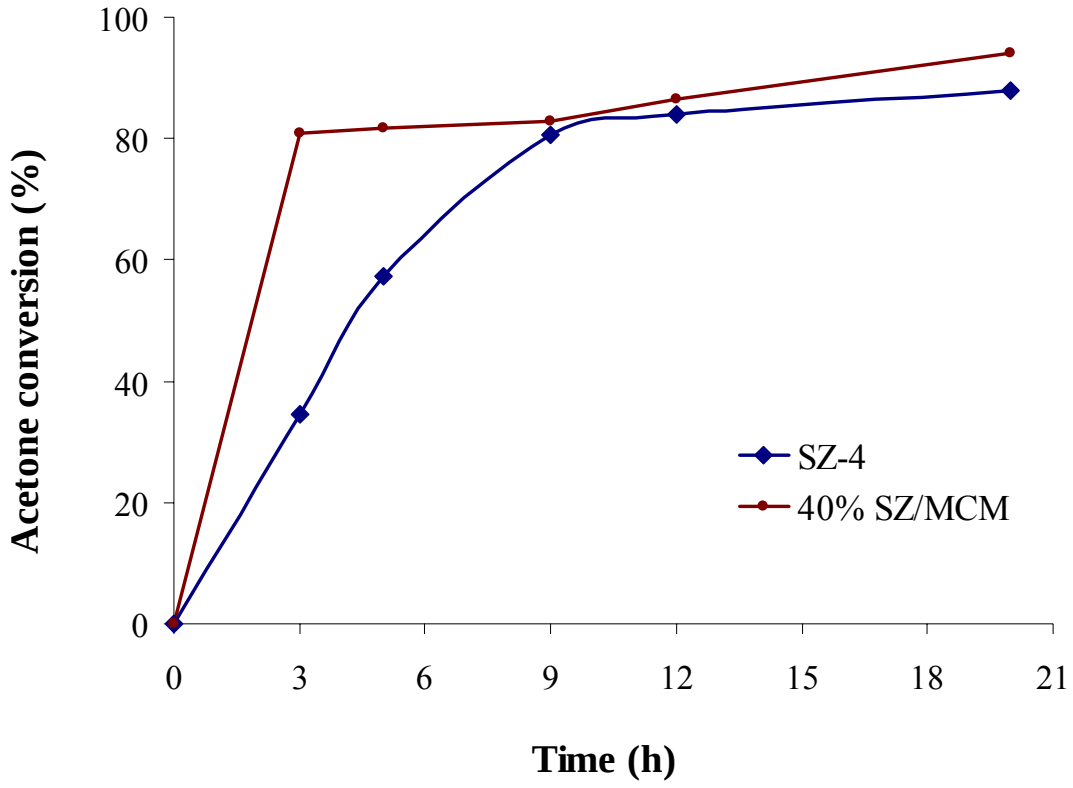


**Figure 6-3: Acetone conversion over sulfated zirconia samples, 40% SZ/MCM and SZ-4 at 150 ºC.**

** The details of the catalyst used are shown in Table 6-1.*

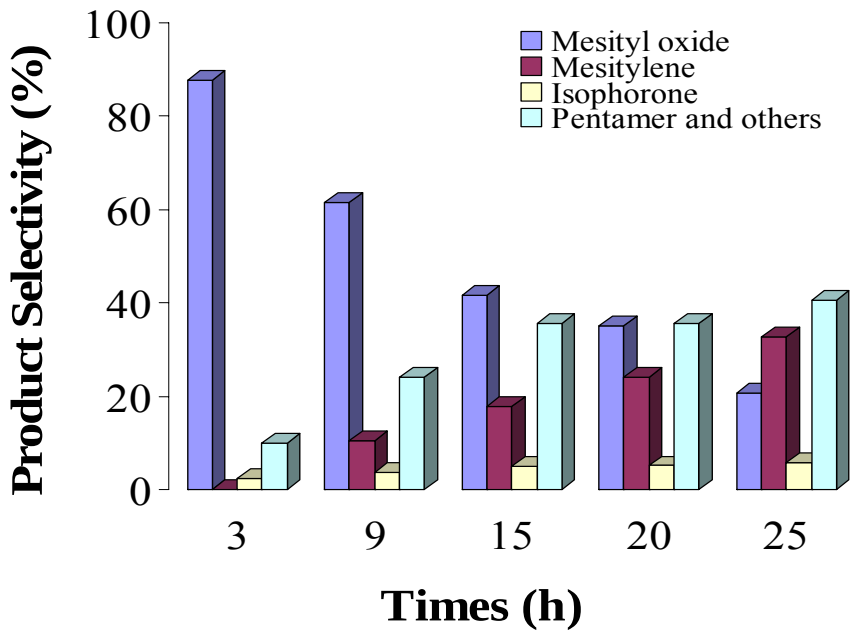


**Figure 6-4: Product distribution resulted from acetone condensation over 40% SZ/MCM sample.**

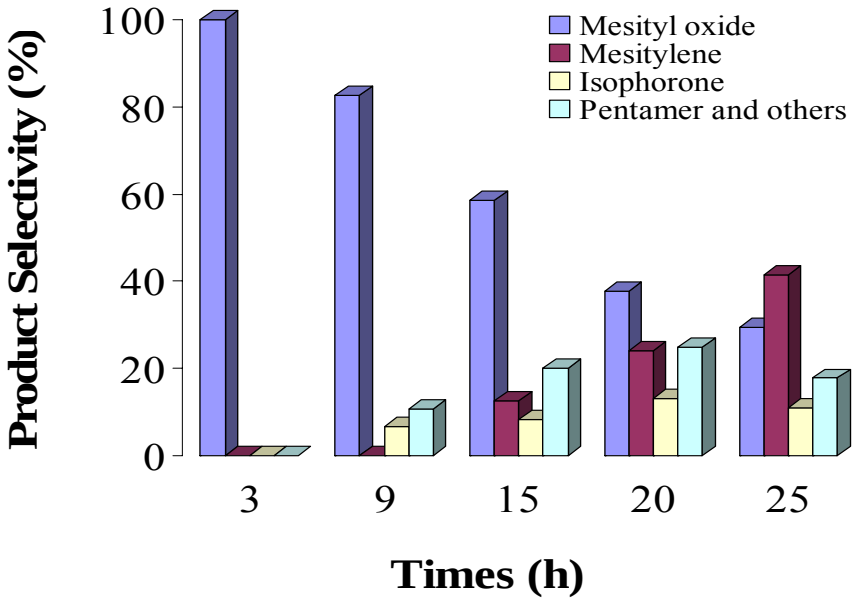


**Figure 6-5: Product distribution resulted from acetone condensation over the sulfated zirconia obtained from zirconium quinoline sulfonates (SZ-4).**

** The details of the catalyst used are shown in Table 6-1.*

The results demonstrated in Figures 6-4 and 6-5 showed that the aldol condensation reaction of acetone initially produced mesityl oxide **2** during the first 3 hours of reaction time. Mesityl oxide is presumably produced from dehydration of the intermediate diacetone alcohol **1**, but none of it was observed at these conditions due to high acidity of the catalyst's surface. It has been reported that the alcohol dehydration process requires low acidic strength sites with pKa of +0.8 [20]. However, when the reaction was performed at room temperature for 24 hours with 10 wt% catalyst (40% SZ/MCM)/ acetone, the primary condensation products were observed which are diacetone alcohol **1** and mesityl oxide **2**. The acetone conversion at these conditions was very low with approximately 92% selectivity for diacetone alcohol and 8% selectivity for mesityl oxide. These results clearly indicate that the selectivity toward the diacetone alcohol is sensitive to the reaction temperature. The high selectivity for diacetone alcohol which was observed at room temperature is presumably due to the fact that dehydration steps as well as further condensation of ketones to higher molecular weight products have high activation energy and occur quite slowly at room temperature.

As shown in Figures 6-1 and 6-2, numerous products are formed when the reaction was performed at 150 ºC. These products generally formed as a result of the self and cross condensation of mesityl oxide with acetone molecules. When the reaction proceeds for longer time, it is shown that the concentration of mesityl oxide was decreased as it was consumed in cross-condensation reaction with acetone to produce isophorone **4**, mesitylene **5**, and pentamer **8** or **9** products. The selectivities towards these products increased with increasing reaction time. Isophorone selectivity was very low compared to the other products due to its instability toward decomposition over strong

acidic sites to give mesitylene **5** or further reaction with mesityl oxide to give the pentamers **8** and **9**. Another possible route for consumption of phorone and isophorone is cracking of such organics over the acid surface at the reaction conditions to evolve carbon dioxide gas. Isophorone selectivity is higher when the reaction was performed over 15% SZ/MCM sample (Figure 6-5) than when it was conducted over 40% SZ/MCM (Figure 6-4). Apparently this is due to the lower acidic sites available on the surface of 15% SZ/MCM sample compared to that of 40% SZ/MCM (Table 6-1). In general, the results showed that the supported sample 40% SZ/MCM is a more active catalyst for the condensation of acetone than the SZ-4 sample. This greater activity is apparently due to the large difference in the specific surface area and surface acidity. Furthermore, the supported sample (40% SZ/MCM) favored the formation of the high molecular weight products such as mesitylene **5** and the pentamers **8** or **9**. This is presumably due to the availability of the large pores provided by the MCM-41 support which facilitates the formation of such kind of bulky products.

**Cyclopentanone condensation:**

The self condensation reaction of cyclopentanone was studied over the prepared sulfated zirconia catalysts. A schematic diagram for the cyclopentanone condensation reaction is shown in Figure 6-6.

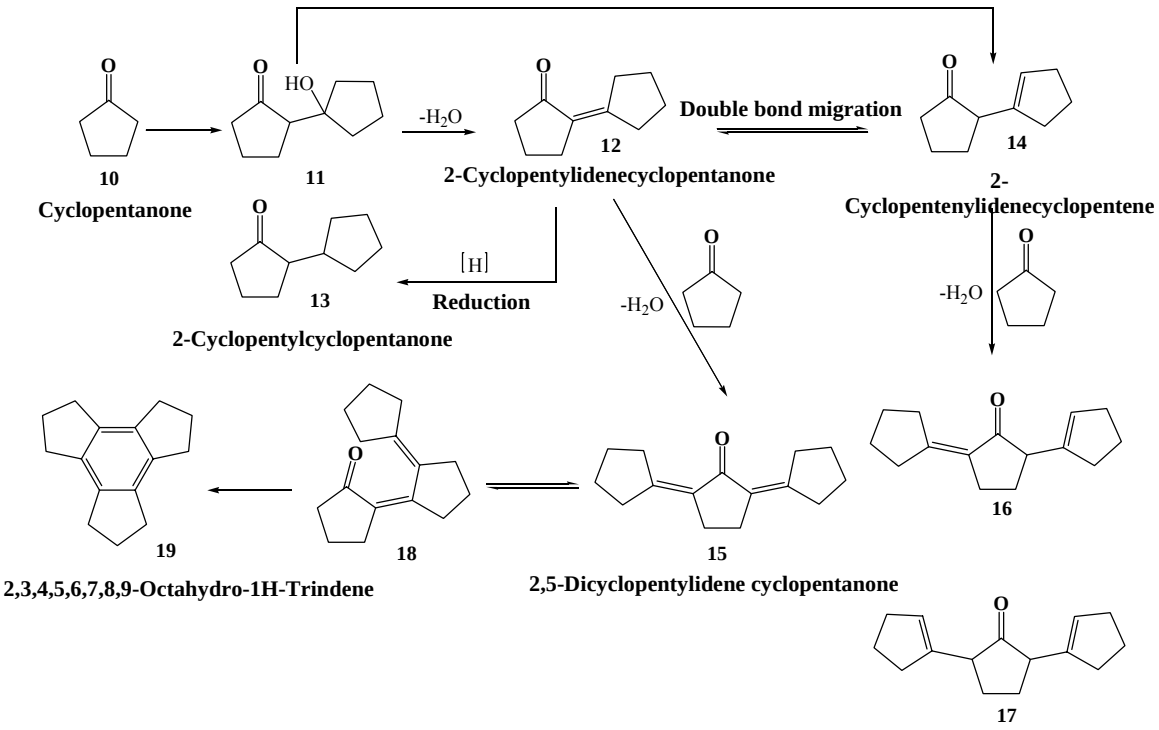


**Figure 6-6: The main products obtained from the condensation reaction of Cyclopentanone (CPO) over sulfated zirconia**

The first steps in the condensation of the cyclopentanone reaction occur over acidic surfaces are quite similar to those observed with the acetone. The reaction involves the protonation of cyclopentanone **10** to form carbonium ions which further react with the enol form of another cyclopentanone molecule to form an alcohol intermediate **11**. As in the case of the acetone condensation reaction, the alcohol intermediate **11** was not observed in the reaction mixture at 150 °C due to the immediate dehydration to give 2-cyclopentylidenecyclopentanone (2-CPYCPE) **12**. This compound can undergoes further secondary reactions over very strong acid sites to yield other products via either protonation or double bond migration. Part of product **12** reduced by hydrogenation of the double bond to form 2-cyclopentylcyclopentanone **13**. However,

the yield of this particular product was very low with a maximum of about 0.5%-1%. 2-cyclopentylidenecyclopentanone **12** can also undergo an isomerization via double bond migration to $\beta,\gamma$ positions to give 2-cyclopentenylidenecyclopentene (2-CPECPE) **14**. The interaction of another enol form of cyclopentanone with either products **12** or **14** followed by dehydration gives a mixture of trimer isomers **15**, **16**, and **17** as shown in Figure 6-6. The mole ratio of the products **15**, **16**, and **17** after 15h reaction time at 150 ºC was 5.2:1.4:1 respectively. Trindene **19** is believed to be formed directly from the trimer **15** through rearrangement to form an intermediate unsymmetrical trimer **18** [21]. Additionally, the ketone conversion as a function of time over 40% SZ/MCM samples is shown in Figure 6-7 while the product distribution of the self condensation reaction of cyclopentanone is shown in Figure 6-8.

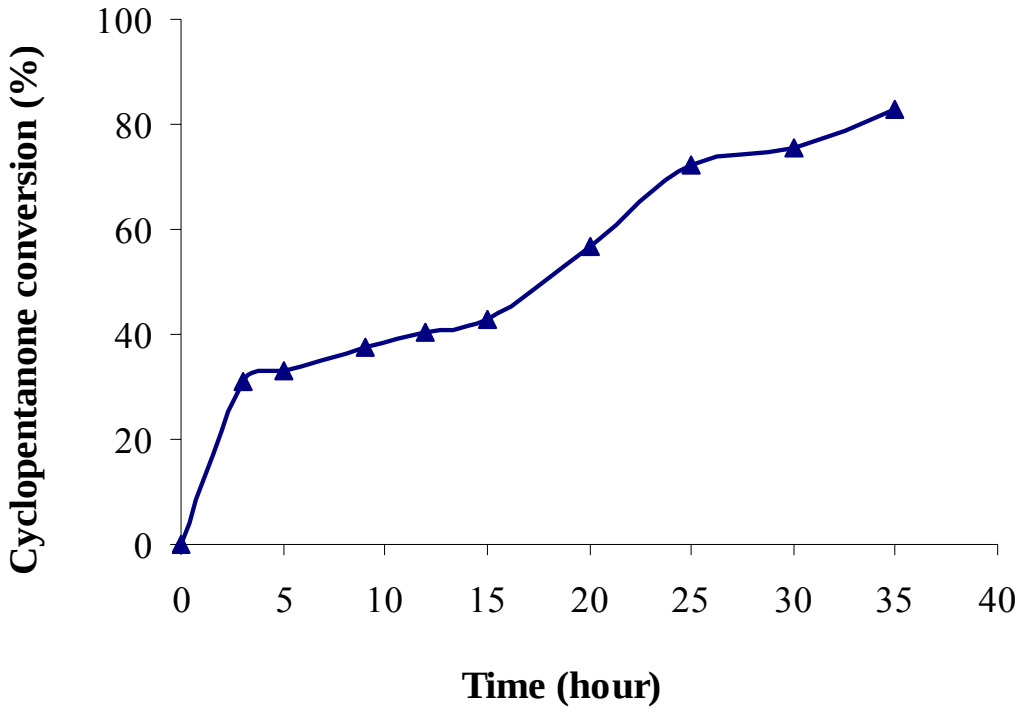


**Figure 6-7: Cyclopentanone conversion over 40% SZ/MCM at 150 ºC.**

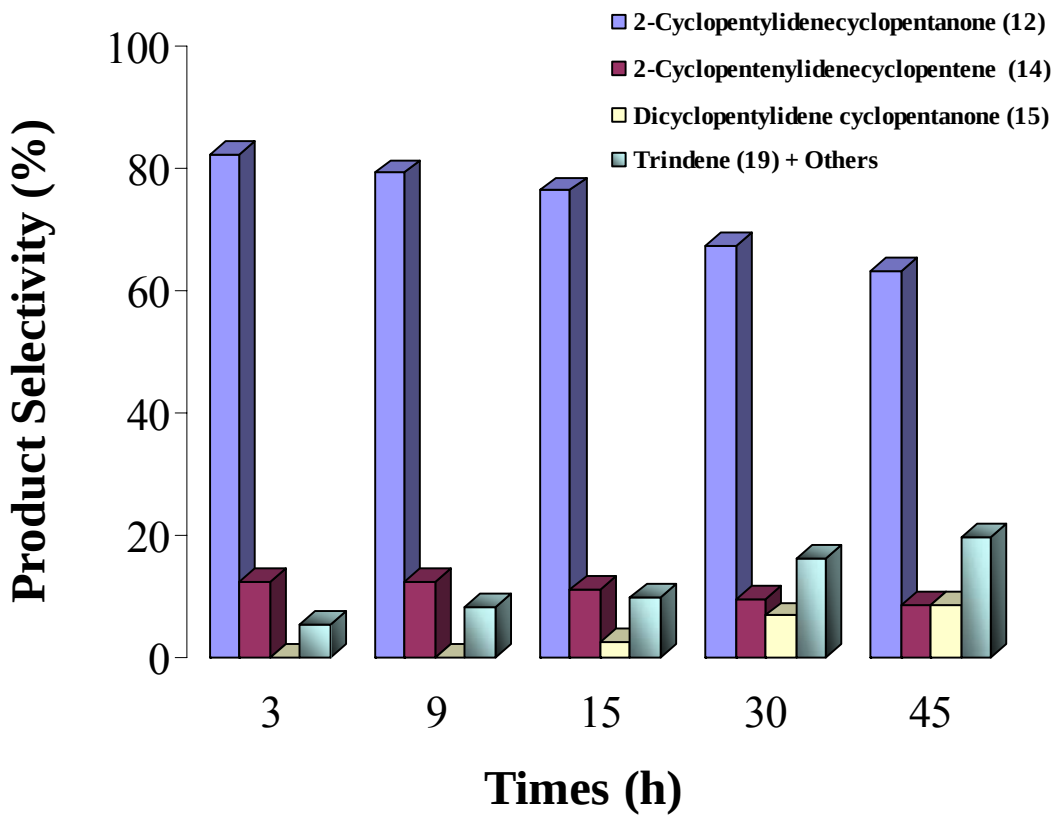


**Figure 6-8: Product distribution resulted from cyclopentanone condensation over 40% SZ/MCM sample.**

The results obtained indicate that at the beginning of the reaction, the main products formed were dimer ketones, such as **12**, and **14**. With increasing reaction time, the yield of trimers and trindene increased while the concentration of the dimer **12** decreased. The results also showed that there was no 2,5-dicyclopentylidene cyclopentanone **15** formed in the early stage of the reaction until the reaction proceeded for 9 hours. This implies that most of the dicyclopentylidene cyclopentanone **15** produced initially further transformed into trindene **19**. However, with prolonged

reaction time, the decrease on activity of the catalyst causes this transformation to slow leading to an increase in the concentration of the trindene.

**Acetophenone condensation:**

Figure 6-9 summarizes the reaction mechanism of acetophenone over sulfated zirconia. The carbonyl group of the acetophenone **20** is protonated to form the conjugate acid carbonium ion which attacks another enol form of acetophenone to form 1,3-diphenyl-3-hydroxy-1-butanone (DPHB) **21**. This then dehydrated to give mainly the cis and trans isomers of dypnone (DPBO) **22,** and **23**. Dypnone is considered an important intermediate as a plasticizer and softening agent. Another dehydration dehydrated product is may be **24**, which was formed via elimination of the hydrogen atom on the primarily methyl group. However, this product was detected in very low concentration due to its lower stability compare to other dypnone isomers.

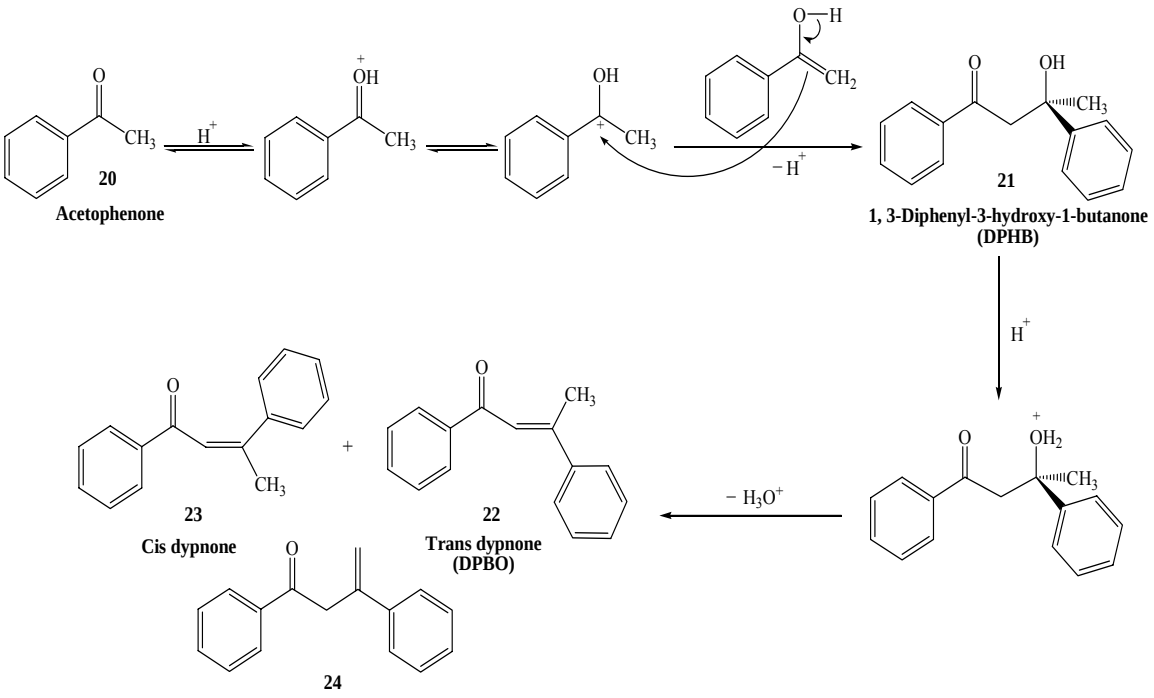


**Figure 6-9: Acetophenone condensation reaction over sulfated zirconia.**

Deactivation of the catalysts occurred, presumably due to coke formation via strong adsorption of dypnone on the catalyst surface or formation of bulky aromatics groups such as triphenylbenzene **25** as illustrated in Figure 6-10. Triphenylbenzene was formed, most likely from condensation of three molecules of acetophenone to give a trialcohol intermediate followed by rapid dehydration to liberate three water molecules. Other possible molecules responsible for acid site deactivation and pore blockage according to Lavaud et al [22] is the product resulting fro condensation of triphenylbenzene with another acetophenone molecule to give an intermediate alcohol **26** which undergoes a dehydration reaction to yield probably a compound with chemical structure ($C_{32}H_{24}$) **27** (Figure 6-10). These bulky aromatic compounds have low volatility and can strongly deposit on the acid surface leading to a catalyst deactivation.

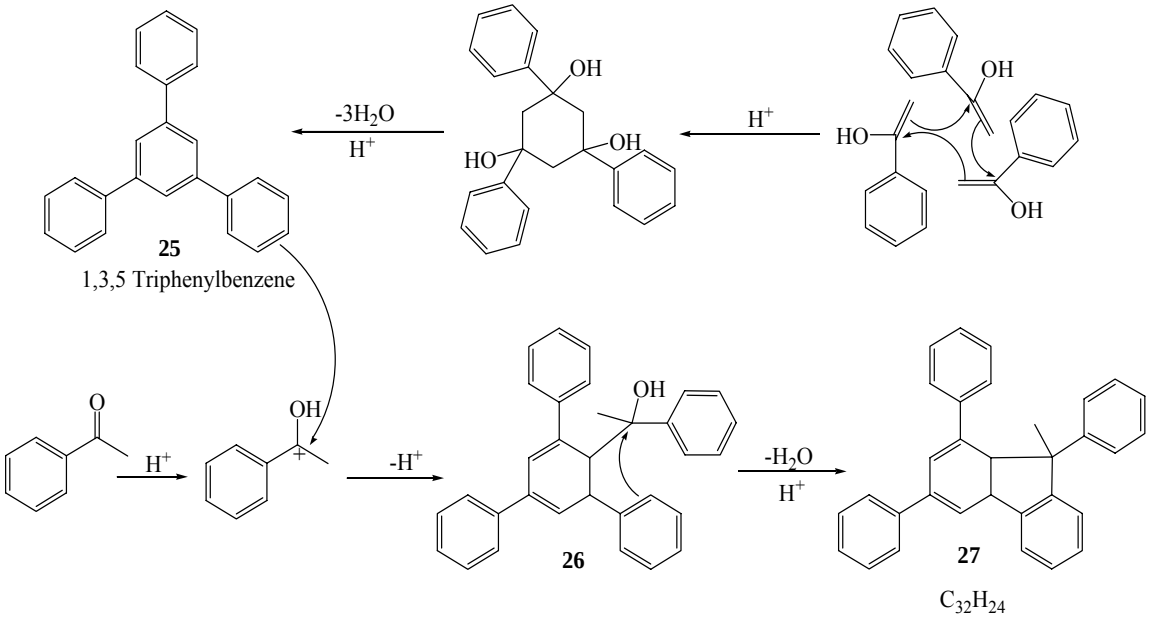


**Figure 6-10: Formation of the possible coke precursors from the acetophenone condensation self reaction.**

Table 6-2 summarizes the product from aldol condensation of acetophenone carried out at 150 °C over various zirconia samples. As in case of acetone and cyclopentanone condensation reactions, no intermediate alcoholic products such as BPHB **21** was observed under these reaction conditions.

**Table 6-2: Acetophenone condensation reaction over sulfated zirconia samples proceeds for 10 hours at 150 ºC.**

| Catalyst code | Acetophenone Conversion (%) | Product Selectivity (%) | | Ratio (trans : cis) |
|---|---|---|---|---|
| | | Dypnone | Others | |
| **SZ-1(1:3)** | 39.7 | 88 | 12 | (1:1) |
| **15% SZ/MCM** | 22.1 | 92.8 | 7.2 | (1:0) |
| ***15% SZ/MCM** | 45.4 | 61.6 | 38.4 | (1:0) |
| **40% SZ/MCM** | 17.9 | 83.7 | 16.3 | (1:0) |
| **SZ-4** | 20.7 | 89.4 | 10.6 | (9:1) |

** The reaction was run for 50 hours.*

The results of the condensation reaction of acetophenone over supported and unsupported sulfated zirconia (Table 6-2) showed that the reaction strongly depends on the number and the distribution of the active acid sites. The catalyst with the highest initial activity was SZ-1(1:3) which also had the highest acidity. However, unlike the supported samples, SZ-1(1:3) showed a rapid deactivation which indicated that the dispersion of the active sites on the surface is extremely important to avoid fast catalyst deactivation. Bulky triphenylbenzene **25** was isolated in the product solution only when the reaction was conducted over the supported sulfated zirconia samples. This implies

that such bulky products, once formed, are protected inside the pores of the MCM and desorb from the catalyst before further polymerization to form coke species or decomposition could occur. Furthermore, when the reaction time prolonged over 15% SZ/MCM sample for about 50 hours, the selectivity toward dypnone was decreased to about 60% and the selectivity for triphenylbenzene at these conditions was increased to 22%. Apparently, the selectivity towards dypnone decreases due to the arising of other competition reactions included the self and cross condensation over the acid sites. Another possible reason for the decrease of the dypnone selectivity is due to an acid cracking mechanism by protonation of the dypnone itself followed by dissociation to give a stable carbocation acylium ion **28** and isopropenylbenzene **29** (Figure 6-11). The acylium ion further reacts with another water byproduct molecule in the solution to give benzoic acid **30**. Such products, however, were observed with very low yield. These products were also observed when the acetophenone condensation reaction was performed at high reaction temperature (350 °C) on zeolite type catalysts [23-24].

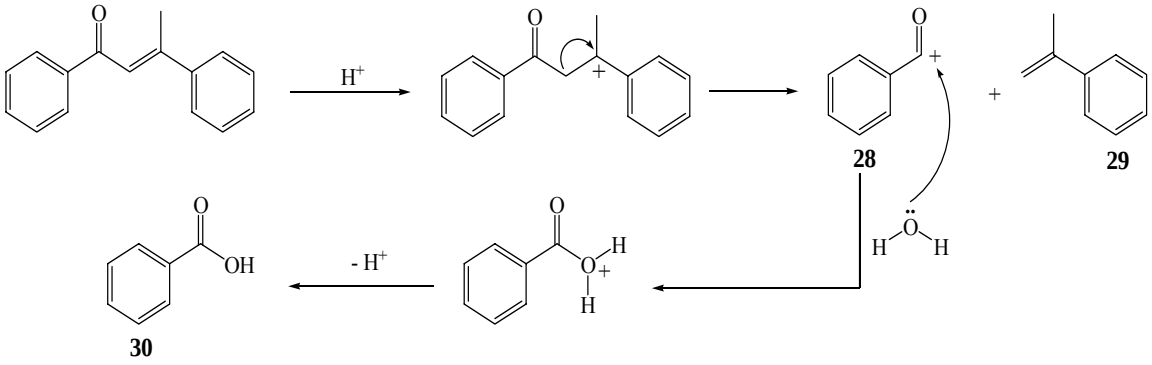


**Figure 6-11: Formation of benzoic acid and isopropenyl benzene from acid cracking of dypnone.**

**Methylisopropyl ketone condensation:**

The mechanistic pathway for the self condensation reaction of methyl isopropyl ketone (MIP) was quite similar to that discussed for other ketones. The reaction was conducted over 40% SZ/MCM sample at 150 °C. Figure 6-12 summarizes the main products formed from this reaction. In this case, however, there are two different enol forms that can be produced; the more stable form (**32)** and the less stable one (**33)** (Figure 6-12).

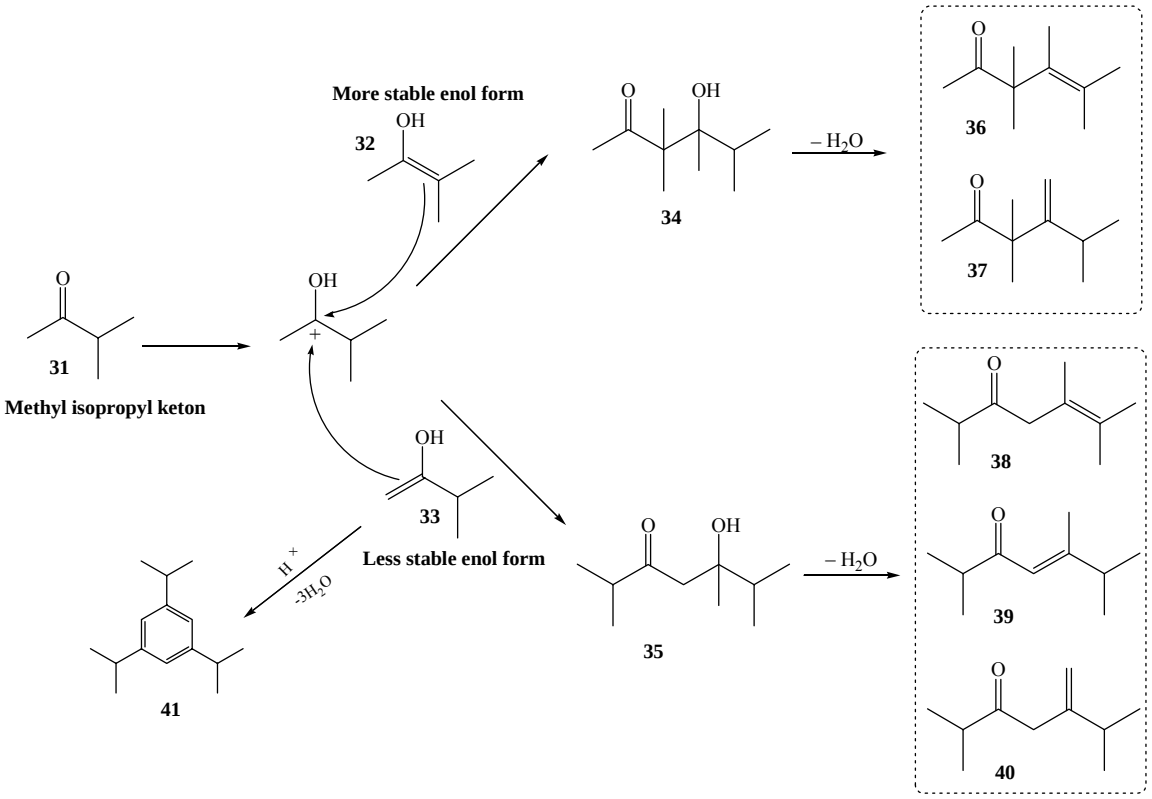


**Figure 6-12: Reaction network for methyl isopropyl ketone condensation over synthesized sulfated zirconia.**

The conversion of metyhlisopropyl ketone over sulfated zirconia is shown in Figure 6-13. The reaction showed a slower initial rate compare to that of other studied

ketones such as acetone and cyclopentanone, and a comparable rate to that of Acetophenone.

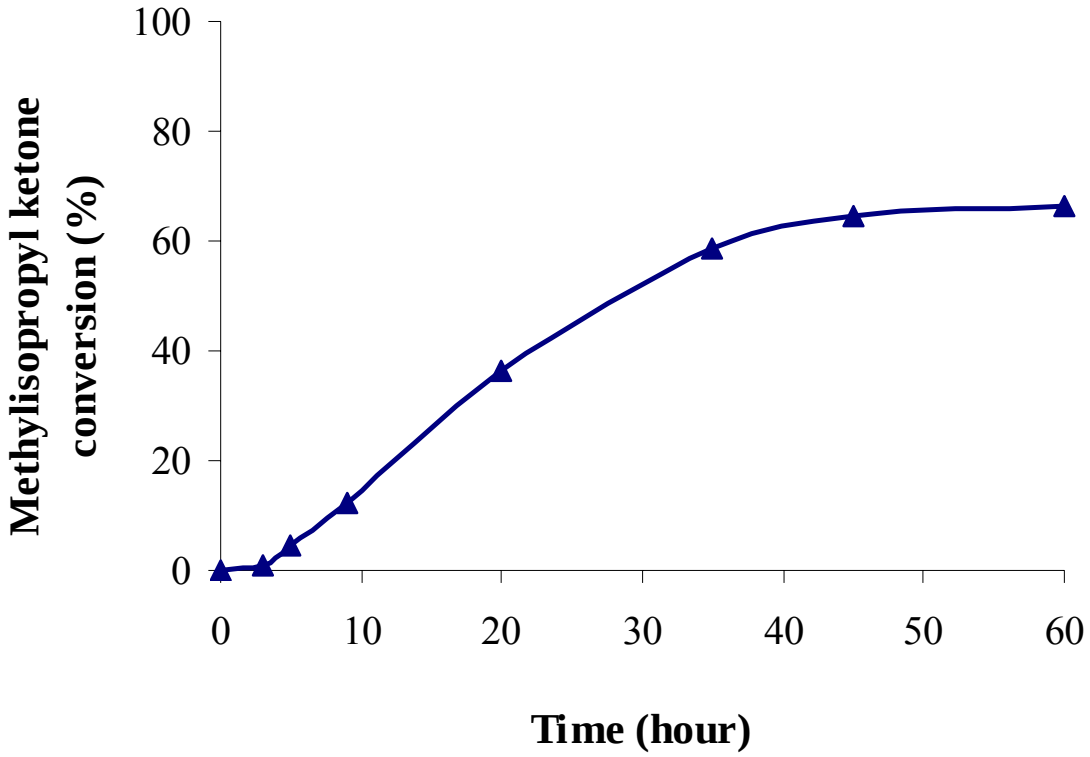


**Figure 6-13: Methylisopropyl ketone conversion over 40% SZ/MCM at 150 °C.**

Unsaturated ketones **36**, **37**, and **38** are the main products formed. These ketones formed as a result of reaction of both enol forms with the protonated ketone molecules to form generally stable unsaturated ketones. The results of the condensation reaction of MIP over the 40% SZ/MCM sample are shown in Table 6-3.

**Table 6-3: Methylisopropyl Ketone condensation reaction over sulfated zirconia sample 40% SZ/MCM at 150 ºC.**

| Reaction Time (h) | MIP conversion (%) | Product Selectivity (%) | | | | |
|---|---|---|---|---|---|---|
| | | **34** | **36** | **35** | **36** | **Others** |
| **9** | 12.3 | 26.8 | 35.9 | 11.9 | 1.8 | 23.6 |
| **20** | 36.3 | 26.3 | 37.5 | 6.9 | 2.2 | 27.1 |
| **35** | 58.7 | 24.5 | 30.5 | 6.4 | 1.2 | 37.4 |
| **45** | 64.6 | 22.8 | 25.7 | 11.18 | 2.9 | 37.4 |
| **60** | 66.4 | 16 | 17.7 | 9.4 | 3.8 | 53.1 |

** The products assigned to each number in the table are shown in figure 6-13.*

The less stable enol form **33** also reacts with the protonated carbocation followed by dehydration to produce three different unsaturated ketones **38**, **39**, and **40** isomers with that only differ in the position of the double bond. Triisopropyl benzene **41** was also observed in very low concentration and is believed to be formed as a result of the self condensation of three less stable enol forms molecules **33** to form a trialcoholic intermediate followed by dehydration.

**Ketones reactivity on the surface of sulfated zirconia:**

Figure 6-14 showed the IR spectra of the adsorption of acetone and cyclopentanone over sulfated zirconia sample (40% SZ/MCM) at room temperature and at the reaction conditions. In the case of acetone adsorption, on sulfated zirconia at room temperature, two different bands that correspond to the carbonyl groups were observed [Figure 6-14 25 °C, a]. The first band at 1720 $cm^{-1}$ is obviously attributed to the weakly

physisorbed ketone species on the surface. The other band at about 1560 $cm^{-1}$ is believed to be attributed to the formation of the enolate acetone species on the surface as in case of adsorption of acetone over zeolite type catalysts [24]. The lower frequency of the latter band is due to the lower C-O double bond character. The enolate band formed as a result of the coordination of the ketones on either the Lewis or Brønsted acid sites.

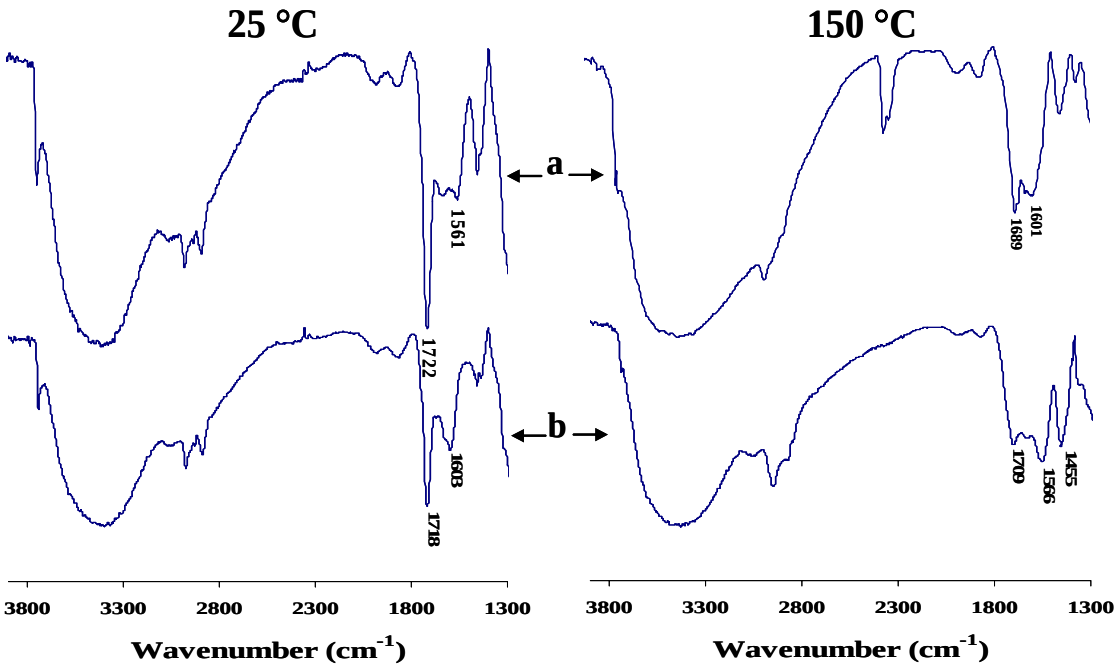


**Figure 6-14: IR spectra of the sulfated zirconia after adsorption of a) acetone and b) cyclopentanone at 25 °C and 150 °C.**

As with acetone, a band at 1718 $cm^{-1}$ was observed for the cyclopentanone adsorption at room temperature [Figure 6-14, 25 °C, b]. This band, which corresponds to the carbonyl group of the cyclopentanone, indicates that the cyclopentanone is physisorbed on the surface. In contrast to the acetone case, however, the band attributed

to the enolate form was not observed. This clearly implies that the protonation of the cyclopentanone at room temperature is not as easy as in case of the protonation of acetone molecules. This maybe is the reason behind the lower initial reactivity of the cyclopentanone compared to that of the acetone [Figures 6-3 and 6-7]. The conversion of acetone was about 80% when the reaction performed for 3 hours while the conversion of cyclopentanone was only about 25% in the same time period. Other evidence for the protonation of acetone at room temperature, as seen earlier, is that acetone reacts on 40% SZ/MCM sample at room temperature with low conversion to produce diacetone alcohol and mesityl oxide while no reaction was occur when cyclopentanone was stirred with 40% SZ/MCM catalyst at 25 °C for two days. Figure 6-15 shows a schematic diagram for the proposed structure of the chemisorbed acetone on the both, Lewis and Brønsted acid sites on sulfated zirconia surface.

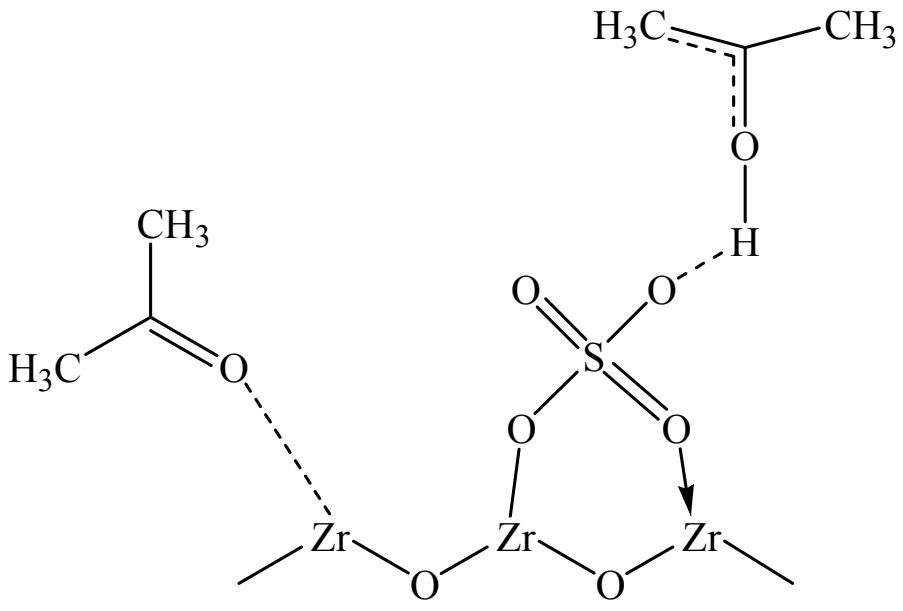


**Figure 6-15: Schematic diagram for acetone chemisorbed on sulfated zirconia.**

Figure 6-14 also shows the IR spectra of the sulfated zirconia after the condensation reaction of acetone and cyclopentanone at 150 °C. The spectra are significantly changed compared to the spectra of the adsorbed ketone at room temperature. In the case of acetone [Figure 6-14,150 °C, a], a strong band at 1689 $cm^{-1}$ was observed which corresponds to the chemisorbed carbonyl groups of the ketone compound such as acetone or mesitylene oxide. The band at 1601 $cm^{-1}$ presumably corresponds to the C=C of the aromatic compound which may be deposited on the surface of the oxide during the reaction. On the other hand, the IR spectrum of the oxide after the condensation of cyclopentanone [Figure 6-14,150 °C, b] shows a strong band at 1710 $cm^{-1}$ corresponding to the weakly physisorbed ketone species on the surface. Additionally, the appearance of a strong band at 1560 $cm^{-1}$ along with another strong band at 1466 $cm^{-1}$ in the IR spectra of the oxide after cyclopentanone condensation at 150 ºC compared to that at room temperature, presumably, suggests the formation of surface carboxylate groups ($RCOO^{-}$). The carboxylate species formed as a result of the oxidation of cyclopentanone or other species at elevated temperature. These surface molecules along with the coke formation probably contributing to the slow reactivity of cyclopentanone compared to that of acetone (the conversion of acetone reaches 80% after reaction for three hours while the conversion of cyclopentanone achieved 80% after 38 hours [Figures 6-3 and 6-7]).

**CONCLUSIONS AND REMARKS:**

In conclusion, sulfated zirconium oxides can catalyze self condensation reactions of several ketones such as acetone, cyclopentanone, and acetophenone. The catalytic

activity and product selectivities are strongly influenced by the nature of the starting ketone (steric properties and accessibility to the active sites) as well as catalyst properties and the surface acidity of the employed sulfated zirconia catalyst. Acidity becomes very critical in the dehydration of the intermediate alcohol to the corresponding α,β-unsaturated carbonyl compounds. However, the reaction temperature also plays an important role in the dehydration process as seen in the case of conversion of diacetone alcohol to mesityl oxide in the acetone condensation reaction. The catalyst deactivation most probably occurs due to the strong chemisorption of ketones over the acid sites or is due to the formation of bulky high molecular weight aromatics which formed via the secondary reactions during the condensation reaction via oligomerization. These aromatics act as a coke precursor leading to the rapid deactivation of the surface of zirconia catalysts. Bulky aromatic products are best prepared using a porous catalyst with high surface area and big cavities that can easily accommodate these species. Furthermore, water molecules that are formed during the condensation reaction can adsorb on the acidic sites on the oxide surface and hence deactivate the catalysts. In general, one can say that the selection of suitable and appropriate reaction conditions and catalytic system is very critical for the optimization of the activity and selectivity for desired products.

**REFERENCES CITED:**


1. O. Veloso, F. Monteiro and F. Sousa-Aguiar, *Stud. Surf. Sci. Catal*. **1991**, *84*, 1913.
2. T. Wierzchawski and W. Zatorski, *J. Cata*l. **1991**, *9*, 411.
3. J. Rode, E. Gee, N. Marquez, T. Uemura and M. Bazagani, *Catal. Lett*. **1991**, *9*, 103.
4. J. Colonge, *Bull. Soc. Chem. Fr.* **1931**, *49*, 426.
5. G. Zhang; H. Hattori and K. Tanabe, *Appl. Catal.* **1988**, *36*, 189.
6. W. Reichles, *J. Catal.* **1980**, *63*, 295.
7. S. Lippert, W. Baumann and K. Thomke, *J. Molec. Catal.* **1991**, *69*, 199.
8. L. Baigrie, *J. Am. Chem. Soc.* **1985**, 107, 3640.
9. T. Komatsu, M. Misuhashi and T. Yshima, *Stud. Surf. Sci. Catal.* **2002**, *142A*, 667.
10. J. Muzart, *Synthesis* **1982**, 60.
11. M. Jerry, *Advance Organic Chemistry*, Wiley, New York, 4th edition, 1992, 938.
12. A. Corma and M. Martin-Aranda , *J. Catal.* **1991**, *130*, 130.
13. V. Bell and H. Gold, *J. Cata*l. **1983**, *79(2)*, 286.
14. W. Xu and D. Raftery, *J. Cata*l., **2001**, *204(1)*, 110.
15. A. Biaglow, J. Sepa, R. Gorte and D. White, *J. Cata*l. **1995**, *151(2)*, 373.
16. T. Solomons, *Organic Chemistry*, Wiley, New York, 7th edition, 1998, p798.
17. J. Cosimo and C. Apesteguia, *J. Molec. Catal. A.* **1998**, *130*, 177.
18. C. Lelkar and A. Schutz, *Appl. Clay Sci.* **1998**, *13*, 417.

19. A. Philippou and M. Anderson, *J. Catal.* **2000**, *189*, 395.

20. F. Delannay, *Chemical Industries (V-15), Characterization of Heterogeneous Catalysis*, Marcel Dekker, INC, New York, 1984, p367.

21. T. Xu, E. Munson and J. How. *J. Am. Chem. Soc.* **1994**, *116*, 1962.

22. N. Lavaud, P. Magnoux, F. Alvarez, L. Melo, G. Giannetto and M. Guisnet *J. Molec. Catal. A* **1999**, *142*, 223.

23. L. Kubelkova, J. Cejka, J. Novakova, V. Bosacek, I. Jirka and P. Jiru, *Stud. Surf. Sci. Catal*. **1989**, *49B*, 1203.

24. L. Kubelkova and J. Novakova, *Zeolite,* **1991***, 11,* 822.

# VITA

Mohammed H. AL-Hazmi

Candidate for the Degree of

Doctor of Philosophy

Thesis: SYNTHESIS, CHARACTERIZATION, AND APPLICATION OF ZIRCONIA AND SULFATED ZIRCONIA DERIVED FROM SINGLE SOURCE PRECURSORS.

Major Field: Chemistry

Biographical:

Education: The author obtained his B.S. degree in General Chemistry from King Saud University, Riyadh, Saudi Arabia in 1995. He also was awarded the Master's degree from the Graduate College at King Saud University in 1999 in Physical Chemistry. Finally, he completed the requirements for the Doctor of Philosophy degree at Oklahoma State University, Stillwater, Oklahoma, in May, 2005.

Publications: The author published several research papers and he was a co-author in several patents dealt with some heterogeneous catalysis topics.

Professional Experience: During his study for the M.S., the author joined The Saudi Basic Industrial Corporation (SABIC) as a researcher at SABIC Industrial Complex for Research and Technology (SABIC R&T). He acquired more than four years experience in research activities related to several heterogeneous catalysis topics in the area of oxidative dehydrogenation and selective oxidation of lower alkanes to value added chemicals, hydrogenation of lower olefins, ammoxidation of $C_3$-$C_4$ olefins, and isomerization and dehydrogenation of normal butane. The projects dealt with designing, synthesis, and characterization of various metal oxide catalysts for the above reactions.

Professional Memberships: American Chemical Society (ACS); Saudi Chemical Society (SCS); Phi Lambda Upsilon (PLU) National Honorary Chemical Society; American Association for the Advancement of Science (AAAS).

Name: Mohammed H. AL-Hazmi Date of Degree: May, 2005

Institution: Oklahoma State University Location: Stillwater, Oklahoma

Title of Study**: SYNTHESIS, CHARACTERIZATION, AND APPLICATION OF ZIRCONIA AND SULFATED ZIRCONIA DERIVED FROM SINGLE SOURCE PRECURSORS.**

Pages in Study: 215 Candidate for the Degree of Doctor of Philosophy

Major Field: Chemistry

**Scope and Method of Study:** The objective of this research was the development of new methods for the synthesis of zirconium oxide and sulfated zirconium oxide based on the preparation and utilization of novel single-source precursors based on zirconium carboxylate and zirconium sulfonate complexes. A variety of carboxylate and sulfonate compounds were treated with zirconium salts to yield new precursors. The oxide products obtained form the thermal pyrolysis of the precursors were analyzed and characterized using several techniques such as powder X-ray diffraction, thermogravimetric analysis and infrared spectroscopy. Additionally, supported sulfated zirconia was successfully obtained by dispersion of the oxide over a high surface area porous silica support known as MCM-41. The ability of the produced sulfated zirconias to catalyze two different industrial reactions was addressed. The first was the alkylation reaction of benzene utilizing ethers such as dibenzyl ether, n-butyl ether, and benzyl methyl ether as alkylating agents. The second reaction was the self aldol condensation reaction of several ketones such as acetone, methyl isopropyl ketone, cyclopentanone and acetophenone.

**Findings and Conclusions:** Oxides obtained from different zirconium carboxylate and sulfonate precursors showed distinctive properties such as surface morphology, surface area, phase composition and crystallite size. This reflected the strong dependency of the final oxide's properties on the precursor complexes. The supported samples were successfully synthesized with high dispersion of the sulfated zirconia on the surface of the MCM-41 while maintaining high surface area and without causing a serious blockage or damage of the support pore structure. The supported samples assisted in the improvement of the thermal stability of the tetragonal phase and the sulfate groups on the surface. Acidic catalysts prepared by these methods showed a higher acid strength than concentrated sulfuric acid. The sulfated zirconias showed a remarkable catalytic activity and selectivity towards the alkylation of aromatics and self ketone aldol condensation reactions.

ADVISOR'S APPROVAL:___ **Dr. Allen Apblett** _____